Dynamical Aspects of Topological Quantum Systems

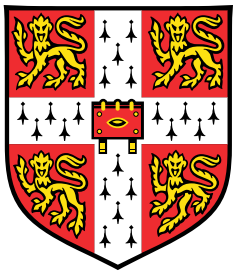

Maximilian McGinley

Supervisor: Prof. Nigel Cooper

Department of Physics
University of Cambridge

This dissertation is submitted for the degree of
Doctor of Philosophy

Christ's College August 2020

To my parents.

Declaration

This thesis is the result of my own work and includes nothing which is the outcome of work done in collaboration except as declared in the Preface, Acknowledgements, and as specified in the text. It is not substantially the same as any that I have submitted, or, is being concurrently submitted for a degree or diploma or other qualification at the University of Cambridge or any other University or similar institution except as declared in the Preface and specified in the text. I further state that no substantial part of my thesis has already been submitted, or, is being concurrently submitted for any such degree, diploma or other qualification at the University of Cambridge or any other University or similar institution except as declared in the Preface and specified in the text. It does not exceed the prescribed word limit for the relevant Degree Committee.

Maximilian McGinley
August 2020

Abstract

Topological phases of matter are understood to be characterized by particular configurations of entanglement encoded within the ground states of many-body quantum systems. In this thesis, we discuss how novel phenomena associated with topological phases can arise in systems that are driven out of equilibrium or coupled to their surroundings, which are not described by ground state physics.

Firstly, we consider systems undergoing unitary time evolution due to some external driving. We show how the entanglement features of the time-dependent wavefunction can be topologically characterized, and demonstrate that these topological properties are reflected in the dynamics of various quantities usually associated with topological phases in equilibrium. We introduce a new non-equilibrium topological classification scheme which can be used to predict whether or not the topological features of a given system will be preserved under time evolution. In brief, this classification captures the fact that certain symmetries (namely antiunitary symmetries) are inevitably broken once the system is driven out of equilibrium; thus any topological phenomena protected by such symmetries cannot be expected to persist in non-equilibrium scenarios.

Secondly, we investigate how topologically non-trivial systems are affected by dissipative effects, i.e. coupling to an external environment. We demonstrate that system-environment interactions facilitate processes in the system that effectively break any antiunitary symmetries, regardless of the symmetries of the microscopic Hamiltonian. Accordingly, those phases that were shown to be unstable against time-dependent driving are also fragile against coupling to an environment. To illustrate the consequences of this fragility, we consider the effects of dissipation on the coherence properties of topological bound states, as well as the conductance properties of chiral and helical topological edge modes. We find that the decoherence rate of the former and the deviation from quantized conductivity of the latter are (not) exponentially suppressed in the inverse temperature when the phase in question is protected by unitary (antiunitary) symmetries. These results regarding open systems can be connected to the same non-equilibrium classification developed in the context of isolated systems undergoing unitary dynamics.

Our findings highlight a distinction between topological phases that are either robust or fragile against non-equilibrium effects and/or system-environment coupling. The ramifications for the use of such systems in quantum technologies are discussed.

Acknowledgements

The work described in this thesis would not have been possible without the help of many people. Most importantly, my thanks go to my supervisor Nigel, who has been a constant source of inspiration and guidance throughout my Ph.D. I have learned so much from him, and he has given me the liberty to pursue my own ideas while always keeping me focussed on what is most important. His insight as a collaborator and thoughtfulness as a mentor has made working with him a formative and enjoyable experience.

I owe a great deal to Andreas Nunnenkamp and Johannes Knolle, whose supervision and advice during my Masters and beyond has proved invaluable. Their enthusiasm and encouragement has helped foster my interest in condensed matter physics, and prepared me for the future. Likewise, I am grateful to have had the chance to work with Simon Lieu.

During my Ph.D I have benefited from helpful discussions with many members of the physics community. I would like to thank Juan Garrahan, Graham Kells, Jan Budich, and Peter Zoller for inviting me to visit their respective research institutes. I have also had the opportunity to broaden my knowledge through attending several conferences and schools, thanks to financial support from the EPSRC, who also funded the research presented in this thesis.

It has been a joy to work and study in the Theory of Condensed Matter group in Cambridge. I am grateful to all those who made my time there so much fun both in and out of work. Particular thanks go to my office mates and amateur social event coordinators Alice and Ollie who proofread parts of this thesis, as well as to Elis, Michael, Chris, Stephen, Angela, Attila, Petr, and many others who are too numerous to name here.

Thanks go to Chris, David, and all my other friends outside of work who have made my time in Cambridge all the more enjoyable. Most of all, thank you to Selena for being patient and supportive of me no matter what, and for reminding me of all the important things in life outside the world of physics.

Finally, to Mum, Dad, Theo, and my whole family, thank you for your limitless love and support without which the last three years would have been a great deal more challenging. Dad – I think those childhood lessons on entropy in the garage have paid off!

Table of contents

Chapter 1

Introduction

The materials one encounters in everyday life are composed of an enormous number of particles, each interacting with one another according to the fundamental laws of physics that govern their behaviour. The details of this complex motion may differ greatly at the microscopic level from one many-body system to another, yet the qualitative properties we observe on macroscopic scales can be remarkably universal, in that they are insensitive to such differences. The intuitive notion of a phase of matter relies on this empirical observation: Many different systems exhibiting the same qualitative features can be classified as belonging to the same phase.

Solids, liquids, and gases are the most familiar classical phases of matter, and were naturally the first to be understood. However, the advent of quantum mechanics has seen the discovery of many more phases with highly counter-intuitive properties. In these many-body systems, the quantum nature of the constituent particles becomes apparent on macroscopic scales, giving rise to rich and exotic phenomena, such as superfluidity, superconductivity, and Bose-Einstein condensation. In an effort to systematically classify the ever-increasing list of phases of matter, Landau developed a paradigm based on the concept of spontaneous symmetry breaking. He recognised that the free energy minima of a system may possess fewer symmetries than the underlying microscopic equations of motion. Accordingly, states belonging to different phases can be distinguished by the ways in which they transform under the action of symmetries. As a typical example, one can use the rotational symmetry of interactions in a system of spins to differentiate between ferromagnetic and paramagnetic phases: A ferromagnet has a net magnetization that spontaneously aligns along a particular direction, whereas a paramagnet exhibits the same rotational symmetry present at the microscopic level.

Landau's paradigm is an extremely powerful tool, and can be successfully applied to highly contrasting physical scenarios. For instance, a solid, governed by Newton's

equations, can be characterised through symmetry-breaking in the same way as a Bose-Einstein condensate, governed by the Schrödinger equation. Indeed, the breaking of a continuous symmetry gives rise to gapless modes that in both cases are referred to as 'sound waves'. Given the power of Landau's approach to describe phase transitions in both classical and quantum systems, one might conclude that quantum mechanics simply offers a new context for symmetry-breaking phases, but that the relevant underlying mechanisms are the same as in classical physics.

However, it has long been known that quantum mechanical few-particle systems can exhibit effects that no classical system can, related to the presence of *quantum entanglement*. It is only in recent years that the rôle of entanglement in many-body systems has been widely appreciated. This newfound understanding has many important consequences for the study of phases of matter: Whereas classical phases can all be understood through the different ways in which the system transforms under symmetries, there exist quantum phases of matter that instead are distinguished by the ways in which the degrees of freedom are entangled. These phases thus do not admit a classical description, and have been termed 'topological phases of matter', for reasons which we will elucidate. Although entanglement is generally very difficult to measure directly, systems belonging to topological phases exhibit many experimentally observable universal phenomena that derive from their unusual entanglement properties, some of which have potential technological use.

While early work on topological phases focussed primarily on electronic systems, today there is a much wider range of experimental platforms in which these topics can be explored. This expansion beyond traditional solid-state experiments requires us to re-examine some of the key assumptions that were previously justified for electronic systems. Perhaps most strikingly, the typical timescales on which these new systems equilibrate are orders of magnitude longer than their electronic counterparts, and so these systems are not necessarily at or near to thermal equilibrium at a given instant in time. This has both motivated and facilitated studies of coherent quantum many-body dynamics in non-equilibrium regimes. Again, this field has benefited greatly from a better understanding of many-body quantum entanglement, and in particular its dynamics. The theoretical progress in non-equilibrium quantum many-body physics has been rapid, both in relation to isolated systems undergoing unitary dynamics, and for open systems, where the additional possibility of entanglement generation between a system and its environment adds to the underlying complexity.

Evidently, if we are to fully understand topological phenomena in this context, we should treat entanglement as a dynamic, rather than a static property. This requires us to revisit some of the central ideas that underpin topological phases of matter. At the broadest level, the aim of this thesis is to elucidate how the entanglement structures and experimental signatures

characteristic of topological phases are affected by the departure from the familiar paradigm of isolated systems at equilibrium. Despite the increased complexity of the underlying many-body physics, our findings reveal a remarkable degree of universality in the resultant dynamics, as well as offering insights into the practical challenges that may arise when utilising topological systems for technological purposes.

1.1 Quantum entanglement in many-body systems

1.1.1 Basics of entanglement

A tacit assumption of classical physics is that there is no fundamental obstruction to specifying and/or determining the state of any given degree of freedom. The same is not true in quantum mechanics. The state of a quantum system is specified by a wavefunction $|\Psi\rangle$, which encodes probability distributions for the outcomes of measurements. When dealing with multipartite systems (i.e. those in which there is a meaningful separation between different degrees of freedom), the axioms of quantum mechanics lead us to conclude that it is not always possible to describe the state of one degree of freedom independently of the others. More precisely, there does not necessarily exist a wavefunction that pertains to some subsystem only and accurately describes the outcomes of measurements therein. In contrast, the state of a classical degree of freedom (coordinates and momenta) can always be specified and in principle measured irrespective of the state of the rest of the system. The term quantum entanglement is introduced to describe this fundamental interdependency that can be established between quantum degrees of freedom.

For instance, a system made up of two spin-half degrees of freedom can be in the state

$$|\Psi_{\text{ent.}}\rangle = \frac{1}{\sqrt{2}}\left(|\uparrow\rangle_1 \otimes |\downarrow\rangle_2 + |\downarrow\rangle_1 \otimes |\uparrow\rangle_2\right) \tag{1.1}$$

where $\{|\uparrow\rangle_i, |\downarrow\rangle_i\}$ are the two eigenstates of the spin operator $\hat{S}_i^z$ for the spin indexed by $i = 1, 2$. In words, the above tells us that if the first spin is up, then the second spin is down, and vice-versa. Clearly, the two spins are entangled. In contrast, the state

$$|\Psi_{\text{unent.}}\rangle = \frac{1}{2}\left(|\uparrow\rangle_1 + |\downarrow\rangle_1\right) \otimes \left(|\uparrow\rangle_2 + |\downarrow\rangle_2\right) \tag{1.2}$$

is not entangled. To be more precise, for the state $|\Psi_{\text{unent.}}\rangle$, a measurement of spin 1 does not affect the outcome of a subsequent measurement of spin 2.

More generally, if the system is divided into degrees of freedom in A and those in its complement B, then given a pure state $|\Psi\rangle$ of the composite system, we can ask whether there is any entanglement between A and B. With such a bipartition in place, it is helpful to consider a construction due to Schmidt (see, e.g. Ref. [175]), who noted that any $|\Psi\rangle$ admits a decomposition

$$|\Psi\rangle = \sum_j \sqrt{\zeta_j}\, |\phi_j\rangle_A \otimes |\chi_j\rangle_B \,, \tag{1.3}$$

where the Schmidt coefficients ζ_j satisfy $0 \leq \zeta_j \leq 1$, $\sum_j \zeta_j = 1$, and $\{|\phi_j\rangle_A\}$ and $\{|\chi_j\rangle_B\}$ are orthonormal bases for the Hilbert spaces of regions A and B, respectively. All these objects depend on the particular $|\Psi\rangle$ in question.

If there is only one non-zero ζ_j, then the wavefunction is factorizable $|\Psi\rangle = |\phi\rangle_A \otimes |\chi\rangle_B$ and there is no entanglement between A and B [cf. Eq. (1.2)]. If, instead, more than one ζ_j is non-zero, then we see from (1.3) that the state of A cannot be defined independently of the state of B [cf. Eq. (1.1)]. Although A cannot be described in terms of a single quantum state, we can still calculate the outcome of measurements of observables on A, i.e. $\langle \hat{O}_A \rangle \coloneqq \langle \Psi | \hat{O}_A | \Psi \rangle$, where the operator $\hat{O}_A$ depends only on degrees of freedom in A. For this purpose, it is helpful to consider the reduced density matrix $\hat{\rho}_A$, which is defined as

$$\hat{\rho}_A \coloneqq \mathrm{Tr}_B \left(|\Psi\rangle \langle \Psi| \right), \tag{1.4}$$

where Tr_B denotes a trace over the degrees of freedom in B only. By writing $\langle \hat{O}_A \rangle = \mathrm{Tr}[\hat{O}_A |\Psi\rangle \langle \Psi|] = \mathrm{Tr}_A[\hat{O}_A \hat{\rho}_A]$, one can see that all observables on A can be determined from $\hat{\rho}_A$; this therefore gives us maximal information about the state of A.

Using the orthonormality of $\{|\chi_j\rangle_B\}$, one can relate the Schmidt decomposition to the eigendecomposition of the reduced density matrix

$$\hat{\rho}_A = \sum_j \zeta_j |\phi_j\rangle_A \langle \phi_j|_A \,. \tag{1.5}$$

Thus we see that the Schmidt coefficients are exactly the eigenvalues of $\hat{\rho}_A$, with eigenvectors $|\phi_j\rangle_A$. If only one ζ_j is non-zero, then we have $\hat{\rho}_A = |\phi\rangle_A \langle \phi|_A$, which is a pure density matrix, and the quantum state of A is well-defined, as expected. Otherwise, $\hat{\rho}_A$ can be interpreted as a statistical ensemble of quantum states – that is, we would obtain the same quantum averages $\langle \hat{O}_A \rangle$ if we supposed that A were in the quantum state $|\phi_j\rangle_A$ with probability ζ_j, and averaged over the corresponding classical statistical ensemble [175]. Note that this uncertainty in the state of A is a fundamental one, rather than being due to some inability to make perfect

measurements of A. Furthermore, from the symmetry of the Schmidt decomposition, we also see that the reduced density matrix for B, $\hat{\rho}_B = \mathrm{Tr}_A(|\Psi\rangle\langle\Psi|)$ has the same eigenvalues as $\hat{\rho}_A$, with eigenvectors $\{|\chi_j\rangle_B\}$.

The Schmidt coefficients $\{\zeta_j\}$ (equivalently, the eigenvalues of $\hat{\rho}_A$) provide a lot of information about the entanglement features of $|\Psi\rangle$, and are referred to as the *entanglement spectrum* [133]. However, it is often convenient to quantify the amount of entanglement between A and B using a single number, which is referred to as an entanglement entropy. The most commonly used of these is the von Neumann entropy

$$S_A := -\mathrm{Tr}\,(\hat{\rho}_A \log \hat{\rho}_A) = -\sum_j \zeta_j \log \zeta_j \tag{1.6}$$

If $S_A \neq 0$, then $|\Psi\rangle$ necessarily features some entanglement between A and B, i.e. more than one ζ_j is non-zero. More generally, the von Neumann entropy can be defined for an arbitrary density operator whose lack of purity may be due to either entanglement with external degrees of freedom, or classical uncertainty in the state of the system (or even a combination of both).

The reduced density matrix, Schmidt decomposition, entanglement spectrum, and entanglement entropy will prove to be useful tools when probing the entanglement properties of both closed and open many-body quantum systems.

1.1.2 Many-body entanglement

When moving to isolated *many-body* systems, one can ask similar questions about entanglement of a pure wavefunction. A particularly important class of wavefunctions are ground states, which are of relevance to isolated systems at equilibrium (and sufficiently low temperature). In this context, there are a thermodynamically large number of degrees of freedom to consider. Moreover, with the exception of extremely long-ranged systems, there is a notion of locality in many-body systems, in that degrees of freedom will only interact with other degrees of freedom that are nearby in space. Understanding *spatially resolved* entanglement features will be of central importance to the study of quantum phases of matter.

A key result in the study of gapped systems at equilibrium is the entanglement area law for ground states [200, 93]. The area law tells us about the structure of entanglement for a ground state $|\Psi_0\rangle$ of a gapped local Hamiltonian[1]. To probe entanglement in a way that is sensitive to the spatial features of the system, we can choose different bipartitions of

[1] In this context, we consider a Hamiltonian to be local if it only couples degrees of freedom that are separated by some finite maximum length; however results are also known for Hamiltonians with terms that decay sufficiently quickly with their range [85].

the system into regions A and B, and consider how the associated entanglement properties depend on the geometric features of A.

The entanglement area law states that if the Hamiltonian of which $|\Psi_0\rangle$ is the ground state is gapped, then as the region A is varied, the entanglement entropy scales with the size of the boundary[2] of A

$$S_A\left[|\Psi_0\rangle\right] = \mathscr{O}(|\partial A|). \tag{1.7}$$

This scaling behaviour holds for any choice of geometry of A – it is thus a very strong condition on the form of $|\Psi_0\rangle$. There are many different arguments justifying the area law, with various different levels of rigour. For an introductory review, see e.g. Ref. [61].

The area law is satisfied when the amount of entanglement between any two degrees of freedom decays sufficiently rapidly with the distance between them. To see this, take the simple case of a large region A that is simply connected. If appreciable amounts of entanglement can only be established over short distances, then degrees of freedom well within the bulk are only entangled with other degrees of freedom in A; thus they do not contribute to the entanglement entropy S_A. Only the degrees of freedom near the boundary of A are appreciably entangled with those outside of A, the number of which scales with the size of the size of the boundary of A. This is in stark contrast with a random state in the Hilbert space, for which any two degrees of freedom can be arbitrarily entangled. In this case, all degrees of freedom will on average contribute a finite amount of entanglement to S_A, resulting in a 'volume law' scaling $S_A = \mathscr{O}(|A|)$.

The constraint (1.7) on the entanglement properties of many-body ground states has many important consequences in a variety of contexts. One of the most notable concerns how wavefunctions can be represented on classical computers. The small amount of entanglement in these area-law states means they can be efficiently captured using far fewer classical parameters than the dimension of the Hilbert space[3]. This allows one to make use of certain variational ansätze for ground state wavefunctions for which the area law is manifestly satisfied, e.g. matrix product states (MPS) [68, 167]. Because the total number of parameters required to specify an MPS scales linearly, rather than exponentially, in the system size, MPS wavefunctions and their generalisations are practical tools for numerically studying ground state physics, forming the basis of various numerical algorithms such as the density matrix renormalization group [237].

[2] To be precise, the statement that the entropy of a region A scales with its boundary ∂A means that there exists some finite constant α such that $S_A \leq \alpha|\partial A|$ for all choices of A.

[3] Strictly speaking, one must consider the scaling of Renyi entropies, which generalize the von Neumann entropy (1.6), to fully determine whether an efficient representation exists [196].

Although it has not always been fully appreciated in this context, the area law nature of ground state wavefunctions also plays an important rôle in topological phases of matter. In the following section, we will see that topological phases can be defined entirely in terms of the entanglement features of ground state wavefunctions, which themselves are heavily constrained by the area law.

1.2 Topology in quantum many-body systems

Phases that are governed by symmetry breaking can be identified using an order parameter: a local observable that vanishes if the relevant symmetries are preserved, and is non-zero if the symmetries are spontaneously broken. For instance, the local magnetization of a spin system is finite in the ferromagnetic phase, and is zero in the paramagnetic phase. In contrast, topological phases cannot be identified through local[4] measurements. Heuristically, this is because topological phases are based on entanglement between distant degrees of freedom, which can only be determined using non-local measurements.

The name 'topological phase of matter' derives from an analogy in mathematics, where the local (geometric) features of a manifold are compared to its global (topological) properties. In that context, a topological invariant refers to some quantity that remains unchanged when the local features of the manifold are continuously deformed. For instance, the sphere and the torus are both orientable two dimensional manifolds that are qualitatively indistinct when one considers their local geometric structure; however, their global properties can be distinguished by an integer-valued topological invariant known as the genus, which effectively counts the number of 'holes' in the surface, see Figure 1.1. Any continuous deformation of either system cannot change the genus, and therefore the sphere cannot be converted to the torus without some discontinuous process, such as 'tearing' the manifold.

As a field of mathematics, the scope of topology is not limited to conventional geometric objects, and can be applied to any structure in which the notion of continuous deformations can be defined. The mathematical objects that are used to describe physical systems can therefore be studied from the perspective of topology. In identifying quantum phases of matter at zero temperature[5], one can look for topological invariants that characterize properties of the many-body ground state wavefunction $|\Psi\rangle$. By their topological nature, these invariants will

[4] This statement of course requires a strict definition of what constitutes as a 'local' measurement. For our purposes, we ask that the observable have support on some simply connected spatial region with a fixed finite size, however the statement may hold under an even more general definition [119].

[5] The reference to ground states in this thesis is strictly only relevant at zero temperature; however, the existence of a bulk gap E_g means that for temperatures $0 \leq T \ll E_g$, a description of the system in terms of a ground state is accurate, with corrections scaling as $e^{-E_g/T}$.

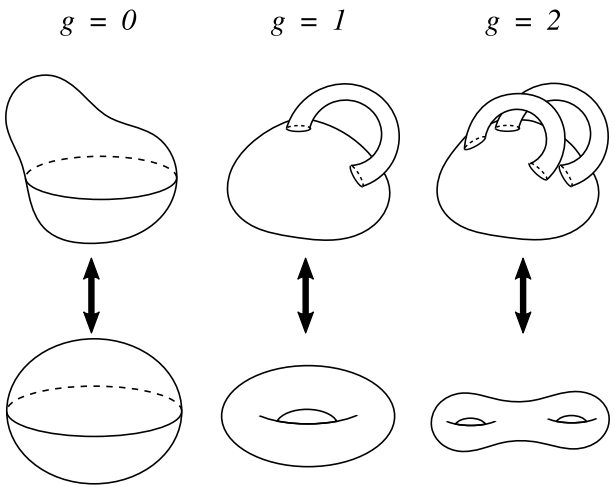

Fig. 1.1 Illustration of the topological properties of two-dimensional closed orientable manifolds. Within the space of such manifolds, one can identify topologically disconnected components, defined such that manifolds belonging to different components cannot be continuously deformed from one to the other. Each component corresponds to a different value of the genus g, which counts how many 'holes' there are in the embeddings drawn here.

remain unchanged when the physical system is continuously deformed (in a manner which we will make precise). Therefore, if a given invariant differs in its value for two quantum many-body systems, then they cannot be converted from one to the other without some discontinuous process. This allows us to associate phases of matter with each possible value of the topological invariant, separated by phase transitions across which the global properties of $|\Psi\rangle$ change discontinuously. These topological properties are intimately connected to the entanglement structures of the ground state wavefunction, as we will describe in Section 1.2.1.

Remarkably, in many cases one finds that the topological invariants used to describe quantum systems are directly related to simple, experimentally accessible observables. The archetypical example is the integer quantum Hall effect, wherein the transverse conductivity of a two-dimensional electron gas is found to be directly related to a topological invariant known as the Chern number (Ch_1) through the following 'TKNN' formula named after the authors of Ref. [212]

$$\sigma_{xy} = \frac{e^2}{2\pi\hbar}\mathrm{Ch}_1. \tag{1.8}$$

The precisely quantized Hall conductance, first measured by von Klitzing et al. [124], is thus a reflection of the topological features of the wavefunction describing the electrons. Rather generally, the entanglement properties of topological systems give rise to many striking phenomena that can be directly observed, as we will review in Section 1.2.3.

1.2.1 Defining topological phases in terms of entanglement

In the spirit of Landau, a key aim in the study of phases of matter is to develop a systematic classification of the topological phases that can arise in nature, providing the means to identify new phases and discover connections between them. To make progress in this direction, it is helpful to have a more precise definition of a topological phase of matter. Indeed while they are all by definition 'not symmetry breaking phases,' the phenomena associated with different topological phases can vary. For instance, a given phase may or may not possess gapless edge modes [232], Abelian and non-Abelian anyons [129, 152], ground state degeneracies [235], surface topological order [222], etc.

In the last decade, a unifying framework for describing a wide variety of topological phases has emerged for this purpose. Central to this understanding is a definition of a *gapped quantum phase of matter* that is based on the entanglement properties of many-body ground states, which we have seen are a special class of wavefunction. While several studies have identified connections between entanglement and topology, one of the first complete pictures was provided by Chen et al. [38], who also recognised the rôle of symmetries in the phase structure of gapped systems. Within their construction, topological phases with markedly different properties – such as free-fermion topological insulators [120] and strongly interacting bosonic SPTs [172] – can be understood on an equal footing. Here we briefly review the framework developed in Ref. [38] used to define topological phases in equilibrium.

As outlined above, we understand topological phases to be associated with the existence of topological invariants that describe the many-body ground state wavefunction. From a mathematical viewpoint, topological invariants pertaining to a particular object can only be defined once one specifies the space to which the object of interest belongs[6] (e.g. the genus is only defined for closed orientable two-dimensional manifolds). One can identify components of this space that are disconnected, in the sense that objects in one component cannot be continuously deformed into objects in another. In this picture, a topological invariant is some quantity whose value depends on which component the object under consideration belongs

[6] Even more formally, one must specify exactly what counts as 'continuous' when moving around this space. In physics, there is usually a natural way to define the allowed continuous deformations.

to. For instance, each disconnected component of the space of two-dimensional manifolds can be associated with a given value of the genus (see Figure 1.1).

A wavefunction of course belongs to the appropriate Hilbert space, which has very simple topological properties. Specifically, any wavefunction can be continuously deformed into any other wavefunction, e.g. by linearly interpolating between the two. Thus there is no way in which we can construct a topological invariant that is well-defined for an arbitrary wavefunction. However, in Section 1.1.2, we saw that ground state wavefunctions of gapped Hamiltonians satisfy an area law. The space of area-law states is much more complex than the full Hilbert space, and may feature disconnected components. Because of this, there may exist ground states that cannot be continuously connected without violating the area law at some point along the deformation. A path between these two states necessarily involves passing through some state that is not the ground state of a gapped Hamiltonian, which represents a quantum phase transition. It is therefore useful to define the following notion of a gapped phase of matter (assuming the absence of symmetries) [94, 38]

Definition 1 (Gapped quantum phases without symmetries) *Two many-body wavefunctions $|\Psi_1\rangle$ and $|\Psi_2\rangle$ that are the ground states of local gapped Hamiltonians $\hat{H}_1$ and $\hat{H}_2$ (therefore having area-law entanglement) belong to the same phase if and only if there is a continuous path of local Hamiltonians connecting $\hat{H}_1$ to $\hat{H}_2$ along which the gap remains open.*

Because the above does not assume the presence of any symmetries, the phases that arise under this definition cannot be symmetry-breaking, and are therefore all topological phases, by definition. Generally, one will be able to define a topological invariant that distinguishes different gapped phases, just as the genus distinguishes manifolds that cannot be continuously connected.

We say that two states belonging to the same phase are adiabatically connected, since the above procedure of continuously varying the Hamiltonian could be done in real time, provided the rate of change is sufficiently slow so as to keep the system in the ground state [94]. Systems in equilibrium that are probed on timescales much longer than the inverse bulk gap will remain within this subset of states, and therefore exhibit universal phenomenology characteristic of the given phase. In order to change the topological properties of a system using adiabatic deformation, one must pass through a critical point where the gap closes.

The authors of Ref. [38] go on to define an area-law wavefunction as being *long-range entangled*[7] (LRE) if it is not in the same quantum phase as a product state in real space, or more generally some reference state with no ground state entanglement. Conversely,

[7] One should not confuse long-range entanglement with the absence of an area law.

short-ranged entangled (SRE) states can be connected to product states. Thus, although the above definition constitutes an equivalence relation between wavefunctions, there is one equivalence class which is singled out as being the set of 'trivial' states, and these are referred to as SRE. Examples of long-ranged entangled states are the ground states of integer and fractional quantum Hall systems[8].

This definition of topological phases is useful when the only constraint imposed on the system in question is the existence of a bulk gap, so that the area law holds. However, in many physical systems, symmetries naturally arise which also constrain the wavefunctions that are accessible. One can ask for a different definition of topological phases that accounts for the presence of symmetries.

We know from Landau's paradigm that symmetries allow for conventional phases wherein the ground states spontaneously break the symmetries of the Hamiltonian. However, it turns out that there also exist quantum phases of matter that do not break any symmetries. To identify new phases that cannot be characterized by either spontaneous symmetry breaking or long-range entanglement, one can consider the space of states that are SRE and respect all the symmetries of the Hamiltonian, and perform the same topological analysis as above to identify new phases. These *symmetry-protected topological phases* (SPTs) are based on the following definition [38]

Definition 2 (Symmetry-Protected Topological Phases) *Two short-range entangled many-body wavefunctions $|\Psi_1\rangle$ and $|\Psi_2\rangle$ that are the ground states of local gapped Hamiltonians $\hat{H}_1$ and $\hat{H}_2$ and do not spontaneously break any symmetries belong to the same symmetry-protected topological phase if and only if there is a continuous path of local Hamiltonians connecting $\hat{H}_1$ to $\hat{H}_2$ along which the gap remains open and all symmetries are preserved throughout.*

Wavefunctions belonging to different SPT phases can be adiabatically deformed from one to the other (since they are SRE), but in this process one must break at least some of the protecting symmetries. If the symmetries are preserved throughout the adiabatic procedure, then one must pass through a quantum phase transition where the gap closes in order to move between such states.

Equilibrium SPT phases are a useful concept for systems that are probed on slow timescales, and possess symmetries that cannot be 'easily' broken, i.e. their presence does not require fine-tuning. Experimentally relevant examples include topological insulators in two and three dimensions [111, 110, 76, 128, 97], which are protected by time-reversal symmetry, and topological crystalline insulators [74, 98, 207], which are protected by space group

[8] Note that long-range entanglement does not necessitate the presence of anyons, and there is thus an alternative definition of topological order associated with excitations possessing fractional statistics [121].

symmetries. We emphasise that SPTs are intrinsically quantum phases: wavefunctions that have no entanglement ('classical states') cannot have non-trivial SPT order [38]. Different patterns of long-range entanglement, symmetry-breaking order, and symmetry-respecting order can be combined to generate even more phases of matter. However, for the purposes of this thesis we will focus primarily on SPTs, which make up the majority of the current experimentally accessible topological phases.

With this rigorous definition in hand, the task of determining the complete set of topological phases for a particular type of system is reduced to a mathematical problem, depending on the spatial dimension, particle statistics, symmetries, etc. Various different methods to explicitly compute this classification of topological phases have been developed, which apply in different contexts. In this dissertation, we will refer mainly to SPTs composed of either weakly interacting fermions, or strongly interacting bosons. The theoretical techniques used to classify these classes of systems will be reviewed in Chapter 3.

Before describing some of the physical properties of topological systems, we wish to point out that gapped quantum systems are by no means the only context in which topological phenomena are known to arise in physics. For example, one can assign meaningful topological invariants to certain gapless systems, including both electronic [11] and photonic[9] [165] systems, and even to some classical systems [101]. In all of these cases, the connections to topology are very much in the same spirit: one looks for properties of the system that do not change as it is continuously varied. However, these notions of topology should be thought of as distinct from the definitions given here, since they do not pertain to a *wavefunction*, but rather describe some dynamical property of the system's excitations. That is, there is no actual (symmetry-protected) topological order present in these systems. In this thesis, we refer exclusively to topological phases of gapped quantum systems. Although it is likely that many of the insights here may prove equally useful to these other contexts, our results cannot necessarily be immediately transferred, and will require more careful analysis.

1.2.2 Bulk-boundary correspondence

Formally, the topological entanglement properties discussed in the previous sections are only well-defined sufficiently[10] far within the bulk of a thermodynamically large system.

[9] The gaplessness of photonic systems, which are well-described by non-interacting bosons, should not be confused with a photonic band gap, which is a range of frequencies in which the *single-particle* Hamiltonian has no eigenvalues. Here, the gap corresponds to the difference in energy between the two lowest *many-body* states.

[10] The existence of a bulk gap ensures that the system possesses a finite correlation length ξ; thus one expects boundary effects to decay with the distance x from the edges as $e^{-x/\xi}$. In gapless systems, one expects an algebraic dependence on x.

Therefore, in a system with open boundaries, there is no *a priori* reason to expect these topological considerations to bear much relevance to the physics near the edge. However, quite generally there turns out to be a fundamental relationship between the topological properties of the bulk of a system and the dynamics near its boundary. This connection has been appreciated since the early days of the integer and fractional quantum Hall effects [92], and is referred to as the bulk-boundary correspondence.

In gapped systems, one can develop a rough intuition for the bulk-boundary correspondence by considering a related scenario: the coupling of a topologically non-trivial and a topologically trivial system at some interface of codimension 1. One can ask how the gap to excitations varies in space. Far away from the interface in both directions, there must be a finite energy cost for excitations, due to the two phases being gapped in the bulk. However, as one approaches the divide from a particular side, the system must somehow adapt such that its topological properties change across the interface. To do so is impossible without either spontaneously breaking the protecting symmetries, or closing the gap to excitations at some point near the boundary.

This argument can similarly be applied to the case where the system is terminated (rather than coupled to a trivial system) to show that the boundary of a topological system must either exhibit spontaneous symmetry breaking, or possess gapless degrees of freedom[11]. In this thesis, we will generally consider scenarios where the latter occurs. For a more rigorous discussion of the relationship between bulk and boundary, see e.g. Ref. [65].

Here we briefly present the basic low-energy theories that describe some specific topological boundary modes which will be studied later in this thesis. The first is a spatially localised (zero-dimensional) edge mode of a one-dimensional superconducting system, while the remainder are extended one-dimensional channels at the boundaries of two-dimensional topological systems.

Majorana bound states

The edge modes of $d = 1$ dimensional SPTs are zero-dimensional (i.e. pointlike) collective degrees of freedom pinned to zero energy. The origin and robustness of these 'zero modes' can be understood using simple toy models, such as the one-dimensional superconducting chain first proposed by Kitaev [122]. In this model, spinless fermions $\hat{c}_j$, $\hat{c}_j^\dagger$ living on lattice

[11] An alternative scenario emerges in three-dimensional systems, where the surface can develop symmetry-preserving topological order [222], but we do not discuss such cases in this thesis.

sites j can be described in terms of a basis of Majorana fermions

$$\begin{aligned}\hat{\gamma}_j^A &:= \hat{c}_j + \hat{c}_j^\dagger \\ \hat{\gamma}_j^B &:= -\mathrm{i}\left(\hat{c}_j - \hat{c}_j^\dagger\right)\end{aligned} \tag{1.9}$$

which are Hermitian $(\hat{\gamma}_j^\alpha)^\dagger = \hat{\gamma}_j^\alpha$, and obey the anticommutation relations $\{\hat{\gamma}_j^\alpha, \hat{\gamma}_k^\beta\} = 2\delta_{jk}\delta^{\alpha\beta}$. Consider the following Hamiltonian, with open boundary conditions

$$\hat{H}_{\text{Kitaev}} = \mathrm{i}J \sum_{j=1}^{N-1} \hat{\gamma}_j^B \hat{\gamma}_{j+1}^A \tag{1.10}$$

where N is the number of sites in the chain. In the original fermion basis, the above is a sum of a hopping term $J(\hat{c}_j^\dagger \hat{c}_{j+1} + \text{h.c.})$ and a nearest-neighbour p-wave superconducting pairing $J(\hat{c}_j^\dagger \hat{c}_{j+1}^\dagger + \text{h.c.})$ with equal weight.

The terms in the above Hamiltonian are illustrated in Figure 1.2 for a chain of length 4. The Majorana operators that appear in the Hamiltonian (1.10) are gapped by an energy J, but at each end of the chain there is one Majorana operator that is decoupled from the bulk. In the limit of a long chain, these two decoupled operators have support on spatially disconnected regions, and thus constitute a non-local Dirac fermion $\hat{d} = \hat{\gamma}_1^A + \mathrm{i}\hat{\gamma}_N^B$ which costs zero energy to excite. The two degenerate edge modes corresponding to the fermionic mode $\hat{d}$ being occupied or unoccupied have opposite fermion parity, and so transitions between them are forbidden as long as the fermion parity of the system is conserved, which it must be in an isolated system. Moreover, the edge mode can only become gapped via a non-local Hamiltonian term $\propto \hat{d}^\dagger \hat{d}$. Therefore, when one adiabatically moves away from the ideal limit (1.10) while preserving locality, the zero energy modes must persist (up to corrections that decay exponentially with the length of the chain [122]). In work not detailed in this thesis, I have investigated how these Majorana modes remain robust in the presence of both spatial disorder and interactions [149].

The protected nature of these non-local Majorana fermion modes in principle gives them the potential to store and manipulate quantum information non-locally over long times. For this reason, topological superconductors, and indeed various other topological phases, have been proposed as candidates for hardware in quantum computation architectures [160, 166]. The intrinsic resilience of these modes against any local Hamiltonian perturbations which may be present in realistic experiments has attracted a great deal of attention in this regard from researchers in physics, mathematics, and computer science [184].

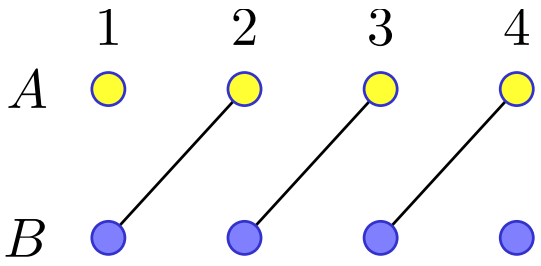

Fig. 1.2 Illustration of the Kitaev chain Hamiltonian (1.10) for a chain of length $N = 4$. Each circle represents a particular Majorana operator, and lines between them represent the bilinear couplings $iJ\hat{\gamma}_j^B\hat{\gamma}_{j+1}^A$. At each end of the chain, a single Majorana operator ($\hat{\gamma}_1^A$ or $\hat{\gamma}_N^B$) is decoupled from all other degrees of freedom. Together, these two Majorana fermions form a topological zero mode $\hat{d} = \hat{\gamma}_1^A + i\hat{\gamma}_N^B$, resulting in degenerate ground states.

It is important to recognise the implicit assumptions that are made when we use the above arguments to claim that these modes offer 'robust' storage of quantum information. What is certainly proven is that the system Hamiltonian $\hat{H}$ possesses degenerate ground states (up to exponentially small corrections) in some finite volume of parameter space wherein the system is in a topological phase. If the system is indeed governed by a static Hamiltonian $\hat{H}$, then a qubit encoded in the ground state subspace will remain undisturbed for long times, even if the desired Hamiltonian is not realized perfectly. However, this analysis gives little indication of what will happen if the system in question is driven out of equilibrium, or coupled to a macroscopic environment. These matters will be addressed in detail throughout this thesis.

Chiral and helical edge channels

In spatial dimensions $d > 1$, topological edge states typically form a gapless $(d-1)$-dimensional continuum of modes, which cannot be gapped out as long as the relevant symmetries are preserved. Perhaps the simplest spatially extended edge mode arises in integer quantum Hall systems at filling factor $\nu \in \mathbb{N}$. The edge modes are composed of ν distinct species of chiral fermions each with a dispersion $\varepsilon(k) \sim v_F k$, where k is a quasi-momentum along the direction of the boundary (see Fig. 1.3). An electron placed at the Fermi level will be energetically constrained to stay within the boundary, since the bulk is gapped[12]. Due to the chiral nature of the edge modes, electrons can only propagate in one direction, determined by the orientation of the magnetic field. Since there are no backward

[12]More generally, the bulk need only possess a *mobility gap*, i.e. a finite energy gap to the nearest eigenstates that are not spatially localized. For example, in quantum Hall systems, quenched disorder renders almost all of the bulk modes immobile with the exception of delocalized states at specific energies, and so at generic filling the bulk is insulating, despite the presence of in-gap bulk modes [116, 105].

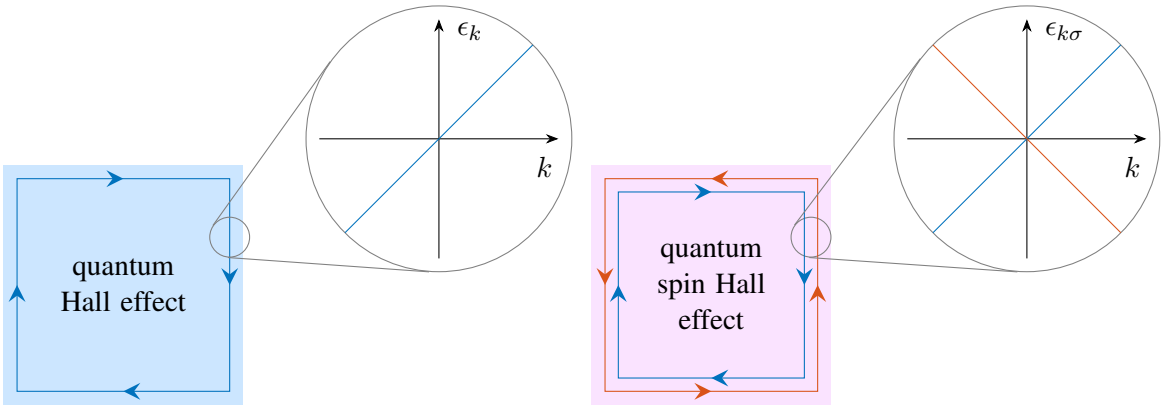

Fig. 1.3 Illustration of the chiral and helical edge modes of quantum Hall and quantum spin Hall insulators, respectively. The systems are gapped in the bulk, and possess one-dimensional gapless boundary modes at their boundary. In the quantum Hall effect, the edge channels are chiral, propagating in one direction only. In the quantum spin Hall effect, the edge channels are helical, propagating in a direction determined by the spin of the electron (or some other internal quantum number) [Eq. (1.11)]. The insets show the low-energy form of the dispersion relation for the edge modes.

moving modes to which the electron can scatter, transport is dissipationless, leading to a quantized edge conductivity of $\sigma_{xy} = N_s \nu e^2/h$, where N_s is the spin degeneracy. Indeed the quantized Hall conductivity associated with the bulk topological invariant [Eq. (1.8)] can be understood as being mediated by these edge channels [92]. The number of channels is related to the bulk topological invariant as $\nu = |\mathrm{Ch}_1|$ under this correspondence, and the direction of propagation is determined by the sign of Ch_1.

Another well-known type of topological edge mode arises in two-dimensional topological insulators protected by time-reversal symmetry, also referred to as quantum spin Hall (QSH) systems [111, 110, 128]. The simplest way to theoretically construct a nontrivial quantum spin Hall system is as follows: Let the system be comprised of two species of fermion (usually associated with opposite electron spin states $\uparrow, \downarrow$) which do not mutually interact, so that the Hamiltonian is $\hat{H} = \hat{H}_\uparrow + \hat{H}_\downarrow$. Let one of the species (say $\uparrow$) be in a non-trivial quantum Hall phase with $\nu = 1$. Then let the Hamiltonian for the opposite species be given by the time-reversed conjugate of this quantum Hall state, i.e. $\hat{H}_\downarrow = \hat{T}\hat{H}_\uparrow\hat{T}^{-1}$, where $\hat{T}$ is the time-reversal operator for a single species of fermion. Since momenta are flipped under time-reversal, the chiral edge modes for each species propagate in opposite directions; thus as a pair, they constitute a *helical* edge channel [241], wherein the 'spin' is locked to the

direction of momentum, see Fig.1.3. The Hamiltonian describing this edge theory is

$$\hat{H} = \sum_{\sigma=\pm 1} \sigma v_F \int \mathrm{d}x\, \hat{\psi}_\sigma^\dagger \mathrm{i}\partial_x \hat{\psi}_\sigma, \tag{1.11}$$

where the spin quantum numbers $\sigma = \pm 1$ correspond to the two spin states $\uparrow$, $\downarrow$, and $\hat{\psi}_\sigma(x)$ annihilates a fermion with spin σ at a coordinate x along the edge.

The crucial observation that makes this construction non-trivial is that these helical modes remain gapless and localised at the edges when the two systems are coupled, so long as the time-reversal symmetry of the combined system ($\hat{T}_{\mathrm{tot}} = \hat{T} \otimes \mathrm{i}\hat{\sigma}^y$, where σ^y is the second Pauli matrix in spin space) is maintained, and the bulk gap remains open. This obstruction to gapping out the edge modes reflects the fact that the system is in a non-trivial SPT phase protected by time-reversal symmetry. Away from the decoupled limit, the edge theory (1.11) will be modified, e.g. by interactions between the two spin states. However, if one is interested in low-energy properties, it is possible to develop a theory that captures the universal aspects of helical edge modes. This theory, known as the helical Luttinger liquid [241, 244], will be discussed in detail in Section 4.4.

Just as in the quantum Hall effect, these modes mediate dissipationless transport at zero temperature, which can be experimentally verified using non-local conductance measurements [183]. Alternatively, their presence can be confirmed using spectroscopic techniques, such as angle-resolved photoemission spectroscopy (ARPES), which reveal the gapless dispersion that is expected from theory [97].

1.2.3 Characteristic phenomena of topological systems

Systems belonging to non-trivial topological phases generally exhibit phenomena characteristic of the phase in question which are 'robust', i.e. the relevant effect persists when the system is perturbed in a permissible way (provided the system remains gapped, close to equilibrium, and respects the relevant symmetries). Although our discussion so far has emphasised the fundamental rôle that entanglement plays in these systems, the experimentally accessible signatures associated with these phases are often *a priori* unrelated to entanglement. Here, we discuss some of the most important effects that generally occur in topological systems at equilibrium.

Topological invariants as physical observables

We have already seen from the relation (1.8) that, in some cases, topological invariants turn out to be related to experimentally accessible quantities, such as the Hall conductance.

Identifying physical observables that are also topological invariants is a very appealing idea when it comes to designing quantum many-body systems: these quantities inherit a natural robustness to imperfections, since they cannot change when the system is deformed away from some ideal limit. This makes topological phases of matter promising candidates for many high-precision technologies. For instance, the quantized Hall conductance has now been measured to one part in 10^{10} [159], and today is utilized in the standard definition of the kilogram [226].

Many of the topological invariants that are relevant for weakly interacting fermionic phases in different spatial dimensions can also be related to other physical observables, allowing them to be directly measured. In one dimension, the relevant invariant is the Chern-Simons invariant (which we will meet in Section 2.3), and is equal to the electric polarization of the system in units of the lattice spacing times the electric charge [118]. This invariant has been directly measured in ultracold atom experiments, wherein non-interacting topological phases have been realised [12]. Similarly, in three dimensions, the magnetoelectric polarisability is determined by a topological invariant [66, 243].

In strongly correlated systems, topological invariants are not always directly related to experimentally accessible observables in this way. The closest analogy in this context is the 'string order parameter': a non-local observable whose long distance scaling can be shown to depend on the value of the relevant invariant [55, 114, 90, 171]. However, rather than directly measuring topological invariants, it is often easier to infer which topological phase the system belongs to by capturing different universal features associated with the phase in question, e.g. the low-energy properties of the edge theories discussed in the previous section.

Universal form of the entanglement spectrum

Although we have discussed the connections between entanglement and topological phases, we have not yet specified any quantitative entanglement properties that can be used to identify a particular topological phase. The entanglement entropy and entanglement spectrum, introduced in Section 1.1.1, can be used for this purpose.

For some topological phases, the scaling behaviour of the entanglement entropy S_A with the size of A can be used to probe topological order [121, 132]. Specifically, the presence of anyonic excitations can be inferred from the subleading corrections to the area law scaling (1.7). However the entanglement entropy does not contain useful information for all topological phases – for instance, SPTs do not display this effect. In general, a single number S_A is insufficient to characterise the topological phase in question.

One of the first uses of the entanglement spectrum in many-body physics was suggested by Li and Haldane [133], who used it to infer properties about fractional quantum Hall states. The entanglement spectrum of course contains much more information than the entanglement entropy, and has proved to be a useful tool for studying a wide class of topological phases of matter. In short, the gapless edge modes which one would expect at a physical boundary appear in the spectrum of reduced density operator $\hat{\rho}_A$ which are localised at the boundary of the region A, as opposed to the physical edge.

In the special case of non-interacting fermionic systems, an intuition for the connection between topology and the entanglement spectrum can be established as follows: For a non-interacting area-law ground state, the reduced density matrix can always be written as $\hat{\rho}_A = e^{-\hat{H}_E}$, where $\hat{H}_E$ (sometimes known as the entanglement Hamiltonian) is local and bilinear in fermion operators on the region A [168]. As such, the single-particle matrix that constitutes $\hat{H}_E$ can be diagonalized. One can use this to show that $\hat{H}_E$ satisfies all the same symmetries as the physical Hamiltonian, and belongs to the same SPT phase [70]. According to the bulk-boundary correspondence, the physical Hamiltonian will feature topologically protected gapless modes at its boundary. Being in the same topological phase, $\hat{H}_E$ must therefore also exhibit gapless modes at the boundary[13] of A (although the exact dispersion will generally differ from the physical Hamiltonian). Therefore, the 'low-energy' states of $\hat{H}_E$ – those that contribute the most to $\hat{\rho}_A$ – are qualitatively equivalent to the boundary theory of the SPT phase in question, allowing the phase to be identified. Rather generally, degeneracies in the entanglement spectrum signal that the wavefunction under consideration is topologically non-trivial. Note that related methods can be developed to establish an analogous connection between SPT order and the spectrum of $\hat{\rho}_A$ in strongly interacting systems [172, 39, 214].

We have seen that the entanglement properties of many-body systems in their ground state can lead to interesting topological phenomena. It is also possible to discuss the *dynamics* of these entanglement structures in systems undergoing time evolution. The relationship between entanglement dynamics and topological order is one of the key subjects of this thesis. Much is already known about the dynamics of entanglement in contexts outside of topology. As we will be making use of some of these results, we will give a brief overview of this topic in the following section.

[13] If the phase in question is protected by spatial symmetries, then the boundary of A may have to be constructed such that it respects that symmetry [74].

1.3 Dynamics of entanglement

During the mid-Twentieth Century, the main motivation for studying quantum many-body physics was to better understand solid-state systems. The extremely fast electronic relaxation times that arise therein made studying real-time dynamics experimentally unfeasible; thus, historically, theorists have largely focussed on understanding quantum many-body systems at or near equilibrium (e.g. linear response theory). However, the past few decades have seen advances in experimental techniques which make it possible to study coherent quantum many-body physics far from equilibrium. As well as improvements in probing electronic systems on ultrafast timescales [192], there are now many new experimental platforms which possess unprecedented degrees of control and coherence over the constituent particles, wherein real-time dynamics can be directly observed. These experiments, such as those based on ultracold atoms [88, 213, 42], trapped ions [180, 106], and Rydberg atoms [19, 89], have brought into focus new theoretical questions regarding non-equilibrium dynamics which were previously regarded as having limited experimental relevance.

Although the departure from equilibrium increases the complexity of the physics that emerges, it is still possible to identify phenomena that are universal, in that they are displayed by a wide range of systems, rather than being specific to a particular scenario. A particular focus has been on the dynamics of entanglement as a system evolves in time, which has consequences for the way in which isolated quantum systems thermalise. In this section, we review aspects of non-equilibrium dynamics in both closed and open many-body quantum systems, and the universal features they exhibit when driven far from equilibrium, with reference to entanglement properties.

1.3.1 Evolution of entanglement and quantum thermalisation

In an isolated quantum system, time evolution is generated by unitary operators. Specifically, if the density operator $\hat{\rho}(0)$ describes the state of a system at $t = 0$, then at a later time t the density matrix is

$$\hat{\rho}(t) = \hat{U}(t,0)\hat{\rho}(0)\hat{U}(t,0)^{\dagger} \tag{1.12}$$

where the time evolution operator $\hat{U}(t_2,t_1)$ has a formal expression

$$\hat{U}(t_2,t_1) = \mathscr{T} \exp\left(-\mathrm{i}\int_{t_1}^{t_2} \mathrm{d}t' \hat{H}(t')\right), \tag{1.13}$$

$\hat{H}(t)$ is the (possibly time-dependent) Hamiltonian, and $\mathscr{T}$ denotes time-ordering. Since $\hat{U}(t_2,t_1)$ is unitary, the spectrum of $\hat{\rho}(t)$ remains constant in time. For example, if $\hat{\rho}(0)$ describes a pure state, then $\hat{\rho}(t)$ is also pure. More generally, the von Neumann entropy of $\hat{\rho}(t)$ [Eq. (1.6)] is unchanged under unitary time evolution.

The constancy of the von Neumann entropy implies that if we start with some small uncertainty in the initial state (small but finite entropy), then this uncertainty remains of the same magnitude for all time. In contrsast, in classical chaotic systems, two initial states that are close by in phase space quickly diverge under time evolution, leading to amplification of uncertainty in the positions and momenta of the constituent particles, and eventually thermalisation. Our intuition suggests (and experiments can verify) that a generic isolated quantum system should also thermalise under its own dynamics; however it is clear from the above that the relevant mechanism cannot be dynamical chaos as defined in a classical sense.

These matters were already apparent to von Neumann in 1929 [227, 82]. His solution was to recognise that we should focus not on the full density matrix, but rather on the outcome of a set of privileged 'physical' operators which are accessible to the experimentalist. We must accept that quantum statistical mechanics can only be successful insofar as measurements of these observables at late times should agree with the predictions of thermodynamic ensembles. There may exist some complicated and highly non-local observables that disagree, but we dismiss these as being inaccessible.

For instance, we could consider only measurements of operators with support in some small spatial region A. Full information about the outcome of these measurements is contained within the (time-dependent) reduced density operator $\hat{\rho}_A(t) \coloneqq \mathrm{Tr}_B\,\hat{\rho}(t)$, defined in analogy to (1.4). Therefore, if the system thermalises then we expect that this reduced density operator will agree with the predictions of statistical mechanics, that is

$$\hat{\rho}_A(t\to\infty) = \mathrm{Tr}_B\,\hat{\rho}_{\text{therm.}} \tag{1.14}$$

where $\hat{\rho}_{\text{therm.}}$ is the state corresponding to the appropriate thermodynamic ensemble. The density operator $\hat{\rho}_{\text{therm.}}$ represents a classical statistical distribution in which all global states that are compatible with any conservation laws are equally likely. Accordingly, $\mathrm{Tr}_B\,\hat{\rho}_{\text{therm.}}$ will have a high entropy. In contrast, the entropy associated with the reduced density matrix $\hat{\rho}_A(t\to\infty)$ cannot be due to classical uncertainty about the state of the system, since $\hat{\rho}(t)$ is known to the same precision as the initial state. Rather, the reduced density matrix is mixed due to the presence of entanglement between A and B. We see that for a quantum system to thermalise under its own dynamics, entanglement must be generated between different degrees of freedom.

Much effort has gone into understanding the precise conditions under which quantum thermalisation occurs (see e.g. Refs. [56, 201, 181, 170, 47]). Theoretical and experimental evidence indicates that the vast majority of many-body[14] systems do indeed thermalise, with some notable exceptions (e.g. many-body localized systems). This ubiquity of thermalisation can be thought of as being due to a general trend by which initially unentangled degrees of freedom tend towards high-entanglement states as they interact [173]. The opposite process, i.e. disentangling under unitary dynamics, must be much less likely to occur, otherwise the inverse of thermalisation would be possible. This highlights the existence of an 'arrow of time' in quantum dynamics, despite the lack of any breaking of microscopic time-reversal symmetry.

This perspective also sheds light on the more traditionally relevant scenario where a quantum system is in contact with an environment. If the system is initialized in a state that is unentangled with its environment, then over time entanglement will be established, and so the entropy of the system density matrix $\hat{\rho}(t)$ will increase irreversibly. If the composite system-plus-environment thermalises, then the system density matrix obeys $\hat{\rho}(t \to \infty) = \hat{\rho}_{\text{therm.}}$ in full, i.e. we do not have to restrict ourselves to small subsystems. Since the entropy of $\hat{\rho}(t)$ changes in time, open systems cannot be governed by unitary dynamics of the form (1.12). Indeed in general, the coupling between system and environment facilitates processes that would be forbidden in an isolated system. In Chapter 4, we will see that these non-unitary processes can lead not only to entanglement entropy production, but also to effects that are detrimental to certain topological systems.

1.3.2 Lieb-Robinson bounds

We see from the previous section that quantum systems thermalize through the spreading of entanglement. A natural question that arises is: how fast can this occur? It turns out that there are certain bounds on how entanglement and correlations (the two of which are closely related [20]) spread in a system, which we briefly survey here.

The unitary dynamics of an isolated system (1.12) can alternatively be treated within the Heisenberg picture, where one considers the time evolution of observables. A Hermitian operator $\hat{A}$ evolves according to the Heisenberg equation of motion

$$\frac{\mathrm{d}}{\mathrm{d}t}\hat{A}(t) = \mathrm{i}[\hat{H}(t), \hat{A}(t)], \tag{1.15}$$

[14] Unlike in classical physics, few-body quantum systems cannot thermalise in the sense defined here. This is because in such systems, there is no longer a meaningful distinction between local (accessible) and non-local (inaccessible) measurements.

where $\hat{H}(t)$ is the (possibly time-dependent) Hamiltonian. In a seminal paper [134], Lieb and Robinson considered the following quantity

$$C_{AB}(t) := \left\| [\hat{A}(t), \hat{B}(0)] \right\|, \tag{1.16}$$

where $\|\cdot\|$ denotes the operator norm, and $\hat{A}$ and $\hat{B}$ are local commuting observables in finite, non-overlapping spatial regions A and B, respectively. A physical interpretation of $C_{AB}(t)$ can be developed as follows: One can think of the action of $\hat{B}(0)$ as a perturbation in the locality of B. At time $t = 0$, this perturbation does not affect the degrees of freedom in A, since they are spatially separated. As the system propagates in time, the influence of the initial action of $\hat{B}(0)$ may spread out. Past some time, the effect of the perturbation may be 'felt' by the degrees of freedom within A, in which case $\hat{A}(t)$ and $\hat{B}(0)$ will fail to commute. Thus, $C_{AB}(t) > 0$ indicates that the initial perturbation at B has propagated to A within a time t. In Ref. [134], it was shown that as long as $\hat{H}$ (here assumed to be time-independent) is local, $C_{AB}(t)$ satisfies a bound

$$C_{AB}(t) \leq a \exp\left(-c[x_{AB} - v_{LR}t]\right) \tag{1.17}$$

for some $a, c, v_{LR} > 0$, where x_{AB} is the minimum distance between two degrees of freedom in A and B. The quantity v_{LR} is known as the Lieb-Robinson (LR) velocity, and depends on the microscopic details of the Hamiltonian. The front $x = v_{LR}t$ is often referred to as a 'light cone' for unitary dynamics, within which operators are appreciably causally related.

The LR bound is tight for a surprisingly wide range of systems: a light cone that propagates with a constant finite velocity is indeed often observed. There are some notable exceptions to this, the most commonly discussed of which are localized systems. In non-interacting Anderson localized systems, the light cone does not spread beyond a fixed distance, and in many-body localized systems, the light cone spreads out logarithmically slowly $x \propto \log t$ [100, 67, 41]. During my PhD I have investigated aspects of correlation spreading in localized systems [150], using a quantity related to $C_{AB}(t)$ known as the out-of-time-order correlator; however I will not discuss that work in this thesis.

Although the LR bound (1.17) only makes reference to the specific quantity (1.16), it has far-reaching consequences for systems both in and out of equilibrium – in fact the area law for ground states follows from this bound [93]. It can also be used to bound how fast correlations [i.e. expectation values of the form $\langle\Psi|\hat{A}(t)\hat{B}(t)|\Psi\rangle - \langle\Psi|\hat{A}(t)|\Psi\rangle\langle\Psi|\hat{B}(t)|\Psi\rangle$] can spread under unitary evolution [20]. For the purposes of this dissertation, perhaps the most important consequence of the Lieb-Robinson bound is the implication for the generation of entanglement under unitary dynamics, which we discuss in the following.

1.3.3 Universal classes of entanglement growth

In the Schrödinger picture, the many-body wavefunction for a system far from equilibrium is time-dependent $|\Psi(t)\rangle$. Thus, one can ask how the entanglement properties of this state change in time.

The most natural quantity to consider is the evolution of entanglement entropy, where one constructs a time-dependent reduced density matrix $\hat{\rho}_A(t) = \mathrm{Tr}_B |\Psi(t)\rangle \langle\Psi(t)|$, and calculates $S(t)$ according to (1.6). This was first explored in certain exactly solvable systems, where one can obtain analytic expressions for $S(t)$, and run efficient numerical simulations [32, 43]. Naturally, the Lieb-Robinson bound puts an upper limit on how fast this entropy can grow: the existence of a linear light cone implies that $S(t)$ must be less than some value that grows linearly in time [20, 62, 216]. Rather commonly, it is observed that $S(t)$ does indeed have a linear dependence bound for all time in the limit of A being infinitely large (although the corresponding rate of entropy growth may be less than that allowed by the LR bound [157]). For a finite size subsystem A, then there exists a time beyond which $\hat{\rho}_A(t)$ becomes maximally entangled[15] with B, at which point the entanglement saturates.

A simple explanation for this universal form of entanglement growth for a quantum quench (i.e. when $\hat{H}(t) = \hat{H}$ is time-independent) in an exactly solvable system was first presented in Ref. [32], which was later shown to hold for more general integrable systems [2]. The initial state is generically highly excited with respect to $\hat{H}$, and will feature some finite density of quasiparticles, which are long-lived thanks to the integrability of $\hat{H}$. If the initial state is a product state, then these quasiparticles are only strictly locally entangled. Under time evolution, pairs of quasiparticles that began on the same site can propagate in opposite directions with some maximum speed, which will be bounded by the Lieb-Robinson velocity $v \leq v_{LR}$. At time t, if a given entangled pair has one quasiparticle in A, and one in B, then it will contribute to $S(t)$ by some amount (which may be random with a fixed mean s_0). Because pairs can only move apart at a finite velocity, the number of such pairs grow linearly in time, until $v_{LR}t = L_A$ (where L_A is the length of the subsystem A), when this number saturates. On average, $S(t)$ will be equal to the number of these pairs times the mean amount of entanglement that they contribute s_0, which agrees with the above universal form.

Although these arguments rely on the existence of long-lived quasiparticles, $S(t)$ displays the same qualitative behaviour in a variety of systems which are strongly correlated [117, 96]. It is believed that this form of entanglement growth applies to systems undergoing a wide range of unitary (not necessary Hamiltonian) evolution, as demonstrated by certain toy

[15] By maximally entangled, we mean that $S_A(t)$ takes its maximal value subject to any constraints that may be imposed by conservation laws [182]. This may be less than the absolute maximum of entanglement that an arbitrary reduced density matrix could possess.

'random unitary circuit' models [157, 35, 224]. Again, localized systems are exceptions to this rule, with entanglement that either saturates quickly, or grows logarithmically in time [251, 14], depending on the absence or presence of interactions.

The limits placed on the rate of entropy growth by the Lieb-Robinson bound implies that there is a limit to how fast quantum thermalization [Eq. (1.14)] can occur. It also justifies the use of certain numerical algorithms used to treat dynamics over short times, e.g. time-dependent DMRG [221, 50]. The LR bound and the associated limit of entanglement growth will prove crucial in our study of the topological properties of isolated systems far from equilibrium.

1.4 Topology in non-equilibrium settings

As well as providing access to new non-equilibrium regimes of many-body physics, the new experimental platforms described in the previous section also provide a new platform for realising topological phases of matter. The unprecedented degree of control over the interactions between the underlying degrees of freedom makes these experiments ideal settings for realising certain topological phases that are difficult to synthesise in traditional solid-state experiments [80, 45]. Recent successes include the realisation of one- and two-dimensional non-interacting topological phases using ultracold atoms in optical lattices [12, 103, 1], as well as an interacting SPT phase in a 1D array of Rydberg atoms [53].

The realisation of topological phases in systems with long coherence naturally raises questions regarding the rôle that topology plays in the coherent dynamics of closed and open quantum systems far from equilibrium. Here we briefly review recent work in this direction.

1.4.1 Floquet topological insulators

One of the simplest ways in which a system can be forced out of equilibrium is by applying periodic driving. In an isolated system, this situation is described by a Hamiltonian that repeats itself exactly after a period T:

$$\hat{H}(t) = \hat{H}(t+T) \qquad\qquad t \in [0,T) \tag{1.18}$$

In a generic system, the dynamics resulting from this drive will not be periodic; rather, the system will eventually heat to infinite temperature due to the provision of an unbounded amount of energy by the drive [48, 130]. However, if the system is prepared in a Floquet eigenstate (an eigenstate of the time evolution operator $\hat{U}(T,0)$ over one period), then the

wavefunction will also oscillate with the same period. Alternatively, if the system is many-body localized, then the heating to infinite temperature will not occur, and periodic dynamics will eventually emerge [115].

This periodic dynamics can be topologically characterized in a manner similar to the study of systems in equilibrium. A simple approach is to look at the 'Floquet Hamiltonian' $\hat{H}_F \coloneqq (\mathrm{i}/T)\ln\hat{U}(T,0)$ and ask which equilibrium phase it belongs to [162]. However, it turns out that periodically driven systems can exhibit topological phases that do not have an undriven analogue, related to the dynamics within a single driving period, which cannot be captured by a Floquet Hamiltonian, and thus have no equilibrium analogue [186]. There has been a great deal of progress in classifying Floquet topological phases in a way which captures these intrinsically non-equilibrium 'anomalous' phases [174, 225, 63, 185].

1.4.2 Emergent topology in quench dynamics

Another simple class of non-equilibrium protocol is a quantum quench, where one prepares an initial state $|\Psi(0)\rangle$ (usually the ground state of some initial Hamiltonian $\hat{H}^{\mathrm{i}}$), and then evolves under some other Hamiltonian $\hat{H}^{\mathrm{f}}$ which is constant in time.

Recently, there has been interest in inferring the (static) topological properties of $\hat{H}^{\mathrm{f}}$ from the resulting quench dynamics. Specifically, in non-interacting systems it has been shown that an 'emergent' type of topology arises in the trajectory of the time-dependent wavefunction $|\Psi(t)\rangle = e^{-\mathrm{i}\hat{H}^{\mathrm{f}}t}|\Psi(0)\rangle$ [229, 84, 245, 249] (as opposed to the wavefunction at some instant in time only). The topological properties of this trajectory can be measured in experiments where a given quench protocol can be run in a reproducible way, with measurements taken at different times for each run. The emergent invariants and the static invariants pertaining to $\hat{H}^{f}$ turn out to be related, which provides a new way of identifying topological phases in experiment [208, 204].

1.4.3 Topology in non-Hermitian systems

A rather different application of concepts from topology in non-equilibrium physics arises in the study of systems that are governed by non-Hermitian Hamiltonians. Although microscopically, all quantum Hamiltonians must be Hermitian, one can construct both classical and quantum systems whose effective equations of motion are governed (or at least well-approximated) by a non-Hermitian time-dependent Schrödinger equation. This includes classical photonic, mechanical, and electrical systems featuring gain or loss [151], as well as quantum systems in certain settings [51, 95, 135].

A great deal of interest in the topological properties of non-Hermitian Hamiltonians has emerged in the last few years. By borrowing ideas from the study of Hermitian systems, one can develop formalisms that can be used to systematically identify different topological phases in this context (albeit, usually at a single-particle level) [250, 113, 83]. The notion of a ground state is not always applicable to these systems, since their description in terms of a non-Hermitian Hamiltonian generally describes some transient behaviour, rather than static properties. However, the topological features of these systems are naturally reflected in their non-unitary dynamics, as can be seen, for instance, near the edges of systems, where topologically protected modes may appear [165]. Recently, I have been involved in work identifying signatures related to non-Hermitian topological invariants in certain Lindblad master equations, which govern the non-unitary time evolution of the system density matrix in open quantum systems [21] (see Section 4.1). This work will not be described in detail here; see Ref. [136].

1.4.4 Topology by dissipation

Dissipation is almost always thought of as being detrimental to the establishment of novel quantum phenomena. However, it has recently become possible to construct experiments wherein the dissipation experienced by the system of interest is explicitly controlled – a concept referred to as 'reservoir engineering' [57, 219]. This possibility turns dissipation from a hindrance into a resource, which can be used to steer quantum systems towards desired states. In particular, there has been much interest in the idea that engineered dissipation can be used to prepare topologically non-trivial wavefunctions [58, 15].

Like the aforementioned work on non-Hermitian Hamiltonians, these studies are centred around the relationships between dissipation and topology; however the phenomena of interest here are quite different. Rather than looking at topologically protected boundary excitations, the central goal of these works is to identify experimentally feasible setups where any initial state of the system $\hat{\rho}(t=0)$ will eventually reach a unique steady state that is 1) pure, and 2) topologically non-trivial [58, 15, 28]. While the first condition is certainly desirable, it generically requires fine-tuning of the system-environment interactions. Nevertheless, even if full purity cannot be achieved, it is also possible to define topological invariants that pertain to mixed states [26], although the connection to physical observables may need to be revised in this case [16].

The above discussions highlight just some of the many ways in which concepts from topology can be incorporated into various scenarios that are not governed by ground state physics. In each case, the topological properties that are identified are specific to the non-

equilibrium setting in question, and are for the most part conceptually distinct from each other. One of the broad goals of this thesis is to identify principles that can be used to understand topological aspects of quantum many-body systems in *general* non-equilibrium settings. As such, we do not expect that our results will necessarily capture all of the features described here, which pertain only to a specific type of non-equilibrium protocol, e.g. periodic driving. However, by placing our emphasis on generality, we expect that our results will be applicable to a broad range of experimentally relevant settings, giving us the means to uncover new universal phenomena.

1.5 Thesis outline

Having introduced the physical concepts and theoretical methods that will be employed throughout this thesis, we present our findings in the following three chapters. Most of the material discussed here has been published during my PhD in the following articles:

- **M. McGinley**, N. R. Cooper
  Topology of one-dimensional quantum systems out of equilibrium. Physical Review Letters **121**, 090401 (2018);

- **M. McGinley**, N. R. Cooper
  Classification of topological insulators and superconductors out of equilibrium. Physical Review B **99**, 075148 (2019);

- **M. McGinley**, N. R. Cooper
  Interacting symmetry-protected topological phases out of equilibrium. Physical Review Research **1**, 033204 (2019);

- **M. McGinley**, N. R. Cooper
  Fragility of time-reversal symmetry protected topological phases. Nature Physics (2020);

- **M. McGinley**, N. R. Cooper
  Elastic backscattering of quantum spin Hall edge modes from Coulomb interactions with non-magnetic impurities. arXiv:2009.14650.

We begin by studying the topological properties of systems far from equilibrium undergoing unitary time-evolution in Chapter 2. We introduce a non-equilibrium topological classification, defined in analogy to the familiar equilibrium classification (Definitions 1 and 2), which can be used to understand the constraints that locality, symmetry, and quantum entanglement

impose on many-body dynamics. We demonstrate that this theoretical construction can be used to predict the non-equilibrium dynamics of certain quantities relevant to topology in a wide range of non-equilibrium scenarios. In Chapter 3, we explain how the methods used to classify topological phases in equilibrium can be adapted to compute the corresponding non-equilibrium classification tables. Finally, in Chapter 4 we investigate the fate of topological phenomena when the system is coupled to external degrees of freedom. Specifically, the influence of system-environment interactions on topological edge modes are studied, and our findings can be related back to the non-equilibrium classification developed in the previous chapters. We summarise our findings in Chapter 5, and suggest potential new directions for future research.

Simultaneously, I have worked on separate projects with other collaborators, which are not described in this dissertation

- **M. McGinley**, J. Knolle, A. Nunnenkamp
  Robustness of Majorana edge modes and topological order: Exact results for the symmetric interacting Kitaev chain with disorder Physical Review B **96**, 241113 (2017);

- **M. McGinley**, A. Nunnenkamp, J. Knolle
  Slow growth of out-of-time-order correlators and entanglement entropy in integrable disordered systems Physical Review Letters, **122**, 020603 (2019);

- S. Lieu, **M. McGinley**, N. R. Cooper
  Tenfold way for quadratic Lindbladians. Physical Review Letters **124**, 040401 (2020).

Chapter 2

Unitary Dynamics

The majority of advances in the field of topological phases have come from studying systems at equilibrium, or close enough so that linear response theory applies. Indeed the formal definition of a topological phase of matter which we encountered in the introduction (Definition 1) is framed in terms of ground states of gapped Hamiltonians, and so its relevance to equilibrium physics is manifest. One of the goals of this thesis is to highlight how and when the topological features familiar from equilibrium are reflected in more general settings beyond this paradigm. This chapter is devoted to systems that remain isolated from their environment, but are driven out of equilibrium through some coherent driving, i.e. time-dependence of the Hamiltonian. As highlighted in Section 1.4, while the applicability of these non-equilibrium scenarios to traditional solid state experiments is somewhat limited, the experimental platforms that are available today make this subject an interesting and readily accessible direction for discovering new physics.

A key result of this chapter is the identification of a classification scheme for quantum many-body wavefunctions which can be used to predict the topological properties of systems as they undergo unitary time evolution. This construction is introduced and motivated in Section 2.1. In the subsequent sections, we consider some specific scenarios, and demonstrate how the non-equilibrium classification can be used to predict the behaviour of various quantities generally associated with topological phases.

2.1 Classifying topology in and out of equilibrium

Before turning to systems out of equilibrium, let us briefly discuss why the definitions of topological phases that we met in Section 1.2.1 are useful in describing equilibrium physics. First of all, it is important to note that although the Definitions 1 and 2 refer explicitly to

gapped Hamiltonians, the topological properties of a given system are in fact fully determined by the ground state wavefunction. This is perhaps best illustrated by a construction due to Chen *et al.* [38]. They showed that the family of adiabatic evolutions between area-law ground states are in one-to-one correspondence with the set of *local unitary transformations*, which are defined as unitary operations that can be sufficiently well-approximated by a local unitary circuit of finite depth. In essence, under such a process entanglement cannot be generated over arbitrarily long distances, ensuring that SRE states cannot become LRE and vice-versa. Therefore, on a formal level, the usual definition of topological phases can be thought of as an equivalence relation between many-body wavefunctions, rather than between Hamiltonians.

Importantly, when it comes to studying physical systems in equilibrium, the equivalence relation in question (namely, whether two wavefunctions can be connected through adiabatic deformation under a symmetry-respecting gapped Hamiltonian) is particularly well motivated. If one ensures that the system is not driven out of equilibrium and that all relevant symmetries are preserved at all times, then the resulting dynamics is indeed adiabatic, and so the state of the system will only explore the space of wavefunctions that make up the given (symmetry-protected) topological phase. Despite its somewhat abstract form, the present definition of topological phases is evidently pertinent to a wide range of physical scenarios in which the system is kept in equilibrium (at sufficiently low temperatures).

Here, we present an alternative topological classification scheme that is of direct relevance to systems driven out of equilibrium, rather than those in their ground state. This construction differs from its equilibrium counterpart in the equivalence relation used to distinguish many-body wavefunctions. Our new definition of topological equivalence naturally encompasses the most general processes that can occur under non-adiabatic Hamiltonian dynamics, subject to the constraints imposed by symmetries. We introduce this non-equilibrium topological classification in the following section, and provide a physical motivation of its definition. The rest of this chapter (and to a certain extent, the rest of this thesis) is then devoted to studying specific classes of non-equilibrium protocols whose dynamics reflects the content of the new classification scheme, highlighting the broad applicability of our results.

To begin, consider some isolated system driven out of equilibrium by a time-dependent Hamiltonian, which is governed by the time-dependent Schrödinger equation

$$\mathrm{i}\frac{\partial}{\partial t}\left|\Psi(t)\right\rangle = \hat{H}(t)\left|\Psi(t)\right\rangle . \tag{2.1}$$

The usual classification of topological phases is *a priori* no longer of relevance to these scenarios, since the evolution of $|\Psi(t)\rangle$ is no longer adiabatic. Indeed in a generic non-equilibrium scenario, the wavefunction explores the space of states accessible under unitary time evolution, compared to equilibrium scenarios where the wavefunction is constrained to stay in the ground state of the instantaneous Hamiltonian. Generally, over arbitrarily long times, the wavefunction will reach all (normalized) states in the Hilbert space due to the ergodicity of dynamics[1].

We saw before that wavefunctions belonging to different quantum phases cannot be interconnected under adiabatic dynamics, i.e. as long as the system remains in equilibrium. However, we see here that all states in the Hilbert space are accessible through non-equilibrium unitary dynamics in the long-time limit. Because the Hilbert space is simply connected, it is impossible to construct a topological invariant that is well-defined for all wavefunctions. We might conclude that topology plays no significant rôle in the dynamics of systems far from equilibrium.

However, let us consider the process by which an area-law wavefunctions $|\Psi_1\rangle$ can evolve into another area-law wavefunction $|\Psi_2\rangle$ under unitary dynamics. A formal expression for the state of the system at intermediate times is given by the solution of (2.1)

$$\begin{aligned} |\Psi(t)\rangle &= \hat{U}(t,0)\,|\Psi_1\rangle\,, \\ \text{where } \hat{U}(t_2,t_1) &:= \mathscr{T}\exp\left(-\mathrm{i}\int_{t_1}^{t_2}\mathrm{d}t'\hat{H}(t')\right). \end{aligned} \tag{2.2}$$

Here, $\mathscr{T}$ is the time-ordering operation. We choose the Hamiltonian $\hat{H}(t')$ such that $|\Psi(t_f)\rangle = |\Psi_2\rangle$ for some final time t_f.

We start with the simpler scenario where no symmetries are required, i.e. the phase is LRE. For some finite time $0 < t < t_f$, we ask about the entanglement structure of $|\Psi(t)\rangle$. By assumption, the initial wavefunction at $t = 0$ obeys an area law (1.7), so $S_A(0) \sim |\partial A|$. In Section 1.3, we saw that there are strict limits on the amount entanglement that can be generated under unitary evolution (so long as the Hamiltonian is local), imposed by the Lieb-Robinson bound. Specifically, for a fixed region A, the entanglement entropy of $\hat{\rho}_A(t)$ as a function of time $S_A(t)$ must be less than some upper bound that grows linearly in time [20]. This is because distant degrees of freedom can only become entangled once they lie within each others' light cone, i.e. for $t \gtrsim x/v_{\text{L.R.}}$, where x is the distance separating them.

[1] This may not be the case when $\hat{H}(t)$ is either constant in time or is strictly periodic in time, and possesses enough spatial disorder to enter a many-body localized phase [158]. However, in this work we are interested in properties that do not depend on the specifics of the driving protocol. Even if the instantaneous Hamiltonian is in an MBL phase, if it is driven in a non-periodic fashion, the dynamics will inevitably be ergodic.

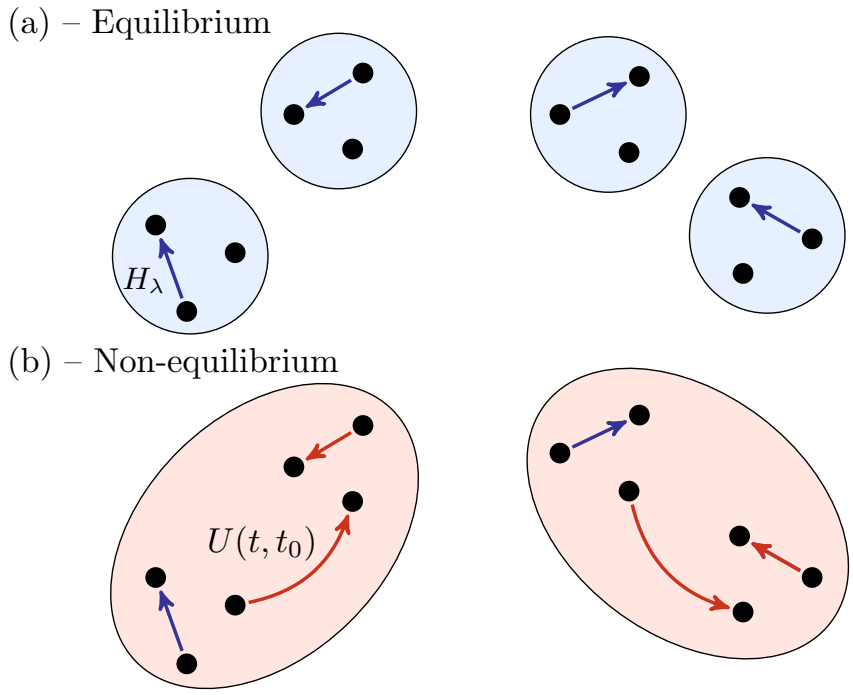

Fig. 2.1 Illustration of equilibrium vs non-equilibrium topological classification. Black dots represent various short-ranged entangled wavefunctions that respect a certain symmetry group G. Panel (a) – In equilibrium, wavefunctions are classified into sets (blue circles) according to whether each can be adiabatically connected through a family of symmetry-respecting Hamiltonians H_λ parametrised by $\lambda \in [0,1]$ (blue arrows). Panel (b) – The non-equilibrium classification partitions wavefunctions into sets (red ellipses) according whether each can be connected through some finite-time unitary evolution $U(t,t_0) = \mathscr{T}\exp[-\mathrm{i}\int_{t_0}^{t} \mathrm{d}t' H(t')]$ ($\mathscr{T}$ = time-ordering) governed by a Hamiltonian $H(t')$ that respects the symmetries in G (red arrows). The latter deformation procedure is strictly more general than the formal, so the non-equilibrium classification is always a subgroup of the equilibrium classification.

The implication is that for some fixed finite time t, the wavefunction $|\Psi(t)\rangle$ still satisfies an area law (see also Ref. [62] for a more rigorous proof).

By definition, as a wavefunction moves continuously within the space of area-law states, it must remain within the same quantum phase (since a phase corresponds to a single disconnected component of the space of area law states, see Section 1.2.1). We have seen that $|\Psi(t)\rangle$ is area-law entangled for t finite, and evolves continuously in time according to (2.1); therefore $|\Psi(t)\rangle$ must belong to the same quantum phase as the initial state $|\Psi(0)\rangle = |\Psi_1\rangle$. This can also be proven using the fact that for finite t, the unitary time-evolution operator $\hat{U}(t,0)$ can be well-approximated by a finite-depth unitary circuit (albeit one whose range increases with time [164]), which according to the notion of local unitary transformations introduced in Section 1.2.1 cannot connect wavefunctions belonging to different quantum

phases. We must conclude that in an infinite system, it will take an infinite time to evolve into a state in a different topological phase. For a finite-size system, the crossover from area- to volume- law happens on a timescale $t^* \sim L/v_{\text{L.R.}}$, which is extensive in the system size.

Therefore, for systems in non-equilibrium scenarios there is still a natural way in which the dynamics is constrained by topology: Instantaneous wavefunctions with different topological properties cannot evolve into each other *in a finite time* (from hereon we understand that 'finite time' implies a sub-extensive time when dealing with a finite-size system). Definition 1 is therefore still a useful construction in this context. We expect that systems undergoing unitary time evolution will continue to exhibit universal behaviour characteristic of the the topological phase in which it is initialised, up to some time that is extensive in the system size (although exactly which observables reflect these topological properties remains to be seen).

Our considerations so far apply to LRE phases with no symmetries, such as the integer and fractional quantum Hall effects. Now let us incorporate symmetries into our discussion. We wish to define an analogue of an SPT classification that applies to systems undergoing unitary time evolution. In equilibrium, we considered ground state wavefunctions that do not spontaneously break the symmetries of the Hamiltonian. It is important to note that, rather naturally, we insist that symmetries are imposed at the level of the Hamiltonian. Indeed, in any experimental set up, one generally has some degree of control over the Hamiltonian, and the wavefunction is subsequently determined through the appropriate Schrödinger equation. With this in mind, we wish to consider the space of states that can are accessible under unitary time evolution generated by a Hamiltonian that respects the relevant symmetries. Again, we distinguish states that can be accessed after arbitrarily long times from those that can be reached in a finite time.

We therefore propose the following definition

Definition 3 (Classification of SPTs Out of Equilibrium) *Two short-range entangled wavefunctions $|\Psi_1\rangle$ and $|\Psi_2\rangle$ both respecting the relevant symmetries are topologically equivalent if and only if $|\Psi_2\rangle$ can be reached from $|\Psi_1\rangle$ through unitary time evolution over a finite time governed by a symmetry-respecting, possibly time-dependent Hamiltonian.*

The set of equivalence classes under this relation constitutes a topological classification of symmetry-protected topological phases different from the usual one (Definition 2), as illustrated in Fig. 2.1. Heuristically, the classification enumerates how many different symmetry-respecting ground-state wavefunctions will remain topologically distinct once they are driven out of equilibrium. Again we emphasise that while this definition is certainly intuitively well-justified, it remains to be shown whether systems driven out of equilibrium do

indeed exhibit behaviour that reflects this topological classification. This will be demonstrated in the remainder of this thesis.

At first sight, one might expect that the above definition would be equivalent to the usual equilibrium classification of SPTs. In terms of locality, we already know that finite-time evolution is equivalent to adiabatic deformation [38]. Indeed, it has been suggested that the topological invariants that characterise these phases are always constants of motion [138, 245], which if true would confirm this simple expectation. However, such arguments overlook an important aspect to do with symmetries. The tight relationship between the symmetries of the Hamiltonian and those of the wavefunction which we are used to in adiabatic settings does not always hold out of equilibrium. This effect, which we refer to as 'dynamically-induced symmetry breaking' (following our work Ref. [145]) is described in the next section.

2.2 Dynamically-induced symmetry breaking

In equilibrium, if a Hamiltonian has a unique ground state, then that ground state will respect all the symmetries of its parent Hamiltonian. The alternative is that some of the symmetries are spontaneously broken, which leads to multiple ground states transforming non-trivially under the action of symmetries. Given that we are not concerned with symmetry-breaking phases of matter here, we assume this not to be the case. With this understood, what can we say about symmetries of the wavefunction out of equilibrium?

First, let us understand the nature of symmetries that can occur in a quantum system. According to Wigner's theorem [238], symmetries must be either linear and unitary, or antilinear and antiunitary. The former type are implemented by a unitary matrix $\hat{U}_S$ acting on Fock space, and the latter are implemented by the product of a unitary matrix and complex conjugation $\hat{U}_A\hat{\mathscr{K}}$. The conditions for a Hamiltonian $\hat{H}$ to satisfy each of the symmetries are

$$\hat{H} = \hat{U}_S \hat{H} \hat{U}_S^\dagger \qquad \text{(Unitary)} \tag{2.3a}$$

$$\hat{H} = \hat{U}_A \hat{H}^* \hat{U}_A^\dagger \qquad \text{(Antiunitary)} \tag{2.3b}$$

The most common type of antiunitary symmetry that one encounters in nature is time-reversal symmetry. This is present, for example, in spin systems for which the external magnetic field vanishes. For the majority of this work, we will only consider non-spatial symmetries, i.e. those for which the operator $\hat{U}_{S,A}$ can be written as a product of unitary matrices on each site $\hat{U}_{S,A} = \hat{u} \otimes \hat{u} \otimes \cdots \otimes \hat{u}$, with each factor acting on the Hilbert space of a

single site. This excludes crystalline symmetries, wherein one also permutes the positions of each site according to the rotations, reflections, and translations that make up the symmetry.

If a wavefunction is left unchanged by a symmetry operation, then we say it respects that symmetry. Because the overall phase of a wavefunction is unphysical, this implies that a symmetry-respecting wavefunction $|\Psi\rangle$ must satisfy

$$|\Psi\rangle = e^{\mathrm{i}\alpha}\hat{U}_S\,|\Psi\rangle\,, \qquad \text{(Unitary)} \tag{2.4a}$$

$$|\Psi\rangle = e^{\mathrm{i}\alpha}\hat{U}_A\,|\Psi\rangle^* \qquad \text{(Antiunitary)} \tag{2.4b}$$

for some phase α. In the absence of symmetry-breaking, when $|\Psi\rangle$ is the ground state of $\hat{H}$, one can verify that (2.3) implies (2.4).

Now let us consider the symmetry properties of wavefunctions far from equilibrium as they undergo unitary dynamics. Suppose that the state is initially prepared in a symmetry respecting state $|\Psi(0)\rangle$ satisfying Eq. (2.4). If the Hamiltonian which governs the time evolution also respects the relevant symmetry, is the wavefunction at a later time $|\Psi(t)\rangle$ symmetry-respecting? When the symmetry is unitary, we can apply $\hat{U}_S$ to $|\Psi(t)\rangle$

$$\begin{aligned}
\hat{U}_S\,|\Psi(t)\rangle &= \hat{U}_S\mathscr{T}\exp\left(-\mathrm{i}\int_0^t \mathrm{d}t'\,\hat{H}(t')\right)|\Psi(0)\rangle \\
&= \mathscr{T}\exp\left(-\mathrm{i}\int_0^t \mathrm{d}t'\,\hat{U}_S\hat{H}(t')\hat{U}_S^\dagger\right)\hat{U}_S\,|\Psi(0)\rangle \\
&= \mathscr{T}\exp\left(-\mathrm{i}\int_0^t \mathrm{d}t'\,\hat{H}(t')\right)e^{-\mathrm{i}\alpha}\,|\Psi(0)\rangle \\
&= e^{-\mathrm{i}\alpha}\,|\Psi(t)\rangle\,,
\end{aligned} \tag{2.5}$$

where in the third line we have exploited Eqs. (2.3a) and (2.4a). Thus the time-evolved wavefunction is still symmetry-respecting, as one would intuitively expect, for example, in a system with reflection symmetry: neither the initial state nor the equations of motion differentiate between the left and right halves of the system.

We now perform the same calculation for the antiunitary symmetry (as I demonstrated in Ref. [145])

$$\begin{aligned}\hat{U}_A |\Psi(t)\rangle^* &= \hat{U}_A \left[\mathscr{T} \exp\left(-\mathrm{i} \int_0^t \mathrm{d}t' \, \hat{H}(t') \right) |\Psi(0)\rangle \right]^* \\ &= \mathscr{T} \exp\left(+\mathrm{i} \int_0^t \mathrm{d}t' \, \hat{U}_A \hat{H}(t')^* \hat{U}_A^\dagger \right) \hat{U}_A |\Psi(0)\rangle^* \\ &= \mathscr{T} \exp\left(+\mathrm{i} \int_0^t \mathrm{d}t' \, \hat{H}(t') \right) e^{-\mathrm{i}\alpha} |\Psi(0)\rangle \\ &\neq e^{-\mathrm{i}\alpha} |\Psi(t)\rangle \,. \end{aligned} \tag{2.6}$$

The presence of the factor of $(-\mathrm{i})$ in the time-ordered exponential is not invariant under antiunitary symmetries, even if the Hamiltonian itself respects the symmetry. Because of this, unitary dynamics will in general break all antiunitary symmetries in any system – this is the phenomenon of dynamically-induced symmetry breaking. The only way to restore the symmetry is through some fine-tuned matching between $\hat{H}(t')$ and the initial state $|\Psi(0)\rangle$, which we do not consider here.

This analysis of symmetries highlights one of the key differences between equilibrium and non-equilibrium dynamics: while antiunitary symmetries are stable in the context of ground state physics, they are unstable against any time-dependent perturbations that may be introduced to the system (either deliberately or inadvertently). Physically, antiunitary symmetry operators induce a reversal of time, possibly combined with some other unitary transformation. This effect therefore makes intuitive sense: the breaking of time-reversal invariance comes through the time-dependence of the Hamiltonian itself. Although this effect is well-known, the associated consequences for topological phenomena in non-equilibrium scenarios have not yet been fully addressed.

Comparing the equilibrium vs. non-equilibrium classification of SPTs (Definition 2, 3), we see that the latter involves deformations where the wavefunction breaks all antiunitary symmetries at intermediate times, unlike the former. There are some simple cases where this difference in symmetry properties can be understood immediately. If all symmetries are unitary, then the deformation procedures for the two constructions are equivalent, and so the equilibrium and non-equilibrium classifications are identical. If all symmetries are antiunitary, then the deformation procedure out of equilibrium is the same as that for the definition of quantum phases with no symmetries present. When dealing with SPTs, the wavefunctions under consideration are all SRE. Thus, once symmetry is broken, there are no quantum phases and the non-equilibrium classification is trivial, i.e. all wavefunctions

are connected under the relevant deformation procedure. If the system in question features a combination of unitary and antiunitary symmetries, then it is less clear how to compute the non-equilibrium classification. We will develop new methods to calculate these cases in Chapter 3.

It is important to note that the non-equilibrium classification for a given group of symmetries is *not* simply given by the equilibrium classification under the subgroup of only unitary symmetries. As an illustrative example, consider fermionic systems in two dimensions with time-reversal symmetry and charge conservation. This combination of symmetries gives rise to two topologically distinct phases in equilibrium: a trivial phase and a quantum spin Hall phase (see Section 1.2.2). With charge conservation only, there are an infinite number of topological phases labelled by the Chern number Ch_1. However, since the wavefunctions being classified are all time-reversal symmetric, they must all have a Chern number of zero, and so are trivial once time-reversal symmetry is dynamically broken. Therefore, although antiunitary symmetries are not preserved under unitary time evolution, their presence is still important in constraining the phases that are accessible in the first place.

Just as the classification of SPT phases in equilibrium allows one to make general predictions about systems that are constrained to remain in their symmetry-respecting ground states, the non-equilibrium classification has physical consequences for isolated systems undergoing unitary time evolution. We highlight some of these consequences in the following sections of this chapter. For the sake of simplicity, some of this discussion will explicitly refer to non-interacting systems, which make up only a subset of all SPT phases. Almost all of these results generalise to the strongly interacting regime, but we will be sure to point out those that are specific to weakly interacting systems. Surprisingly, the non-equilibrium classification also bears relevance to scenarios where the system is not isolated; these matters are discussed in Chapter 4.

2.3 Topological bulk indices of one-dimensional free-fermion systems

Some of the simplest systems that exhibit non-trivial SPT order exist in one spatial dimension (1D), and can be well described using non-interacting fermions. Prototypical models within this class include the Kitaev chain [122] and the Su-Schreiffer-Heeger model [203]. Before investigating non-equilibrium physics, we briefly review the structure of equilibrium topological phases in 1D free-fermion systems (i.e. those that admit a single-particle description), and the methods used to analyse them.

2.3.1 Symmetries and classification in equilibrium

A notable success in the theory of free-fermion topological phases was the classification of topological insulators and superconductors within the 'tenfold way' [177, 193, 120, 187]. This encompasses non-interacting fermionic systems with non-spatial symmetries (i.e. excluding crystalline symmetries such as rotation and reflection). In this case, the many-body Hamiltonian is bilinear in fermion operators

$$\hat{H} = \sum_{ij} \hat{c}_i^\dagger(k) H_{ij}(k) \hat{c}_j(k)\,, \tag{2.7}$$

where $\hat{c}_j^\dagger(k)$ creates a fermion in a basis state $j = 1,\ldots,n$ with quasimomentum k belonging to the Brillouin Zone. The different basis states include other quantum numbers such as spin, or position within the unit cell. Note that, for pedagogical reasons, we are treating systems with discrete translation invariance; however all the phases that we consider here are stable in the presence of perturbations that break translation symmetry. One can calculate the Bloch wavefunctions, which are given by the eigenvectors of the single-particle Hamiltonian

$$H(k)\,|u^n(k)\rangle = E_n(k)\,|u^n(k)\rangle\,. \tag{2.8}$$

Here, $n = 1,\ldots,N$ labels the bands. The many-body ground state of this system is a Slater determinant of all orbitals having negative energy $E_n(k) < 0$ (we have set the chemical potential to zero without loss of generality). Because the system is gapped, all bands are either completely occupied, or completely unoccupied.

Symmetries of non-interacting systems impose certain constraints on the single particle Hamiltonian $H(k)$. If one considers only non-spatial symmetries, then there are four possibilities for the form of this constraint

$$UH(k)U^\dagger = H(k) \qquad \text{(Unitary)} \tag{2.9a}$$
$$U_T H(-k)^* U_T^\dagger = H(k) \qquad \text{(Time-reversal)} \tag{2.9b}$$
$$U_C H(-k)^* U_C^\dagger = -H(k) \qquad \text{(Particle-hole)} \tag{2.9c}$$
$$U_S H(k) U_S^\dagger = -H(k) \qquad \text{(Chiral)} \tag{2.9d}$$

where the unitary matrices $U_{T,C,S}$ determine exactly how the symmetry is implemented, and satisfy $U_T U_T^* = \pm 1$, $U_C U_C^* = \pm 1$, $(U_S)^2 = +1$ [44]. Free fermion phases have the special property that unitary symmetries of the type (2.9a) can always be eliminated by choosing a basis in which U is diagonal, wherein $H(k)$ becomes block diagonal, and each block can be topologically characterized individually [187]. We therefore restrict our attention to the latter

	Symmetries			Spatial Dimension d							
Class	U_T	U_C	U_S	0	1	2	3	4	5	6	7
A	0	0	0	$\mathbb{Z}$	0	$\mathbb{Z}$	0	$\mathbb{Z}$	0	$\mathbb{Z}$	0
AIII	0	0	1	0	$\mathbb{Z}$	0	$\mathbb{Z}$	0	$\mathbb{Z}$	0	$\mathbb{Z}$
AI	+	0	0	$\mathbb{Z}$	0	0	0	$2\mathbb{Z}$	0	$\mathbb{Z}_2$	$\mathbb{Z}_2$
BDI	+	+	1	$\mathbb{Z}_2$	$\mathbb{Z}$	0	0	0	$2\mathbb{Z}$	0	$\mathbb{Z}_2$
D	0	+	0	$\mathbb{Z}_2$	$\mathbb{Z}_2$	$\mathbb{Z}$	0	0	0	$2\mathbb{Z}$	0
DIII	−	+	1	0	$\mathbb{Z}_2$	$\mathbb{Z}_2$	$\mathbb{Z}$	0	0	0	$2\mathbb{Z}$
AII	−	0	0	$2\mathbb{Z}$	0	$\mathbb{Z}_2$	$\mathbb{Z}_2$	$\mathbb{Z}$	0	0	0
CII	−	−	1	0	$2\mathbb{Z}$	0	$\mathbb{Z}_2$	$\mathbb{Z}_2$	$\mathbb{Z}$	0	0
C	0	−	0	0	0	$2\mathbb{Z}$	0	$\mathbb{Z}_2$	$\mathbb{Z}_2$	$\mathbb{Z}$	0
CI	+	−	1	0	0	0	$2\mathbb{Z}$	0	$\mathbb{Z}_2$	$\mathbb{Z}_2$	$\mathbb{Z}$

Table 2.1 Periodic table of topological insulators and superconductors in equilibrium [177, 193, 120, 187]. The ten Altland-Zirnbauer symmetry classes are defined according to the presence of time-reversal [U_T, Eq. (2.9b)], particle-hole [U_C, Eq. (2.9c)], and chiral [U_S, Eq. (2.9d)] symmetries. The notation $+$ ($-$) indicates that the relevant unitary matrix satisfies $U_{T,C}U_{T,C}^* = +1$ (-1). For each symmetry class and spatial dimension, an Abelian group (0, $\mathbb{Z}_2$, $\mathbb{Z}$, or $2\mathbb{Z}$) is provided, the elements of which represent different topological phases. The classification in spatial dimension $(d+8)$ is the same as that in d dimensions.

three symmetries only. Note that in superconducting systems, particle-hole symmetry (PHS) arises not as a physical symmetry, but is due to a redundancy in the Bogoliubov-de Gennes equations [18].

Depending on the presence or absence of each of these symmetries, the system in question belongs to one of ten Altland-Zirnbauer symmetry classes [6] (see the first four columns of Table 2.1). Within a particular symmetry class, one can determine how many topological phases of matter there exist in each spatial dimension, i.e. how many different single-particle Hamiltonians there exist which cannot be continuously interconnected without closing the gap. The full classification was first derived in Refs. [177, 193, 120, 187], and is presented in the latter columns of Table 2.1. The table exhibits a remarkable repeating structure, because of which it is sometimes referred to as the periodic table of topological insulators and superconductors [120].

The classification is particularly simple to understand in one dimension, wherein all free-fermion phases can be identified using the appropriate topological bulk index, known as the Chern-Simons invariant CS_1 (equivalently the Zak phase α_Z [248])

$$\mathrm{CS}_1 \equiv \frac{\alpha_Z}{2\pi} = \frac{\mathrm{i}}{2\pi} \sum_{n\,\mathrm{occ.}} \int_{\mathrm{BZ}} \mathrm{d}k \, \langle u^n(k) | \partial_k u^n(k) \rangle \,, \tag{2.10}$$

where the sum runs over occupied bands only. The Bloch wavefunctions $|u^n(k)\rangle$ are assumed to vary sufficiently smoothly with k, and be periodic in the Brillouin Zone – this is only possible thanks to the area-law nature of the ground state [125]. Roughly speaking, this quantity is an analogue of the Chern number Ch_1 for one-dimensional systems, which can also be expressed as an integral of the $|u^n(k)\rangle$ over the whole Brillouin Zone (see Section 3.1.1).

In general, CS_1 is only defined modulo 1, since unitary rotations within the space of occupied Bloch functions do not change the many-body ground state, but can change CS_1 by an integer (such transformations are referred to as gauge transforms [239]). Within the unit interval over which the index is unambiguous, it can take any value. However, if a particle-hole or chiral symmetry is present, then this quantity becomes quantized to a half-integer [24]. In this case, CS_1 cannot change as the ground state is continuously deformed, provided that the relevant symmetries are enforced; it can thus be used as a topological invariant[2]. Furthermore, in the presence of time-reversal and/or chiral symmetries, the integer part of the expression (2.10) can be given physical meaning. It is simple to show that out of the ten Altland-Zirnbauer symmetry classes, five can support a quantized bulk index that can take multiple inequivalent values – these are the classes that possess non-trivial topological phases. The equilibrium topological classification can be inferred from the set of possible values of CS_1, which is summarized in column 5 of Table 2.2.

2.3.2 Symmetries of the time-evolved state

We now turn to non-equilibrium dynamics in free-fermion systems, following our treatment in Ref. [145]. Our first consideration is of symmetries of the wavefunction, which we expect will prove important from the discussion of Section 2.2. Specifically, we anticipate that dynamically-induced symmetry breaking will occur for some of the symmetries (2.9).

In equilibrium the symmetries of a Hamiltonian $\hat{H}$ are naturally inherited by its ground state wavefunction $|\Psi\rangle$. In the context of free-fermion systems, it is convenient to express the symmetry constraints on the ground state in terms of the single-particle density matrix

$$\rho_{ij}(k) \coloneqq \left\langle \Psi \middle| \hat{c}_i^\dagger(k)\hat{c}_j(k) \middle| \Psi \right\rangle \sum_{n\,\mathrm{occ.}} \langle i|u^n(k)\rangle \langle u^n(k)|j\rangle \,, \tag{2.11}$$

where $|i\rangle$, $|j\rangle$ are single-particle basis states, and the sum runs over occupied bands only. By its Gaussian nature, $|\Psi\rangle$ is uniquely specified by $\rho_{ij}(k)$. The symmetries (2.9) in turn impose

[2] One can show that ground state wavefunctions possessing different values of CS_1 are indeed in different equilibrium SPT phases, in the sense of Definition 2.

the following constraints on the single-particle density matrix [187]

$$U_T \rho(-k)^* U_T^\dagger = \rho(k) \qquad \text{(Time-reversal)} \tag{2.12a}$$
$$U_C \rho(-k)^* U_C^\dagger = \mathbb{1}_N - \rho(k) \qquad \text{(Particle-hole)} \tag{2.12b}$$
$$U_S \rho(k) U_S^\dagger = \mathbb{1}_N - \rho(k). \qquad \text{(Chiral)} \tag{2.12c}$$

Unlike the Hamiltonian symmetries (2.9), this characterization of the ground state admits a natural generalization out of equilibrium.

For concreteness, we will consider the following non-equilibrium protocol, which is rather general: At time $t = 0$, the system is prepared in the ground state of an initial Hamiltonian $\hat{H}^{\mathrm{i}}$, possessing a certain set of symmetries. The system then evolves under the (possibly time-dependent) Hamiltonian $\hat{H}^{\mathrm{f}}(t)$, which is assumed to respect the same set of symmetries. We consider properties of the wavefunction at some later time t. A similar analysis also applies when the symmetry properties of the Hamiltonian change in time; however we will not cover these scenarios in this thesis.

The single particle density matrix evolves as $\rho(t,k) = U(t,0;k)\rho(0,k)U(t,0;k)^\dagger$ under the single-particle time evolution matrix, defined in analogy to the many-body version [Eq. (2.2)]

$$U(t_2,t_1;k) = \mathscr{T} \exp\left(-\mathrm{i}\int_{t_1}^{t_2} dt' \, H^{\mathrm{f}}(t';k)\right), \tag{2.13}$$

where $H^{\mathrm{f}}(t,k)$ is the first quantized Bloch Hamiltonian for the final Hamiltonian $\hat{H}^{\mathrm{f}}(t)$. By replacing $\rho(k)$ with $\rho(t,k)$ in (2.12), we can determine whether the symmetries of the initial state are preserved after a time t. We find [145]

$$U_T \rho(-k,t)^* U_T^\dagger = \rho(k,-t) \qquad \text{(Time-reversal)} \tag{2.14a}$$
$$U_C \rho(-k,t)^* U_C^\dagger = \mathbb{1}_N - \rho(k,t) \qquad \text{(Particle-hole)} \tag{2.14b}$$
$$U_S \rho(k,t) U_S^\dagger = \mathbb{1}_N - \rho(k,-t). \qquad \text{(Chiral)} \tag{2.14c}$$

where we have used $\rho(k,-t)$ to denote a fictitious system time-evolved by a time $+t$ under the Hamiltonian $-H^{\mathrm{f}}(t)$. In general $\rho(k,-t) \neq \rho(k,t)$, and so we infer that TRS and chiral symmetries of the state are *not* preserved under dynamics, whereas PHS is preserved.

Although the PHS relation (2.9c) involves complex conjugation, it is important to note that as a many-body symmetry operator, it is in fact unitary. It is distinguished from conventional unitary symmetries in that it exchanges fermionic creation and annihilation operators. After applying a PHS transformation to the quadratic Hamiltonian (2.7), the

creation and annihilation operators can be anticommuted to restore their order, resulting in a factor of (-1) and a transposition of $H_{ij}(k)$, hence the form (2.9c). Based on our expectations from Section 2.2, the fact that PHS is represented by a unitary operator in Fock space explains why it is preserved under time evolution. Similarly, chiral symmetry (being the product of TRS and PHS) is represented by an antiunitary in Fock space, and so is subject to dynamically-induced symmetry breaking.

2.3.3 Dynamics of the bulk invariant

With knowledge of the symmetry properties of the time-evolved state, we are now in a position to consider its topological properties. One of the simplest questions one can answer is how the bulk index CS_1 behaves under time evolution. Although CS_1 is generally used to characterize ground states, the expression (2.10) can be evaluated for any set of Bloch functions, including those of the time evolved state $|u^n(k,t)\rangle = U(t,0|k)\,|u^n(k,0)\rangle$. Here, we consider the time-dependent bulk index $\mathrm{CS}_1(t)$, focussing on the five symmetry classes that possess non-trivial topological phases in 1D, and demonstrate how the non-equilibrium classification defined in Section 2.1 can be used to predict its dynamics.

All area-law Gaussian wavefunctions that possess particle-hole symmetry (classes BDI, D, DIII, and CII) must have a CS invariant quantized to 0 or $1/2$ up to the addition of an integer [24]. As we have shown, this symmetry is preserved under time evolution, and so the time-dependent $\mathrm{CS}_1(t)$ must also be quantized for $t > 0$. Moreover, assuming that all Hamiltonians are smooth in k-space, the time evolution constitutes a continuous interpolation between the initial and final states parametrized by the time t, along which $\mathrm{CS}_1(t)$ remains well-defined. Along such a continuous path, the bulk index cannot change discontinuously, and so we conclude that the fractional part of $\mathrm{CS}_1(t)$ must be constant in time when PHS is present.

States which do not possess PHS can have a CS invariant quantized to half-integer values if there is a chiral symmetry (class AIII). We have argued above that chiral symmetry will in general undergo dynamically-induced symmetry breaking. Thus, for $t > 0$ the CS invariant need no longer be quantized, and one expects $\mathrm{CS}_1(t)$ to vary in time. This leads to the surprising finding that even when the initial and final Hamiltonians satisfy the same (chiral) symmetry at all times the bulk index becomes time-dependent.

Thus, through considering the symmetry properties of wavefunctions after some time evolution, we are able to make general predictions about the dynamics of the bulk index far from equilibrium: there are cases in which it remains quantized and constant, and those in which it can vary continuously in time. However, it remains to be seen to what extent the bulk

Sym. Class	U_T	U_C	U_S	$\mathrm{CS}_1(t=0)$	$\mathrm{CS}_1(t) \bmod 1$	Classification
AIII	0	0	1	$\mathbb{Z}/2^*$	Varies $[0,1)$	0
BDI	+	+	1	$\mathbb{Z}/2^*$	Const. $\{0,1/2\}$	$\mathbb{Z}_2$
D	0	+	0	$\mathbb{Z}/2 \bmod 1$	Const. $\{0,1/2\}$	$\mathbb{Z}_2$
DIII	−	+	1	$\mathbb{Z} \bmod 2^*$	Const. 0	0
CII	−	−	1	$\mathbb{Z}^*$	Const. 0	0

Table 2.2 Topological characterizations of 1D free-fermion systems in and out of equilibrium. The five non-trivial Altland-Zirnbauer symmetry classes in 1D are defined by the presence of time-reversal, particle-hole and chiral symmetries (U_T, U_C, U_S, respectively) according to Eq. (2.9), and we list the possible values that $\mathrm{CS}_1(t=0)$ can take in the ground state of systems belonging to each symmetry class. Asterisks denote cases for which CS_1 must be evaluated in a gauge specified by the time-reversal or chiral symmetries. After time evolving under a Hamiltonian in the same symmetry class, the fractional part of $\mathrm{CS}_1(t)$ either varies in time, or stays fixed to its initial value. The possible values of $\mathrm{CS}_1(t) \mod 1$ are given, which determine the topological classification out of equilibrium.

index, calculated in this simple way, encodes the *topological* features of the time-evolving state.

One may naïvely expect that the topological properties of the initial state are preserved as long as $\mathrm{CS}_1(t)$ does not vary in time (as occurs for all non-trivial classes other than AIII). However, this argument overlooks the gauge dependence of the bulk index. An individual measurement of $\mathrm{CS}_1(t)$ at some time t is still only defined modulo 1. In equilibrium, we were able to resolve this ambiguity when time-reversal and/or chiral symmetries were present, using a choice of gauge related to those symmetries. However, both these symmetries are generically broken under dynamics, and these gauges are no longer well-defined. Therefore, we should not ascribe any physical meaning to the integer part of $\mathrm{CS}_1(t)$ once dynamically-induced symmetry breaking occurs. There is thus no way to topologically distinguish wavefunctions with the same $\mathrm{CS}_1(t)$ modulo 1.

In symmetry classes DIII and CII, which both have a time-independent $\mathrm{CS}_1(t)$, the bulk index must be an integer (not a half-integer). Although the time-reversal symmetry allowed different initial states to be topologically distinguished, the fractional part $[\mathrm{CS}_1(t) \bmod 1]$ will always be zero, regardless of the initial state. In these cases, the topological features of the initial state are *not* reflected in the time-evolved wavefunction. In contrast, systems in classes D and BDI can have a bulk index quantized to a half-integer, which remains distinct from those states with $\mathrm{CS}_1(t) \bmod 1 = 0$ when driven out of equilibrium. In column 6 of table 2.2, we list the possible values that $[\mathrm{CS}_1(t) \bmod 1]$ can take after time evolution, which informs us whether different time-evolved states in the same symmetry class can be topologically distinguished from each other.

A careful treatment of the dynamics of the bulk index therefore allows us to distinguish two fundamentally different behaviours in topological systems far from equilibrium. In the first (classes D and BDI), at least some of the topological features of the initial state, as encoded by $\mathrm{CS}_1(t=0) \mod 1$, are exhibited in the time evolved state. In the second (classes AIII, DIII, and CII), the time-evolved state contains no information about the topological features of the initial state. Indeed, in Ref. [145], we explicitly showed that in these latter cases, initial wavefunctions in different topological phases can evolve into the same state.

These considerations are specific to one-dimensional non-interacting fermionic systems, but reflect the more general principles encapsulated by the non-equilibrium topological classification introduced in Section 2.1. The constraints imposed by symmetries on the dynamics of the bulk invariant allow us to identify obstructions to time-evolving between certain wavefunctions under dynamics governed by a symmetry-respecting wavefunction. We can understand those wavefunctions that have $[\mathrm{CS}_1(t) \mod 1]$ non-quantized or equal to zero as being trivial in the non-equilibrium classification, and those with a bulk invariant quantized to $1/2$ as non-trivial.

The non-equilibrium classification refers to *finite-time* unitary evolution, which as we discussed ensures that the wavefunctions in question remain area-law entangled. In a finite-size system of length L, we saw that the time of evolution must be less than some maximum time set by the Lieb-Robinson bound $t < L/v_{\mathrm{L.R.}}$. It is therefore prudent to consider what happens to $\mathrm{CS}_1(t)$ as this critical time is approached. For a non-interacting wavefunction, the Bloch wavefunctions $|u^n(k,t)\rangle$ will vary with k on a momentum scale on the order of $\xi(t)^{-1}$, the inverse of the correlation length of the wavefunction. (The correlation length is defined such that components $\rho_{ij}(t)$ are sufficiently small for $|i-j| \gtrsim \xi(t)$, and will grow at most linearly in time, due to the Lieb-Robinson bound [20].) Around the critical time, the correlation length becomes on the order of L, i.e. correlations span the whole system. The momentum states in a finite system are discrete, separated by intervals of $\delta k = 2\pi/L$, and so the derivative in Eq. (2.10) is only well defined when $|u^n(k,t)\rangle$ varies on momentum scales less than δk, i.e. $\xi(t)^{-1} \lesssim 2\pi/L$. Thus, beyond the critical time $L/v_{\mathrm{L.R.}}$, derivatives in momentum space become poorly defined, which in turn invalidates the definition of $\mathrm{CS}_1(t)$. This confirms our expectations based on the arguments of Section 2.1, and also demonstrates the relationship between topological properties out of equilibrium and the dynamics of correlations, both of which are constrained by the Lieb-Robinson bound.

We note that in strongly interacting 1D systems, the CS invariant is no longer appropriate for characterizing topology. In this case the relevant topological invariants do not have a simple closed-form expression like Eq. (2.10), but are more complicated mathematical

structures (which we will discuss in Section 3.2). Although in these cases one cannot define a notion of a time-dependent bulk index, one can still conduct a similar analysis by considering which topological features of the wavefunction remain well-defined after dynamically-induced symmetry breaking.

2.3.4 Measuring the bulk invariant in experiment

In equilibrium, many bulk topological indices are directly related to physical observables, such as the relation between the Chern number and the Hall conductivity [Eq. (1.8)]. This holds in one dimension: Although the CS invariant [Eq. (2.10)] appears to be a complex quantity which would require full wavefunction tomography to measure, it can in fact be deduced from the bulk polarization of the system, i.e. the displacement of the fermions in the system with respect to the centres of the unit cell. Here I show that this relationship still holds out of equilibrium. The time derivative of the polarization of a material is given by the current in the bulk, which in a system with discrete translation symmetry is given by the group velocity operator $\partial_k \hat{H}_k$. Upon summing over all bands and all quasimomenta, this gives

$$\begin{aligned}
\langle j(t)\rangle &= \frac{1}{2\pi}\sum_{n\,\mathrm{occ.}}\int_{\mathrm{BZ}} \mathrm{d}k\, \langle u_k^n(t)|\partial_k \hat{H}_k(t)|u_k^n(t)\rangle \\
&= \frac{1}{2\pi}\sum_{n\,\mathrm{occ.}}\int_{\mathrm{BZ}} \mathrm{d}k\, \left\{\partial_k\left[\langle u_k^n(t)|\hat{H}_k(t)|u_k^n(t)\rangle\right] - \langle u_k^n(t)|\hat{H} f_k(t)|\partial_k u_k^n(t)\rangle - \langle \partial_k u_k^n(t)|\hat{H}_k(t)|u_k^n(t)\rangle\right\} \\
&= \frac{i}{2\pi}\sum_{n\,\mathrm{occ.}}\int_{\mathrm{BZ}} \mathrm{d}k\, \left[\langle \partial_t u_k^n(t)|\partial_k u_k^n(t)\rangle + \langle u_k^n(t)|\partial_t\partial_k u_k^n(t)\rangle\right] \\
&= \frac{d}{dt}\mathrm{CS}_1. \qquad (2.15)
\end{aligned}$$

We have integrated by parts, and used the periodicity of $|u_k^n\rangle$ in the BZ. Thus, the time variation of $\mathrm{CS}_1(t)$ can be directly measured in experiment as a current. Note that no assumption of any form of adiabaticity is required. This result contrasts with the Chern number in 2D for which the relationship with the Hall conductance does not hold out of equilibrium [31, 215].

We have numerically verified that this relationship between the CS invariant and local current holds, even within the bulk of a finite system. We consider a model of spinless fermions, represented by operators $\hat{\psi}_j$, $\hat{\psi}_j^\dagger$ acting on the sites labelled by j, with a hopping

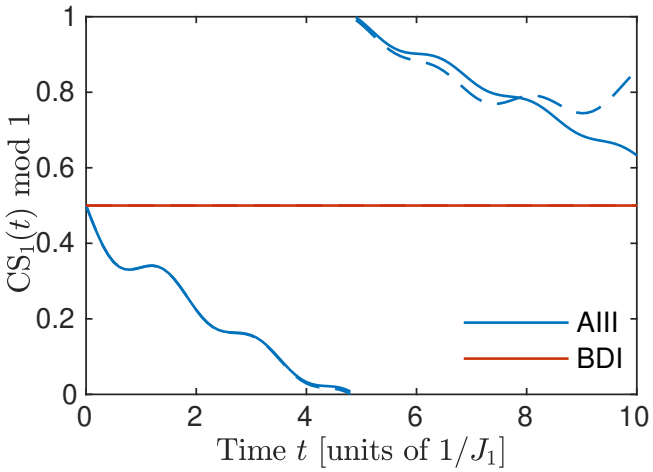

Fig. 2.2 Panel (a): Time-dependent CS invariant of a hopping model of spinless fermions [with Hamiltonian given by Eq. (2.16)], calculated as a bulk integral in k-space (solid lines), compared with the polarization $Q_B(t)$ of a 24-site system with open boundary conditions, using same hopping parameters (dashed lines). $Q_B(t)$ is calculated as the expectation value of the number of particles within the one half of the system. The red lines are for a system in class BDI and the blue lines are for a class AIII system. The parameters for the quenches are $(J_1, J_2) = (0.3, e^{i\alpha}) \to (0.8\, e^{i\alpha}, 1)$ with $B_{1,2} = 0.05$ throughout; $\alpha = 0$ for class BDI and $\alpha = 0.4$ for class AIII. The observables in the finite sample match the dynamics of the bulk invariants even out of equilibrium, until correlations span the whole system at which point the discrete nature of k-space invalidates Eq. (2.15).

Hamiltonian

$$\hat{H} = -\sum_j (J_1 \hat{\psi}^\dagger_{2j+1} \hat{\psi}_{2j} + J_2 \hat{\psi}^\dagger_{2j+2} \hat{\psi}_{2j+1} + B_1 \hat{\psi}^\dagger_{2j+3} \hat{\psi}_{2j} + B_2 \hat{\psi}^\dagger_{2j+4} \hat{\psi}_{2j+1} + \text{h.c.}) \tag{2.16}$$

In general, the model possesses only a chiral sublattice symmetry (class AIII), but if all hopping amplitudes are real, TRS and PHS are also present (class BDI). We consider a quantum quench of this model, in which the ground state of (2.16) for a particular set of parameters is prepared, and then time-evolved under a Hamiltonian with a different set of parameters. Specifically, we choose $(J_1, J_2, B_1, B_2) = (0.3, e^{i\alpha}, 0.05, 0.05)$ before the quench (ensuring that the initial state is topological $\mathrm{CS}_1 \bmod 1 = 1/2$), and $(J_1, J_2, B_1, B_2) = (0.8e^{i\alpha}, 1, 0.05, 0.05)$ after the quench, where $\alpha = 0.4$ or $\alpha = 0$ for systems in classes AIII and BDI, respectively. Figure 2.2 shows the time variation of the CS invariants for AIII and BDI systems, calculated as bulk integrals. This is compared to the bulk polarization $Q_B(t)$ in a finite system with the same hopping amplitudes, calculated as the particle number in the right subsystem B (see inset). The gauge-invariant part of $Q_B(t)$ equals $\mathrm{CS}_1(t)$ up to an integer, until correlations span the whole system. Thus in 1D, the change in the CS invariant is directly measurable as particle accumulation.

2.4 Entanglement spectrum dynamics

We have so far seen that systems undergoing unitary dynamics are constrained explore the space of wavefunctions that are equivalent to the initial state in the sense defined by the non-equilibrium classification. Any quantity that witnesses the topological properties of ground state wavefunctions should therefore reflect this classification. One such object is the entanglement spectrum (See Section 1.2.3), which is the subject of this section.

2.4.1 Evolution of the entanglement spectrum

As in Section 2.3, we consider a scenario in which the system is prepared in some initial state, and then evolves for a finite time under a symmetry-respecting time-dependent Hamiltonian. We are interested in the eigenvalues of the reduced density matrix $\hat{\rho}_A(t) = \mathrm{Tr}_B |\Psi(t)\rangle \langle\Psi(t)|$ at later times.

We presume that the initial state features entanglement spectrum degeneracies characteristic of the topological phase that it belongs to. For concreteness, we will address a particular class of one-dimensional systems, namely topological superconductors in symmetry classes D, BDI, and DIII, which appeared in our discussion of bulk indices (See Table 2.2); however,

the arguments we provide will apply more generally to other SPT phases. The models under consideration are realized in mean-field descriptions of superconducting systems, whose Bogoliubov-de Gennes equations can be described using a basis of Majorana fermions $\hat{\gamma}_j^\alpha$, as described in Section 1.2.3. Any Hamiltonian that is bilinear in these Majorana operators inherits a particle-hole symmetry satisfying $U_C U_C^* = +1$ [18]. If no other symmetries are present, the system belongs to class D. If time reversal symmetry is added, then the system belongs to class BDI (DIII) if the fermions have integer (half-integer) spin (which determines the sign of $U_T U_T^*$).

From Table 2.2, we see that there exist an infinite number of phases in class BDI, labelled by different values of the integer-valued winding number $\nu := 2 \times \mathrm{CS}_1$ (as calculated in a particular gauge). In equilibrium, the winding number determines how many zero-energy modes are present at each edge. Each of the $|\nu|$ modes can be described by a single Majorana operator. On a given edge, all the modes are composed of Majorana operators of the same flavour (A or B). Any bilinear Hamiltonian term that respects the time-reversal symmetry must couple an A-fermion to a B-fermion [since a term of the form $\hat{H} = \mathrm{i}\hat{\gamma}_j^A \hat{\gamma}_k^A$ is not invariant under time-reversal, due to the factors of i in Eq. (1.9)], therefore these edge modes cannot be gapped out by a Hamiltonian, unless time-reversal symmetry is explicitly broken. Note that in our discussion of superconducting systems, Hamiltonian terms consisting of an odd number of fermion operators are not considered, since these terms are forbidden by the conservation of fermion parity[3].

Now, when driven out of equilibrium, the reduced density matrix of the time-evolved state $\hat{\rho}_A(t) = \mathrm{Tr}_B |\Psi(t)\rangle \langle\Psi(t)|$, and in turn the entanglement Hamiltonian $\hat{H}_E(t) = -\log \hat{\rho}_A(t)$, will evolve continuously in time. In Section 1.2.3, we saw that the entanglement Hamiltonian will possess topologically protected zero-modes if the wavefunction under consideration has SPT order; thus, by assumption, $\hat{H}_E(t=0)$ will possess $|\nu|$ edge modes, protected by the symmetries of the initial state. We know from Section 2.3.2 that time-reversal symmetry will generically undergo dynamically-induced symmetry breaking, but particle-hole symmetry will be preserved. Thus, for $t > 0$ time-reversal symmetry-breaking terms will be introduced in $\hat{H}_E(t)$. The $|\nu|$ gapless Majorana modes at each edge can therefore gap out; however particle-hole symmetry (which is preserved in time) demands that they gap out in pairs (since Hamiltonian terms that are linear in Majorana operators violate the conservation of fermion parity). If $|\nu|$ is even (CS_1 is an integer), then all the modes gap out; if $|\nu|$ is odd (CS_1 is a half-integer), then one mode will be left remaining, and the entanglement spectrum will exhibit a degeneracy at times $t > 0$. We see that the condition for entanglement degeneracies

[3] Particle-hole symmetry and fermion parity symmetry are two equivalent descriptions of the symmetries that arise in superconducting systems, and are often used interchangeably.

to persist after time evolution is the same as the condition for the bulk index to remain non-trivial out of equilibrium, i.e. $\mathrm{CS}_1 \mod 1 = 1/2 \Leftrightarrow |\nu|$ is odd. Thus, as long as the time-evolved wavefunction remains topologically non-trivial, the time-dependent entanglement spectrum continues to exhibit degeneracies; however, one can no longer distinguish between wavefunctions whose winding number differs by two.

In class D, the only non-trivial phase has one Majorana mode per edge, and so the degeneracies of such systems out of equilibrium are the same as in equilibrium. In the non-trivial phase of class DIII, a Majorana Kramers pair appears at each edge [25], corresponding to opposite spin states. Because there are an even number of Majorana modes at each edge, these will gap out after time evolution, and so edge degeneracies are not preserved in these systems.

All these results regarding the presence of entanglement degeneracies are connected to the existence of topological invariants that remain robust out of equilibrium, which in turn can be inferred from the non-equilibrium classification. Indeed, the relationship between our classification and the dynamics of the entanglement spectrum can be interpreted in a simple intuitive way: Wavefunctions that are trivial under the non-equilibrium classification by definition can be locally deformed to a product state without breaking any unitary symmetries. Product states are fully unentangled, and so do not exhibit entanglement degeneracies. Therefore, if there were a topological obstruction to gapping out the entanglement spectrum of the time-evolved wavefunction, then it could not be deformed into a product state. Clearly, entanglement degeneracies that remain robust under time evolution necessarily imply that the system is non-trivial in the non-equilibrium classification.

Our results point to universal behaviour in the dynamics of the entanglement spectrum far from equilibrium. The presence or absence of degeneracies can be predicted without knowledge of the microscopic details of the system; one only needs to know which non-equilibrium class the initial state belongs to. We expect that other quantities related to the topological properties of ground state wavefunctions will behave analogously far from equilibrium, e.g. string order parameters [55, 114, 90, 171].

2.4.2 Numerical simulations

To illustrate the connection between topology and the dynamics of the entanglement spectrum in higher dimensions, we perform numerical simulations of quantum quenches in certain two-dimensional systems. Specifically, we consider models models due to Haldane [91] and to Kane and Mele [111] which have become prototypical examples of topological insulators in symmetry classes A and AII, respectively. The edge modes associated with the topological

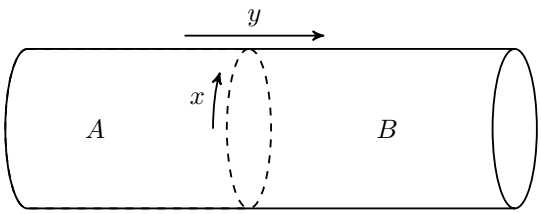

Fig. 2.3 Geometry of the entanglement cut for 2D systems with periodic boundary conditions in the x direction and open boundary conditions with a large system size in the y direction. The dashed line represents the divide between regions A and B.

phases to which these systems belong were described in Section 1.2.2, and will be reflected in the entanglement spectrum of the ground states of each model.

The Haldane model describes spinless fermions $\hat{c}_i^{(\dagger)}$ hopping on a honeycomb lattice (with sublattices A and B), with Hamiltonian

$$\hat{\mathscr{H}}_{\text{Hal}} = J_1 \sum_{\langle j,k\rangle} (\hat{c}_j^\dagger \hat{c}_k + \text{H.c.}) + J_2 \sum_{\langle\langle j,k\rangle\rangle} \left(e^{\mathrm{i}\phi_{jk}} \hat{c}_j^\dagger \hat{c}_k + \text{H.c.} \right) + m \sum_{j\in A} \hat{c}_j^\dagger \hat{c}_j - m \sum_{j\in B} \hat{c}_j^\dagger \hat{c}_j. \quad (2.17)$$

where $\langle j,k\rangle$ denotes nearest neighbours, and $\langle\langle j,k\rangle\rangle$ denotes next-nearest neighbours. The phases ϕ_{jk} originate from a staggered magnetic flux, and are equal to $+\phi$ for anti-clockwise hopping about their common nearest neighbour, and $-\phi$ for clockwise hopping. The mass term m serves to break the inversion symmetry of the lattice. The model possesses two bands corresponding to the sublattice degree of freedom, and realises Chern numbers of 0, $+1$, and -1 for various different parameter regimes.

The Kane-Mele model has the same honeycomb structure, but features spinful fermions $\hat{c}_{i,\alpha}^{(\dagger)}$ where $\alpha = \uparrow, \downarrow$. Instead of a complex hopping (which breaks TRS), the model features a spin-orbit interaction as well as a Rashba interaction. The Hamiltonian is

$$\begin{aligned}\hat{\mathscr{H}}_{\text{KM}} = {} & J_1 \sum_{\langle j,k\rangle,\alpha} (\hat{c}_{j,\alpha}^\dagger \hat{c}_{k,\alpha} + \text{H.c.}) + \mathrm{i}\eta_{\text{s.o.}} \sum_{\langle\langle j,k\rangle\rangle,\alpha,\beta} \nu_{j,k} \hat{c}_{j,\alpha}^\dagger \sigma^z_{\alpha,\beta} \hat{c}_{k,\beta} \\ & + \mathrm{i}\lambda_{\text{R}} \sum_{\langle j,k\rangle,\alpha,\beta} \hat{z} \cdot (\vec{\sigma} \times \vec{r}_{j,k})_{\alpha,\beta} \hat{c}_{j,\alpha}^\dagger \hat{c}_{k,\beta} + m \sum_{j\in A,\alpha} \hat{c}_{j,\alpha}^\dagger \hat{c}_{j,\alpha} - m \sum_{j\in B,\alpha} \hat{c}_{j,\alpha}^\dagger \hat{c}_{j,\alpha}. \quad (2.18)\end{aligned}$$

where $\nu_{j,k} = -1$ $(+1)$ for clockwise (anti-clockwise) next-nearest neighbour hopping, and $\vec{r}_{j,k}$ is a unit vector in the direction from site j to k. We have also included the inversion symmetry-breaking mass term. When $\eta_{\text{s.o.}}$ is sufficiently strong, this model enters a topological quantum spin Hall phase.

The topological invariant pertaining to the former system is the Chern number, which is preserved under unitary dynamics [30, 49]. The latter system is in a topological phase

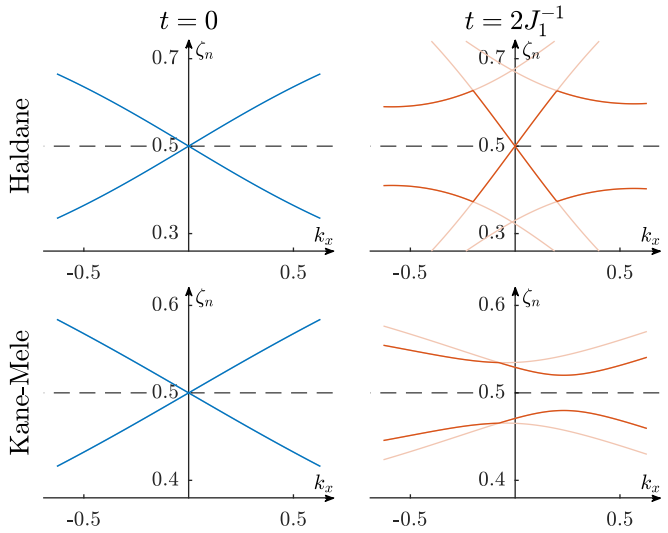

Fig. 2.4 Dynamics of the single-particle entanglement spectrum for the Haldane model (top) and the Kane-Mele model (bottom). In both systems, we start with a topologically non-trivial initial state at $t = 0$ (left), and then time-evolve under a different Hamiltonian by a time $t = 2J_1^{-1}$. The entanglement spectrum of the time-evolved state is plotted (right). In the Haldane model, for which the bulk index is preserved in time, the spectrum remains gapless after time evolution. However, in the Kane-Mele model, which is trivial under the non-equilibrium classification, the edge state becomes gapped at finite times.

protected by time-reversal symmetry only, which is antiunitary, and so must be trivial in our non-equilibrium classification. Therefore, in this case the relevant bulk topological properties will not be preserved under unitary dynamics. For the Haldane model, we expect that the chiral edge modes in the entanglement spectrum of the initial state will remain gapless under time evolution. In the Kane-Mele model, we expect that the helical edge theory describing the low-energy modes of the entanglement spectrum (see Section 1.2.2) will be perturbed by TRS-breaking operators upon time-evolution, e.g. $\hat{\psi}_+^\dagger \hat{\psi}_- + \text{H.c.}$ [using the notation of Eq. (1.11), where $\hat{\psi}_{+(-)}$ annihilates a right-(left-)handed fermion]. The entanglement modes will accordingly acquire a gap.

In each simulation, we apply periodic boundary conditions in the x direction and make the entanglement cut perpendicular to the y direction so that the wavevector k_x is a good quantum number, as illustrated in Figure 2.3.

In our simulation, the initial states are ground states of the Hamiltonians (2.17), (2.18) for a certain set of parameters. We then time-evolve under Hamiltonians with different parameters, and look at the entanglement spectrum of the state after some finite time t_f, which we choose to be $2J_1^{-1}$ in both cases. For the Haldane model quench, we choose $(J_1, J_2, \phi, m)_{t=0} = (1, 0.3, 0.4, 0.1)$, and then change the phase to $(\phi)_{t>0} = -0.2$. For the

Kane-Mele model quench, we choose $(J_1, \eta_{\text{s.o.}}, \lambda_{\text{R}}, m)_{t=0} = (1, 0.5, 0.1, 0.2)$, and then change the spin-orbit coupling to $(\eta_{\text{s.o.}})_{t>0} = 1.5$. Using the method of Peschel [168], one can infer the single-particle entanglement spectrum from the equal-time correlation matrix on the region A. The results are shown in Figure 2.4. We see that the entanglement spectrum of the Haldane model remains gapless after the quench, however in the TRS-protected Kane-Mele model, the entanglement edge mode becomes gapped after the quench. This is consistent with our expectations.

2.5 Response of edge modes to noise

So far, we have studied the dynamics of quantities that, from a theoretical perspective, are extremely useful in identifying topological properties, but are difficult to access in experiment far from equilibrium (with the exception of the CS invariant in one dimension, and the entanglement spectrum in a certain class of Hamiltonians [52]). These properties characterize certain structures in the bulk of the system. On the other hand, many of the proposed technological applications of these phases rely on the topological protection of gapless modes at the edge. For instance, the quantized transverse conductance in the quantum Hall effect is carried along chiral edge modes [92], and the protected Majorana edge modes in 1D systems have potential as hardware in certain quantum computation architectures [122] (see Section 1.2.3). From a practical point of view, it is important to understand how these edge modes behave in systems driven out of equilibrium, and whether the features that facilitate their applications remain robust in this context. Furthermore, given the intimate relationship between bulk and boundary physics in equilibrium, it is natural to ask whether a link exists between the fate of topological invariants and the dynamics of edge modes in non-equilibrium scenarios.

2.5.1 Classical noise

In this section, we will be concerned with systems that are subjected to classical noise: some term in the Hamiltonian that varies stochastically in time. This type of non-equilibrium dynamics can be used to describe a number of different physical scenarios, such as experimental setups where the control over the Hamiltonian is not perfect. Our non-equilibrium classification scheme is well-suited to treat this type of drive, since its conclusions are not specific to the particular way in which the system is driven out of equilibrium. We therefore aim to leverage our results to make universal predictions about the dynamics of edge modes in the presence of noise.

We model the coupling of a system to a classical noise source as follows: The dynamics is described by a time-dependent Hamiltonian $\hat{H}(t)$ that is the sum of the unperturbed part $\hat{H}_0$ and a noise Hamiltonian $\hat{V}(t)$ which can be decomposed into an arbitrary number M of independent channels, each varying stochastically:

$$\hat{V}(t) = \sum_{\alpha=1}^{M} \eta_\alpha(t)\hat{V}_\alpha. \tag{2.19}$$

Without loss of generality, all noise operators $\hat{V}_\alpha$ are assumed to be Hermitian. Crucially, we demand that they are invariant under all the relevant symmetries of the system. The signals $\eta_\alpha(t)$ are real, have zero mean, and are mutually uncorrelated. We consider Gaussian noise, which can be completely characterized by the second moment

$$\overline{\eta_\alpha(t)\eta_\beta(t')} = \delta_{\alpha\beta}\tilde{S}_\alpha(t-t'), \tag{2.20}$$

where $\tilde{S}_\alpha(t-t')$ is the inverse Fourier transform of the noise spectral function $S_\alpha(\omega)$. Overlines denote averages over noise realisations. For scenarios in which time-reversal symmetry is relevant, it is natural that the noise source also be invariant under the reversal of time $\tilde{S}_\alpha(t) = \tilde{S}_\alpha(-t)$, i.e. there is no statistical bias between forward and backward directions of time – this type of noise could therefore be achieved by coupling to a classical bath which is itself governed by time-reversal symmetric equations of motion. Even when this is enforced, a particular realization of the noise will not be invariant under $t \to -t$. This fact will prove crucial when discussing the robustness of edge modes that are protected by antiunitary symmetries.

2.5.2 Coupling to edge modes

We are interested in the effect of noise on systems that exhibit topologically protected edge modes. For concreteness, we will restrict our attention to one-dimensional superconducting systems that possess Majorana-type edge modes (the same classes as those considered in Section 2.4.1). However, unlike before, we will not assume that the system admits a non-interacting description.

In a closed, time-independent system, these edge modes give rise to a degenerate ground state subspace with an energy splitting that is exponentially small in the system size [122]. They are therefore capable of storing quantum information coherently over times that scale inversely with this splitting, making these systems potential platforms for certain quantum

computation architectures [112]. A question of both theoretical and technological importance is whether this coherence survives the introduction of non-equilibrium effects.

In the following, we will consider models that feature two Majorana zero-energy modes at each edge, which is the minimum number for the ground state subspace to form a two-level system. (We will work in a given fermion parity sector, since the number of fermions in the system can only ever change by an even number.) We denote these modes as $\hat{\gamma}^{\alpha}_{\lambda}$, with $\lambda = \mathrm{L}, \mathrm{R}$ denoting the two ends of the system and $\alpha = 1, 2$ labelling the two modes on each end. In addition to fermion parity symmetry, each system possesses some extra symmetry ensuring that there are no Hamiltonian matrix elements which can couple the two $\hat{\gamma}^{\alpha}$ on the same edge – this is the origin of their protection in an isolated system. The symmetry may be unitary (e.g. spin rotation invariance) or antiunitary (e.g. time-reversal symmetry). In the odd fermion parity sector, we have the constraint $\hat{\gamma}^1_{\mathrm{L}}\hat{\gamma}^1_{\mathrm{R}}\hat{\gamma}^2_{\mathrm{L}}\hat{\gamma}^2_{\mathrm{R}} = +1$. The two remaining states are spanned by $|0\rangle$ and $|1\rangle$, which are eigenstates of $\mathrm{i}\hat{\gamma}^1_{\mathrm{L}}\hat{\gamma}^2_{\mathrm{L}}$ with eigenvalue -1 and $+1$, respectively.

An arbitrary qubit can be encoded in the edge modes as

$$|\Psi(t=0)\rangle = \alpha\,|0\rangle + \beta\,|1\rangle\,, \tag{2.21}$$

with $|\alpha|^2 + |\beta|^2 = 1$. A good quantum memory will allow α and β to be recovered after some time (up to an overall unphysical phase of the wavefunction). Processes that modify the complex phase between α and β represent decoherence, and will lead to loss of quantum information. Changes of the magnitude of α and β correspond to the loss of classical information. When the Hamiltonian is time-independent, $|0\rangle$ and $|1\rangle$ are eigenstates with identical energies, and so the state $|\chi\rangle$ is indeed preserved. We now wish to determine whether this still holds in the presence of classical noise.

Models of classical noise are often simplified by taking the limit of 'white noise', where the noise correlators tend to a delta function $\tilde{S}_{\alpha}(t-t') \propto \delta(t-t')$. In the frequency domain, this implies that a given noise signal will feature components of arbitrarily high frequency. Because the fluctuation rate of the noise signal exceeds the gap of the system E_g, bulk excitations will be produced in pairs at a rate that can be estimated from Fermi's golden rule: $\Gamma \sim V^2 \nu(E_g)$, where V quantifies the strength of the noise signal $\|\hat{V}(t)\|$, and $\nu(E_g)$ is the density of bulk states. A single excited bulk mode can propagate to the edge of a system, allowing for the fermion parity of the edge modes to change, and in turn decoherence of the topological qubit. Indeed in the long time limit, the whole system will generically heat to an infinite temperature state, since the noise can increase the energy of the system without bound. These 'direct' heating processes have been well understood previously [81, 99].

For this reason, we will consider the case when $S_\alpha(\omega)$ has a finite width (equivalently, for $\tilde{S}_\alpha(t-t')$ having a finite correlation time). If the spectral function is negligible for frequencies above E_g, then bulk excitations will not occur, and the edge modes will remain decoupled from the bulk. Does this energetic protection then guarantee the coherence of the edge modes? To answer this question, we must consider the dynamics within the ground state subspace, and in particular how it is constrained by symmetries.

2.5.3 Decoherence processes

The systems we consider respect unitary and/or antiunitary symmetries, generated by operators $\hat{U}_S$, $\hat{U}_A$, respectively [Eq. (2.3)]. Within the ground state subspace, the symmetry operations have the effect of toggling between $|0\rangle$ and $|1\rangle$

$$\hat{U}_S|0\rangle = |1\rangle \qquad \text{(Unitary)} \tag{2.22a}$$

$$\hat{U}_A|0^*\rangle = |1\rangle \qquad \text{(Antiunitary)} \tag{2.22b}$$

One can verify that either of these symmetries combined with fermion parity conservation is sufficient to ensure degeneracy of the the ground state subspace[4]. The unitary symmetry is relevant for a system that is composed of two decoupled superconducting chains, for which the fermion parity of each chain is separately conserved, and each chain is in symmetry class D. The antiunitary symmetry is relevant for time-reversal symmetric topological superconductors (in symmetry classes BDI and DIII).

For concreteness, we consider the following preparation and measurement protocol: At the initial time, the system is prepared in the state (2.21) in the absence of noise, i.e. when $\hat{V}(t=0)=0$. The noise is then gradually turned on, and the system proceeds to evolve for a time t_f under a particular noise signal. After this time, the noise is ramped down again, and the state of the system is then measured. Thus the noise signals over the whole sequence start and end at $\eta_\alpha(t=0)=\eta_\alpha(t=t_f)=0$. The specific form of this protocol makes the measurement process at the final time unambiguous, since one can clearly distinguish $|0\rangle$ and $|1\rangle$ at the initial and final times. We will not specify the exact way in which the noise is ramped up and down, understanding that this will not affect our conclusions regarding long-time dynamics; however, we will make use of the fact that each noise trajectory executes a loop in parameter space. We are interested in whether α, β can be recovered at the final time t_f.

[4] We assume that the Hamiltonian is local, meaning the two edges cannot be coupled, and so $\langle i\hat{\gamma}_L^1\hat{\gamma}_L^2\rangle$ is a good quantum number within the ground state subspace

Because the noise is low-frequency, the time-dependent wavefunction can be captured by an adiabatic ansatz

$$|\Psi(t)\rangle = c_0(t)\,|0_{\hat{V}[\eta(t)]}\rangle + c_1(t)\,|1_{\hat{V}[\eta(t)]}\rangle \tag{2.23}$$

where $|0_{\hat{V}[\eta(t)]}\rangle$ and $|1_{\hat{V}[\eta(t)]}\rangle$ are the instantaneous ground states of the Hamiltonian $\hat{H}_0 + \sum_{\alpha=1}^{M} \eta_\alpha(t)\hat{V}_\alpha$, which governs the time evolution at time t. Clearly, $c_0(0) = \alpha$, $c_1(0) = \beta$. A realistic model of noise will feature only local terms, which cannot change the fermion parity in each edge separately; thus $|c_{0,1}(t)|$ are constant in time (assuming we work in a gauge such that $|0_{\hat{V}(t)}\rangle$ and $|1_{\hat{V}(t)}\rangle$ have definite fermion parity on each edge). We therefore need only consider the net phase difference accumulated between the two coefficients.

Now, time evolution is governed by the time-dependent Schrödinger equation

$$\mathrm{i}\frac{\mathrm{d}}{\mathrm{d}t}\,|\Psi(t)\rangle = \left(\hat{H}_0 + \hat{V}(t)\right)|\Psi(t)\rangle\,. \tag{2.24}$$

We insert the adiabatic ansatz (2.23) into Eq. (2.24) to find equations of motion for the coefficients

$$\mathrm{i}\frac{\mathrm{d}c_1(t)}{\mathrm{d}t} = \varepsilon[\eta(t)]c_1(t) - \mathrm{i}\left\langle 1_{\hat{V}[\eta(t)]} \middle| \frac{\mathrm{d}}{\mathrm{d}t} 1_{\hat{V}[\eta(t)]} \right\rangle \tag{2.25}$$

where $\varepsilon[\eta(t)]$ is the instantaneous energy of $|1_{\hat{V}[\eta(t)]}\rangle$, which is always instantaneously degenerate with $|0_{\hat{V}[\eta(t)]}\rangle$. In deriving this equation of motion, we have used

$$\left\langle 1_{\hat{V}[\eta(t)]} \middle| \frac{\mathrm{d}}{\mathrm{d}t} 0_{\hat{V}[\eta(t)]} \right\rangle = 0, \tag{2.26}$$

since the two ground states have opposite fermion parity on each edge, which itself is a good quantum number for all times. A similar equation for $c_0(t)$ can also be derived.

The first term in Eq. (2.25) gives rise to a dynamical phase, and can be eliminated by a parametrization

$$c_1(t) = \tilde{c}_1(t)\exp\left(-\mathrm{i}\int_0^t \mathrm{d}t'\,\varepsilon[\eta(t')]\right) \tag{2.27}$$

such that $\tilde{c}_1(t)$ obeys the equation of motion (2.25) without the first term on the right hand side. The last term of (2.25) is identified as a geometric contribution to the phase of $|\Psi(t)\rangle$. We will find it useful to define the Abelian Berry connection, which is a vector in the

M-dimensional parameter space [spanned by the noise coordinates η^α, as in (2.19)]

$$\begin{aligned}\vec{\mathscr{A}}_{11}[\eta] &:= \left\langle 1_{\hat{V}[\eta]} \middle| \frac{\partial}{\partial \vec{\eta}} 1_{\hat{V}[\eta]} \right\rangle \\ &= \lim_{\delta\vec{\eta}\to 0} \frac{\langle 1_{\hat{V}[\eta]} | 1_{\hat{V}[\eta+\delta\eta]}\rangle - 1}{\delta\vec{\eta}},\end{aligned} \tag{2.28}$$

and $\mathscr{A}_{00}(t)$ is defined analogously. Normalization of $|1_{\hat{V}[\eta+\delta\eta]}\rangle$ requires $\mathscr{A}^*_{11}[\eta] = -\mathscr{A}_{11}[\eta]$. Through this, we write

$$\left\langle 1_{\hat{V}[\eta(t)]} \middle| \frac{\mathrm{d}}{\mathrm{d}t} 1_{\hat{V}[\eta(t)]} \right\rangle = \frac{\mathrm{d}\vec{\eta}(t)}{\mathrm{d}t} \cdot \vec{\mathscr{A}}_{11}[\eta]. \tag{2.29}$$

Note that, although the ground state subspace is degenerate, we do not need to consider a non-Abelian Berry connection, since rotations between the two ground states require a transfer of fermions from one edge to the other, which is a forbidden by locality.

The coherence properties of the qubit can be inferred from the time-dependence of the relative phase of the coefficients. This can be extracted by integrating the equation of motion Eq. (2.25)

$$\begin{aligned}&\frac{c_0(t)}{c_1(t)} = \frac{\alpha}{\beta} e^{\mathrm{i}\phi(t)}, \\ &e^{\mathrm{i}\phi(t)} = \exp\left[-\int_0^t \mathrm{d}t' \frac{\mathrm{d}\vec{\eta}(t')}{\mathrm{d}t'} \left(\mathscr{A}_{11}[\eta(t')] - \mathscr{A}_{00}[\eta(t')] \right) \right].\end{aligned} \tag{2.30}$$

Here, $\phi(t)$ is a real function of time, and is gauge dependent for $t < t_\mathrm{f}$. However, since the noise signal completes its loop in parameter space, its value at $t = t_\mathrm{f}$ is physical, and represents the angle of dephasing between the two states for the particular noise realization under consideration.

The symmetries of the system naturally constrain the form of the geometric phases induced by the noise. Let us first consider the unitary symmetry. From the relation (2.22a), and assuming the Hamiltonian to instantaneously respect the symmetries, we have $|1_{\hat{V}[\eta]}\rangle = \hat{U}_S |0_{\hat{V}[\eta]}\rangle$ for all values of the parameters η. This implies

$$\langle 1_{\hat{V}[\eta]} | 1_{\hat{V}[\eta+\delta\eta]}\rangle = \langle 0_{\hat{V}[\eta]} | \hat{U}_S^\dagger \hat{U}_S | 0_{\hat{V}[\eta+\delta\eta]}\rangle = \langle 0_{\hat{V}[\eta]} | 0_{\hat{V}[\eta+\delta\eta]}\rangle . \tag{2.31}$$

From the definition (2.28), this implies that

$$\mathscr{A}_{11}[\eta] = \mathscr{A}_{00}[\eta]. \qquad \text{(Unitary)} \tag{2.32}$$

In this case, the phases in the exponential of (2.30) cancel, and the phase induced for a particular noise realization is necessarily zero. We conclude that when the protecting symmetry is unitary, the quantum information in the Majorana modes will remain coherent in the presence of noise.

We now turn to the antiunitary symmetry. In this case, the instantaneous ground states are related by Eq. (2.22b)

$$\begin{aligned} \langle 1_{\hat{V}[\eta]} | 1_{\hat{V}[\eta+\delta\eta]} \rangle &= \langle 0^*_{\hat{V}[\eta]} | \hat{U}_A^\dagger \hat{U}_A | 0^*_{\hat{V}[\eta+\delta\eta]} \rangle \\ &= \langle 0_{\hat{V}[\eta]} | 0_{\hat{V}[\eta+\delta\eta]} \rangle^* \\ \Rightarrow \mathscr{A}_{11}[\eta] &= -\mathscr{A}_{00}[\eta], \qquad \text{(Antiunitary)} \end{aligned} \tag{2.33}$$

where we have used the fact that the Berry connection is pure imaginary. The geometric phases for the two ground states therefore do not cancel in Eq. (2.30), and dephasing will generically occur when the phase in question is protected by antiunitary symmetries. This is natural, since Berry phases are complex quantities, which are not invariant under the action of antiunitary symmetries.

When the protecting symmetry is antiunitary and the Berry connections do not cancel, we can estimate the amount of dephasing over a total time t_f. Because the preparation and measurement steps occur in the absence of noise ($\eta_\alpha(t=0) = \eta_\alpha(t=t_f) = 0$), the parameters $\eta_\alpha(t)$ execute a loop in parameter space, so Stokes' theorem can be employed to calculate the dephasing angle

$$\phi(t_f) = -2\mathrm{i} \oint_{\eta(t)} \mathrm{d}\vec{\eta}\,' \cdot \vec{\mathscr{A}}_{11}[\eta'] = -2\mathrm{i} \iint \mathrm{d}S \cdot \Omega_{11}[\eta'] \tag{2.34}$$

where the loop integral in parameter space follows the trajectory determined by the noise realization under consideration, and the double integral is over a surface bounded by that loop. Here $\Omega_{11}[\eta']$ is the Berry curvature at the point η' in parameter space

$$\Omega_{11}^{\alpha\beta}[\eta] = \frac{\partial}{\partial \eta_\alpha} \mathscr{A}_{11}^{\beta}[\eta] - \frac{\partial}{\partial \eta_\beta} \mathscr{A}_{11}^{\alpha}[\eta] \tag{2.35}$$

If the noise amplitudes are small, then the parameters $\vec{\eta}(t)$ explore only a small region of parameter space around the origin, and in this region the Berry flux can be assumed to be a constant tensor[5] $\Omega_{11}^{\alpha\beta}[\eta] \approx \Omega_{11}^{\alpha\beta}$. When there are two noise channels $M = 2$, the Berry

[5] It may be that the Berry curvature tensor vanishes at $\eta_\alpha = 0$, in which case one must expand $\Omega_{11}^{\alpha\beta}[\eta]$ to lowest non-trivial order in η_α, and perform the same calculation. However, this scenario only occurs when the system parameters are fine-tuned, and thus we do not consider this case explicitly here.

phase is approximately given by the signed area swept out by $\vec{\eta}(0 \leq t \leq t_f)$ times the off diagonal value of the Berry curvature Ω_{11}^{xy}. (The same results can be obtained for larger M by projecting onto a two-dimensional surface orthogonal to the Berry flux.) This area can be calculated as

$$A(t_f) = \int_0^{t_f} \mathrm{d}t\, \eta_y(t) \frac{\mathrm{d}\eta_x(t)}{\mathrm{d}t} \tag{2.36}$$

where $\eta_{x,y}$ are the two components of $\vec{\eta}$. In this case we have $\phi(t_f) \approx 2A(t_f)\Omega_{11}^{xy}$.

Now, in a typical run of the experiment, the fidelity $F(t)$ with which the qubit can be extracted after a time t_f is given by the noise-average of $e^{\mathrm{i}\phi(t_f)}$, which for Gaussian noise can be calculated using the cumulant expansion

$$F(t) = \exp\left(-\overline{\phi(t)^2}/2\right) \approx \exp\left(-2\Omega_{11}^{xy}\overline{A(t_f)^2}\right). \tag{2.37}$$

This requires us to calculate the second moment of the swept area

$$\begin{aligned}\overline{A(t_f)^2} &= \int_0^{t_f} \mathrm{d}t \int_0^{t_f} \mathrm{d}t' \overline{\eta_y(t)\eta_y(t')} \frac{\mathrm{d}\eta_x(t)}{\mathrm{d}t} \frac{\mathrm{d}\eta_x(t')}{\mathrm{d}t'} \\ &= \int_0^{t_f} \mathrm{d}t \int_0^{t_f} \mathrm{d}t' \tilde{S}_{xx}(t-t') \frac{\partial^2}{\partial t \partial t'} \tilde{S}_{yy}(t-t').\end{aligned} \tag{2.38}$$

At times t_f much longer than the noise correlation time, we can integrate over the sum and difference of t and t', discarding the corrections at the boundaries of the integral to give

$$\overline{A(t_f)^2} \approx \frac{1}{2} \int_0^{2t_f} \mathrm{d}v \int_{-t_f}^{t_f} \mathrm{d}u\, \tilde{S}'_{xx}(u)\tilde{S}'_{yy}(u). \tag{2.39}$$

We take the correlators $\tilde{S}_{\alpha\alpha}(t)$ to be on the order of V^2 times a dimensionless function of (t/τ_n), where V is the typical strength of the noise and τ_n is the noise correlation time. This dimensionless function will be peaked with a width of order 1, such that the integral over u in the above becomes independent of t_f. We therefore estimate the swept area to be

$$\overline{A(t_f)^2} \sim \frac{t_f V^4}{\tau_n} \tag{2.40}$$

Finally, since the Berry curvature will scale as E_g^{-2}, where E_g is the bulk gap, we find that the qubit fidelity decays exponentially in time

$$F(t_f) = \exp\left(-\gamma t_f\right) \tag{2.41}$$

where the rate γ scales as

$$\gamma \sim \frac{V^4}{\tau_n E_g^4} \tag{2.42}$$

Note that this form for the decoherence rate is qualitatively different from that corresponding to processes in which the bulk is excited (which for a thermal bath has Arrhenius form $\gamma \sim e^{-E_g/T}$).

We see that the dynamically-induced breaking of antiunitary symmetries within the zero-energy edge mode subspace leads to decoherence of quantum information when low-frequency classical noise is present. Most generally, we expect that quantum information will only be robust against such noise if the edge modes can be protected by the unitary symmetries alone – this is equivalent to the condition for a system to be non-trivial in the non-equilibrium classification. Note that, because we have considered low-frequency noise, correlations do not propagate into the bulk of the system. Therefore, the usual caveat regarding finite-time unitary evolution that must be satisfied to make use of the non-equilibrium classification is no longer required, and the classification can be applied to make predictions about long-time physics.

Again, we emphasise that the noise correlation function need not break time-reversal symmetry on average for this dephasing to occur [i.e. we consider the case $\tilde{S}_\alpha(t) = \tilde{S}_\alpha(-t)$]. The dephasing occurs because each realization of the noise will not be invariant under the reversal of time, leading to a phase rotation of $\phi(t_f)$ [Eq. (2.30)]. Even though the distribution of $\phi(t_f)$ is even by time-reversal symmetry, dephasing will occur.

2.5.4 Implications for other non-equilibrium protocols

Models featuring classical noise are generally somewhat phenomenological: the random fluctuation of the Hamiltonian is designed to represent some external process that is effectively random, and occurs independently of the system, i.e. the state of the system does not influence whatever object is giving rise to the noise term. Such models can capture certain types of open systems, which suggests that the the connection between decoherence of quantum information and the non-equilibrium classification may hold in other types of open system. In Chapter 4, we will demonstrate that the classification actually applies much more generally to the dynamics of topological systems coupled to environment, even though the connection to dissipative dynamics is less clear from Definition 3.

However, even if a noisy model is not appropriate for describing the system in question, one can still draw conclusions from the results of the previous sections regarding the ability

of edge modes to store quantum information. Indeed, the angle of dephasing between the two ground states (2.30) can be calculated for any single choice of time-dependent Hamiltonian $\hat{H}(t)$ (assuming it only has frequency components below the gap); this then made it possible to then average over all choices of Hamiltonian trajectory in the noisy case [Eq. (2.37)]. Crucially, for systems that are trivial in the non-equilibrium classification, this angle will depend on the specifics of the particular $\hat{H}(t)$, whereas it is identically zero for systems that are non-trivial in the non-equilibrium classification. In the former case, a reconstruction of the initially stored qubit based on measurements at a later time t_f requires exact knowledge of $\hat{H}(t)$ for $0 \leq t \leq t_f$. If one is not able to determine the microscopic Hamiltonian exactly for all time, then this will lead to uncertainty in the readout of the qubit. Furthermore, even if $\hat{H}(t)$ is known exactly, the problem of determining the state of the system at $t = 0$ from measurements at $t = t_f$ may be classically intractable (e.g. if the system is strongly interacting, time evolving backwards over long times may be exponentially hard).

In contrast, for systems that are non-trivial in the non-equilibrium classification, the angle of dephasing is zero independently of the trajectory of $\hat{H}(t)$. In these cases, any lack of knowledge of the Hamiltonian or inability to simulate the dynamics of the system is not important, and the measurements of the system at $t = t_f$ allows one to fully characterize the qubit stored at $t = 0$.

2.5.5 Numerical simulations

We confirm these theoretical predictions with some numerical simulations of systems that possess Majorana edge modes. We consider three one-dimensional systems in symmetry classes DIII and BDI. As explained in Section 2.3.3, systems in the former class are unstable out of equilibrium, whereas systems in the latter class remain topologically non-trivial under dynamics if the winding number is odd (see Table 2.2). For this reason, we wish to compare systems in class BDI with different values of the topological index, and we expect that only

those which are odd will be protected. The three models we consider, therefore, are

$$\hat{\mathscr{H}}^{\mathrm{DIII}} = \sum_{j,\sigma}\left[\frac{1}{2}\mu_j\hat{c}^\dagger_{j\sigma}\hat{c}_{j\sigma} + J_j\hat{c}^\dagger_{j\sigma}\hat{c}_{j+1\,\sigma} + \Delta_j\hat{c}^\dagger_{j\sigma}\hat{c}^\dagger_{j+1\,\sigma}\right] + \sum_j\left[\Delta^{(s)}_j\hat{c}^\dagger_{j\uparrow}\hat{c}^\dagger_{j\downarrow} + \alpha^R_j\left(\hat{c}^\dagger_{j\uparrow}\hat{c}_{j+1\downarrow} + \hat{c}^\dagger_{j\downarrow}\hat{c}_{j+1\uparrow}\right)\right] + \mathrm{h.c.}; \tag{2.43a}$$

$$\hat{\mathscr{H}}^{\mathrm{BDI}}_{\nu=1} = \sum_{j,\beta}\left[\frac{1}{2}\mu_{j\beta}\hat{c}^\dagger_{j\beta}\hat{c}_{j\beta} + J_{j\beta}\hat{c}^\dagger_{j\beta}\hat{c}_{j+1\,\beta} + \Delta_{j\beta}\hat{c}^\dagger_{j\beta}\hat{c}^\dagger_{j+1\,\beta}\right] + \mathrm{h.c.}; \tag{2.43b}$$

$$\hat{\mathscr{H}}^{\mathrm{BDI}}_{\nu=2} = \sum_{j}\left[\frac{1}{2}\mu_j\hat{c}^\dagger_j\hat{c}_j + J_j\hat{c}^\dagger_j\hat{c}_{j+1} + \Delta_j\hat{c}^\dagger_j\hat{c}^\dagger_{j+1} + J^{(2)}_j\hat{c}^\dagger_j\hat{c}_{j+2} + \Delta^{(2)}_j\hat{c}^\dagger_j\hat{c}^\dagger_{j+2}\right] + \mathrm{h.c.}\,. \tag{2.43c}$$

Model (2.43a) features fermions $\hat{c}_{j\sigma}$ with a spin-1/2 index σ; model (2.43b) features fermions $\hat{c}_{j\beta}$ where the label $\beta = 1,2$ distinguishes two disconnected chains; and Model (2.43c) features spinless fermions $\hat{c}_j$. The various terms featured in the models, all of which can vary spatially, are a chemical potential μ_j; a Rashba spin-orbit coupling term α^R_j; a single-particle hopping amplitude J_j; and a p-wave (s-wave) superconducting pairing amplitude Δ ($\Delta^{(s)}$). The p-wave superconducting and hopping amplitudes can couple fermions either 1 or two sites apart – this difference allows us to access both the $\nu = 1$ and $\nu = 2$ phases in the class BDI cases. Each single-particle Hamiltonian will respect PHS ($U_C U_C^* = +1$) due to the redundancy of the Bogoliubov-de Gennes description [18]. In addition, when the parameters are real, both systems satisfy a TRS. In the spinful system (2.43a) the TRS is symplectic ($U_T U_T^* = -1$), putting it in class DIII. On the other hand, the latter two models possess a TRS satisfying $U_T U_T^* = +1$ due to the spinless nature of the fermions, and hence belong to class BDI.

The chains are duplicated ($\beta = 1,2$) in the model of (2.43b) so that each of the three systems possesses two Majorana modes on each edge. As before, we work in the odd fermion parity sector, within which the ground state is twofold degenerate, spanned by $|0\rangle$, $|1\rangle$ with different eigenvalues of $\mathrm{i}\hat{\gamma}^1_{\mathrm{L}}\hat{\gamma}^2_{\mathrm{L}}$. In models (2.43a) and (2.43c) the zero modes are protected against being gapped out by time-reversal symmetry, whereas in model (2.43b) the protection stems from a unitary symmetry (a conservation of fermion parity in each chain separately). We subject each system to two low-frequency noise channels, with a Lorentzian spectrum $S_\alpha(\omega) \propto (\omega^2 + \Gamma^2)^{-1}$ where the width Γ is much less than the bulk gap.

To quantify the loss of information due to dephasing, we use the 'recovery fidelity' developed by the authors of Ref. [144], wherein the robustness of class D Majorana-based memories to global fluctuations was studied. This quantity characterizes the extent to which the initial information stored can be recovered by some optimal recovery process. To calculate the fidelity, the authors consider two initial pure qubit states, labelled by $+,-$ which are

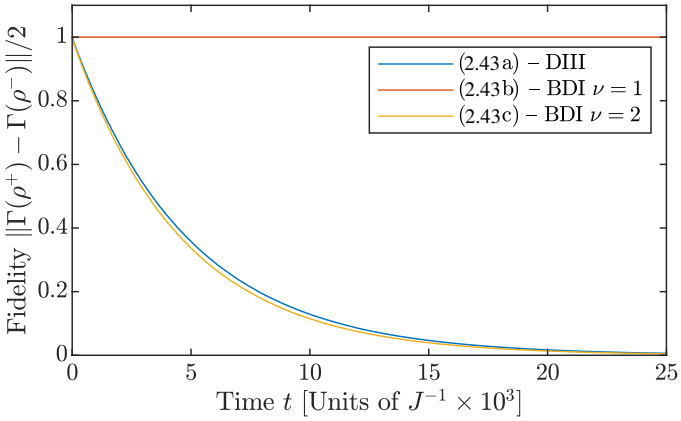

Fig. 2.5 Decoherence of Majorana qubit memories due to temporal noise, as witnessed by the recovery fidelity [Eq. (2.44)]. We compare three systems in $d = 1$ [with Hamiltonians given in Eq. (2.43)], in symmetry classes DIII and BDI. Based on the dynamics of bulk invariants, the topological properties of models (2.43a) and (2.43c) are unstable out of equilibrium, whereas model (2.43b) is stable. This is reflected in the fidelity of storage in the associated Majorana modes when local Lorentzian (TRS) noise is present: The fidelity for the stable model (2.43b) saturates at a constant value, indicating the preservation of the qubit, whereas the initial state information stored in the unstable models decays away completely, indicating that there is no measurement which can be made to extract the initial qubit state.

opposite on the Bloch sphere, i.e. states such that the density matrix in the Majorana subspace is $\hat{\rho}_{\pm} = \hat{\rho}_0^{\text{Bulk}} \otimes \hat{(}1 \pm \hat{\sigma}^x)/2$, where $\hat{\rho}_0^{\text{Bulk}}$ is the ground state density matrix of the bulk, and the $\hat{\sigma}^x$ acts in the Majorana subspace. These initial states are then evolved for a time t under the same realization of the noise potential, and the states obtained from different realizations are averaged to obtain mixed density matrices $\hat{\rho}_{\pm}(t)$. In Ref. [144] it was shown that the optimal process that one can perform to extract the qubit after a time t has a fidelity

$$F^{\text{opt}}(t) = \frac{2}{3} + \frac{1}{6} \|\Gamma_+(t) - \Gamma_-(t)\|_{\text{op}} \tag{2.44}$$

Here, $\|\cdot\|_{\text{op}}$ is the operator norm (which returns the largest eigenvalue), and $\Gamma_{\pm}(t)_{jk} \coloneqq \text{Tr}[\hat{\rho}_{\pm}(t)\hat{\gamma}_j\hat{\gamma}_k]$ is the covariance matrix, where j,k label the set of Majorana operators in the system.

We calculate the time dependence of the fidelity for each of the models (2.43) and plot the results in Figure 2.5. All Hamiltonian parameters are site-independent, except for the noise terms, which act on the two leftmost sites. The initial Hamiltonian parameters chosen are: $(\mu, J, \Delta, \Delta^{(s)}, \alpha^R)^{\text{DIII}} = (0.25, 1, 1, 0.3, 0.2)$ in model (2.43a); $(\mu, J, \Delta)^{\text{BDI}}_{\nu=1} = (0.25, 1, 1)$ in (2.43b); and $(\mu, J, J^{(2)}\Delta, \Delta^{(2)})^{\text{BDI}}_{\nu=2} = (0.25, 0.2, 1, 0.3, 1)$. These values are chosen such that the systems are all in the desired phases, and have approximately equal decay lengths

for the Majorana wavefunctions. Noise is introduced at each edge through an explicit time dependence of μ_j and $\Delta_j^{(s)}$ in (2.43a); $\mu_{j\beta=1,2}$ and Δ_j in (2.43b); and μ_j and Δ_j in (2.43c) (with $j = 1,2$ on the left edge, and $j = N-1,N$ on the right edge). In $\hat{\mathscr{H}}^{\mathrm{BDI}}_{\nu=1}$, the noise signals on the two disconnected wires are independent and uncorrelated. These noise signals have an amplitude such that the root mean square of the signal $\sqrt{C(t=0)} = 0.1$. We choose the width of the Lorentzian noise spectrum to be small $\Gamma = 0.02$, so as to minimise coupling of the edges and bulk. The length of each chain is $N = 24$, and the density matrices are averaged over 20 noise realisations.

In model (2.43b), the non-equilibrium classification that we derived using is non-trivial, which we argue ensures that qubits do not decohere. As expected, the recovery fidelity is unaffected by the noise, and remains at 1. On the other hand, models (2.43a) and (2.43c) are trivial out of equilibrium according to our classification. In these cases, the recovery fidelity decays until the states which started with opposite qubit values become indistinguishable from one another. There is thus no way of extracting the qubit in these cases where the system topology is destroyed by non-equilibrium effects.

Chapter 3

Computing the Non-Equilibrium Classification

In the previous chapter, we defined a topological classification for systems driven far from equilibrium, and demonstrated how it can be used to predict universal behaviour in a variety of non-equilibrium scenarios. The aim of this chapter is to explicitly compute this classification for a wide variety of systems with physically relevant symmetries. Although there are some simple cases for which the non-equilibrium classification can be immediately determined given knowledge of the equilibrium classification (see Section 2.2), in many cases new theoretical methods must be developed to obtain the desired results. The mathematical formalisms that are appropriate to the task in hand may depend on the system's dimensionality and particle statistics, as well as the presence or absence of interactions, and whether spatial and/or non-spatial symmetries are to be included. We will focus on two regimes here: non-interacting fermionic systems within the tenfold way (Section 3.1), and interacting bosonic SPTs with non-spatial symmetries (Section 3.2). In each case, we will briefly review how the equilibrium classification is constructed, and then describe how we can generalize the relevant techniques to derive the non-equilibrium classifications. Our results are summarised in Tables 3.1 and 3.3 for free-fermion and interacting boson systems, respectively.

3.1 Tenfold way

As described in Section 2.3, the tenfold way encompasses non-interacting fermionic systems with non-spatial symmetries [Eqs. (2.9)]. The equilibrium topological classification of the tenfold way is provided in Table 2.1. Its periodic structure is evident: the classification for a given symmetry class is related to that of another symmetry class by an appropriate shift

of spatial dimension. To derive the classification and understand its periodic structure, a number of methods can be used, such as those based on topological terms in nonlinear sigma models [193, 194], or K-theory [120]. We find that the method that is most easily adapted for our purposes is dimensional reduction, which is based on establishing mappings between topological ground states in different spatial dimensions and different symmetry classes that preserve all topological phase boundaries. We first review how this method can be used to derive the equilibrium table, before using it to compute the non-equilibrium classification. As in Chapter 2, our discussion will mostly refer to systems with discrete translation invariance, however the phases in question are all stable against symmetry-preserving perturbations that break this invariance.

3.1.1 Dimensional reduction in equilibrium

The starting point of the dimensional reduction procedure is to determine the set of topological phases and associated bulk invariants in the absence of symmetries (class A). The invariants are all functionals of the Bloch wavefunctions $|u^n(k)\rangle$. A central quantity in the following is the non-Abelian Berry connection in momentum space

$$\mathscr{A}^{nm}(k) = A_\mu^{nm}(k)\mathrm{d}k^\mu := \langle u^n(k)\,|\,\mathrm{d}u^m(k)\rangle\,. \tag{3.1}$$

$\mathscr{A}^{nm}(k)$ is a differential 1-form with matrix structure from the band indices, which run over occupied bands only (we will use Latin letters $n, m, \ldots$ to index the bands, and Greek letters $\mu, \nu, \ldots$ for the components of the momentum space). The associated Berry curvature is a gauge-invariant 2-form

$$\mathscr{F}^{nm}(k) = \frac{1}{2}F_{\mu\nu}^{nm}(k)\mathrm{d}k^\mu \wedge \mathrm{d}k^\nu := \mathrm{d}\mathscr{A}^{nm} + (\mathscr{A}\wedge\mathscr{A})^{nm}. \tag{3.2}$$

The nth Chern character is then defined as [187]

$$\mathrm{ch}_n(k) = \frac{1}{n!}\,\mathrm{Tr}\left(\frac{\mathrm{i}\mathscr{F}}{2\pi}\right)^n \tag{3.3}$$

In $d = 2n$ spatial dimensions, the Chern character can be integrated over the Brillouin zone to obtain the nth Chern number, which is quantized to an integer (assuming that the Bloch functions $|u^n(k)\rangle$ describe an area-law entangled many-body wavefunction)

$$\mathrm{Ch}_n := \int_{\mathrm{BZ}} \mathrm{ch}_n(k) \in \mathbb{Z}. \tag{3.4}$$

These bulk indices generalise the first Chern number Ch_1, which we encountered in the context of the quantum Hall effect [212]. The Chern numbers serve as topological invariants in even-dimensional systems; in systems with odd spatial dimension, there are no free-fermion phases in the absence of symmetry [193].

Starting from this simple classification for systems without any symmetries, dimensional reduction can be used to classify systems with symmetries. The details of this procedure depend on whether the system in question features a chiral symmetry or not. We therefore consider the two cases separately here.

Non-chiral symmetry classes

Topological phases with different nth Chern numbers may or may not be compatible with the addition of symmetries. For example, if time-reversal symmetry is imposed on a two-dimensional system, then the first Chern number necessarily vanishes. Similarly, chiral symmetry forces all Chern numbers to vanish. However, for particular combinations of symmetries and spatial dimensions, the Chern number is unrestricted – the entries in Table 2.1 for which this is the case are termed the 'even primary series'. The equilibrium classification of these systems is denoted '$\mathbb{Z}$' (i.e. the group[1] of integers, representing the different possible values of Ch_n). For certain other combinations of d and symmetry class, the Chern number is restricted to take only even values, in which case we denote the classification as '$2\mathbb{Z}$'[2].

Note that in these systems, the topological properties of the system persist even when the symmetry is broken. Therefore, in the framework of Chen et al. [38], these systems are long-range entangled, rather than SPT ordered. Despite this distinction, the equilibrium and non-equilibrium topological properties of these systems can understood on the same footing.

The dimensional reduction procedure is based on embedding the Brillouin zone (BZ) of the physical d-dimensional system within the BZ of a $(d+r)$-dimensional system, in a way such that all symmetries are preserved. For example, in a four-dimensional time-reversal symmetric system (class AII), one can restrict the Bloch functions $|u^n(k_1,\ldots,k_4)\rangle$ to the three-dimensional subspace $k_1 = \pi$, and obtain a valid description of three-dimensional time-reversal symmetric system [154]. Given that the four dimensional system belongs to the even primary series, one can try to learn about the topology of a physical three-dimensional system from the Chern number of its parent.

[1] Each entry of the classification table has an Abelian group structure. The group operation represents a 'stacking' of two systems, e.g. if two systems with Chern numbers $n_1, n_2 \in \mathbb{Z}$ are coupled together without closing the gap of the combined system, then the full system has a Chern number of $n_1 + n_2$ [120].

[2] The group $2\mathbb{Z}$ is of course isomorphic to $\mathbb{Z}$, but we include the 2 to signify that only even topological invariants are permitted.

Using this approach, one finds that for each member of the even primary series in d dimensions, the classification in dimensions $(d-1)$ and $(d-2)$ is $\mathbb{Z}_2$. These entries termed the first and second descendants, respectively [177]. Let us prove this for the four-dimensional class AII example. (All other descendants of the primary series can be understood in analogous ways.) As in Section 2.3.2, we will make use of the ground state single-particle density matrix $\rho(k)$ rather than the Hamiltonian, since this formulation can be naturally generalized to the non-equilibrium problem.

Consider a 3D TRS ground state characterized by the density matrix $\rho(\vec{k})$ as our physical system. To understand whether this system is in an SPT phase, one can attempt to adiabatically connect it to some trivial reference state ρ^{ref}, which can be chosen to be independent of $\vec{k}$ thus representing a uniform product state. One can always construct a one-parameter family of states $\rho_4(\vec{k},\theta)$ that continuously connects the physical system $\rho(\vec{k})$ at $\theta = 0$ to ρ^{ref} at $\theta = \pi$. TRS will generally be broken for $0 < \theta < \pi$ (indeed this will be necessary if $\rho(\vec{k})$ is topologically non-trivial). Now one can close this path into a loop $\theta \in (-\pi, \pi]$ by invoking a 'super-TRS' condition

$$\rho_4(-\vec{k},-\theta) = U_T \rho_4(\vec{k},\theta)^* U_T^\dagger \qquad\qquad 0 \leq \theta \leq \pi, \tag{3.5}$$

where U_T is the TRS operator. Since $\rho(\vec{k})$ and ρ^{ref} respect TRS, this loop can be made without any discontinuities. If θ is reinterpreted as an extra momentum variable in 4D, then $\rho_4(\vec{k},\theta)$ describes a four dimensional TRS insulator. Since class AII in $d = 4$ belongs to the even primary series, this 'parent' system can be characterized by the second Chern number Ch_2.

Because the reference Hamiltonian ρ^{ref} is $\vec{k}$-independent, the regions of the 4D Brillouin zone at $\theta = \pm\pi$ can be contracted to a single point. The higher dimensional momentum space is therefore topologically equivalent to a 'suspension' $\Sigma(\text{BZ})$, as illustrated in Figure 3.1. The second Chern number is the integral of the Chern form ch_2 over $\Sigma(\text{BZ})$ [Eq. (3.4)], which can be split into two contributions from $\theta > 0$ and $\theta < 0$, i.e. the North and South hemispheres. Following Teo and Kane [209], one can show that the super-TRS condition (3.5) implies that the two contributions are equal, and so we need only consider one hemisphere, which we call $\Sigma^N(\text{BZ})$. The Chern form ch_2 is exact, which means it can be written as a total derivative of a lower differential form, called the Chern-Simons form Q_{2n-1}, i.e. $\text{ch}_n = \text{d}Q_{2n-1}$ (here we have $n = 2$) [187]. Thus, using Stokes' theorem the integral over $\theta > 0$ can be computed as a surface integral on the boundary $\theta = 0$, i.e. the physical BZ, giving

$$\text{Ch}_2 = 2\int_{\Sigma^N(\text{BZ})} \text{ch}_2 = 2\int_{\text{BZ}} Q_3 =: 2\text{CS}_3, \tag{3.6}$$

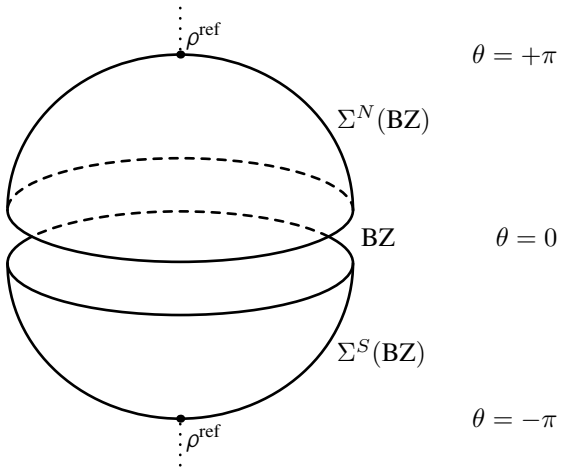

Fig. 3.1 The physical Brillouin zone (BZ) as the equator of a higher dimensional momentum space parametrized by $(\vec{k}, \theta)$. At the poles $\theta = \pm\pi$, the BZ is contracted to a point, representing the $\vec{k}$-independent reference state. The higher dimensional BZ is a suspension of the physical BZ, denoted $\Sigma(\text{BZ})$.

where CS_3 is the Chern-Simons (CS) invariant (the three-dimensional generalisation of CS_1). Because this latter integral is evaluated on the physical BZ, this invariant can be explicitly calculated from $\rho(k)$.

The CS invariant is gauge invariant only up to an integer. This gauge dependence reflects the fact that different embeddings of $\rho(\vec{k})$ in the 4D BZ can yield Chern numbers that differ by an even integer. Therefore, $[\text{Ch}_2 \bmod 2]$ (or equivalently $\text{CS}_3 \bmod 1$) is an unambiguous $\mathbb{Z}_2$-valued topological invariant that pertains to the 3D system – this relates the first descendant (3D) to the primary series (4D) in class AII.

An entirely analogous construction can be used to relate a 2D class AII insulator to a 3D parent system. Again, the topology of the higher-dimensional insulator is inherited by the lower-dimensional system, and one finds a $\mathbb{Z}_2$ index that characterizes two-dimensional systems, known as the Fu-Kane (FK) invariant. However, applying this procedure again to 1D systems fails (see Ref. [177] for details). Note also that entries with $2\mathbb{Z}$ classifications do not have descendants, since if the Chern number is always even, then the CS invariant of the lower-dimensional system must always be 0 mod 1.

Chiral Symmetry Classes

The above construction relates topological classifications in different spatial dimensions for the same symmetry class, and only applies to those classes with no chiral symmetry. One can also construct dimensional reduction procedures that relate systems in different symmetry classes. The simplest case involves systems with only chiral symmetry (class

AIII) in odd spatial dimensions. The procedure has to be slightly modified from the above. Given a state $\rho(\vec{k})$ which respects chiral symmetry [Eq. (2.12c)], we can uniquely specify a higher-dimensional state via [210]

$$\rho_{d+1}(\vec{k},\theta) = \rho(\vec{k})\cos(\theta/2) - \frac{1}{2}U_S\sin(\theta/2) + \frac{1}{2}\left[1-\cos(\theta/2)\right] \qquad \theta \in [-\pi,\pi), \quad (3.7)$$

where U_S is the chiral symmetry operator, and the last term enforces the correct trace. Again, $\rho_{d+1}(\vec{k},\theta)$ is k-independent at $\theta = \pm\pi$, so the higher dimensional BZ is a suspension (Fig. 3.1). The addition of a term proportional to U_S breaks the chiral symmetry, and so the $(d+1)$-dimensional Hamiltonian belongs to class A and is characterizable by a Chern number $\mathrm{Ch}_{(d+1)/2}$. It can be rigorously shown that under the mapping (3.7), topologically distinct physical systems have parents with different Chern numbers, and vice-versa [210]. A simple (albeit less precise) way to see how the Chern number of $\rho_{d+1}(\vec{k},\theta)$ relates to the topology of $\rho(\vec{k})$ is by noticing that the higher dimensional system obeys an unusual symmetry

$$U_S\rho_{d+1}(\vec{k},\theta)U_S^\dagger = 1 - \rho_{d+1}(\vec{k},-\theta) \quad (3.8)$$

which implies that the Chern character $\mathrm{ch}_{(d+1)/2}(\vec{k},\theta)$ is again even under $\theta \to -\theta$. By arguments analogous to those used to derive Eq. (3.6), we then have $\mathrm{Ch}_{(d+1)/2} = 2\times \mathrm{CS}_d \bmod 2$, which quantizes the Chern-Simons invariant to a half integer modulo 1. Moreover, there exists a gauge specified by the chiral symmetry operator in which the integer part of CS_d is unambiguously determined and we have $\mathrm{Ch}_{(d+1)/2} = 2\mathrm{CS}_d$ (without the modulo 2)[3]. Therefore, two systems whose dimensional extensions (3.7) have different Chern numbers cannot be adiabatically connected while maintaining chiral symmetry. These systems are accordingly $\mathbb{Z}$-classified.

If the physical system also respects TRS and PHS (classes BDI, DIII, CII, and CI), then we can still use the mapping (3.7). In this case the symmetry of the higher dimensional system changes according to [for $d \to (d+1)$ dimensions] [187]

$$\mathrm{AIII} \to \mathrm{A}; \quad \mathrm{BDI} \to \mathrm{D}; \quad \mathrm{CII} \to \mathrm{C}; \quad \mathrm{DIII} \to \mathrm{AII}; \quad \mathrm{CI} \to \mathrm{AI}. \quad (3.9)$$

These relations determine the ordering of the symmetry classes given in Table 2.1. As before, topologically distinct physical systems map onto topologically distinct parents and vice-versa. This holds regardless of whether the parent is classified by a Chern number,

[3] See Ref. [187], Eq. (41) and the discussion therein for a details of the gauge dependence of the various quantities discussed here.

Chern-Simons invariant, etc. Therefore, the physical system has the same classification as in $(d+1)$ dimensions in the symmetry class given by (3.9). This completes the derivation of the tenfold way in equilibrium.

3.1.2 Dimensional reduction out of equilibrium

Having described how the equilibrium classification can be obtained using dimensional reduction procedures, we now adapt these methods in order to derive the non-equilibrium classification, following our analysis in Ref. [146]. To do so, we introduce a non-equilibrium version of dimensional reduction in the following way: Starting with an initial state $\rho(k,t=0)$ belonging to a particular symmetry class in d dimensions, we construct the higher-dimensional insulator in $(d+r)$ dimensions $\rho_{(d+r)}(k,\theta,t=0)$ in the appropriate manner for the equilibrium classification (θ is an r-dimensional vector). The physical (d-dimensional) system evolves under the final Hamiltonian $H^{\mathrm{f}}(k,t)$. We then dimensionally extend this final Hamiltonian to $H^{\mathrm{f}}_{(d+r)}(k,\theta,t)$ and consider the time-evolution of the higher-dimensional system, whilst ensuring that the $\theta=0$ subspace remains true to the physical system. By examining the time-evolved state in $(d+r)$ dimensions $\rho_{(d+r)}(k,\theta,t)$, we can infer the topological properties of the physical time-evolved system. Importantly, as in equilibrium, our conclusions regarding the topology of the physical system should be independent of the choice of embedding in this higher dimensional space; however one should be restricted to embeddings which respect the relevant symmetries of the system, e.g. by enforcing the super-TRS condition (3.5).

Although the dimensional reduction parameter θ is often interpreted as a time coordinate which traces out an adiabatic evolution of the ground state, one should not confuse this parameter with the physical (generally non-adiabatic) time evolution in our non-equilibrium protocol. Instead, θ can be thought of as a coordinate which labels a one-parameter family of independent non-equilibrium protocols.

Having described the general procedure, we now systematically construct our non-equilibrium table of topological insulators, considering each series in turn.

Primary series in $d=2n$

As previously discussed, the primary series in even dimensions refers to the $\mathbb{Z}$-valued entries of the equilibrium table, and these systems are classified by the Chern numbers. Each member of the even primary series possesses at most one symmetry which, roughly speaking, is irrelevant for the topology of the system, since the classification is neither restricted nor enriched by its addition.

Class	Symmetries			Spatial dimension d							
	U_T	U_C	U_S	0	1	2	3	4	5	6	7
A	0	0	0	$\mathbb{Z}$	0	$\mathbb{Z}$	0	$\mathbb{Z}$	0	$\mathbb{Z}$	0
AIII	0	0	1	0	$\mathbb{Z} \to 0$	0	$\mathbb{Z} \to 0$	0	$\mathbb{Z} \to 0$	0	$\mathbb{Z} \to 0$
AI	+	0	0	$\mathbb{Z}$	0	0	0	$2\mathbb{Z}$	0	$\mathbb{Z}_2 \to 0$	$\mathbb{Z}_2 \to 0$
BDI	+	+	1	$\mathbb{Z}_2$	$\mathbb{Z} \to \mathbb{Z}_2$	0	0	0	$2\mathbb{Z} \to 0$	0	$\mathbb{Z}_2 \to 0$
D	0	+	0	$\mathbb{Z}_2$	$\mathbb{Z}_2$	$\mathbb{Z}$	0	0	0	$2\mathbb{Z}$	0
DIII	−	+	1	0	$\mathbb{Z}_2 \to 0$	$\mathbb{Z}_2 \to 0$	$\mathbb{Z} \to 0$	0	0	0	$2\mathbb{Z} \to 0$
AII	−	0	0	$2\mathbb{Z}$	0	$\mathbb{Z}_2 \to 0$	$\mathbb{Z}_2 \to 0$	$\mathbb{Z}$	0	0	0
CII	−	−	1	0	$2\mathbb{Z} \to 0$	0	$\mathbb{Z}_2 \to 0$	$\mathbb{Z}_2$	$\mathbb{Z} \to \mathbb{Z}_2$	0	0
C	0	−	0	0	0	$2\mathbb{Z}$	0	$\mathbb{Z}_2$	$\mathbb{Z}_2$	$\mathbb{Z}$	0
CI	+	−	1	0	0	0	$2\mathbb{Z} \to 0$	0	$\mathbb{Z}_2 \to 0$	$\mathbb{Z}_2 \to 0$	$\mathbb{Z} \to 0$

Even primary Even descendants Odd primary Odd descendants $2\mathbb{Z}$ series

Table 3.1 Classification of topological insulators and superconductors out of equilibrium. The non-equilibrium classification describes the equivalence classes of symmetry-respecting wavefunctions that cannot be mutually connected under finite-time unitary evolution (see Section 2.1). The ten symmetry classes of the ten-fold way are listed on the left, and defined by the presence (+,−, 1) or absence (0) of time-reversal (U_T), particle-hole (U_C), and chiral (U_S) symmetries [6, 193]. For each symmetry class and spatial dimension d, the equilibrium and non-equilibrium classifications are given. A single entry indicates that the classification does not change out of equilibrium, and the notation $G_1 \to G_2$ indicates that the classification changes from G_1 in equilibrium to G_2 out of equilibrium. The different series of the classification are coloured as described in the main text and labelled below the table. Systems in dimension $d > 7$ have the same classification as the corresponding system in $(d-8)$ dimensions (Bott periodicity).

Because the Chern number is a discrete topological invariant that is always well-defined, it must remain constant in time out of equilibrium, independently of any symmetry properties (as discussed in Section 2.1). This behaviour has been explicitly proved for two dimensional systems in previous studies [72, 188, 49, 30]. Wavefunctions with different Chern numbers therefore cannot be connected under finite-time unitary evolution, and so the non-equilibrium classification is the same as the equilibrium classification ($\mathbb{Z}$). The primary series in $d = 2n$ are coloured black in Table 3.1.

As we found for the one-dimensional bulk index CS_1, finite-size systems possess a time L/v_{LR} beyond which the discrete nature of momentum space makes the derivatives in Eq. (3.1) poorly defined, and so it is meaningless to consider the dynamics of the Chern number. These scenarios fall outside the scope of the non-equilibrium classification, since they involve unitary evolution over times that are extensive in the system size.

First and second descendants in $d = 2n-1$ and $d = 2n-2$

The first and second descendants of the even primary series are derived by dimensionally extending the physical system, as described in Section 3.1.1. We can consider the dynamics of the higher-dimensional system to inform us about topological properties of the descendants when driven far from equilibrium.

If the descendants are PHS-protected (class D in $d = 0,1$ and class C in $d = 4,5$), then we can dimensionally extend the initial state and final Hamiltonian in a PHS-symmetric way. Because PHS is unitary (and thus does not undergo dynamically-induced symmetry breaking), this ensures that $\rho_{(d+r)}(k,\theta,t)$ will respect PHS for all time. We can then apply the usual arguments that relate the topological properties of $\rho(k,t)$ and $\rho_{(d+r)}(k,\theta,t)$ to the time-evolved state. Since the higher-dimensional system belongs to the even primary series, its Chern number remains well-defined and constant in time (Section 3.1.2). Accordingly, the topological properties of the physical system cannot change in time. The non-equilibrium classification for these systems is therefore the same as in equilibrium ($\mathbb{Z}_2$).

Analogously, if the descendants are TRS-protected (class AII in $d = 2,3$ and class AI in $d = 6,7$), then we extend the initial state and final Hamiltonian in a TRS-respecting way [Eq. (3.5)]. However, for $t > 0$ the $(d+r)$-dimensional extended state $\rho_{(d+r)}(k,\theta,t)$ will not respect TRS due to dynamically-induced symmetry breaking. Although the Chern number of the parent system remains constant in time, it can no longer be used to infer properties of the physical system, because of the breaking of TRS. More explicitly, for first descendants, we find that the relationship (3.6) between Ch_n and CS_{2n-1} no longer holds, because the contributions to Ch_n for $\theta > 0$ and $\theta < 0$ are not equal once TRS is dynamically broken. The CS invariant will therefore no longer be quantized, and will vary continuously in time, as

we saw for class AIII in $d = 1$ (Section 2.3.3). The non-equilibrium classification for these systems must therefore be trivial, since there is no obstruction to time-evolving between TRS-respecting wavefunctions belonging to different SPT phases. The second descendants, being derived from the first descendants, must also be trivial out of equilibrium[4]. All the cases covered in this section are marked in blue in Table 3.1.

Primary series in $d = (2n-1)$

We now turn to $\mathbb{Z}$-classified systems that feature a chiral symmetry, i.e. the odd primary series. Let us start with the case where the only symmetry present is chiral (class AIII in $d = 2n-1$). These systems are related to class A systems in $(d+1)$ dimensions via the extension (3.7). The symmetry (3.8), which is inherited from the chiral symmetry of the phyical system, allowed us to relate the Chern-Simons invariant of the physical system CS_d to the Chern number of the parent $\mathrm{Ch}_{(d+1)/2}$ (although only modulo 2). However, chiral symmetry is broken under time evolution. Eq. (3.8) is then no longer true, and the arguments used to relate the two systems do not hold. As we saw for the TRS descendants, the contributions to the Chern number from the two hemispheres $\theta > 0$ and $\theta < 0$ are no longer equal, and so CS_d is not quantized. The non-equilibrium classification for systems in class AIII is therefore trivial.

For members of the odd primary series that possess TRS and PHS in addition to chiral symmetry, we must consider how the classification is affected by the symmetries of the higher-dimensional system. In particular, the parent Hamiltonian will respect either TRS or PHS, according to Eq. (3.9). If the parent possesses TRS (as for DIII and CI, which have class AII and AI parents, respectively), then the above arguments are unchanged, since TRS will be dynamically broken. The non-equilibrium classification is therefore trivial. However, if the higher dimensional system possesses PHS (as for BDI and CII, which have class D and C parents, respectively), then we must account for this extra symmetry. We have seen that the contributions to $\mathrm{Ch}_{(d+1)/2}$ from the two hemispheres are equal if either PHS or the symmetry (3.8) is present. While the latter is dynamically broken, the former is not. Therefore, for these classes the relation $\mathrm{Ch}_{(d+1)/2} = 2 \times \mathrm{CS}_d \bmod 2$ still holds for $t > 0$, although the integer part of CS_d can no longer be resolved. The non-equilibrium classification is then reduced from $\mathbb{Z}$ to $\mathbb{Z}_2$. In essence, once chiral symmetry is broken, the primary series for classes BDI and

[4]Unlike the first descendants, the relevant bulk index for second descendants (the Fu-Kane invariant [75]), does not vary in time [138]; however the above argument highlights that the FK invariant is no longer appropriate for capturing topological properties far from equilibrium. Indeed, the FK invariant must be calculated in a gauge specified to the TRS operator in order to be unambiguously defined, and once TRS is dynamically broken this gauge is no longer well-defined.

CII are reduced to first descendants of the class D and C primary series, respectively. The odd primary series are marked in red in Table 3.1.

First and second descendants in $d = (2n-1)-1$ and $d = (2n-1)-2$

The non-equilibrium classification for the descendants in chiral symmetry classes can be understood in a similar way to the odd primary series. In equilibrium, the dimensionally extended system (3.7) respects either TRS or PHS [Eq. (3.9)]. Again, due to dynamically-induced symmetry breaking, we cannot rely on TRS or chiral symmetry to relate the classifications of the physical system to the parent for $t > 0$, and so in classes DIII and CI the non-equilibrium classification is trivial. For the first descendants in classes BDI and CII, the parent systems are themselves first descendants in classes D and C respectively. Once chiral symmetry is broken, the physical system can be understood as a PHS-protected second descendant. The non-equilibrium classification is $\mathbb{Z}_2$.

However, if we go to one lower dimension, then a generalisation of the above arguments would require us to interpret the physical system as a *third* descendant of the even primary series. As shown in Ref. [177], one cannot derive a topological invariant in such a way. Even though PHS is preserved, there is no topological invariant that we can define for the system that relies only on PHS, and so the non-equilibrium classification for these systems is trivial. The systems studied in this section are marked in orange in Table 3.1.

$2\mathbb{Z}$ classified systems

The only systems that remain to be classified are those which have a $2\mathbb{Z}$ classification in equilibrium; these occur four dimensions below the primary series. In even dimensions, these are classified by the Chern number just as in the primary series, but the extra symmetry implies that the Chern number must be even [187]. We can employ exactly the same reasoning as in Section 3.1.2 to show that this even Chern number must be constant in time, and so the non-equilibrium classification is the same as in equilibrium.

In odd dimensions the $2\mathbb{Z}$ systems are classified in the same way as the odd primary series, with the understanding that only even topological indices are possible. We have seen that for the odd primary series, the relevant invariants either become non-quantized (classes CI and DIII), or their parity is preserved (classes BDI and CII). However, since the initial state must have a topological invariant of even parity, all states become topologically equivalent out of equilibrium, and the classification is trivial. The systems covered in the above are coloured green in Table 3.1.

3.1.3 Structure of the non-equilibrium tenfold way

Having considered all symmetry classes in all spatial dimensions, we arrive at our non-equilibrium classification for the tenfold way given in Table 3.1. Some comments on its structure are required.

The fact that PHS is the only symmetry that is preserved under dynamics indicates that the wavefunction will belong to one of the symmetry classes A, D, or C for $t > 0$. The equilibrium classification of these classes therefore acts as a 'upper bound', in that the non-equilibrium entry must be a subgroup of the corresponding equilibrium entry A, D, or C. The reason that the non-equilibrium classification is not simply given by the equilibrium classification in the corresponding class is that antiunitary symmetries can still prevent certain topological phases from being realised in the first place, despite not being preserved under time evolution. For instance, TRS forbids a non-trivial Chern insulator in two dimensions, and so the non-equilibrium classification is not $\mathbb{Z}$, but 0. In $d = 3$ and 7, the equilibrium classifications of classes A, D, and C are all 0, hence all non-equilibrium classifications in $d = 3$ and 7 are 0.

The equilibrium table exhibits two forms of periodicity: Firstly, the table is invariant if all spatial dimensions are shifted by $d \to d+8$. This is naturally also seen in our non-equilibrium table, since all our arguments are invariant under such an eightfold dimensional shift. The equilibrium table is also invariant if the dimension is increased by one and the symmetry classes are all shifted down in the order that they are given in Table 3.1 (for real and complex classes separately). This full periodicity is not reflected in the non-equilibrium classification, because of the differences between the three symmetries: only PHS is preserved out of equilibrium. However, a subset of this periodicity survives. For each of the real symmetry classes, there is another class in which the same types of symmetry are present, but the quantities $U_T U_T^*$ and $U_C U_C^*$ have opposite sign – these appear four rows above or below. Because PHS and TRS are respectively preserved and broken independently of these values, our arguments can still be applied when the spatial dimension is shifted by $d \to d+4$, and these pairs of symmetry classes are all swapped.

3.2 Interacting bosonic SPTs

While the topological phases within the tenfold way are robust against weak interactions, they all have free-fermion representatives. In contrast, some SPTs do not admit a non-interacting description, and these are referred to as strongly interacting, or strongly correlated phases. In particular, all topological phases of bosons must be of this kind, since the ground states of non-interacting bosonic systems are trivial condensates. In this section, we derive the

non-equilibrium classification for interacting bosonic SPTs with non-spatial symmetries, the results of which are summarised in Tables 3.2 and 3.3.

The single-particle quantities discussed in the previous section do not contain enough information to encode the various topological properties relevant to interacting SPTs. Instead of working with $\rho(k)$, we must instead adopt the theoretical technology used to describe many-body wavefunctions with area-law entanglement, since these are the states that are relevant for our classification. As already mentioned in Section 1.1.2, there exist particular many-body wavefunction ansätze for which the area law is manifestly satisfied. The most commonly used are matrix-product states [68, 167] (MPS) and their generalization to higher dimensions, known as projected entangled-pair states (PEPS) [218, 220]. Not only are these wavefunctions useful from a computational perspective, but they also allow one to construct analytical arguments regarding the topological properties of ground state wavefunctions. Specifically, through studying the space of all possible symmetry-respecting MPS and PEPS wavefunctions, a classification of bosonic SPT phases in equilibrium has been put forward[5]. For simplicity, we find it helpful to first consider one-dimensional systems. We review how the classification is derived, and then generalise those arguments to construct the non-equilibrium classification. We then explain how our methods pertaining one-dimensional can be extended to all spatial dimensions, using group cohomological methods.

3.2.1 One dimensional interacting SPTs in equilibrium

The methods used to classify one-dimensional bosonic SPTs were first developed in Refs. [172, 39, 195, 40, 171]. Because the ground states of the systems in question satisfy an area law, we can make use of the matrix product state (MPS) representation [93, 196] (see Section 1.1.2), which takes the form [68, 167]

$$|\Psi\rangle = \sum_{i_1,i_2,\ldots,i_L} \mathrm{Tr}\left[A^{[1]}_{i_1} A^{[2]}_{i_2} \cdots A^{[N]}_{i_N}\right] |i_1, i_2, \cdots, i_N\rangle \,. \tag{3.10}$$

Here, $|i_1, i_2, \cdots, i_N\rangle$ are product states labelled by the on-site quantum numbers $\{i_k = 1, \ldots, s\}$ with local Hilbert space dimension s, and each $A^{[k]}_{i_k}$ is a $D \times D$ matrix that parametrizes the wavefunction. Although the bond dimension D is arbitrary, a wavefunction with area law entanglement can be efficiently captured using some fixed finite choice of D.

[5] In those works, and in this paper, the theoretical framework covers only pure SPTs, which excludes systems with surface intrinsic topological order, among other exotic phases in spatial dimension $d \geq 3$ [222, 228, 29, 234].

Importantly, not only can all ground states be well approximated by an MPS, but also all MPS states are the unique ground state of some local Hamiltonian[6] [68]. Therefore, a topological characterization of the space of MPS wavefunctions is equivalent to a classification of topological phases in the sense of Definition 2. Such a classification can be obtained by enumerating the inequivalent ways in which the matrices $A^{[k]}_{i_k}$ can transform under the action of symmetries [39].

If the wavefunction respects a group of symmetries G, then this imposes restrictions on the $A^{[k]}_{i_k}$. If the symmetries are realised by on-site unitary operations, $U(g) = u(g) \otimes u(g) \otimes \cdots \otimes u(g)$ (where each unitary $u(g)$ is a $s \times s$ matrix acting on one site only), then the condition for $|\Psi\rangle$ to respect the symmetry is [40]

$$\sum_{j=1}^{s} u(g)_{ij} A_j = \alpha(g) R^{-1}(g) A_i R(g) \tag{3.11}$$

where $\alpha(g)$ is a g-dependent phase factor, $R(g)$ is a $D \times D$ matrix, and for simplicity we have assumed translational invariance, dropping the superscript labels on the A (however we will only be interested in topological invariants that remain well defined when translation symmetry is broken). A crucial observation made in Refs. [39, 172] is that to be consistent with the group structure of G, the matrices $R(g)$ need only respect the multiplication rule of G up to a phase factor: $R(g_1 g_2) = \omega(g_1, g_2) R(g_1) R(g_2)$, where $\omega(g_1, g_2)$ is a modulus-1 complex number known as the factor system. This implies that the $R(g)$ form a one-dimensional *projective representation* of the symmetry group G, as opposed to a linear representation which satisfies $R(g_1 g_2) = R(g_1) R(g_2)$. It was shown [39] that wavefunctions belong to the same SPT phase if and only if their projective representations are equivalent, in the sense that they can be related through multiplying one by a linear representation[7]. Therefore, the topological phase to which the ground state $|\Psi\rangle$ belongs is entirely determined by the equivalent class of the factor system $\omega(g_1, g_2)$.

The analysis when G features both unitary and antiunitary elements follows similarly. In bosonic systems, G will factorize as $G = G_T \times \mathbb{Z}_2^T$ or $G = G_T \rtimes \mathbb{Z}_2^T$, where the group $\mathbb{Z}_2^T = \{1, T\}$ contains a group element T corresponding to a time-reversal symmetry, and the choice depends on whether time-reversal commutes with the other group elements or

[6] The MPS (or PEPS in higher dimension) must further satisfy certain (generalised) injectivity conditions, which are satisfied as long as the system does not spontaneously break symmetry [40, 240].

[7] If translation invariance is also imposed on the system, then $\alpha(g)$ is a good quantum number, and cannot change unless the gap closes, or the symmetries and/or translation invariance is broken. However, we will only be concerned with SPT phases that are robust against translational symmetry breaking here.

not[8]. Time-reversal acts on the Hilbert space as $V(T) = v \otimes v \otimes \cdots \otimes vK$, where K is the complex conjugation operator and v is an on-site unitary. For our purposes, one can assume that $vv^* = 1$ without loss of generality[9]. Just as for unitary symmetries, the MPS can be classified according to the way in which it transforms under the action of the whole symmetry group. The unitary subgroup G_T generates the same data as described above. In addition to this, the MPS must also transform consistently under the action of the antiunitary element T. This implies that

$$\sum_{j=1}^{s} v_{ij} A_j^* = M^{-1} A_i M \tag{3.12}$$

for some $D \times D$ matrix M. To be consistent with the $\mathbb{Z}_2^T$ group product $T^2 = 1$, we must have $MM^* = \beta(T)\mathbb{1}_D$, where $\beta(T) = \pm 1$ [40]. The two choices of $\beta(T)$ correspond to the two distinct antilinear projective representations of $\mathbb{Z}_2^T$.

The objects so far [$\omega(g_1, g_2)$ and $\beta(T)$] quantify how the group product is represented for G_T and $\mathbb{Z}_2^T$ separately; however one also needs to understand how group products between unitary and antiunitary elements are realised. By applying the symmetries (3.11) and (3.12) in different orders, the authors of Ref. [40] demonstrated that, when $G = G_T \times \mathbb{Z}_2^T$ (i.e. $TgT = g$), the projective representations must satisfy a projective commutation relation

$$M^{-1} R(g) M = \gamma(g) R(g)^* \tag{3.13}$$

where $\gamma(g)$ is a phase factor that forms a linear 1D representation of G_T. The matrices $R(g)$ are only unambiguously defined up to multiplication by a 1D linear representation of G [see Eq. (3.11)], which in turn changes $\gamma(g)$ by the square of that representation. Therefore, two systems with phase factors $\gamma(g)$ that belong to different elements of the quotient group $\mathscr{G}/\mathscr{G}_2$ cannot be adiabatically connected (here $\mathscr{G}$ is the group of 1D representations of G_T, and $\mathscr{G}_2$ is the group of those representations which are squares of other representations). When $G = G_T \rtimes \mathbb{Z}_2^T$, one replaces $R(g)$ with $R(g^{-1})$ on the right-hand side to account for the fact that elements of G_T do not commute with time-reversal, and the same arguments can be applied.

[8] Most generally, G is a group extension of its unitary subgroup G_T by an antiunitary group $\mathbb{Z}_2^T$: $1 \to G_T \to G \to \mathbb{Z}_2^T \to 1$ which might not split as a direct or semi-direct product [153]. A notable exception is half-integer-spin fermionic systems with a time-reversal symmetry satisfying $T^2 = P_f$ (P_f is the fermion parity operator), which has a $\mathbb{Z}_4^T$ structure $\{I, T, P_f, TP_f\}$.

[9] In a system for which $vv^* = -1$, the unit cell can be doubled, after which one has $vv^* = 1$ [39]. In doing this, one loses information about certain topological invariants that depend upon translation invariance, which we are not concerned with here.

On the one hand, in comparison to the classification for only unitary symmetries G_T, these new relations give rise to new topological phases as indicated by the possible values of $\beta(T)$, $\gamma(g)$. On the other hand, combining this relation with (3.11), one finds that the imposition of an antiunitary symmetry means that $\omega(g_1,g_2)$ must square to unity, which implies that some of the phases that existed under the symmetry G_T are not compatible with the presence of TRS (specifically, those with $\omega^2 \neq 1$). To summarise, different topological phases under a on-site symmetry group $G_T \times \mathbb{Z}_2^T$ featuring a time-reversal part are

1. The equivalence class of the factor system $\omega(g_1,g_2)$, which must satisfy $\omega^2 = 1$
2. The projective representation of $\mathbb{Z}_2^T$, $\beta(T) = \pm 1$
3. The projective commutation relation between symmetry transformations in G_0 and $\mathbb{Z}_2^T$, $\gamma(g) \in \mathscr{G}/\mathscr{G}_2$

(3.14)

While the above refers to bosonic models, 1D fermionic models can also be captured using the same arguments through a Jordan-Wigner transformation [40]. In that context, one must also include phases which result from a spontaneous breaking of the $\mathbb{Z}_2^P$ fermion parity symmetry, which results in boundary Majorana modes.

3.2.2 One dimensional interacting SPTs out of equilibrium

Compared to the equilibrium classification, the range of deformations that one can make in the non-equilibrium classification is wider (Definition 3). Specifically, when time-evolving from one symmetry-respecting wavefunction to another, antiunitary symmetries can be broken at intermediate times. Since finite-time evolution preserves the area law nature of the wavefunctions in question, the MPS ansatz can still be used (albeit with a bond dimension that typically grows exponentially in time [176]). Following our treatment in Ref. [147], we compute the non-equilibrium classification by determining how the symmetry properties of the matrices $A_{i_k}^{[k]}$ change as the system evolves in time.

As explained in Section 2.2, if the system only possesses unitary symmetries, then we expect that finite-time evolution and adiabatic deformation are equivalent, and the non-equilibrium classification will be the same as in equilibrium. More explicitly, the object used to topologically characterize the wavefunction [the equivalence class of $\omega(g_1,g_2)$] is a discrete quantity and remains well-defined throughout the evolution process; therefore, it cannot be changed under such a continuous deformation procedure.

Now consider the case where the system is invariant under both unitary and antiunitary symmetries. Take $G = G_T \times \mathbb{Z}_2^T$ for now, so that the initial state is characterized by the objects

listed in Eq. (3.14). (The $G_T \rtimes \mathbb{Z}_2^T$ case proceeds in the same way.) Because of dynamically induced symmetry breaking, the wavefunction at intermediate times will only respect the symmetries in G_T. This means that some of the data used to topologically characterize the original wavefunction may not be well-defined. In particular, because Eq. (3.12) no longer holds, the objects $\beta(T)$ and $\gamma(g)$, each of which relate to the matrix M, become meaningless. Therefore, even if $|\Psi_1\rangle$ and $|\Psi_2\rangle$ have inequivalent $\beta(T), \gamma(g)$ [but equivalent $\omega(g_1, g_2)$], they can still be connected via finite-time unitary evolution under a symmetry-respecting Hamiltonian. If they differ with respect to $\omega(g_1, g_2)$, which remains well-defined throughout the evolution, then they cannot be connected in this way, and belong to different non-equilibrium classes.

The objects that can still distinguish wavefunctions in the non-equilibrium classification are simply those that characterise the equilibrium topology of systems that only respect the symmetry subgroup G_T. Note, however, that the non-equilibrium classification is not simply given by the equilibrium classification of this reduced symmetry group, since the states $|\Psi_1\rangle$, $|\Psi_2\rangle$ must belong to phases that are compatible with the full symmetry group $G_T \times \mathbb{Z}_2^T$. From Eq. (3.14), we see that TRS requires the representations to satisfy $\omega^2 = 1$, which comprise only a subgroup of the equilibrium classification for G_T-symmetric systems. Therefore, if at least one antiunitary symmetry is present, then the non-equilibrium classification is given by the equivalence classes of projective representations of G_T; subject to the constraint $\omega^2 = 1$.

We list the classification groups for certain symmetry groups of physical relevance in Table 3.2. In many cases, the non-equilibrium classification is trivial, since the equilibrium classification of G_T (without the TRS part) is itself trivial. More subtle cases include the time-reversal invariant spin chains with full rotation invariance $\mathrm{SO}(3) \times \mathbb{Z}_2^T$. In this case, the equilibrium classification is $\mathbb{Z}_2 \times \mathbb{Z}_2$; the first group factor accounting for $\beta(T) = \pm 1$ and the second accounting for the two projective representations of $\mathrm{SO}(3)$ [which are integer-spin and half-integer-spin linear representations of its double cover $\mathrm{SU}(2)$]. Only the latter object is well-defined once TRS is dynamically broken, and so the non-equilibrium classification reduces from $\mathbb{Z}_2 \times \mathbb{Z}_2$ to $\mathbb{Z}_2$.

We can also make connection with the non-equilibrium classifications of 1D free-fermion systems derived in Section 2.3.3 using the Jordan-Wigner transform approach, where one-dimensional fermion systems are mapped onto boson systems with an extra $\mathbb{Z}_2^p$ symmetry, representing conservation of fermion parity [40]. In that context, the single-particle symmetries that constitute the 10 Altland-Zirnbauer symmetry classes must be re-interpreted as symmetry groups of the auxiliary spin system (although in some cases one needs to specify whether the free Hamiltonian represents a superconductor or an insulator [155]). Spinless

Symmetry group	Equilibrium	Non-eq.
Bosonic:		
$\mathbb{Z}_2^T$	$\mathbb{Z}_2$	0
$\mathrm{U}(1)\times\mathbb{Z}_2^T$	$\mathbb{Z}_2\times\mathbb{Z}_2$	0
$\mathrm{U}(1)\rtimes\mathbb{Z}_2^T$	$\mathbb{Z}_2\times\mathbb{Z}_2$	0
$\mathbb{Z}_n\times\mathbb{Z}_2^T$	$\mathbb{Z}_2\times\mathbb{Z}_{(2,n)}$	0
$\mathbb{Z}_n\rtimes\mathbb{Z}_2^T$	$\mathbb{Z}_2\times\mathbb{Z}_{(2,n)}$	0
$\mathbb{Z}_n\times\mathbb{Z}_m\times\mathbb{Z}_2^T$	$\mathbb{Z}_2\times\mathbb{Z}_{(2,n)}\times\mathbb{Z}_{(2,m)}\times\mathbb{Z}_{(2,n,m)}$	$\mathbb{Z}_{(2,n,m)}$
$\mathrm{SO}(3)\times\mathbb{Z}_2^T$	$\mathbb{Z}_2\times\mathbb{Z}_2$	$\mathbb{Z}_2$
Fermionic:		
$\mathbb{Z}_2^F\times\mathbb{Z}_2^T$ (BDI)	$\mathbb{Z}_8$	$\mathbb{Z}_2$
$\mathbb{Z}_4^{T,F}$ (DIII)	$\mathbb{Z}_2$	0
$\mathrm{U}(1)\times\mathbb{Z}_2^T$ (AIII)	$\mathbb{Z}_4$	0

Table 3.2 Non-equilibrium classification of 1D fermionic and bosonic interacting SPT phases protected by onsite symmetry group $G = G_T \times \mathbb{Z}_2^T$ or $G = G_T \rtimes \mathbb{Z}_2^T$. The group G_T contains all unitary symmetries, and $\mathbb{Z}_2^T = e, T$, where T represents time-reversal, and is realised by an antiunitary operator. $\mathbb{Z}_4^{T,F}$ is the cyclic group $\{1, T, P_f, TP_f\}$, representing time-reversal symmetry and fermion parity P^f for half-integer spin fermions. Here (n,m) is the greatest common divisor of integers n and m. The non-equilibrium classification for symmetry groups only featuring unitary elements are identical to the equilibrium classification, which can be found in Ref. [37]. We also include some fermionic systems which are interacting analogues of the non-interacting symmetry classes within the ten-fold way; the Cartan labels for the corresponding Altland-Zirnbauer class are also given in brackets.

superconductors with time-reversal symmetry, which correspond to class BDI in the tenfold way, possess a $\mathbb{Z}_2^F \times \mathbb{Z}_2^T$ symmetry group when transformed to a spin system ($\mathbb{Z}_2^F$ represents fermion parity, whilst $\mathbb{Z}_2^T$ is time-reversal symmetry with $T^2 = +1$). Our previous finding that the classification of these systems is reduced from $\mathbb{Z}$ in equilibrium to its $\mathbb{Z}_2$ subgroup out of equilibrium is consistent with the results of this section. When interactions are included, the equilibrium classification is reduced from $\mathbb{Z}$ to $\mathbb{Z}_8$ [71], consisting of one trivial phase, 3 phases where T, P_f are unbroken, but TRS is projectively realised, and 4 phases where the fermion parity symmetry is spontaneously broken (in the spin language), and T is realised projectively in different ways. After TRS is dynamically broken, the first 3 non-trivial phases are all indistinguishable from the trivial phase, and the latter 4 phases remain non-trivial, but mutually indistinguishable, hence the $\mathbb{Z}_2$ non-equilibrium classification, the same as in the non-interacting case. We find similar agreement for spinful time-reversal symmetric superconductors with (AIII) and without (DIII) $\mathrm{U}(1)$ spin-rotation invariance (because $T^2 = P_f$, we use $\mathbb{Z}_4^{T,F}$, the cyclic group $\{I, T, P_f, TP_f\}$ which is relevant only in fermionic systems).

3.2.3 Extending to higher dimensions

The arguments regarding projective representations of the symmetry groups are specific to 1D, since they rely on the matrix-product state ansatz (3.10). To generalize to higher dimensional systems whose ground states possess area-law entanglement, one must consider more general tensor-network states, such as projected entangled-pair states (PEPS) [218, 220]. In these states, one replaces the matrix product in Eq. (3.10) with the contraction of a tensor network where each node represents a site of the lattice. As described in Ref. [37], the natural algebraic structure for classifying bosonic SPT phases in this context is the cohomology group $\mathscr{H}^{(1+d)}[G, \mathrm{U}_T(1)]$, where d is the spatial dimension ($\mathrm{U}_T(1)$ is defined below). A full introduction to group cohomology and its relevance to SPT phases can be found in Ref. [37]; however, we will briefly summarize its structure here.

The principles underpinning how SPT phases are classified in higher dimensions are no different from 1D, but some technical aspects of the arguments are altered. It turns out to be more convenient not to explicitly separate TRS from the unitary symmetries as we did above, (which previously resulted in additional data β, γ). This can be achieved by specifying how the symmetry transformations $g \in G$ act on wavefunctions, such that the antiunitary nature of TRS is captured. To be specific, we define the action of each group element $g \in G$ on complex phases $a \in \mathrm{U}(1)$ via the product $g \cdot a$ such that $g \cdot a = a^*$ if g is antiunitary, and $g \cdot a = a$ otherwise. $\mathrm{U}_T(1)$, which consists of the Abelian group $\mathrm{U}(1)$ combined with the operation $\cdot$, is referred to as a G-module.

Symmetry group	Spatial dimension d			
	0	1	2	3
$\mathbb{Z}_2^T$	0	$\mathbb{Z}_2$	0	$\mathbb{Z}_2$
	0	0	0	0
$\mathrm{U}(1)\times\mathbb{Z}_2^T$	0	$\mathbb{Z}_2^{\times 2}$	0	$\mathbb{Z}_2^{\times 3}$
	0	0	0	0
$\mathrm{U}(1)\rtimes\mathbb{Z}_2^T$	$\mathbb{Z}$	$\mathbb{Z}_2$	$\mathbb{Z}_2$	$\mathbb{Z}_2^{\times 2}$
	$\mathbb{Z}$	0	0	0
$\mathbb{Z}_n\times\mathbb{Z}_2^T$	$\mathbb{Z}_{(2,n)}$	$\mathbb{Z}_2\times\mathbb{Z}_{(2,n)}$	$\mathbb{Z}_{(2,n)}^{\times 2}$	$\mathbb{Z}_2\times\mathbb{Z}_{(2,n)}^{\times 2}$
	$\mathbb{Z}_{(2,n)}$	0	$\mathbb{Z}_{(2,n)}$	0
$\mathbb{Z}_n\rtimes\mathbb{Z}_2^T$	$\mathbb{Z}_n$	$\mathbb{Z}_2\times\mathbb{Z}_{(2,n)}$	$\mathbb{Z}_{(2,n)}^{\times 2}$	$\mathbb{Z}_2\times\mathbb{Z}_{(2,n)}^{\times 2}$
	$\mathbb{Z}_n$	0	$\mathbb{Z}_{(2,n)}$	0
$\mathbb{Z}_n\times\mathbb{Z}_m\times\mathbb{Z}_2^T$	$\mathbb{Z}_{(2,n)}\times\mathbb{Z}_{(2,m)}$	$\mathbb{Z}_2\times\mathbb{Z}_{(2,n)}\times\mathbb{Z}_{(2,m)}\times\mathbb{Z}_{(2,n,m)}$	$\mathbb{Z}_{(2,n)}^{\times 2}\times\mathbb{Z}_{(2,m)}^{\times 2}\times\mathbb{Z}_{(2,n,m)}^{\times 2}$	$\mathbb{Z}_2\times\mathbb{Z}_{(2,n)}^{\times 2}\times\mathbb{Z}_{(2,m)}^{\times 2}\times\mathbb{Z}_{(2,n,m)}^{\times 4}$
	$\mathbb{Z}_{(2,n)}\times\mathbb{Z}_{(2,m)}$	$\mathbb{Z}_{(2,n,m)}$	$\mathbb{Z}_{(2,n)}\times\mathbb{Z}_{(2,m)}\times\mathbb{Z}_{(2,n,m)}$	$\mathbb{Z}_{(2,n,m)}^{\times 2}$
$SO(3)\times\mathbb{Z}_2^T$	0	$\mathbb{Z}_2^{\times 2}$	$\mathbb{Z}_2$	$\mathbb{Z}_2^{\times 3}$
	0	$\mathbb{Z}_2$	0	0

Table 3.3 Non-equilibrium classification of bosonic interacting symmetry-protected topological orders in physical spatial dimensions, as captured by Eq. (3.20). Systems are protected by various onsite symmetry groups $G = G_T \times \mathbb{Z}_2^T$ or $G = G_T \rtimes \mathbb{Z}_2^T$, where G_T is realised unitarily and $\mathbb{Z}_2^T = e, T$, where T represents time-reversal, and is realised with an antiunitary operator. Here (n,m) is the greatest common divisor of integers n and m. The non-equilibrium classification for symmetry groups without the time-reversal part are identical to the equilibrium classification, which can be found in Ref. [37]. For each symmetry group, we provide two rows, the first being the equilibrium classification taken from Ref. [37], and the second being the non-equilibrium classification discussed in Section 3.2.3 derived in Appendix A. Systems with translational invariance also possess weak indices, which out of equilibrium are still given by products of the non-equilibrium classification in lower spatial dimensions.

The key object used in Section 3.2.1 was the factor system of the projective representation $\omega(g_1,g_2)$, which quantifies how the representation fails to respect the group product $R(g_1)R(g_2) = \omega(g_1,g_2)R(g_1g_2)$. If TRS is included within G, then the factor system $\omega : G^{\times 2} \to \mathrm{U}_T(1)$ is formally a map from 2 group elements to the G-module $\mathrm{U}_T(1)$ which is the only object needed to specify an SPT phase. The structure of these maps can be understood in the framework of group cohomology, which more generally concerns maps from n group elements to an arbitrary G-module M. The space of such maps is denoted $\mathscr{C}^n[G,M] = \{\omega : G^{\times n} \to M\}$.

Now define a 'differential' operator $d_n : \mathscr{C}^n[G,M] \to \mathscr{C}^{n+1}[G,M]$ which returns a function of $(n+1)$ elements of G

$$\begin{aligned}(d_n\omega)(g_1,\ldots,g_{n+1}) &= [g_1\cdot\omega(g_2,\ldots,g_{n+1})]\\ &\times \omega^{(-1)^{n+1}}(g_1,\ldots,g_n)\prod_{i=1}^{n}\omega^{(-1)^i}(g_1,\ldots,g_{i-1},g_ig_{i+1},\ldots g_n).\end{aligned} \tag{3.15}$$

The precise form of the differential operator is not important; we need only know that d_n is a homomorphism, and $d_{n+1}\circ d_n = 0$. This last identity justifies the nomenclature, since the same identity is satisfied by the exterior derivative in differential geometry.

One considers the infinite family of groups $\{\mathscr{C}^n[G,M] : n \geq 0\}$ (where we understand $\mathscr{C}^0[G,M] = M$) along with the maps $\{d_n\}$ between them, which together constitute a *cochain complex*

$$\mathscr{C}^0[G,M] \xrightarrow{d_0} \mathscr{C}^1[G,M] \xrightarrow{d_1} \mathscr{C}^2[G,M] \xrightarrow{d_2} \mathscr{C}^3[G,M] \xrightarrow{d_3} \cdots \tag{3.16}$$

An element of $\mathscr{C}^n[G,M]$ is referred to as an n-cochain.

If an n-cochain ω_n can be written $\omega_n = d_{n-1}\omega_{n-1}$ for some ω_{n-1} (i.e. $\omega_n \in \mathrm{im}\, d_{n-1}$), one says that it is exact, and if it satisfies $d_n\omega_n = 0$ (i.e. $\omega_n \in \ker d_n$), then one says that it is closed. From $d_{n+1}\circ d_n = 0$, all exact n-cochains are closed. However, not all closed cochains are exact. The nth cohomology group of this complex quantifies this asymmetry; it is defined as the quotient group

$$\mathscr{H}^n[G,M] := \ker(d_n)/\,\mathrm{im}(d_{n-1}), \tag{3.17}$$

or in words, 'the equivalence classes of cochains that are closed, but cannot be interconverted through multiplying by an exact cochain'. If, for a particular G-module M, all closed chains are exact, then every cohomology group is trivial, and the sequence (3.16) is a long exact sequence.

Returning to the 1D case, the natural quantities to deal with are factor systems, which are elements of $\mathscr{C}^2[G,\mathrm{U}_T(1)]$. Note, however, that not all such functions from $G^{\times 2}$ to $\mathrm{U}_T(1)$ can describe valid projective representations. One can think of the condition that $\omega \in \ker(d_2)$ as a statement that ω is the factor system of a valid projective representation. Two projective representations ω, ω' are considered to be equivalent if they are related by a 1D linear representation through $\omega(g_1,g_2) = \omega'(g_1,g_2)\beta(g_2)^{s(g_1)}\beta(g_1)/\beta(g_1g_2)$ for some $\beta \in \mathscr{C}^1[G,\mathrm{U}_T(1)]$ [38], since such a change can be absorbed into $\alpha(g)$ in Eq. (3.11). Here, $s(g_1) = \pm 1$ depending on whether g_1 is an antiunitary element. Using Eq. (3.15), this equivalence relation for ω, ω' can be written as $\omega = \omega' \times (d_1\beta)$. Two factor systems ω, ω' obeying this relation therefore belong to the same class in the quotient group $\mathscr{H}^2[G,\mathrm{U}_T(1)]$, as defined by Eq. (3.17). We see that the cohomology group is the natural structure for classifying inequivalent factor systems, which in turn allows us to classify 1D SPTs. More generally, different SPT phases in d spatial dimensions are captured by elements of $\mathscr{H}^{1+d}[G,\mathrm{U}_T(1)]$ [37].

We now describe how the above construction of cohomology groups can be applied to our non-equilibrium classification. As in 1D, we must consider a unitary evolution $|\Psi(t)\rangle$ between symmetric SRE wavefunctions $|\Psi_1\rangle$ at $t = 0$, and $|\Psi_2\rangle$ at $t = 1$. Dynamically induced symmetry breaking means that at intermediate times $0 < t < 1$, $|\Psi(t)\rangle$ will respect only a subgroup of the symmetries $G_T \leq G$, in which only unitary elements are kept. We must understand which topological data remain well-defined throughout the evolution, since only these data will restrict whether $|\Psi_1\rangle$ and $|\Psi_1\rangle$ can be unitarily connected.

At time $t = 0$, the object $\omega_0 \in \mathscr{C}^n[G,\mathrm{U}_T(1)]$, which belongs to one of the equivalence classes of $\mathscr{H}^n[G,\mathrm{U}_T(1)]$, characterizes how an initial PEPS state $|\Psi_1\rangle$ transforms under the full symmetry group G in dimension $d = n-1$. However, $|\Psi(t>0)\rangle$ can only be understood through its behaviour under symmetry transformations within the subgroup G_T. We should therefore take the function $\omega_0 : G^{\times n} \to \mathrm{U}_T(1)$ and restrict it to the domain $G_T^{\times n}$, yielding $\omega_T := \omega_0|_{G_T}$. This object is sufficient to characterize the topology of $|\Psi(t)\rangle$, but does not do so uniquely. For the same reasons as in equilibrium, we must identify how ω_T fits into the cohomology group corresponding to the reduced set of symmetries.

Note that ω_T is an element of $\mathscr{C}^n[G_T,\mathrm{U}(1)]$ [we drop the subscript T on the module since by definition all elements of G_T are unitary and have trivial action on $\mathrm{U}_T(1)$]. The groups $\mathscr{C}^n[G_T,\mathrm{U}(1)]$ form their own cochain complex, and for each n we can define the restriction map $\mathrm{res}_n : \mathscr{C}^n[G,\mathrm{U}(1)] \to \mathscr{C}^n[G_T,\mathrm{U}(1)]$, defined as above. Importantly, the restriction map

is a homomorphism, and the following diagram is commutative [198]

$$\begin{array}{ccccccc} \mathscr{C}^0[G,\mathrm{U}_T(1)] & \xrightarrow{d_0} & \mathscr{C}^1[G,\mathrm{U}_T(1)] & \xrightarrow{d_1} & \mathscr{C}^2[G,\mathrm{U}_T(1)] & \xrightarrow{d_2} & \cdots \\ \downarrow{\scriptstyle \mathrm{res}_0} & & \downarrow{\scriptstyle \mathrm{res}_1} & & \downarrow{\scriptstyle \mathrm{res}_2} & & \\ \mathscr{C}^0[G_T,\mathrm{U}(1)] & \xrightarrow{d_0^T} & \mathscr{C}^1[G_T,\mathrm{U}(1)] & \xrightarrow{d_1^T} & \mathscr{C}^2[G_T,\mathrm{U}(1)] & \xrightarrow{d_2^T} & \cdots \end{array} \tag{3.18}$$

i.e. restriction preserves which elements are exact and which are closed. Here, we use d_n^T to denote the differential maps on the bottom cochain complex. It is well known in cohomology that this restriction from G to any subgroup in turn induces a homomorphism on the cohomology groups, called the restriction functor [198]

$$\mathrm{Res}_n : \mathscr{H}^n[G,\mathrm{U}_T(1)] \to \mathscr{H}^n[G_T,\mathrm{U}(1)]. \tag{3.19}$$

We use a capitalized Res_n to denote the restriction functor on cohomology groups.

To construct Res_n explicitly, one can consider how the restriction map res_n affects the components of Eq. (3.17). First, consider $\ker(d_n)$, i.e. the group of closed n-cochains within $\mathscr{C}^n[G,\mathrm{U}_T(1)]$. Since the differentials and restrictions commute, any closed element of $\mathscr{C}^n[G,\mathrm{U}_T(1)]$ will still be closed when restricted to an element of $\mathscr{C}^n[G_T,\mathrm{U}(1)]$. Restriction therefore defines a map between the two kernels $\mathrm{res}_n : \ker(d_n) \to \ker(d_n^T)$. Note, however, that not all closed elements of $\mathscr{C}^n[G_T,\mathrm{U}(1)]$ can be written as the restriction of some closed element of $\mathscr{C}^n[G,\mathrm{U}_T(1)]$.

For $n = 2$ ($d = 1$), this is the statement that a valid projective representation of G becomes a valid projective representation of G_T after restriction, but that not all projective G_T-representations can be extended to projective G-representations. In the context of higher-dimensional SPT phases (for $n > 2$), one can replace the notion of a valid projective G-representation with a valid action of the symmetry G on the wavefunction ansatz of choice, as specified by some $\omega_n \in \mathscr{C}^n[G,\mathrm{U}_T(1)]$. The previous paragraph simply states that if $|\Psi_1\rangle$ transforms in a consistent way under G, then it must also transform consistently under G_T, but that the converse is not necessarily true.

Similarly, thanks to the commutative diagram above, res_n maps elements of $\mathrm{im}(d_{n-1})$ to elements of $\mathrm{im}(d_{n-1}^T)$, i.e. exact cochains remain exact after restriction. Again, not all exact cochains of the reduced group G_T can be expressed as restrictions of exact cochains of G. Two cochains ω_1, ω_2 which are inequivalent as elements of $\mathscr{H}^n[G,\mathrm{U}_T(1)]$ must satisfy $\omega_1 \neq \omega_2 \times (d_{n-1}\beta)$ for all $\beta \in \mathscr{C}^{n-1}[G,\mathrm{U}_T(1)]$. However, after restriction to G_T they may become equivalent as elements of $\mathscr{H}^n[G_T,\mathrm{U}(1)]$, since one may have $\omega_1 = \omega_2 \times (d_{n-1}^T \beta_T)$ for an element $\beta_T \in \mathscr{C}^{n-1}[G_T,\mathrm{U}_T(1)]$.

The restriction functor Res_n between the cohomology groups defined in (3.19) is constructed through the action of res_n on $\ker(d_{n+1})$ modulo the transformations defined by $\mathrm{im}(d_n^T)$, in the sense defined above. It has an image

$$\mathrm{im}\,(\mathrm{Res}_n) = \mathrm{im}\left(\ker(d_{n+1}) \xrightarrow{\mathrm{res}_n} \ker(d_{n+1}^T)\right) / \mathrm{im}(d_n^T). \tag{3.20}$$

The above object (3.20) constitutes the non-equilibrium classification for bosonic systems in spatial dimension $d = n-1$. Each element of this group represents a collection of symmetry-respecting SRE wavefunctions which can be mutually connected via finite-time unitary evolution under a symmetry-respecting Hamiltonian.

In the Appendix, we describe a method for computing the image of the restriction map by making use of the Hochschild-Serre spectral sequence [13]. The non-equilibrium classification for all pure bosonic SPT phases computed using this method is given in Table 3.3.

Chapter 4

Open Quantum Systems

All physical systems interact with their surroundings to some degree. Thus, any theoretical model in which the system is isolated can only ever approximate the true dynamics that is realised in a given experiment. Of course the relative simplicity of isolated systems makes them easier to understand, and so typically theoretical predictions are first made based on analyses of closed systems. However, we must always re-examine these predictions in light of the fact that the experimental system is in fact open, and thus subject to dissipative effects.

In some scenarios, by either providence or design, the influence of the environment only leads to small quantitative corrections to the original calculations. For instance, in atomic physics one often takes advantage of electronic states that have very slow spontaneous emission rates. If the timescale of the experiment is short compared to the lifetime of the atomic states being probed then the interactions between the atom and its environment (the electromagnetic vacuum) will have little bearing on the dynamics. However, in many settings dissipation becomes relevant on much shorter timescales, and so a more careful treatment is required.

Much in the spirit of this thesis, an important practical question to address is: How do system-environment interactions affect the topological phenomena that have been predicted based on treatments of isolated systems? *Prima facie*, there are some reasons to expect that topological systems could be particularly susceptible to dissipative effects:

1. Topological phases are often associated with very precisely quantized responses, e.g. the Hall conductivity (1.8). Even if the system-environment coupling is weak, corrections to these responses could easily be large compared to the precision with which they are expected to be quantized. Unless there is some reason why the environment cannot change the relevant response function, it is likely that dissipation will be the limiting factor preventing improvements to quantization.

2. As explained in Section 1.2.2, one of the most promising potential technological applications of topological phases is in the context of quantum information processing. In isolated systems, topological bound states (e.g. Majorana zero modes) are expected to store quantum information over timescales that are exponentially large in the system size. Quite generally, one expects that the influence of an environment will become stronger over time, and so environment-induced decoherence may prove to be problematic at late times, even if it occurs slowly.

3. Topological phases are underpinned by the entanglement properties of ground state wavefunctions. However, once the system is open, entanglement can be generated between the system and environment. Once the state of the system becomes mixed, it becomes unclear whether systems can be topologically distinguished in a meaningful way that bears relevance to experimental observables.

These cursory considerations suggest that we should not always expect topological phenomena to show the same degree of robustness in open systems as they do in isolated systems; thus the effects of dissipation warrant proper consideration. Nevertheless, the remarkable precision with which the quantized Hall response in two dimensional electron gases has been measured [226] already demonstrates that there exist realistic scenarios where phenomena associated with topological phases persist despite the interactions between system and environment. One of the central aims of this chapter is to identify general conditions under which the experimentally accessible signatures of topological phases can survive away from the isolated system limit.

This is by no means the first time that issues relating to topology in open quantum systems have been addressed, and there are many other questions which one can ask in this context (see Sections 1.4.3 and 1.4.4). As with the previous chapter, our focus here will be on generality. In most experimental setups, one generally has little control over the structure of the environment or the way in which it is coupled to the system. It is therefore important to develop an understanding which can be applied to a generic open system, not requiring any fine-tuning.

The main result of this chapter can be summarised as follows: Topological phenomena protected by antiunitary symmetries, e.g. time-reversal symmetry (TRS), are inevitably compromised by coupling to an environment. This effect can be intuitively understood by making connections to the arrow of time in quantum mechanics. It is well-known that interactions between a system and its environment can lead to the demise of TRS in the sense that the system propagates irreversibly (see Section 1.3.1); here we demonstrate that the same mech-

anism facilitates processes which spoil phenomena protected by TRS, including certain SPTs.

Before starting any analysis, it is important to first specify exactly what we mean by an open system in the context of topological phases, which we discuss in Section 4.1. Naturally, symmetries play an important rôle in our analysis, and we consider the symmetry properties of open quantum systems, which we discuss in Section 4.2. Using a simple few-body model, we show that the fragility of antiunitary symmetries against system-environment coupling is manifest in the structure of time-dependent perturbation theory. In Section 4.3, we test our newfound intuition regarding symmetry protection in open systems by calculating the environment-induced decoherence rate of topological bound states. The decoherence rate is shown to be exponentially small when the protecting symmetries are unitary $\tau_{\text{coh}}^{-1} \sim e^{-E_g/T}$ (T is the environment temperature), whereas the decoherence is only algebraically suppressed $\tau_{\text{coh}}^{-1} \sim T^{\eta}$ for antiunitary symmetries. We then consider the conductance properties of one-dimensional topological edge channels in Section 4.4, and find an analogous dichotomy in the temperature dependence of the conductance. Finally in Section 4.5, we discuss the wider implications of our findings, and establish some connections to the non-equilibrium classification developed in Chapter 2.

4.1 What is an open quantum system?

In an open quantum system, we distinguish degrees of freedom in the system from those in the environment. The Hilbert space of the combined system and environment (which we refer to as the 'composite system' from hereon) is a tensor product

$$\mathscr{H} = \mathscr{H}_S \otimes \mathscr{H}_E \tag{4.1}$$

where $\mathscr{H}_S$ and $\mathscr{H}_E$ are the Hilbert spaces for the system and environment, respectively. The dynamics is governed by the microscopic Hamiltonian

$$\hat{H} = \hat{H}_S \otimes \hat{\mathbb{1}}_E + \hat{\mathbb{1}}_S \otimes \hat{H}_E + \hat{H}_{SE} \tag{4.2}$$

where $\hat{H}_S$, $\hat{H}_E$ are the system and environment Hamiltonians, respectively, and $\hat{H}_{SE}$ couples the two.

At first sight, this construction appears somewhat unphysical. There is no fundamental principle that informs us how to decide which degrees of freedom belong to the system, and which belong to the environment. Indeed from a reductionist viewpoint, the division of the total Hilbert space (4.1) seems entirely unnecessary. However, in practice the open quantum

system formalism proves to be an indispensable tool without which theoretical progress is almost impossible. In a realistic scenario, attempts to analyse the composite system using techniques developed to study isolated systems will inevitably run into problems: Firstly, the environment is typically very large. (In principle, $\mathscr{H}_E$ represents the rest of the observable universe!) In the composite approach, one would have to analyse the dynamics of the system and environment to a good accuracy, which is generally unfeasible. Secondly, even if one had the analytic and/or computational power to address the full dynamics governed by the Hamiltonian (4.2), often one does not even have a good quantitative description of the environment Hamiltonian $\hat{H}_E$.

The key principle underpinning the open quantum system approach is that the dynamics of the system is often insensitive to the precise details of the environment. Thus, even if we only have coarse information about the environment, it is still possible to develop analytical and computational methods that accurately describe the system. Of course, to do so, one first has to decide where the boundary between system and environment lies. The open system approach will be most successful if the bipartition (4.1) is chosen sensibly, and in many scenarios a natural choice presents itself. Typically, the system contains all the degrees of freedom that can be explicitly controlled and/or measured in the given experiment, whereas the environment features those that are not directly accessible, and are relatively unstructured.

When studying topological systems, there is another reason to distinguish between system and environment. The concept of a topologically non-trivial phase is only strictly well-defined under certain conditions. In particular, for the phases that we consider in this thesis, the system can only be topologically classified if it is gapped in the bulk. In many settings, there are extraneous gapless degrees of freedom which make it impossible to identify topological properties at the level of the composite system. Therefore, from a theoretical perspective it is useful to choose a bipartition (4.1) in a way that allows one to topologically classify the system unambiguously. The formalisms developed to study topological phases in isolated systems can then be harnessed.

With this in mind, let us specify the scenarios that we will address in the rest of this chapter. We will consider systems that are in a well-defined topologically non-trivial gapped phase (mainly focussing on SPT order here) in the limit of being decoupled from the rest of the universe, i.e. we assume that $\hat{H}_S$ has a finite bulk gap E_g and possesses a non-trivial ground state in the sense of Definition 2 in Section 1.2. The system will then be coupled to other degrees of freedom that we refer to as the environment. In the present context, we understand that *the environment contains all degrees of freedom that would preclude a topological classification of $\hat{H}_S$ if they were considered to be part of the system*. For example, for topological band insulators in solid state systems, there are always core electronic bands

which lie well below the Fermi level – these extra degrees of freedom can be safely thought of as part of the system, since gapped bands can always be added to a system without changing its topological properties [120]. In contrast, acoustic phonons are gapless, and therefore must be included in the environment. Even gapped optical phonons may need to be included in the environment, since their dimensionality does not always coincide with the topological phase under considerations (e.g. two dimensional electron gases in the quantum Hall regime will still be coupled to three dimensional phonons). Importantly, unlike the previous chapters, the systems we consider here are not necessarily far from equilibrium – in fact we will mainly consider environments at thermal equilibrium.

In many cases, the influence of the environment can be treated using the powerful methods developed in the wider context of open quantum systems. Perhaps the most useful tool is the concept of a master equation – an equation of motion describing the time evolution of the reduced density matrix for the system $\hat{\rho}_S(t) \coloneqq \mathrm{Tr}_E\, \hat{\rho}(t)$. For instance, under a particular set of conditions (discussed in Section 4.3), the evolution of $\hat{\rho}_S(t)$ can be described by a quantum Markov process, which roughly speaking means that the system dynamics is only dependent on the instantaneous state of the system, and not on its past trajectory. The most general equation of motion describing such a system is known as the Lindblad master equation[1], which has the form [137]

$$\frac{\mathrm{d}\hat{\rho}_S(t)}{\mathrm{d}t} = \mathscr{L}[\hat{\rho}] = -\mathrm{i}[\hat{H}_{\mathrm{eff}}, \hat{\rho}_S(t)] + \sum_\mu \gamma_\mu \left[\hat{L}_\mu \hat{\rho}_S(t) \hat{L}_\mu^\dagger - \frac{1}{2}\{\hat{L}_\mu^\dagger \hat{L}_\mu, \hat{\rho}_S(t)\}\right] \tag{4.3}$$

where the effective Hamiltonian $\hat{H}_{\mathrm{eff}}$ is a Hermitian operator and the 'jump operators' $\{\hat{L}_\mu\}$ are a set of non-Hermitian operators, orthonormal under the Hilbert-Schmidt operator inner product $(\hat{A}, \hat{B}) \coloneqq (\mathrm{Tr}\, \mathbb{1}_S)^{-1}\, \mathrm{Tr}\, \hat{A}^\dagger \hat{B}$, and each associated with a decay rate γ_μ. The object $\mathscr{L}$, sometimes referred to as the Lindbladian, is a superoperator – a linear mapping between operators.

Of course, while the approximations made in deriving a master equation may be accurate, some information about the environment is inevitably lost in reducing the system dynamics to the Lindblad form. One must therefore bear in mind that the true dynamics of the system is governed by the composite Hamiltonian. For instance, in this chapter, we will see examples where the standard 'Born-Markov' derivation for the jump operators $\{\hat{L}_\mu\}$ and effective Hamiltonian $\hat{H}$ fails to capture important effects that are present at the level of the microscopic Hamiltonian. Moreover, some of the systems considered in this chapter will not even be amenable to open quantum system methods, which rely on the environment having sufficiently little internal structure. We will consider one such scenario in Section

[1] also known as the Lindbladian, or the Gorini-Kossakowski-Sudarshan-Lindblad (GKSL) master equation

4.4, where a two-level system is coupled to the edge modes of a two-dimensional topological insulator. There, Kondo-like resonances arise which require a full analysis of the composite Hamiltonian (4.2) in its entirety.

Having specified what we mean by an open system in the context of topological phases and introduced some of the concepts we will be using, we now discuss the symmetry properties of open quantum systems, which we expect to be of particular importance to SPTs.

4.2 Symmetry protection in open systems

The majority of previous studies where topological aspects of open quantum systems have been considered begin with an effective equation of motion describing the dynamics of the system: either a Lindblad master equation (4.3) [58, 15, 28, 217] or non-Hermitian Hamiltonian [83, 113, 250]. In these studies, symmetries are imposed *a posteriori* on this approximate equation of motion, using formalisms described in e.g. Ref. [23]. Instead, our starting point is the full system-environment Hamiltonian (4.2). This allows us to define symmetries at the microscopic level, and we can later ask how those fundamental symmetries are reflected in the effective equations of motion.

In the following, we will find it useful to employ the following decomposition of the system-environment coupling (which can always be made):

$$\hat{H}_{SE} = \sum_{\alpha=1}^{M} \hat{A}_\alpha \otimes \hat{B}_\alpha, \tag{4.4}$$

where $\hat{A}_\alpha$ and $\hat{B}_\alpha$ are Hermitian operators acting on the system and environment, respectively, and M is the number of 'coupling channels'.

Suppose now that the system Hamiltonian $\hat{H}_S$ possesses symmetry-protected features, i.e. properties that remain robust within a range of parameter space provided that a suitable symmetry of the Hamiltonian is maintained. We anticipate that any such features will be spoiled by the system-environment coupling if $\hat{H}_{SE}$ does not respect the relevant symmetries. Therefore, a natural scenario to consider is one where the full Hamiltonian $\hat{H}$ respects the same set of symmetries as $\hat{H}_S$. For example, in topological superconductors possessing Majorana zero modes (see Section 1.2.2), the protecting symmetry is conservation of fermion parity, which will always be respected by any physical Hamiltonian. The isolated system possesses degenerate ground states with opposite fermion parity (corresponding to different states of the non-local Majorana fermion) within which quantum information can be robustly stored over long times. However, once the system-environment coupling is turned on,

fermions can tunnel in/out of the system, even if $\hat{H}$ conserves fermion parity overall. This allows for transitions between the degenerate ground states, and in turn decoherence of the Majorana mode [178]. This 'quasiparticle poisoning' effect is one of several well-known examples where the environment spoils the topological properties of the system, even when the composite Hamiltonian is symmetry-respecting.

Evidently, the issue is that the symmetry of $\hat{H}$ pertains to the combined system and environment, whereas the symmetry-protected phenomena we are interested in, e.g. coherence of quantum information, are properties of the system alone. In the Majorana fermion example, we can remedy this by suppressing processes where an odd number of fermions are transferred between system and environment. In terms of the decomposition (4.4), this amounts to demanding that each coupling operator $\hat{A}_\alpha$ conserve the fermion parity in the system (which can be achieved in experiment using e.g. Coulomb blockade effects [169, 112, 163]). These considerations point to a more general strategy for ensuring symmetry protection in the open system, wherein one ensures that every component of the Hamiltonian $\{\hat{A}_\alpha\}$, $\{\hat{B}_\alpha\}$, $\hat{H}_S$ and $\hat{H}_E$ is symmetry-respecting. One might expect that this scenarios of this type – which we focus on throughout this chapter – would be sufficiently protected, since each $\hat{A}_\alpha$ obeys the same constraints as the original Hamiltonian $\hat{H}_S$: they are both Hermitian and symmetry-respecting. Here we will show that this intuition can fail: when the protecting symmetry is antiunitary (e.g. TRS), protection is lost *regardless of the symmetries of* $\hat{A}_\alpha$.

To understand why TRS and other antiunitary symmetries are unable to offer protection in open quantum systems, it is instructive to analyse a simple few-body model, following the approach we introduced in Ref. [148]. Consider an isolated spin-3/2 with Hamiltonian $\hat{H}_S = E_g(\hat{S}^z)^2$, with twofold degenerate ground states $|^1\!/_2\rangle$ and $|^{-1}\!/_2\rangle$. As long as a suitable symmetry is enforced, the two ground states will remain degenerate as $\hat{H}_S$ is varied. For instance, the degeneracy can be protected by TRS (Kramers' theorem), or alternatively by a unitary group of rotations by π about the principle axes, generated by $\hat{R}_{x,y,z} = e^{i\pi\hat{S}^{x,y,z}}$ [172]. This eigenstate property is reflected in the dynamics of the system: If we encode a qubit in the degenerate subspace, $|\psi\rangle_S = \alpha\,|^1\!/_2\rangle + \beta\,|^{-1}\!/_2\rangle$, then time evolution under $\hat{H}_S$ leaves this state undisturbed and the qubit can be reliably recovered. Even if $\hat{H}_S$ is weakly perturbed, the overlap $|\langle\psi(0)|\psi(t)\rangle|^2$ will remain close to 1 for all time provided the appropriate symmetries are maintained.

We can ask how this symmetry-protected coherence is affected by coupling to an environment. Insight can be gained from considering the simple limit $\hat{H}_E = 0$, and computing the time dependent wavefunction for the composite system $|\Psi(t)\rangle$ using time-dependent perturbation theory in $V \sim \|\hat{H}_{SE}\|$, the characteristic strength of the system-environment coupling. At time

$t = 0$, the system and environment are initialized in a factorized state $|\Psi(0)\rangle = |\psi\rangle_S \otimes |\chi\rangle_E$[2]. We write the time-evolved wavefunction as $|\Psi(t)\rangle = |\Psi(0)\rangle + \sum_{j=1}^{\infty} |\Psi^{(j)}(t)\rangle$, where $|\Psi^{(j)}(t)\rangle$ is the contribution at jth order in perturbation theory. At first order in V, we have

$$|\Psi^{(1)}(t)\rangle = -\mathrm{i}t \sum_{\alpha} \hat{\Pi}_{\mathrm{GS}} \hat{A}_\alpha |\psi\rangle_S \otimes \hat{B}_\alpha |\phi\rangle_E \tag{4.5}$$

where $\hat{\Pi}_{\mathrm{GS}}$ projects onto the degenerate ground state subspace of the system S. For generic $\{\hat{A}_\alpha\}$, the system becomes entangled with the environment (since $|\Psi(t)\rangle$ cannot be written in a factorized form), leading to decoherence of the qubit. Note also that decoherence still occurs even if $\hat{H}_{SE}$ is itself symmetric, but the operator $\hat{A}_\alpha$ are symmetry-violating. However, if all $\{\hat{A}_\alpha\}$ respect the same symmetry as the Hamiltonian $\hat{H}_S$, then these operators can only act trivially within the degenerate subspace, i.e. $\hat{\Pi}_{\mathrm{GS}} \hat{A}_\alpha |\psi\rangle_S = a_\alpha |\psi\rangle_S$ by the same arguments that forbid a symmetry-respecting Hamiltonian from coupling the two states (see Section 4.3 for a more formal justification of this argument). This gives $|\Psi(t)\rangle = |\psi\rangle_S \otimes (1 - \mathrm{i}t \sum_\alpha a_\alpha \hat{B}_\alpha) |\phi\rangle_E$, so the system remains unperturbed. This lends credence to the simple expectation, stated above, that coherence is preserved if the operators $\{\hat{A}_\alpha\}$ are invariant under the symmetries of $\hat{H}_{\mathrm{S}}$ that protect the degeneracy.

However, as indicated before, this hypothesis turns out to be incorrect in general. This can be seen already from the second order corrections in V:

$$|\Psi^{(2)}(t)\rangle = \frac{-\mathrm{i}t}{E_{\mathrm{g}}} \sum_{\alpha\beta} \hat{\Pi}_{\mathrm{GS}} \hat{A}_\alpha \hat{\Pi}_{\mathrm{Ex}} \hat{A}_\beta |\psi\rangle_S \otimes \hat{B}_\alpha \hat{B}_\beta |\phi\rangle_E \,, \tag{4.6}$$

where $\hat{\Pi}_{\mathrm{Ex}} := \hat{\mathbb{1}}_S - \hat{\Pi}_{\mathrm{GS}}$ projects onto excited states $|^{\pm 3}/_2\rangle$. (In deriving the expression (4.6), we have assumed that the coupling is gradually turned on at a rate slower than E_{g}, and neglected contributions $\propto |\Psi(0)\rangle$.) Equation (4.6) captures processes that occur via a virtual excited state, hence the factor of E_{g}^{-1} [see Fig. 4.1b].

We can use the same arguments as above to determine whether transitions within the ground state subspace will occur. Here, rather than considering $\hat{A}_\alpha$, we must consider the matrix elements of the operators

$$\hat{C}_{\alpha\beta} := \hat{A}_\alpha \hat{\Pi}_{\mathrm{Ex}} \hat{A}_\beta \tag{4.7}$$

Being composed of symmetry-respecting operators, $\hat{C}_{\alpha\beta}$ is itself invariant under the relevant symmetries; however, it is generically non-Hermitian, and so might not obey the same

[2] By linearity, this calculation can also be applied to the case where the environment is initialized in a mixed state i.e. $\hat{\rho}(t=0) = |\psi\rangle_S \langle\psi|_S \otimes \hat{\rho}_E$

constraints as a symmetry-respecting Hamiltonian. We therefore decompose $\hat{C}_{\alpha\beta} = \hat{X}_{\alpha\beta} + \mathrm{i}\hat{Y}_{\alpha\beta}$, where $\hat{X}_{\alpha\beta} \coloneqq (\hat{C}_{\alpha\beta} + \hat{C}_{\beta\alpha})/2$, and $\hat{Y}_{\alpha\beta} \coloneqq -\mathrm{i}(\hat{C}_{\alpha\beta} - \hat{C}_{\beta\alpha})/2$ are both Hermitian. Now, if the protecting symmetries are unitary, then both $\hat{X}_{\alpha\beta}$ and $\hat{Y}_{\alpha\beta}$ are also symmetry-respecting Hermitian operators, and so cannot cause transitions between different ground states. Similar arguments can be used to show that transitions are forbidden at all orders in perturbation theory.

However, due to the factor of $(-\mathrm{i})$ required by Hermiticity, $\hat{Y}_{\alpha\beta}$ will *not* be invariant under antiunitary symmetries, such as time-reversal. If the ground state degeneracy is protected by antiunitary symmetries, then $\hat{C}_{\alpha\beta}$ can act non-trivially within the ground state subspace for $\alpha \neq \beta$. For example, consider $\hat{A}_1 = (\hat{S}^x)^2$ and $\hat{A}_2 = \{\hat{S}^x, \hat{S}^z\}$, which are both invariant under time-reversal symmetry; The product $\hat{C}_{12}$ is proportional to $\mathrm{i}\hat{S}^y$ when projected onto the ground state subspace. Thus, generically we expect that the quibit will decohere. The only exception is if $\hat{H}_{SE}$ is factorizable, i.e. $M = 1$; however this requires fine-tuning. Although the limit $\hat{H}_E = 0$ precludes an estimation of a corresponding decoherence rate, we see that the perfect coherence enjoyed by the isolated system is fragile against coupling to an environment if the protecting symmetries are antiunitary.

While the above analysis refers explicitly to the spin-3/2 model, it highlights a much more general issue regarding symmetry protection in quantum systems. The problem stems from the fact that there is no way to consistently define antiunitary symmetries on a subsystem of some larger Hilbert space. To see why this is so, consider the following state of a two-qubit system (as suggested in Ref. [171])

$$|\Psi\rangle = \frac{1}{\sqrt{2}}\left[|\uparrow\rangle_A \otimes |\downarrow\rangle_B + (\mathrm{i}\,|\downarrow\rangle_A) \otimes |\uparrow\rangle_B\right] \equiv \frac{1}{\sqrt{2}}\left[|\uparrow\rangle_A \otimes |\downarrow\rangle_B + |\downarrow\rangle_A \otimes (\mathrm{i}\,|\uparrow\rangle_B)\right] \tag{4.8}$$

If one were to apply an antiunitary operator that acted on the subsystem A only, the outcome would depend on how we choose to separate the complex phases between A and B, which is unphysical.

This 'non-local' property of TRS plays an important rôle in the emergence of the arrow of time in quantum mechanics: Interactions between a quantum system and its surroundings enable processes that effectively break TRS for the system regardless of the presence of any microscopic symmetries, leading to effectively irreversible dynamics (see Section 1.3.1). Here, we show that this same mechanism leads to an inherent fragility of TRS-protected phenomena. In the above, even if every component of the Hamiltonian ($\{\hat{A}_\alpha\}$, $\{\hat{B}_\alpha\}$, $\hat{H}_S$, and $\hat{H}_E$) were TRS-invariant, the relevant protection occurs not at the level of the system Hilbert space, but on the composite system-environment Hilbert space. This is much like

the scenarios described above where symmetries were imposed on $\hat{H}$, but not the individual $\hat{A}_\alpha$. Thus, without explicit control over the environment, the system will not exhibit any desired TRS-protected properties (e.g. coherence of quantum information). In essence, the system-environment interactions mediate processes that would be forbidden by TRS in an isolated system. In contrast, it *is* possible to define a unitary symmetry that pertains only to the system and not to the environment, under which the relevant phenomena can remain protected at non-zero coupling.

Note that although this effective breaking of TRS can be intuitively understood within the context of the arrow of time, the consequences of our findings are more general. While irreversibility only strictly emerges in the limit of an infinitely large environment, the symmetry-breaking effects we consider here occur regardless of the number of degrees of freedom present. In Section 4.4, we will discuss a scenario where a single spin-1/2 coupled to a system via operators $\hat{A}_\alpha$ that are TRS-invariant still leads to TRS-forbidden processes in the system.

By looking at the structure of perturbation theory generated by the microscopic Hamiltonian (4.2), we have identified an important distinction between unitary and antiunitary symmetries in open quantum systems. At this point, it is helpful to establish some relationships between our findings and previous complementary works where symmetry properties of Lindblad master equations were studied [17, 23, 3, 141, 161, 136]. For unitary symmetries, one can define so-called 'weak' and 'strong' symmetries of the Lindbladian $\mathscr{L}$ [Eq. (4.3)]. If $\hat{U}_S$ is a symmetry operator acting on the system only, then one can formally define symmetries in two different ways [23]

$$\mathscr{L}[\hat{U}_S\hat{\rho}_S\hat{U}_S^\dagger] = \hat{U}_S\mathscr{L}[\hat{\rho}_S]\hat{U}_S^\dagger \tag{4.9a}$$

$$\mathscr{L}[\hat{U}_S\hat{\rho}_S] = \hat{U}_S\mathscr{L}[\hat{\rho}_S] \tag{4.9b}$$

We say that $\mathscr{L}$ respects a weak symmetry if (4.9a) is satisfied, and a strong symmetry if both conditions (4.9a) and (4.9b) are satisfied. The latter also implies a similar relation for symmetries acting from the right $\mathscr{L}[\hat{\rho}_S\hat{U}_S^\dagger] = \mathscr{L}[\hat{\rho}_S]\hat{U}_S^\dagger$.

Since the Lindbladian is constructed so as to approximate the dynamics governed by the Hamiltonian (4.2), any symmetries of $\mathscr{L}$ will be dicated by those of $\hat{H}$. For instance, if the total Hamiltonian $\hat{H}$ is invariant under a composite unitary symmetry $(\hat{U}_S \otimes \hat{U}_E)^\dagger \hat{H}(\hat{U}_S \otimes \hat{U}_E) = \hat{H}$ (where $\hat{U}_E$ determines how the symmetry transforms the environment), then it is straightforward to show that any Lindbladian describing the dynamics of the system must obey the weak condition (4.9a). Similarly, if every $\hat{A}_\alpha$ is invariant under the unitary symmetry

$\hat{U}_S$, then the strong condition (4.9b) also follows [211]. Our findings in this section can be thought of as a statement that the time-reversal symmetry of the coupling operators $\hat{A}_\alpha$ will *not* be reflected as a symmetry of $\mathscr{L}$, unlike the unitary case. Indeed any attempts to generalise the strong symmetry (4.9b) to the antiunitary case will end up being inconsistent, for reasons analogous to the discussion of Eq. (4.8). In contrast, one can define an analogous weak antiunitary symmetry for the Lindbladian

$$\mathscr{L}[\hat{T}_S\hat{\rho}_S^*\hat{T}_S^\dagger] = \hat{T}_S\mathscr{L}[\hat{\rho}_S]^*\hat{T}_S^\dagger \tag{4.10}$$

which is guaranteed if the composite system is time-reversal symmetric $(\hat{T}_S\otimes\hat{T}_E)^\dagger\hat{H}^*(\hat{T}_S\otimes\hat{T}_E)=\hat{H}$. (The time-reversal operator for the composite system can be written $\hat{T}=(\hat{T}_S\otimes\hat{T}_E)\hat{K}$, where $\hat{K}$ denotes complex conjugation.) These weaker symmetries (4.9a) and (4.10) are generally insufficient to ensure that the symmetry-protected features of the closed system will persist to the open regime. However, their presence still puts certain constraints on the dynamics of the open system, and one can identify other properties of $\mathscr{L}$ that can be protected by such a symmetry. (We will not discuss these cases in this thesis; see Refs. [217, 136] for some examples.)

4.3 Coherence properties of topological bound states

Having discussed the symmetry properties of open quantum systems in general, we are now in a position to analyse the effects of an environment on topological phases. In particular, our findings naturally have implications for SPTs. In this section, we will consider systems possessing topological bound states – collective degrees of freedom that remain spatially localized and gapless as long as the relevant symmetries are enforced. Such states can arise at the edges of one-dimensional (1D) SPTs [65], as well as within lattice defects of higher-dimensional systems [209].

Let us first consider the properties of isolated systems possessing topological bound states. Provided that all bound states are located far apart from one another compared to the correlation length of the system, we can focus on dynamics within the vicinity of just one[3]. Accordingly, the eigenstate structure of the system Hamiltonian $\hat{H}_S$ closely resembles that of the spin-3/2 model considered above: The system is gapped in the bulk, and so almost all eigenstates have energy $\geq E_\mathrm{g}$, while the remaining N_S states are all ground states $\hat{H}_S|j\rangle = 0$, $j=1,\ldots,N_S$, corresponding to different configurations of the bound state. The

[3] In systems possessing Majorana zero modes, one may need to keep track of an additional bound state far from the region of interest to ensure that the system is composed of a whole number of Dirac fermions.

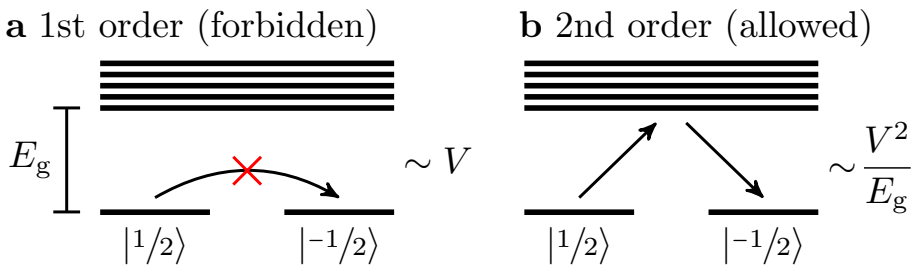

Fig. 4.1 Decoherence mechanisms for topological bound states coupled to an environment. The spectrum of $\hat{H}_S$ possesses N_S ground states whose degeneracy is protected by symmetry (here we draw $N_S = 2$ ground states $|1/2\rangle$ and $|{-1}/2\rangle$). All excited states are above the gap E_g. This picture applies to both systems possessing topological bound states (section 4.1), as well as few-body models, such as the spin-3/2 in Section 4.2. If the environment is at a temperature $T \ll E_g$, then transitions to excited states are thermally activated, and occur at an exponentially slow rate $\sim e^{-E_g/T}$. **a**, Direct transitions between ground states are forbidden by symmetry if the coupling operators $\hat{A}_\alpha$ [Eq. (4.4)] respect the relevant symmetries. **b**, If the protecting symmetry is TRS (or any antiunitary symmetry), then indirect transitions are allowed regardless of the symmetries of $\hat{A}_\alpha$. These proceed via a virtual excited state, and the corresponding matrix elements scale as V^2/E_g [see Eq. (4.6)].

ground state subspace $\mathscr{H}_{GS} = \text{span}(|j\rangle) \subset \mathscr{H}_S$ forms a N_S-dimensional irreducible projective representation of the protecting symmetry group G. According to Schur's Lemma [246], any symmetry-respecting Hermitian operator $\hat{H}$ must act like the identity operator within $\mathscr{H}_{GS}$, i.e. $\hat{\Pi}_{GS}\hat{H}\hat{\Pi}_{GS} \propto \hat{\Pi}_{GS}$. This explains why the degeneracy cannot be lifted by a symmetry-respecting Hamiltonian perturbation.

In an isolated system, any quantum information encoded within these topological bound states will remain coherent, thanks to their protected degeneracy. However, our newfound intuition suggests that if the SPT is protected by (anti-)unitary symmetries, then the topological bound state will (not) remain coherent when the system is coupled to an environment. More precisely, we expect that those phases that can be trivialized by explicitly breaking all antiunitary symmetries will exhibit decoherence. (This already suggests some relationship between the results of this chapter and the non-equilibrium classification developed in Chapter 2; we will discuss this connection more in Section 4.5.) To confirm our hypothesis, we will derive a master equation describing the dynamics of the system, from which a decoherence time τ_{coh} for the bound states can be extracted. This helps us to identify generic conditions under which quantum information can be reliably stored in these systems for long times.

4.3.1 The Born-Markov approximation

The problem of deriving a master equation for the system density matrix $\hat{\rho}_S(t)$ from a microscopic Hamiltonian $\hat{H}$ is a standard one. A number of approximations must be made in order to reach a tractable expression for $\mathrm{d}\hat{\rho}_S(t)/\mathrm{d}t$, one of which is usually to do with the relative strength of the three terms in (4.2). (Unlike the simple analysis of Section 4.2, we do not neglect $\hat{H}_E$ here.) In the vast majority of studies involving open quantum systems, the Born-Markov approximation is employed, which roughly speaking amounts to keeping only terms of second order in the system-environment coupling strength V (this is discussed in more detail in the following section). Within this approximation, a master equation can be derived using standard techniques. We first introduce the two-time correlation functions for the environment

$$\tilde{\Gamma}_{\alpha\beta}(t) \coloneqq \mathrm{Tr}_E\left(\hat{\rho}_E \hat{B}_\alpha(t)\hat{B}_\beta(0)\right) = \int \frac{\mathrm{d}\varepsilon}{2\pi} e^{-\mathrm{i}\varepsilon t}\Gamma_{\alpha\beta}(\varepsilon), \tag{4.11}$$

and the associated spectral functions $\Gamma_{\alpha\beta}(\varepsilon)$. We work in the interaction picture with respect to $\hat{H}_0 = \hat{H}_S \otimes \hat{\mathbb{1}}_E + \hat{\mathbb{1}}_S \otimes \hat{H}_E$; thus $\hat{B}_\alpha(t) \coloneqq e^{\mathrm{i}\hat{H}_E t}\hat{B}_\alpha e^{-\mathrm{i}\hat{H}_E t}$. Here $\hat{\rho}_E$ is the density matrix describing the state of the environment at time $t = 0$, which for the purposes of this thesis we will take to be thermal $\hat{\rho}_E = Z^{-1}\,\mathrm{Tr}_E\, e^{-\beta\hat{H}_E}$, where $Z = \mathrm{Tr}_E\, e^{-\beta\hat{H}_E}$. In terms of these spectral functions, the master equation is (see Ref. [21] for a derivation)

$$\frac{\mathrm{d}\hat{\rho}_S}{\mathrm{d}t} = -\mathrm{i}[\hat{H}_S + \hat{H}_{LS}, \hat{\rho}_S] + \sum_{\omega,\alpha,\beta} \Gamma_{\alpha\beta}(\omega)\left[\hat{A}_\beta(\omega)\hat{\rho}_S\hat{A}^\dagger_\alpha(\omega) - \frac{1}{2}\left\{\hat{A}^\dagger_\alpha(\omega)\hat{A}_\beta(\omega), \hat{\rho}_S\right\}\right], \tag{4.12}$$

where $\hat{A}_\alpha(\omega)$ is the component of $\hat{A}_\alpha$ that lowers the energy of the system by an amount ω. Explicitly,

$$\hat{A}(\omega) \coloneqq \sum_{\varepsilon'-\varepsilon=\omega} \hat{\Pi}_\varepsilon \hat{A}_\alpha \hat{\Pi}_{\varepsilon'} \tag{4.13}$$

where $\hat{\Pi}_\varepsilon$ is the projector onto the eigenspace of $\hat{H}_S$ with energy ε. Evidently, $\hat{A}_\alpha(\omega)^\dagger = \hat{A}_\alpha(-\omega)$. The Lamb shift Hamiltonian can be written

$$\hat{H}_{LS} = \sum_{\omega,\alpha,\beta} S_{\alpha\beta}(\omega)\hat{A}_\alpha(\omega)^\dagger\hat{A}_\beta(\omega) \tag{4.14}$$

where $S_{\alpha\beta}(\omega)$ is the antisymmetrized two-time correlator $2\mathrm{i}S_{\alpha\beta}(\varepsilon) = \int \mathrm{d}t\ \mathrm{sgn}(t)e^{-\mathrm{i}\varepsilon t}\Gamma_{\alpha\beta}(t)$. While Eq. (4.12) does not quite resemble the general Lindblad master equation $\mathrm{d}\hat{\rho}_S(t)/\mathrm{d}t =$

$\mathscr{L}[\hat{\rho}_S(t)]$, it can be brought into the form (4.3) by diagonalizing $\Gamma_{\alpha\beta}(\omega)$ separately for each ω [21]. The dynamics described by this master equation is therefore an example of a quantum Markov process: at any given time t, the future trajectory $\hat{\rho}_S(t' > t)$ is entirely determined by $\hat{\rho}_S(t)$ through an evolution operator $\mathscr{U}(t',t) = e^{(t'-t)\mathscr{L}}$ that depends only on the difference between times $t' - t$.

Suppose now that the system in question is an SPT hosting topological bound states. We can ask whether quantum information stored therein remains coherent under the dynamics described by the master equation (4.12). We therefore consider an initial state within the ground state subspace $\rho_S(0) \in \mathscr{H}_{\mathrm{GS}}$, and ask whether information about $\rho_S(0)$ can be recovered at late times. Regardless of any symmetry considerations, there will generically be terms in the sum (4.12) with $\omega < 0$ that can induce transitions out of the ground state subspace at some rate τ_{ex}^{-1}. These incoherent processes generate entanglement between the system and environment, leading to decoherence of the system. Moreover, the bulk excitations are mobile, and so quantum information can be carried away from the vicinity of the bound state, and one will not be able to reconstruct the initial state from local measurements [178]. These excitations must therefore be suppressed in order to protect the coherence of the bound state.

The most natural scenarios in which bulk excitations are suppressed are those where the environment temperature T is small compared to the bulk gap $T \ll E_{\mathrm{g}}$. In this case, transitions to excited states are thermally activated and thus exponentially slow. More concretely, if the environment is in a thermal state, then spectral functions will obey the Kubo-Martin-Schwinger relation $\Gamma_{\alpha\beta}(\varepsilon) = e^{\varepsilon/T}\Gamma_{\beta\alpha}(-\varepsilon)$ [142]. Therefore, they will be exponentially suppressed for large negative arguments $\Gamma_{\alpha\beta}(-|\varepsilon|) \sim e^{-\beta|\varepsilon|}$. Since the system possesses a bulk gap, the relevant terms in (4.12) will be those with $\omega \leq -E_{\mathrm{g}}$, i.e. an energy of at least E_{g} must be transferred from environment to system. These are suppressed by a factor $\tau_{\mathrm{ex}}^{-1} \sim \Gamma_{\alpha\beta}(-E_{\mathrm{g}}) \sim e^{-E_{\mathrm{g}}/T} \ll 1$, and hence can be neglected. While there are other contexts in which bulk excitations are suppressed (e.g. if the bandwidth of the environment is much less than E_{g}), we will focus on the low-temperature regime in the following. Note that the effects of thermally generated excitations on the coherence properties of topological bound states have been considered elsewhere [81].

We are now left with transitions that occur within the ground state subspace, which here are described by terms in the sum with $\omega = 0$, as well as the part involving the Lamb shift $\hat{H}_{LS}$. If the coupling operators $\hat{A}_\alpha$ and $\hat{B}_\alpha$ respect the symmetries required to protect the ground state subspace, then we must have $\hat{\Pi}_{\mathrm{GS}}\hat{A}_\alpha(0)\hat{\Pi}_{\mathrm{GS}} \propto \hat{\Pi}_{\mathrm{GS}}$ and $\hat{\Pi}_{\mathrm{GS}}\hat{H}_{LS}\hat{\Pi}_{\mathrm{GS}} \propto \hat{\Pi}_{\mathrm{GS}}$

by Schur's Lemma[4]. It follows that within the Born-Markov approximation, $\mathrm{d}\hat{\rho}/\mathrm{d}t = 0$ up to corrections that scale as $e^{-E_\mathrm{g}/T}$, and so the bound state remains coherent for long times. In contrast, if $\hat{A}_\alpha$ are not invariant under the relevant symmetries, then direct transitions within the ground state subspace are allowed, and the bound state will decohere at a rate on the order of the eigenvalues of the matrix $\Gamma_{\alpha\beta}(\omega = 0)$.

This analysis is analogous to the lowest order treatment of the spin-3/2 model in Section 4.2 [Eq. (4.5)], and the conclusions we draw are similar: decoherence occurs only if $\hat{A}_\alpha$ are not invariant under the relevant symmetries. The differences between unitary and antiunitary symmetries are not yet evident. This is perhaps to be expected – the Born-Markov approximation captures only the leading order terms in V, whereas we saw in Section 4.2 that the effective breaking of antiunitary symmetries is manifest in higher order terms in perturbation theory. We therefore need to develop methods that allow us to capture these indirect processes occurring via an intermediate virtual state [Fig. 4.1]. To do so, it is helpful to first discuss the general validity of the Born-Markov approximation, and understand how one can improve upon it.

4.3.2 Beyond Born-Markov

In Eq. (4.12), the influence of the environment on the system comes through the spectral functions $\Gamma_{\alpha\beta}(\omega)$, or equivalently the time-domain correlators $\tilde{\Gamma}_{\alpha\beta}(t)$. There are two scales associated with these quantities: their magnitude, and the typical range in time over which they decay, which we call τ_m, the 'memory time' of the environment[5]. The former is related to the strength of $\hat{H}_{SE}$ through $\tilde{\Gamma}_{\alpha\beta}(t=0) = \langle \hat{B}_\alpha \hat{B}_\beta \rangle \sim V^2$. The latter represents a timescale over which the observable $\hat{B}_\alpha$ returns to its equilibrium value under its own dynamics after being perturbed by the operator $\hat{B}_\beta$.

Being based on a perturbative expansion in the system-environment coupling, the validity of the Born-Markov approximation clearly relies on V being sufficiently small. Additionally, the fact that the resulting master equation is Markovian suggests that the memory time τ_m must also be small: If τ_m were very long, then the environment would be gradually driven

[4]For unitary symmetries, the only condition required to invoke Schur's Lemma is that $\hat{A}_\alpha$ and $\hat{H}_S$ are invariant under the symmetry operation. For antiunitary symmetries, $\hat{B}_\alpha$ and $\hat{H}_E$ must also be symmetry-respecting, else $\Gamma_{\alpha\beta}(\omega)$ and $S_{\alpha\beta}(\omega)$ will generically be complex [see Eq. (B.18)] and the ground state degeneracy will generically be split by the Lamb shift. Note that all of these conditions are met if we demand that $\hat{A}_\alpha$ and the composite Hamiltonian $\hat{H}$ are both symmetry-respecting.

[5]The correlation functions can only strictly decay as $|t| \to \infty$ if the environment is composed of infinitely many degrees of freedom. However, any effects due to the finite size of the environment will generally occur over a timescale on the order of the inverse level spacing of $\hat{H}_E$ (the 'Heisenberg time'), which is exponentially large in the size of the environment and so is usually longer than experimental timescales.

away from its initial state by the system, and in turn the dissipative forces felt by the system at late times would be different from those felt at early times. The question of how small τ_{m} has to be for the dynamics of the system to be Markovian is a subtle one, which is discussed in some detail in Appendix B (see also references therein). In short, one must compare τ_{m} to a third timescale τ_S, which captures the rate of change of the system density matrix, i.e. the time it takes for the state of the system to change appreciably. If

$$\tau_{\mathrm{m}} \ll \tau_S, \tag{4.15}$$

then the dynamics of the system is Markovian over coarse-grained timescales larger than τ_{m}. Therefore, provided we are not interested in resolving timescales shorter than τ_{m}, the system can be accurately described by a Lindblad master equation: $\mathrm{d}\hat{\rho}(t)/\mathrm{d}t = \mathscr{L}[\hat{\rho}(t)]$ for some time-independent generator $\mathscr{L}$ of the form (4.3). It is not always clear *a priori* which quantities determine τ_S; however one can work on the basis of the assumption (4.15) and check that it is indeed satisfied self-consistently at the end of the calculation.

We can understand the Lindblad master equation as a contribution to the true dynamics of the system that is of leading order in τ_{m}/τ_S. The Born-Markov approximation can be thought of as an additional perturbative expansion of $\mathscr{L}$ on top of this, which is truncated at second order in V. (More precisely, the relevant dimensionless perturbative parameter is $\tau_{\mathrm{m}}V$ [107].) Evidently, improvements to the Born-Markov approximation can be made by including higher order corrections in either one of these parameters. Based on the intuition developed in Section 4.2, we expect that decoherence mechanisms for topological bound states protected by antiunitary symmetries will arise at fourth order in V (since the square of the relevant matrix element scales as V^4; see Fig. 4.1b), and so we will extend the expansion in $\tau_{\mathrm{m}}V$, rather than τ_{m}/τ_S. We do not rule out the possibility that higher order terms in τ_{m}/τ_S, which generate fully non-Markovian dynamics, may also give rise to decoherence processes not present in Eq. (4.12). However, we expect that the inclusion of these additional effects will not change our qualitative conclusions – namely that dissipation induces processes that would be forbidden by antiunitary symmetries in an isolated system. Therefore, in the following we will work in regimes where (4.15) is satisfied, and our derivation will be on the basis that the master equation will be of Lindblad form.

All that remains now is to obtain an expression for the Linablad generator $\mathscr{L}$ that contains effects that are higher-order in $\tau_{\mathrm{m}}V$. Our calculation (the details of which can be found in Appendix B) is based on computing $\hat{\rho}_S(t)$ for times $\tau_{\mathrm{m}} \ll t \ll \tau_S$ using time-dependent perturbation theory to fourth order in V and comparing with the formal solution of the master equation $\hat{\rho}_S(t) = \hat{\rho}_S(0) + t\mathscr{L}[\hat{\rho}_S(0)] + \mathscr{L}^2[\hat{\rho}_S(0)]/2! + \cdots$. The necessary coarse-graining can then be performed with the help of the Laplace transform. Again, we work in the regime

$T \ll E_{\mathrm{g}}$, such that transitions to excited states occur at a negligibly slow rate. Provided that the composite system is invariant under at least one antiunitary symmetry (which is the case in the scenarios of interest here), the Lindblad generator can be written

$$\frac{\mathrm{d}\hat{\rho}_S(t)}{\mathrm{d}t} = -\mathrm{i}[\hat{H}_S, \hat{\rho}_S(t)] + \mathscr{L}^{(2)}[\hat{\rho}_S(t)] + \mathscr{L}^{(4)}[\hat{\rho}_S(t)] + \mathscr{O}([\tau_{\mathrm{m}} V]^6) \tag{4.16}$$

where $\mathscr{L}^{(2)}$ is the Born-Markov expression (4.12), and the fourth order correction to the Lindbladian $\mathscr{L}^{(4)}$ is

$$\begin{aligned}\mathscr{L}^{(4)}[\hat{\rho}_S] = \sum_{\substack{\alpha_1,\ldots,\alpha_4 \\ \omega_1,\omega_2 \geq E_{\mathrm{g}}}} \int \frac{\mathrm{d}\varepsilon}{4\pi} \Gamma_{\alpha_4\alpha_1}(\varepsilon)\Gamma_{\alpha_3\alpha_2}(-\varepsilon) \Big(\hat{C}_{\alpha_1\alpha_2}(\omega_1,\varepsilon)\hat{\rho}_S \hat{C}_{\alpha_4\alpha_3}(\omega_2,-\varepsilon) \\ - \frac{1}{2}\left\{ \hat{C}_{\alpha_1\alpha_2}(\omega_1,\varepsilon)\hat{C}_{\alpha_4\alpha_3}(\omega_2,-\varepsilon)\,,\, \hat{\rho}_S \right\} \Big) - \mathrm{i}[\hat{H}^{(4)}_{LS}, \hat{\rho}_S],\end{aligned} \tag{4.17}$$

where

$$\hat{C}_{\alpha\beta}(\omega,\varepsilon) \coloneqq \hat{\Pi}_{\mathrm{GS}} \left[\frac{\hat{A}_\alpha(\omega)\hat{A}^\dagger_\beta(\omega)}{\omega-\varepsilon} + \frac{\hat{A}_\beta(\omega)\hat{A}^\dagger_\alpha(\omega)}{\omega+\varepsilon} \right] \hat{\Pi}_{\mathrm{GS}}. \tag{4.18}$$

The equation (4.17) can be used to analyse the incoherent dynamics of both few-body and many-body systems possessing degenerate ground states in regimes where the environment temperature $T \ll E_{\mathrm{g}}$ and the system is prepared in a ground state. We do not provide an expression for the correction to the Lamb shift $\hat{H}^{(4)}_{LS}$ here; we need only know that it is Hermitian and constructed from products of $\hat{A}_\alpha(\omega)$ with real coefficients. As with the lower-order expression (4.12), the above is not manifestly in the diagonal Lindblad form (4.3), however it can in principle be cast into this form by standard methods [21].

4.3.3 Estimating the decoherence rate

Having derived the general master equation to fourth order in V, we can apply it to our scenarios of interest, namely systems with topological bound states coupled to an environment. We immediately notice that the quantity (4.18) resembles the operator $\hat{C}_{\alpha\beta}$ which we encountered in our analysis of the spin-3/2 model in Section 4.2. Again, if the symmetries protecting the ground state subspace are unitary, then both the Hermitian and antihermitian components of $\hat{C}_{\alpha\beta}(\omega,\varepsilon)$ are constrained by Schur's Lemma, and so $\hat{C}_{\alpha\beta}(\omega,\varepsilon) \propto \hat{\Pi}_{\mathrm{GS}}$. Similarly, the Lamb shift $\hat{H}^{(4)}_{LS}$ is Hermitian and inherits all the symmetries of the composite Hamiltonian $\hat{H}$; thus it also acts like the identity within the ground state subspace. The master equation then reduces to $\mathrm{d}\hat{\rho}_S/\mathrm{d}t = 0$, and we conclude that the bound state can only decohere through

thermally activated processes at this order. Moreover, if we were to compute the master equation at $(2n)$th order in V, we see from the structure of perturbation theory that non-thermally-activated transitions would be generated by analogous operators $\hat{C}_{\alpha_1\ldots\alpha_n}$ composed of products of n operators $\hat{\Pi}_{\mathrm{GS}}\hat{A}_{\alpha_1}(\omega_1)\cdots\hat{A}_{\alpha_n}(\omega_n)\hat{\Pi}_{\mathrm{GS}}$, which are projected onto the ground state subspace to ensure conservation of energy. Any such product can be decomposed into Hermitian and antihermitian components, which again must both be proportional to $\hat{\Pi}_{\mathrm{GS}}$ by Schur's Lemma, and thus will be unable to cause transitions. We conclude that for unitary symmetries, the coherence time scales as $\tau_{\mathrm{coh}} \sim e^{E_{\mathrm{g}}/T}$ at all orders in perturbation theory.

In contrast, if an antiunitary symmetry is required to protect the bound state, then the antihermitian component $\hat{Y}_{\alpha\beta}(\omega,\varepsilon) \coloneqq -\mathrm{i}[\hat{C}_{\alpha\beta}(\omega,\varepsilon) - \hat{C}_{\beta\alpha}(\omega,\varepsilon)]/2$ can act non-trivially within the ground state subspace, generating non-thermally-activated transitions that would be forbidden by TRS in the absence of an environmental[6]. The decoherence rate is then no longer exponentially suppressed.

To estimate the typical magnitude of τ_{coh}^{-1} in this case, we note that the integral over ε in (4.17) is dominated by the region $|\varepsilon| \lesssim T$, while $\omega_{1,2} \geq E_{\mathrm{g}} \gg T$. We can therefore expand the denominators in (4.18) in powers of ε/ω. The zeroth order terms are Hermitian, and so do not contribute to $\hat{Y}_{\alpha\beta}(\omega,\varepsilon)$. We therefore have $\hat{Y}_{\alpha\beta}(\omega,\varepsilon) \approx (\varepsilon/\omega^2)\hat{D}_{\alpha\beta}(\omega)$ for some appropriate ε-independent dimensionless operator $\hat{D}_{\alpha\beta}(\omega)$, up to corrections that are higher order in T/E_{g}. We therefore expect that τ_{coh}^{-1} is of the order of the integral $K_{\{\alpha_i\}} \coloneqq E_{\mathrm{g}}^{-4}\int \mathrm{d}\varepsilon\, \varepsilon^2 \Gamma_{\alpha_4\alpha_1}(\varepsilon)\Gamma_{\alpha_3\alpha_2}(-\varepsilon)$.

To make progress, we can consider a particularly simple yet widely applicable model for the environment consisting of a bath of harmonic oscillators $\hat{H}_B = \sum_k \omega_k \hat{b}_k^\dagger \hat{b}_k$ (with canonical commutation relations $[\hat{b}_q, \hat{b}_{q'}^\dagger] = \delta_{qq'}$). For simplicity, we consider linear system-environment coupling $\hat{B}_\alpha = \sum_q g_{\alpha q}\hat{b}_q + g_{\alpha q}^*\hat{b}_q^\dagger$. Since the bath is presumed to be time-reversal symmetric, we have $g_{\alpha q}^* = g_{\alpha q}$. Following Caldeira and Leggett [33], we define the bath spectral density $J_{\alpha\beta}(\omega) \coloneqq \sum_q g_{\alpha q}^* g_{\beta q}\delta(\omega-\omega_q)$. The spectral functions are then given by $\Gamma_{\alpha\beta}(\omega) = \Theta(\omega)[1+n_B(\omega)]J_{\alpha\beta}(\omega) + \Theta(-\omega)n_B(-\omega)J_{\beta\alpha}(-\omega)$, where $n_B(\omega) = (e^{\omega/T}-1)^{-1}$ is the Bose distribution function. The bath spectral density is normalised such that $\int_0^\infty \mathrm{d}\omega J_{\alpha\beta}(\omega) = \mathrm{Tr}[\hat{B}_\alpha^\dagger \hat{B}_\beta] \sim V^2$, and is typically characterised by a power-law at small frequencies with exponent s, and a cutoff at large frequencies $\omega \gtrsim \omega_{\mathrm{c}}$, e.g. $J_{\alpha\beta}(\omega) \sim V^2\omega^s\omega_{\mathrm{c}}^{-s-1}e^{-\omega/\omega_{\mathrm{c}}}$ (however only the low-frequency behaviour of $J_{\alpha\beta}(\omega)$ matters here, provided $\omega_{\mathrm{c}} \gg T$). The most common case $s=1$ is referred to as 'Ohmic'. Simple power-counting arguments lead

[6] Despite the presence of these TRS-forbidden processes, the master equation still obeys a 'weak' TRS symmetry [Eq. (4.10)], which is due to the time-reversal symmetry of the composite Hamiltonian $\hat{H}$.

to an estimate for the decoherence time

$$\tau_{\text{coh}} \sim \frac{E_{\text{g}}^4 \omega_c^{2+2s}}{V^4 T^{3+2s}} \tag{4.19}$$

We note that since $\tau_S \sim \tau_{\text{coh}}$ and $\tau_{\text{m}} \sim \omega_c^{-1}$, the condition (4.15) required to derive the master equation is self-consistently satisfied for all sensible choices of parameters ($V \ll E_g$, $T \ll \omega_c$).

Although the exact dependence of τ_{coh} on on T may vary slightly for more structured environments, we can conclude that topological bound states protected by antiunitary symmetries generally decohere at a rate that that scales only algebraically with the environment temperature, rather than exponentially. This is consistent with our intuition that phenomena protected by antiunitary symmetries are intrinsically fragile against coupling to an environment, as described in Section 4.2.

Having studied the fate of topological bound states in the presence of an environment in detail, we now turn to the edge modes of higher-dimensional systems. Again, we find that the physics that emerges is qualitatively different depending on whether the topological phase is protected by unitary or antiunitary symmetries.

4.4 Conductance properties of topological edge modes

Thanks to the spatially localized nature of topological bound states, the low-energy properties of the systems considered in the previous section are particularly simple. The ground state subspace is formed of just a few discrete states, which are well-separated in energy from the bulk excitations. This helped us to derive the master equation Eq. (4.17), which captures the effects of the important 'indirect' processes generated by the system-environment coupling.

The aim of this section is to provide a similar analysis of the effects of an environment on systems that possess boundary modes of spatial dimension one, e.g. the chiral and helical edge states introduced in Section 1.2.2. Such modes can arise at the boundaries of two-dimensional SPTs [65], or as 'hinge' modes of three-dimensional higher-order SPTs protected by spatial symmetries [190]. In an isolated system, their topological nature protects them against being gapped out or localized by any local perturbations unless the relevant symmetries are broken explicitly or spontaneously. Accordingly, particles within these channels can propagate without reflection, giving rise to characteristic transport signatures, e.g. the quantum Hall effect. However, if the system is perturbed by coupling to an environment, the same arguments regarding robustness cannot necessarily be applied. Even if explicit or spontaneous symmetry

breaking does not occur, we anticipate that antiunitary symmetries will be effectively broken in the sense discussed in Section 4.2. This suggests that if the phase in question is protected by antiunitary symmetries, then the robust transport signatures expected of the isolated system may be compromised, even when the temperature is well below the bulk gap $T \ll E_g$.

One might hope that the master equation formalism used in the previous section, and in particular the expression Eq. (4.17), could be applied in this context. However, some of the approximations made in its derivation do not necessarily apply here. For instance, we assumed that the intermediate virtual state in the decoherence process [Fig. 4.1b] is a bulk excitation of energy $\geq E_g$, ensuring that the denominators in (4.18) are large; however, here there is a continuum of excitations with energies inside the bulk gap. A somewhat related problem is that perturbation theory is not necessarily as well controlled in this context as it is for topological bound states. Indeed thermodynamically large gapless systems are often subject to non-perturbative effects, as occurs in the Kondo problem [126]. Furthermore, since the system Hamiltonian is non-trivial within the low-energy subspace, the timescale of the system evolution τ_S will likely be faster than the scale associated with the dissipative part of the evolution governed by $\hat{H}_{SE}$, casting doubt on the validity of the Markovian assumption (4.15). We will therefore take a different approach based on analysing the composite Hamiltonian (4.2). Due to the increased complexity of the problem, we will not be able to derive results that are as quantitative as before, but we will obtain qualitatively correct expressions for the relevant transport coefficients that are valid in physically realistic regimes.

We will mainly focus on helical edge modes throughout this section, since they are experimentally relevant and relatively simple to understand. Moreover, they can be protected by either time-reversal symmetry (antiunitary) or spin-rotation symmetry (unitary), and so we can study how the transport properties depend on the presence or absence of each.

4.4.1 Dynamical impurity coupled to helical electrons

In Section 1.2.2, we encountered a simple model describing the dynamics of electrons in helical edge modes, in which non-interacting fermions with spin $\uparrow$ ($\downarrow$) propagate with a speed v_F in the $+x$ ($-x$) direction [Eq. (1.11)]. However, in a realistic experimental setting, this simple Hamiltonian is unlikely to be accurate. For instance, Coulomb interactions between the fermions will likely be present, as well as spin textures in momentum space due to spin-orbit coupling, which itself may even be spatially inhomogeneous [46, 78]. Therefore, we need a more general theory that can account for these perturbations. The solution is the helical Luttinger liquid (HLL) theory [241, 244], which is in its simplest form a bosonized version of the Hamiltonian (1.11) with interactions included. The theory involves fields $\hat{\phi}(x)$,

$\hat{\theta}(x)$, which obey the canonical commutation relations $[\hat{\phi}(x), \nabla\hat{\theta}(x')/\pi] = \mathrm{i}\delta(x-x')$. The HLL Hamiltonian is[7]

$$\hat{H}_{\mathrm{HLL}} = \frac{u}{2\pi}\int \mathrm{d}x \frac{1}{K}(\nabla\hat{\phi})^2 + K(\nabla\hat{\theta})^2 \tag{4.20}$$

Here, the Luttinger parameter K is a dimensionless number that quantifies the strength of interactions. One can develop some intuition for the above theory by starting with the non-interacting Hamiltonian (1.11) supplemented with density-density interactions, and employing the bosonization identity

$$\hat{\psi}_\sigma(x) = \left(\frac{1}{2\pi\xi}\right)^{1/2} \hat{F}_\sigma e^{\mathrm{i}\sigma(k_F - \pi/L)} e^{\mathrm{i}\hat{\theta}(x) - \mathrm{i}\sigma\hat{\phi}(x)} \tag{4.21}$$

where ξ is a short-distance cutoff, k_F is the Fermi momentum, and $\hat{F}_\sigma$ are the Klein factors, included to ensure that fermionic statistics are obeyed[8]. (For an introduction to bosonization and the precise meaning of the all the quantities in Eq. (4.21), see e.g. Refs. [223, 79, 77].) One finds that the original fermionic theory maps exactly onto (4.20), and expressions can be found for u and K in terms of the Fermi velocity v_F and interaction strength [79]. However, the HLL theory can be employed much more generally. The Hamiltonian (4.20) emerges as the long-wavelength fixed point of a renormalization group (RG) flow starting from a 'bare' Hamiltonian that includes many TRS-respecting perturbations other than spatially uniform contact interactions. The effect of these perturbations on low-energy physics can be captured through a renormalization of u and K, and so their values may differ from the expression obtained using the mapping (4.21). Since the bare theory may be rather complex and hard to characterize, we will not attempt to relate u and K to microscopic quantities, and will instead treat them as phenomenological parameters. Nevertheless, quite generally $K < 1$ ($K > 1$) corresponds to repulsive (attractive) interactions.

Note that in this context, the UV cutoff for the theory is not set by the lattice spacing, but by the gap E_{g}, above which bulk degrees of freedom become important. Thus,

$$\xi \sim \frac{u}{E_{\mathrm{g}}}, \tag{4.22}$$

[7] We adopt the convention for the normalization of the bosonic fields used in Ref. [79]. Some expressions found here will differ from those in other sources through various signs and factors of $\sqrt{\pi}$ and K, but all physical quantities are the same.

[8] The Klein factors can be safely ignored here, since we will be working in a fixed fermion number sector [79]. In scenarios where fermions can enter and leave the system, they must be treated more carefully.

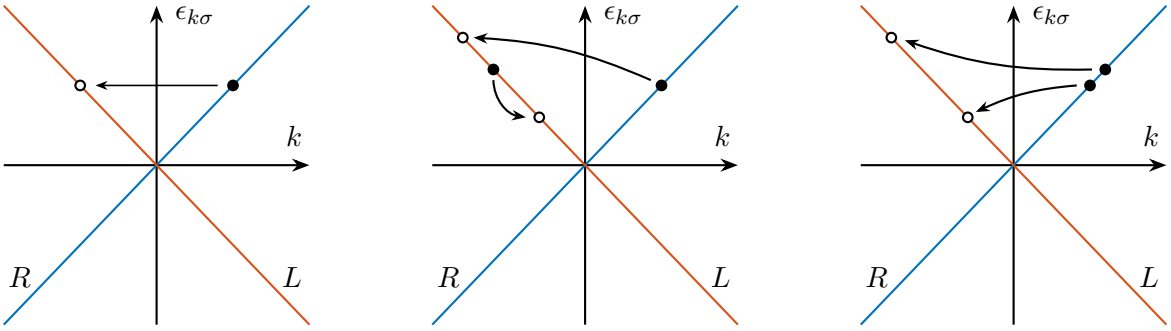

(a) single p. elastic **(b)** single p. inelastic **(c)** two p. inelastic

Fig. 4.2 Various backscattering mechanisms for helical edge modes illustrated in momentum space. The single-particle dispersion relation $\varepsilon_{k\sigma} = \sigma v_F k$ is shown in blue and red for forward- and backward-moving fermions, respectively. (**a**) Elastic single-particle scattering is generated by the operator (4.25), which is odd under time-reversal and so forbidden in an isolated system. (**b**, **c**) Single- and two-particle inelastic backscattering processes are generated by the TRS-invariant operators (4.26) and (4.27), respectively. These operators are RG-irrelevant, and so the associated resistance is suppressed at low temperatures.

which can also be interpreted as the penetration depth of the helical edge modes into the bulk (cf. the magnetic length in the quantum Hall effect [233]). The exact dependence of the short-distance cutoff on u, E_g depends on the details of the regularization procedure being used, and so ξ is a non-universal length scale.

Since the helical liquid arises at the edge of a symmetry-protected phase, we expect that the fixed point theory (4.20) will be stable only if a suitable symmetry is preserved. As mentioned, one such symmetry is TRS, which in the bosonized representation is implemented by the transformation

$$\hat{\phi}(x) \to \hat{\phi}(x) + \frac{\pi}{2}, \qquad \hat{\theta}(x) \to -\hat{\theta}(x), \qquad \mathrm{i} \to -\mathrm{i}. \tag{4.23}$$

(Using Eq. (4.21), one can verify that the fermion operators transform in the appropriate way.) The edge modes can alternatively be protected by certain unitary symmetries, such as the $\mathrm{U}(1)$ group corresponding to rotations of the electron spin about the z axis. A rotation by angle χ is implemented as

$$\hat{\phi}(x) \to \hat{\phi}(x) + \chi \qquad \hat{\theta}(x) \to \hat{\theta}(x). \tag{4.24}$$

To get some insight into how these symmetries can protect the helical edge modes, consider the perturbation

$$\cos\left[2\hat{\phi}(x)\right] \propto \hat{\psi}_+^\dagger(x)\hat{\psi}_-(x) + \text{H.c.} \tag{4.25}$$

This term gives rise to elastic single-particle backscattering[9], where a right-moving electron scatters into a left-moving mode of the same energy (see Fig. 4.2a). Such a process can generate non-zero resistance in the edge modes. Moreover, for finite repulsive interactions this perturbation is RG-relevant, and is in fact capable of driving the system away from the HLL fixed point towards a gapped insulating phase at low temperatures [109, 108, 241]. However, it is forbidden by either TRS or spin rotation symmetry in an isolated system.

Consider instead the TRS-invariant perturbations

$$:\nabla^2\hat{\theta}(x)\cos\left[2\hat{\phi}(x)\right]: \propto \hat{\psi}_+^\dagger(x)\hat{\psi}_-(x)\nabla\left[\hat{\psi}_+^\dagger(x)\hat{\psi}_+(x) - \hat{\psi}_-^\dagger(x)\hat{\psi}_-(x)\right] + \text{H.c.} \tag{4.26}$$

$$\cos\left[4\hat{\phi}(x)\right] \propto \hat{\psi}_+^\dagger(x)\hat{\psi}_+^\dagger(x+\alpha)\hat{\psi}_-(x)\hat{\psi}_-(x+\alpha) + \text{h.c.} \tag{4.27}$$

(The colons in Eq. (4.26) denote normal ordering of the product between $\hat{\theta}$ and $\hat{\phi}$ operators, which means the divergent quantity $\langle\nabla^2\hat{\theta}(x)\cos[2\hat{\phi}(x)]\rangle$ is to be subtracted [79, 77]. We have also used a point splitting regularization for the fermion operators in (4.27).) The former describes single-particle inelastic backscattering, while the latter represents correlated two-particle backscattering process.

In the non-interacting limit $K = 1$, it is helpful to view these processes in momentum space (see Fig. 4.2 b,c). Unlike the elastic process, these transitions involve electrons exchanging energy. Due to Fermi exclusion, the resistance associated with these processes must therefore decrease as temperature is lowered [191]. Quite generally, time-reversal symmetry ensures that matrix elements between single-particle states with the same energy but opposite helicity must vanish [27], and so any TRS-respecting backscattering operator must be inelastic and will be suppressed at low temperatures (at least for weak interactions). For an arbitrary interaction strength K, the temperature-dependence of the resistance can be inferred from the scaling dimensions of the bosonic operators, giving T^{2K+2} and T^{8K-2} for the perturbations (4.26) and (4.27), respectively. We see that for sufficiently weak interactions (K close to 1), both these operators are RG-irrelevant [241]. One can verify that spin rotation symmetry (4.24) also forbids any relevant backscattering operators, thus protecting

[9] We have used the identity (4.21) to convert bosonic operators to fermionic ones in Eq. (4.25). However one should remember that the HLL Hamiltonian describes a low-energy effective theory, and so the renormalized fields $\hat{\phi}(x)$, $\hat{\theta}(x)$ may not actually be related to the bare electron operators in such a simple way. Nevertheless, one can gain a better intuitive appreciation for the various perturbations considered here by considering their fermionic representation.

the conductance of the HLL.

Let us now discuss how this picture can change when the system is coupled to external degrees of freedom. Again we can analyse the microscopic symmetries of the open system by decomposing the system-environment interaction as a sum of terms $\hat{H}_{SE} = \sum_\alpha \hat{A}_\alpha \otimes \hat{B}_\alpha$, with $\hat{A}_\alpha$ acting on the system and $\hat{B}_\alpha$ acting on the environment [Eq. (4.4)]. If the operators $\hat{A}_\alpha$ acting on the system break the relevant symmetries, then we expect that the perfect conductance of the edge modes will be compromised, much like the coherence of topological bound states. A well-studied example of this is a magnetic impurity interacting with the HLL through an exchange coupling

$$\hat{H}_{\text{exch}} = J\vec{S}_{\text{HLL}}(x) \cdot \vec{S}_{\text{imp}}, \tag{4.28}$$

where $\vec{S}_{\text{HLL}}(x)$ and $\vec{S}_{\text{imp}}$ are the spin operators acting on the HLL and impurity, respectively. Evidently, the operators acting on the system break both TRS and spin rotation (although the symmetries of the composite system are preserved). Therefore, the impurity will couple to the HLL via the relevant operator (4.25), which was previously forbidden by TRS. This results in elastic single-particle backscattering accompanied by a flip of the impurity spin, which again leads to imperfect transport at low temperatures[10] [139, 206].

Since it is clear that scenarios of this type do not exhibit perfect conductance, we will instead assume that the coupling operators $\hat{A}_\alpha$ respect the relevant symmetries. Based on our findings in the previous sections, we already anticipate that transitions forbidden by TRS in the isolated system will still occur, and that these arise beyond leading order in the system-environment interaction strength. We will illustrate this point using a simple model for the environment, namely a two-level system (TLS).

Effective two-level systems are thought to be ubiquitous in condensed matter systems [8], forming the basis of certain models of '$1/f$ noise' [60, 231]. As a physically motivated example, the TLS could describe the two lowest charge configurations of some nearby structure. If this structure is formed of an even number of electrons, the TRS operator acting on the TLS obeys $\hat{T}^2 = +1$. Without loss of generality, we choose a basis that is diagonal in the two charge configurations wherein $\hat{T} = \hat{K}$, where $\hat{K}$ the complex conjugation operator.

[10] Since the exchange coupling is RG-relevant (marginally relevant for $K = 1$), the renormalized interaction becomes non-perturbatively strong at very low temperatures $T \lesssim T_K = [\alpha J/v(K-1)]^{1/(K-1)}$. It is then no longer possible to ignore the bulk electrons, which for $T \ll T_K$ form a 'Kondo singlet' with the impurity, the environment-induced backscattering becomes suppressed, and quantized conductance is restored [139]. If there are many impurities distributed along the edge, the helical mode may become insulating even in the limit of strictly zero temperature [7].

This gives

$$\hat{H}_E = E_{\rm sp}\hat{S}^z + \Delta\hat{S}^x, \tag{4.29}$$

where $\hat{S}^{x,y,z}$ are the spin-1/2 operators, satisfying $[\hat{S}^\mu, \hat{S}^\nu] = \mathrm{i}\varepsilon^{\mu\nu\kappa}\hat{S}^\kappa$; $(\hat{S}^\mu)^2 = 1/4$. Physically, we can interpret $E_{\rm sp}$ as the difference in energy between the low-energy charge configurations of the structure, and Δ as the tunnelling matrix element between the two. Assuming no tunnelling of fermions between the TLS and the quantum spin Hall insulator, the predominant system-environment interactions are likely to be electrostatic in nature, which naturally gives rise to couplings for which both $\hat{A}_\alpha$ and $\hat{B}_\alpha$ are TRS-invariant and independent of the fermion spin. The interaction will generically take the form

$$\hat{H}_{SE} = \int \mathrm{d}^2\vec{r}\,\hat{\rho}_{\rm el}(\vec{r}) \otimes \left[\hat{S}^x V_x(\vec{r}) + \hat{S}^z V_z(\vec{r})\right], \tag{4.30}$$

where $\hat{\rho}_{\rm el}(\vec{r})$ is the density operator for the bare electrons, and $V_{x,z}(\vec{r})$ are arbitrary real functions of the spatial coordinate $\vec{r}$, which we presume to be smooth on the scale of α, and localized near some point $x = 0$ along the edge. This interaction captures the dependence of both the splitting $E_{\rm sp}$ and tunnelling matrix element Δ on the distribution of electrons in the system.

4.4.2 Renormalization group analysis

Having defined our model for a dynamical two-level impurity coupled to a quantum spin Hall insulator via electrostatic interactions, we now consider its low-energy properties. At temperatures $T \lesssim E_{\rm g}$, the system-environment interaction (4.30) can be projected onto the edge mode degrees of freedom described by the HLL Hamiltonian (4.20). As mentioned, the relationship between the bare electron operators and those of the effective low-energy theory are highly non-trivial, but we can determine which terms can arise based on their symmetry properties. For instance, the elastic backscattering operator (4.25) is forbidden, since the system operators $\hat{A}_\mu = \int \mathrm{d}^2\vec{r}\hat{\rho}_{\rm el}(\vec{r})V_\mu(\vec{r})$ ($\mu = x,z$) are invariant under TRS. In contrast, terms involving TRS-respecting operators acting on the HLL such as (4.26), (4.27) are not forbidden, and so will generically appear (unless the system possesses some other symmetry that forbids it). Moreover, since the system-environment interaction is quasi-local, we can perform a gradient expansion of the fields $\hat{\phi}(x)$, $\hat{\theta}(x)$ about the point $x = 0$, which is well-controlled at low energies. Therefore, all perturbations can be expressed in terms of the fields and their spatial derivatives evaluated at $x = 0$.

There are infinitely many terms allowed by symmetry, but for illustrative purposes we will only explicitly consider two particular terms

$$\hat{H}_{SE} = J_1 \nabla^2 \hat{\phi} \otimes \hat{S}^z + J_2 : \nabla\hat{\theta} \cos[2\hat{\phi}] : \otimes \hat{S}^x + \cdots \tag{4.31}$$

with all fields evaluated at $x = 0$. [The normal ordering is with respect to the product of $\nabla\hat{\theta}$ and $\cos[2\hat{\phi}]$.] In the fermion representation, the second term represents single-particle inelastic backscattering (see Eq. (4.26) and Fig. 4.2b), and the field $\nabla^2\hat{\phi}(x)$ maps to the gradient of the fermion density $\nabla\hat{\rho}_{\rm f}(x)$. The coefficients $J_{1,2}$ will depend in some complicated way on the microscopic details of the QSHE system in question as well as the profiles $V_{x,z}(\vec{r})$ in (4.30), but neither are constrained by time-reversal symmetry.

Since all the operators acting on the HLL that appear in $\hat{H}_{SE}$ are TRS-even, we know that they are RG-irrelevant at tree level, and therefore will not strongly alter the low-temperature conductance properties at leading order in perturbation theory. The reason we consider them here is that under RG transformations that include loop corrections, they can generate perturbations that would be forbidden by symmetry in the bare Hamiltonian, and these new terms may be RG-relevant. In particular, we will demonstrate that these two couplings generate a term proportional to the single-particle elastic backscattering operator (4.25).

To show this, we will need to compute the one-loop beta functions for the HLL-TLS theory, which can be done using the operator product expansion method; see, e.g. Ref. [34]. This procedure is best described in the imaginary time path integral formalism. Define the decoupled fixed point action

$$S_0\big[\phi, \vec{S}\,\big] = S_{\rm WZ}\big[\vec{S}\,\big] + \frac{1}{2\pi K}\int_0^\beta {\rm d}\tau \int {\rm d}x\, u(\partial_x\phi)^2 + \frac{1}{u}(\partial_\tau\phi), \tag{4.32}$$

where τ is imaginary time, $\beta = 1/T$ is the inverse temperature, $\vec{S}(x,\tau)$ is the pseudospin field for the TLS, and $S_{\rm WZ}$ is the Wess-Zumino action for a spin-$1/2$ [5]. (We do not require an expression for the latter, since we will evaluate spin correlators in the operator formalism.) Following Ref. [109], we have integrated out the $\hat{\theta}(x)$ field using the operator equation of motion

$$\partial_\tau\hat{\phi} = {\rm i}uK\partial_x\hat{\theta}. \tag{4.33}$$

Without loss of generality, the perturbation can be written

$$S_1\big[\phi, \vec{S}\,\big] = \sum_\nu \sum_{\mu=0,x,y,z} g_{\nu\mu} \int_0^\beta \frac{{\rm d}\tau}{\sigma^{1-\Delta_\nu}} A_\nu[\phi](\tau)\, S^\mu(\tau), \tag{4.34}$$

where $A_\nu[\phi](\tau)$ are functionals of the field $\phi(x,\tau)$ at the time τ, and $S^\mu(\tau)$ are the field-theoretic representations of the four Pauli matrices ($S^0(\tau) = 1/2$). Here, $\sigma = \xi/u$ is a short-time cutoff of the order of the inverse bulk gap [see Eq. (4.22)]. Note that the splitting $E_{\rm sp}$ and tunnelling Δ [Eq. (4.29)] are included in the perturbation S_1, which ensures that S_0 is a fixed-point theory. Because the HLL only couples to the TLS at a single point $x = 0$ and the unperturbed action is scale invariant, we can demand that the functionals $A_\nu[\phi](\tau)$ are scaling operators, meaning that

$$\langle A_{\nu_1}(\tau_1/\lambda)\cdots A_{\nu_n}(\tau_n/\lambda)\rangle = \left(\prod_{a=1}^{n}\lambda^{\Delta_{\nu_a}}\right)\langle A_{\nu_1}(\tau_1)\cdots A_{\nu_n}(\tau_n)\rangle\,. \tag{4.35}$$

for positive scaling factors λ. The exponents Δ_ν are known as the scaling dimensions for the operators $A_\nu(\tau)$. This implies that the two-point correlators follow a power law behaviour $\langle \mathscr{T} A_\nu(\tau)A_\nu(\tau')\rangle = C_\nu|\tau-\tau'|^{-2\Delta_\nu}$. We normalize the operators A_ν such that C_ν are dimensionless, and hence the coupling constants $g_{\nu\mu}$ in (4.34) are also dimensionless. Both coupling terms in Eq. (4.31) are manifestly scaling operators, however a more general operator can be decomposed into terms each obeying (4.35) [34].

We can now formally express the partition function $\mathscr{Z} = \mathrm{Tr}\, e^{-\beta\hat{H}}$ for the perturbed theory in terms of expectation values with respect to S_0

$$\begin{aligned}\frac{\mathscr{Z}}{\mathscr{Z}_0} = \sum_{n=0}^{\infty}(-1)^n \sum_{\substack{\nu_1\ldots\nu_n\\ \mu_1\ldots\mu_n}}\left(\prod_{a=1}^{n} g_{\nu_a\mu_a}\right)\int_0^\beta \frac{\mathrm{d}\tau_1}{\sigma^{1-\Delta_{\nu_1}}}\int_0^{\tau_1-\sigma}\frac{\mathrm{d}\tau_2}{\sigma^{1-\Delta_{\nu_1}}}\cdots\int_0^{\tau_{n-1}-\sigma}\frac{\mathrm{d}\tau_n}{\sigma^{1-\Delta_{\nu_n}}}\\ \times\langle A_{\nu_1}(\tau_1)\cdots A_{\nu_n}(\tau_n)\rangle\,\langle S^{\mu_1}(\tau_1)\cdots S^{\mu_n}(\tau_n)\rangle\end{aligned} \tag{4.36}$$

where $\mathscr{Z}_0$ is the partition function for the action S_0. Here, we impose a short-time cutoff by demanding that the time coordinates τ_i are always separated by a time of at least $\sigma \sim E_{\rm g}^{-1}$. Although crude, this cutoff procedure is accurate enough to determine the one-loop beta function [34].

This type of expansion forms the basis of a study of the Kondo model by Anderson, Yuval, and Hamann [247, 9]. To help provide some physical intuition, they identified Eq. (4.36) with the grand partition function for a one-dimensional classical gas of particles[11] interacting via long-range forces governed by the correlators of A_ν and S^μ, subject to a hardcore constraint $|\tau_i - \tau_j| \geq \sigma$. In this analogous classical system, imaginary time τ plays the rôle of the spatial coordinate, the length of the system is β, and $g_{\nu\mu}$ are fugacities for the various 'flavours' of

[11] The factor of $(-1)^n$ does not appear in a classical partition function. In the Kondo problem, it can be removed by a spin rotation, but the same is not necessarily true here. Nevertheless, the physical picture provided by this mapping is helpful.

particle, which we assume to be small. The Anderson-Yuval-Hamann RG scheme involves integrating out configurations in which two particles are separated by a distance $\sigma \leq \Delta t < b\sigma$, and then rescaling the coordinate τ by a factor b^{-1} to restore the original cutoff σ.

For an infinitesimal RG step $b = 1 + \delta\ell$ in the dilute gas regime $g_{\nu\mu} \ll 1$, configurations in which more than two particles are separated by $\Delta\tau < b\sigma$ are rare enough to be neglected. The integration step can then be performed by replacing the two nearby particles by a single particle (possibly of a different flavour), chosen such that the potential felt by the other particles far away is unchanged. This effectively changes the fugacity of the new particle. We therefore need to study correlators of the form

$$\left\langle \mathscr{T}_\tau A_\nu(\tau) A_{\nu'}(\tau') \Phi_S(\{\tau_i\}) \right\rangle \tag{4.37}$$

where $\mathscr{T}_\tau$ denotes imaginary time ordering, and $\Phi_S(\{\tau_i\})$ is a product of operators at times $\{\tau_i\}$ that are well-separated from times τ, τ'. The operator product expansion (OPE) specifies how the correlators (4.37) behave as the time coordinates τ, τ' approach one another, which is precisely the information we need here. The OPE takes the form

$$\lim_{\varsigma\to 0} \mathscr{T}_\tau A_\nu(\bar\tau + \varsigma/2) A_{\nu'}(\bar\tau - \varsigma/2) = \lim_{\varsigma\to 0} \sum_{\nu''} \frac{c_{\nu\nu';\nu''}(\varsigma)}{|\varsigma|^{\Delta_\nu + \Delta_{\nu'} - \Delta_{\nu''}}} A_{\nu''}(\bar\tau) \tag{4.38}$$

The above operator equation should be understood in a weak sense, being only valid when substituted into correlators of the form (4.37). Here the dimensionless functions $c_{\nu\nu';\nu''}(\varsigma)$ are either constant in ς or proportional to $\operatorname{sgn}\varsigma$. The form of the denominator follows from the scaling identity (4.35) [34].

In an isolated system, the OPE for the system operators suffices to determine the one-loop RG equations. The symmetries of the fixed point action and the operators A_ν, $A_{\nu'}$ are preserved under this process[12]. However, in our case the RG also depends on the OPE for the spin fields $S^\mu(\tau)$, which we write as

$$\mathscr{T}_\tau S^\mu(\bar\tau + \varsigma/2) S^{\mu'}(\bar\tau - \varsigma/2) = \sum_{\mu''} d_{\mu\mu';\mu''}(\varsigma) S^{\mu''}(\bar\tau), \tag{4.39}$$

again to be understood in a weak sense. The coefficients $d_{\mu\mu';\mu''}(\varsigma)$ can be evaluated in the operator representation

$$d_{\mu\mu';\mu''}(\varsigma) = \frac{1}{4}\delta_{\mu\mu'} + \frac{\mathrm{i}}{2}\operatorname{sgn}(\varsigma)\varepsilon_{\mu\mu'\mu''} \qquad (\mu,\mu',\mu'' \in \{x,y,z\}) \tag{4.40}$$

[12] We have been careful to avoid any spurious time-reversal symmetry breaking in the OPE by using the symmetrized time coordinate $\bar\tau = (\tau + \tau')/2$.

Generalising the proofs given in Refs. [34, 73], we find that after the infinitesimal RG step, $\mathscr{Z}$ will be left invariant if the fugacities $g_{\nu\mu}$ are renormalized by

$$\frac{\mathrm{d}g_{\nu\mu}}{\mathrm{d}\ell} = (1-\Delta_\nu)g_{\nu\mu} - \sum_{\substack{\nu'\nu''\\ \mu'\mu''}} g_{\nu'\mu'}g_{\nu''\mu''}f^{\mu'\mu'';\mu}_{\nu'\nu'';\nu} \tag{4.41}$$

where

$$f^{\mu'\mu'';\mu}_{\nu'\nu'';\nu} = \frac{1}{2}\left[c_{\nu'\nu'';\nu}(+\sigma)d_{\mu'\mu'';\mu}(+\sigma) + c_{\nu'\nu'';\nu}(-\sigma)d_{\mu'\mu'';\mu}(-\sigma)\right] \tag{4.42}$$

Because $d_{\mu'\mu'';\mu}(\varsigma)$ has a nontrivial dependence on ς for $\mu' \neq \mu''$, system operators that would be forbidden by TRS in an isolated system can actually generated under the RG. This is best illustrated using the two terms we introduced in Eq. (4.31). After substituting for $\hat{\theta}$ using (4.33),the scaling dimensions of the fields $\nabla^2\phi$ and $\mathrm{i}\partial_\tau\phi\cos[2\phi]$ are $\Delta_1 = 2$ and $\Delta_2 = 1+K$, respectively. With proper normalization, the system operators in question can be written as $u^2\sigma\nabla^2\phi(\tau)$ and $\sigma^{-K}\mathrm{i}\partial_\tau\phi\cos[2\phi]$, and the fugacities are $g_{1z} = J_1/(u^2\sigma)$ and $g_{2x} = -J_2/uK$. The OPE can be computed using the fact that the HLL Hamiltonian is a free theory, and so Wick's theorem applies to correlators (4.37).

$$\begin{aligned}&\left[u^2\sigma\nabla^2\phi(\bar{\tau}+\varsigma/2)\right]\times\left[\sigma^{-K}:\mathrm{i}\partial_\tau\phi(\bar{\tau}-\varsigma/2)\cos[2\phi(\bar{\tau}-\varsigma/2)]:\right]\\ =&\frac{-\mathrm{i}K}{\varsigma^3}\left[\sigma^{-K}\cos(2\phi(\bar{\tau}))\right]+\cdots\end{aligned} \tag{4.43}$$

where we have omitted other less relevant operators. The above comes from the contribution in which the $\nabla^2\phi$ operator is Wick contracted with $\mathrm{i}\partial_\tau\phi$, which can be evaluated using the short-distance expression for the Green's function $\langle\phi(x,\tau)\phi(0,0)\rangle = (K/4)\log[x^2+u^2\tau^2]+$ const. [79]. Note that the coefficient is odd in ς, and so without the TLS operators the two terms in (4.42) would cancel. However, since S^x and S^z are non-commuting, the coefficients $d_{\mu'\mu'';\mu}(\varsigma)$ introduce an additional factor of $\operatorname{sgn}\varsigma$ [Eq. (4.40)], and so this cancellation does not occur. An operator of the form

$$(y/\sigma)\times S^y \otimes \cos[2\hat{\phi}] \tag{4.44}$$

is therefore generated under the RG, even though the time-reversal symmetry of the electrostatic interactions forbids a non-zero bare value of the dimensionless coupling constant y.

The scaling dimension for the above term is $\Delta = K$, and so RG equation for y is

$$\frac{\mathrm{d}y}{\mathrm{d}\ell} = (1-K)y - Kg_{1z}g_{2x} + \cdots \tag{4.45}$$

where the ellipses denote other combinations of irrelevant operators that combine to generate the operator (4.44). Since $1-K \geq 0$ for the physically realistic case of repulsive interactions, the coupling y is marginal or relevant, and so for large ℓ the right hand side will be dominated by the first term, giving $y(\ell) \approx y_0 e^{(1-K)\ell}$. The constant of proportionality y_0 is determined by the early stages of the RG flow, i.e. for $\ell \lesssim 1$. During this stage, the irrelevant couplings g_{1z} and g_{2x} (among others) which are allowed by symmetry drive the system away from the stable region of parameter space $y = 0$; see Fig. 4.3. Once a non-zero y is generated, the RG trajectories will flow away from the HLL fixed point.

Thus, in general the low-energy properties of the HLL-TLS system are governed by an effective low-energy Hamiltonian

$$\hat{H}_{\mathrm{eff}} = \hat{H}_{\mathrm{HLL}} + E_{\mathrm{sp}}\hat{S}^z + \Delta\hat{S}^x + (y/\sigma)\hat{S}^y \otimes \cos[2\hat{\phi}] \tag{4.46}$$

In this Hamiltonian, we have excluded terms that are RG-irrelevant. However, the influence of these terms is implicitly accounted for through the renormalized coupling y. If only g_{1z} and g_{2x} are considered, then the solution of (4.45) gives $(y/\sigma) \sim J_1 J_2/\sigma^2 u^3$ (up to dimensionless constants). However, since there are in principle infinitely many such terms contributing to the right hand side of (4.45), y will be treated as a phenomenological parameter.

We see that even though the interactions between the TLS and the HLL only involve TRS-invariant operators acting on the system, the TRS-odd operator (4.25), which generates elastic single-particle backscattering, is generated at low energies. In the non-interacting limit $K = 1$, one can understand the mechanism behind this effect in a single-particle description. The effective operator captures second order transitions generated by the two terms in Eq. (4.31). The operators acting on the system are $\hat{A}_1 := \nabla^2\hat{\phi}$ (which facilitates forward-scattering) and $\hat{A}_2 :=: \nabla\hat{\theta}\cos[2\hat{\phi}]:$ (which facilitates inelastic back-scattering[13]; see Fig. 4.2b). The two operators combined can mediate an indirect transition from a right-mover to a left-mover of the same energy (Fig. 4.4). This transition can occur in two ways depending on whether the forward- or back-scattering operator is applied first. Without the spin operators, the two paths would destructively interfere due to TRS [241]. However, since $\hat{S}^z$ and $\hat{S}^x$ anticommute, the additional phase factors acquired by the spin lead to constructive, rather than destructive,

[13] In the process depicted in Figure 4.2b, single-particle inelastic backscattering is accompanied by a forward-scattering process of another electron, so as to conserve energy. Here, such a process is not required, since the intermediate state is off-shell. Crucially, the second order elastic backscattering mechanism here involves scattering of just one electron – all others do not undergo a transition.

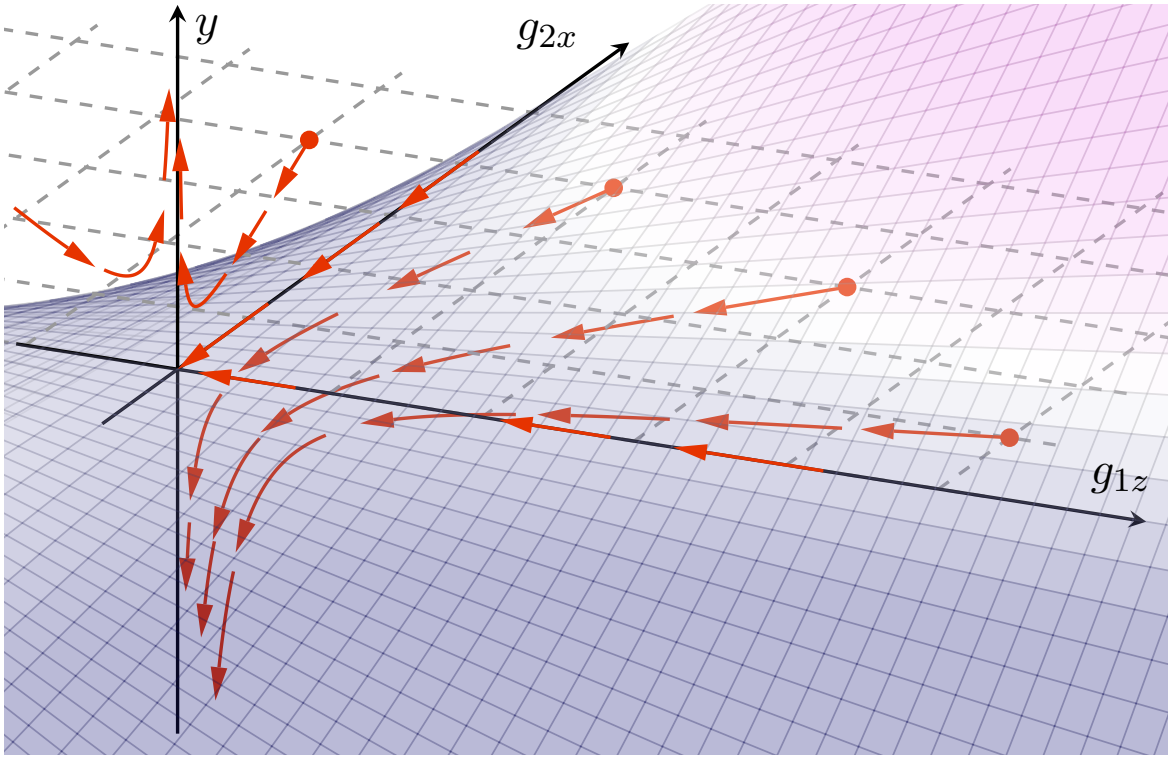

Fig. 4.3 Illustration of the RG flow for the three coupling constants in Eq. (4.45). Being composed of TRS-invariant operators, the couplings g_{1z} and g_{2x} are generically present in the bare Hamiltonian [Eq. (4.31)]. These couplings are irrelevant, and so flow to zero. The coupling y [Eq. (4.44)] involves the TRS-odd operator $\cos[2\hat{\phi}]$, and so must have a bare value of zero for electrostatic system-environment interactions. Various points in the g_{1z}-g_{2x} plane (grey grid) are drawn as red dots, and the subsequent RG flows are sketched. If the bare values of g_{1z} and g_{2x} are both non-zero, then the initial point does not lie on the basin of attraction (shaded area, defined by $y = [K/(1-K)]g_{1z}g_{2x}$), and so a non-zero y is generated along the flow, with a sign determined by the product $g_{1z}g_{2x}$. If either one of g_{1z} or g_{2x} are zero, then the bare value lies in the basin of attraction, and the RG flows to the fixed point $y = 0$. However, generically we expect that there will be at least one pair of couplings that have non-zero bare values and can combine under RG to generate non-zero y, rendering the fixed point theory (4.20) unstable.

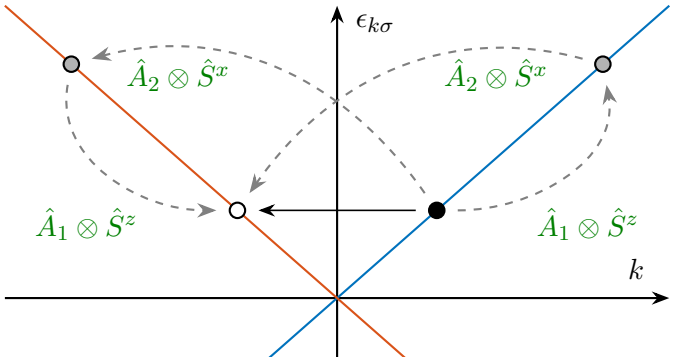

Fig. 4.4 Single-particle mechanism for the generation of the effective coupling (4.44). The HLL and TLS are coupled via two terms $\hat{H}_{SE} = \hat{A}_1 \otimes \hat{S}^z + \hat{A}_2 \otimes \hat{S}^x$, where $\hat{A}_2$ and $\hat{A}_1$ generate forward and backward scattering, respectively [see Eq. (4.31)]. A right mover (black dot) can scatter to a left mover (white dot) through an indirect transition proceeding via an intermediate virtual state (grey dots). While the two pathways (grey arrows) would cancel each other out due to TRS in the absence of the spin operators, the non-commutativity of $\hat{S}^x$, $\hat{S}^z$ means that elastic backscattering is in fact generated.

interference. The system then behaves as if the TLS were coupled to the HLL via TRS-odd operators, such as those that arise in the exchange coupling with a magnetic impurity [Eq. (4.28)].

Although the single-particle picture is less general, it makes the analogy to the indirect decoherence processes in topological bound states much clearer (compare Figs. 4.1 and 4.4). Note that the effective breaking of TRS for the system again requires more than one coupling channel to be present. Additionally, this generation of symmetry-breaking operators acting on the system is specific to antiunitary symmetries: Any two operators that are invariant under a unitary symmetry acting on the system can only generate other operators that are also invariant under the same symmetry. Therefore, if the HLL is protected by a unitary symmetry [e.g. spin rotation (4.24)] and the bare system-environment coupling only features operators acting on the HLL that are invariant under that symmetry, then the conductance of the edge modes will be as robust as it was in the isolated system.

4.4.3 Transport properties

Having determined the form of the low-energy effective Hamiltonian for the HLL-TLS system [Eq. (4.46)], we can now determine the relevant transport coefficients. In particular, we will focus on electrical conductance, which is commonly used as an experimental signature of the QSHE [128, 183]. Before undertaking any formal calculations, we can use RG arguments to predict how the residual resistance induced by the TLS will scale as a function of the relevant

experimental parameters in certain regimes. For convenience, we first rewrite the effective Hamiltonian (4.46) in a basis in which the TLS pseudospin is rotated

$$\hat{H}_{\text{eff}} = \hat{\mathbb{1}} \otimes \hat{H}_{\text{HLL}} + (h/\sigma)\hat{S}^z \otimes \hat{\mathbb{1}} + (y/\sigma)\hat{S}^y \otimes \cos[2\hat{\phi}] \tag{4.47}$$

where $h := \sigma\sqrt{E_{\text{sp}}^2 + \Delta^2}$. Both h and y are dimensionless numbers describing the strength of the two perturbations away from the fixed point Hamiltonian. For repulsive interactions $K < 1$, they are both relevant, with scaling dimensions $\Delta_h = 0$, $\Delta_g = K$. Therefore, if the coupling constants at a given scale σ are $h(\sigma)$ and $y(\sigma)$, then at tree level their renormalized values at new scale σ' are $h(\sigma') = (\sigma/\sigma')^{-1}h(\sigma)$, $y(\sigma') = (\sigma/\sigma')^{K-1}y(\sigma)$. At finite temperature, frequency, or voltage, the RG will flow towards the IR until a scale $\sigma^* \sim 1/E^*$ is reached, where $E^* = \max(T, \omega, eV)$ [109]. If at this point the effective couplings are still perturbatively small $h(\sigma^*), y(\sigma^*) \ll 1$, then we can trust the tree level RG treatment, and treat y perturbatively. The dominant contributions to the resistance δR induced by the TLS should scale as $\delta R \propto [y(\sigma^*)]^2 \sim (E^*)^{2K-2}$.

As the temperature, frequency, and voltage are lowered, one of the couplings $h(\sigma^*), y(\sigma^*)$ will eventually become non-perturbatively strong (order unity). The bare values $h(\sigma)$, $y(\sigma)$ appearing in the Hamiltonian (4.47) determine energy scales on which this occurs

$$E_h = \sigma^{-1}h(\sigma) \equiv \varepsilon \qquad\qquad E_y = \sigma^{-1}[y(\sigma)]^{-1/(K-1)}. \tag{4.48}$$

The scale E_y is an analogue of the Kondo temperature for our problem[14].

If $E_h \gg E_y$, then the renormalized splitting coefficient $h(\sigma^*) = \varepsilon\sigma^*$ becomes large at an energy scale for which $y(\sigma^*)$ is still small. In this case, the tree level analysis is no longer reliable, and we do not expect simple power-law dependence on E^*. However, we should still be able to obtain an accurate expression for the resistance by using methods that are perturbative in y and exact in h. In Appendix C we derive expressions for the resistance of the HLL in this regime, for either non-zero frequency ω or finite bias V. The expressions simplify greatly when two of the energy scales T, ω, eV are set to zero. At finite temperature, we have a DC linear resistance

$$\delta R_{\text{DC}}(T) = R_K \times \frac{\pi^2 y^2}{8}(2\pi\sigma T)^{2K-2}\,\text{sech}\left(\frac{\varepsilon}{2T}\right)\frac{|\Gamma(K + i\varepsilon/2\pi T)|^2}{\Gamma(2K)}, \tag{4.49}$$

[14] Unlike in the Kondo problem, y is marginal in the non-interacting limit $K \to 1$ even at the one-loop level. This means that in the absence of interactions, E_y is at least as small as $\sim \exp(-\text{const} \times [y(\sigma)]^{-2})$, depending on whether multi-loop corrections make y relevant. This differs from the usual $\sim \exp(-\text{const} \times [y(\sigma)]^{-1})$ scaling.

where $R_K = 2\pi\hbar/e^2 = 25.812\,807\ldots\mathrm{k}\Omega$ is the von Klitzing constant, and $\varepsilon = \sigma h = \sqrt{E_{\mathrm{sp}}^2 + \Delta^2}$ is the difference in energy of the TLS eigenvalues. In the non-interacting limit $K \to 1$, the DC resistance simplifies to $\delta R_{\mathrm{DC}} = R_K \times (\pi^2 y^2/8) \times (\varepsilon/T)/\sinh(\varepsilon/T)$. At finite frequency, the real part of the resistance is

$$\mathrm{Re}\,\delta R_{T=0}(\omega) = \begin{cases} 0 & |\omega| < \varepsilon, \\ R_K \times \dfrac{\pi^2 y^2}{4\sigma|\omega|} \dfrac{(\sigma[|\omega| - \varepsilon])^{2K-1}}{\Gamma(2K)} & |\omega| \geq \varepsilon; \end{cases} \tag{4.50}$$

(An expression for the imaginary part, which describes a phase shift of the conductance rather than backscattering, can be found in Appendix C.) The DC resistance at finite bias is

$$\delta R_{T=0}(V) = \begin{cases} 0 & eV \leq \varepsilon/K, \\ \dfrac{\pi^2 y^2}{4eK|V|\sigma} \dfrac{(\sigma[eK|V| - \varepsilon])^{2K-1}}{\Gamma(2K)} & e|V| > \varepsilon/K. \end{cases} \tag{4.51}$$

The expressions (4.49), (4.50), and (4.51) explicitly depend on the cutoff timescale $\sigma \sim E_{\mathrm{g}}$ and the difference between the eigenenergies of the TLS ε, which are non-universal properties of the system in question. However, in units of $(e^2/2\pi) \times y^2(\sigma\varepsilon)^{2K-2}$, the residual resistance δR can be written as a universal function of $\tilde{T} := T/\varepsilon$, $\tilde{\omega} := \omega/\varepsilon$, and $e\tilde{V} := eV/\varepsilon$. We plot δR along the $\tilde{T}$, $\tilde{\omega}$, and $\tilde{V}$ axes for various values of the Luttinger parameter K in Figure 4.5.

As anticipated, in the limit $E^* \gg \varepsilon$, we recover the tree level scaling expression $\delta R \sim (E^*)^{2K-2}$. As T, ω, and eV are reduced below $E_h = \varepsilon$, the TLS becomes 'frozen' in its ground state. Transitions to the excited state, which are necessary to induce backscattering, become energetically suppressed. For example, for $T \ll \varepsilon$, the linear DC resistance δR_{DC} [Eq. (4.49)] is thermally activated $\sim e^{-\varepsilon/T}$. Since the freeze-out truncates any further growth of $y(\sigma^*)$, these results can be trusted all the way down to zero temperature, frequency, and voltage, except perhaps in the vicinity of resonances, which appear in the expressions for the AC and finite bias resistance at sufficiently strong interactions $K < 1/2$ and zero temperature. (For finite temperature, we expect that these resonances will be broadened with a width $\sim T$.)

Finally, we consider the opposite regime $E_h \ll E_y$, in which the HLL-TLS coupling becomes non-perturbatively strong before the freeze-out scale E_h is reached. At energies below E_y, the effective coupling strength y/σ becomes of the order of the bulk gap E_{g}. This not only invalidates our perturbative treatment of y, but also means that we can no longer safely ignore the bulk degrees of freedom. We expect that the TLS will strongly hybridize with the system as a whole, such that the composite system (including both bulk degrees of freedom and the TLS) can be treated as an isolated quantum spin Hall insulator with a

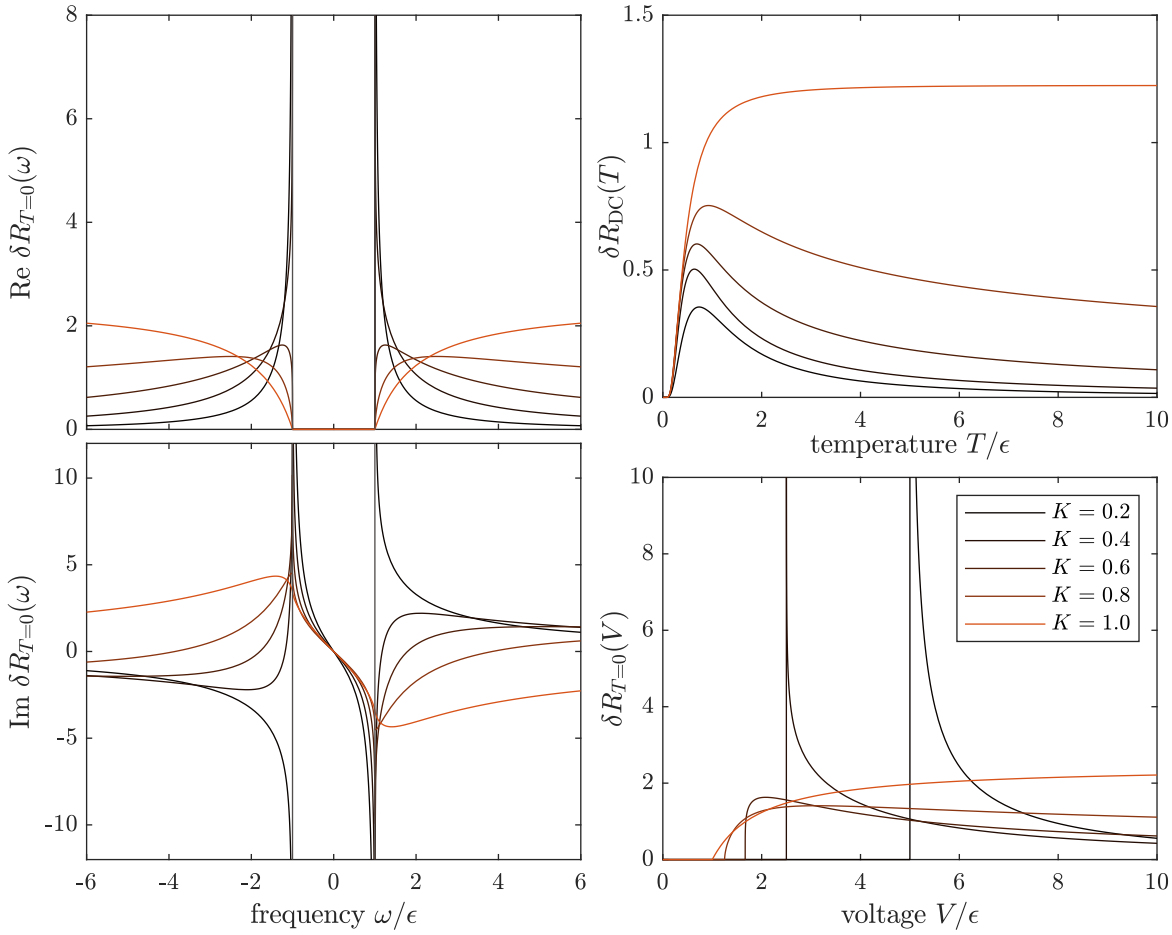

Fig. 4.5 Residual resistance δR of the HLL-TLS system governed by the low-energy effective Hamiltonian (4.46), plotted in units of $(e^2/2\pi) \times y^2(\sigma\varepsilon)^{2K-2}$. Left (both panels): real and imaginary parts of the AC resistance at zero temperature and linear response. Top right: DC resistance in linear response. Bottom right: DC resistance at finite bias and zero temperature. For $K < 1/2$, singularities in the AC and finite bias conductance appear. At energy scales well below ε, the resistance is either thermally activated $\sim e^{-\varepsilon/T}$, or completely suppressed.

bulk gap of the same order as the original system. (The same occurs for magnetic impurities [Eq. (4.28)] at scales below the Kondo temperature [139].) This composite system will possess helical edge modes, which are drastically modified in the vicinity of the TLS, but still capable of conducting. In this regime, the dominant backscattering will be those that were allowed by symmetry in the isolated system [Eqs. (4.26), (4.27)], again giving a positive power-law dependence on T, ω, and eV.

Summary of Section 4.4

In this section, we considered the effect of electrostatic interactions between the helical edge modes of a quantum spin Hall insulator and some external structure, which we modelled as a two-level system. Because the charge density operators for the two systems are time-reversal symmetric and spin-agnostic, the system-environment coupling only features operators acting on the HLL that are invariant under the symmetries that can protect it, namely TRS (4.23) and spin-rotation (4.24) [in contrast to an exchange coupling (4.28)]. Therefore, the contributions to backscattering at leading order in these couplings will be suppressed in the same fashion as a symmetry-respecting perturbation in an isolated system. However, we demonstrated that under an RG-transformation, new operators are generated which include TRS-odd operators acting on the HLL. The most important of these is the relevant operator (4.44), which generates elastic backscattering [Fig. 4.2a] accompanied by a transition in the TLS. Unlike the irrelevant perturbations, the contributions to the resistance δR from this term do not decrease as the temperature, frequency, and voltage are lowered, provided that the largest of these energy scales is above the cutoffs E_h and E_g [Eq. (4.48)]. In this regime, we have $\delta R \sim (E^*)^{2K-2}$, where $E^* = \max(T, \omega, eV)$. For E^* below the cutoff scales, the dynamics of the TLS becomes frozen, either due to the level splitting ε, or because the TLS strongly hybridizes with the bulk electrons in the spin Hall insulator. Either way, the higher-order backscattering mechanism, which relied on the dynamical nature of the environment, is suppressed, and the resistance takes the same form as one would expect for an isolated system. The typical resistance profile as a function of the relevant energy scale is illustrated in Figure 4.6 (ignoring any resonant effects). Since the main features that determine the resistance profile are the scaling dimension of the elastic backscattering operator and a single cutoff scale E_{cut}, we expect that this qualitative form also applies when the HLL is coupled to other kinds of few-body systems. The resistance profile almost exactly resembles the resistance profile that would be induced by a magnetic impurity (see Ref. [139]). Thus, as expected from the discussion in previous sections, we see that scenarios where the coupling operators $\hat{A}_\alpha$ are TRS-invariant are no more protected than those where $\hat{A}_\alpha$ break the protecting symmetries.

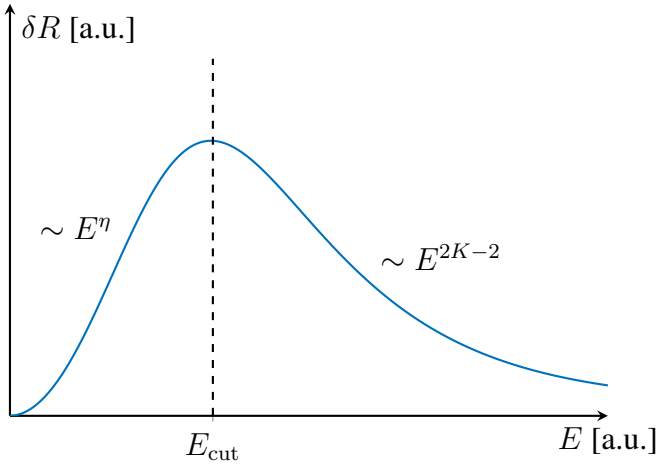

Fig. 4.6 Sketch of the typical resistance profile of a HLL coupled to a few-body system via electrostatic interactions, as a function of the relevant energy scale E (either temperature, frequency, or voltage). Below the cutoff scale E_{cut}, the few-body system becomes effectively frozen, and elastic backscattering is suppressed. The dominant backscattering mechanisms are then inelastic processes, leading to a resistance that vanishes as a power law wih $\eta > 0$.

Although the resistance of the HLL vanishes in the limit of strictly zero temperature, frequency, and voltage, the scales governing the suppression of backscattering E_h and E_g are non-universal, and can in principle take any value. If a given sample features many TLSs interacting with the HLL at different points along the edge, one of them may by chance have a cutoff scale below the temperature of the experiment. This would lead to a contribution to the residual resistance that scales as E^{2K-2} (right hand side of Fig. 4.6). Moreover, spatially-resolved conductance measurements would be able to identify locales where such an efficient elastic backscatterer is present. It is possible that this mechanism could account for deviations from quantized conductivity in experiments on quantum spin Hall systems [205, 86, 59, 69, 242] – for instance, in some experiments, backscattering is indeed mainly present at a handful of 'scattering sites' [127]. However, our description of the external system as a TLS is rather crude, and we have not yet determined the strength of the elastic backscattering that could be expected based on a microscopic description of a given experiment. Therefore more work will need to be done to determine whether this mechanism can quantitatively account for the observed residual resistances seen in these experiments.

Nevertheless, our results exemplify the more general principle described in Section 4.2 regarding the protection of topological phases by time-reversal symmetry. While we have focussed on an environment described by a TLS, a similar effect can in principle occur when an HLL is coupled to any kind of environment. That is, under an RG transformation operators analogous to the elastic backscattering term (4.44) will generically appear (provided there are at least two system-environment coupling channels). More precisely, the most relevant terms that arise will be products of the TRS-odd operator $\cos[2\hat{\phi}]$ with a TRS-odd operator acting on the environment. For example, electron-phonon interactions (which are predominantly electrostatic) could in principle lead to a coupling of the form $\cos[2\hat{\phi}] \otimes \sum_k \mathrm{i} g_k (\hat{b}_k - \hat{b}_k^\dagger)$,

where $\hat{b}_k$ is the annihilation operator for a phonon mode k. Importantly, in these scenarios, the temperature-dependence of the resistivity is not constrained by the time-reversal symmetry of the HLL, but instead depends on the non-universal properties of the environment in question.

Finally, although our results for the resistivity of the HLL bear some resemblance to the decoherence rate of topological bound states (Section 4.3), there are some quantitative differences between the two. Even in the isolated limit, the HLL displays some residual resistance that is only suppressed as a power-law in temperature, compared to the thermally activated temperature dependence of the decoherence time. However, one should note that these power-law corrections only arise when the only protecting symmetry is TRS. If spin-rotation symmetry (4.24) is imposed, then the resistance becomes thermally activated $\delta R \sim e^{-E_g/T}$. (This simply follows from the fact that the combination of charge conservation and spin conservation means the number of left- and right-moving electrons are separately conserved, except for any transitions to bulk excited states.) Therefore, even before an environment is introduced, there seems to be a dichotomy between unitary vs. antiunitary symmetry protection. (It has been suggested that the presence of inelastic backscattering mechanisms in the isolated TRS-protected HLL could be interpreted as being due to the helical electrons acting as their own bath[15].) Nevertheless, topological bound states and the HLL are alike in that for each case, the environment facilitates processes that are forbidden by TRS in the isolated system – namely, decoherence and *elastic* backscattering, respectively.

4.5 Relation to the non-equilibrium classification

The non-equilibrium classification that was introduced in Chapter 2 and computed in Chapter 3 is defined in terms of the wavefunctions of isolated systems. Its relevance to open systems is therefore not immediately clear, particularly given that the systems considered here are at or close to equilibrium. Nevertheless, the results of this chapter bear some resemblance to those described before, and so it is worth considering what relationships can be established between them. In particular, we found that while unitary symmetries can be meaningfully defined in non-equilibrium and/or dissipative scenarios, antiunitary symmetries become ill-defined.

Physically, the difference between the two types of symmetry is that in many-body systems, antiunitary symmetries always describe time-reversal, possibly combined with some other unitary transformation. Loosely speaking, the reversal of time only makes sense when applied to the entire universe (or at least to all objects that the system in question is in contact with). More concretely, in this chapter we saw that antiunitary symmetries cannot be applied

[15] Michael Zaletel (private communication)

to a subspace of some larger Hilbert space in a consistent way [see Eq. (4.8)]. Our results regarding unitary dynamics can also be understood through this perspective: Any time-dependence of the Hamiltonian in an isolated system should capture some physical process that is extrinsic to the system, which could in principle be modelled quantum mechanically. For example, we can think of a quench of the optical lattice in a cold atom experiment as an explicit time-dependence of the potential felt by the atoms, or as a transition between different photon occupation states of the surrounding electromagnetic field. If we were to adopt the latter picture, we could understand the breaking of TRS for the system using the arguments developed in this chapter. Thus the symmetry-breaking effects described in the two parts of this thesis are really one and the same.

This principle is perhaps best illustrated by comparing our results regarding the coherence properties of topological bound states in the presence of noise (Section 2.5) versus the presence of a quantum environment (Section 4.3). The temporal fluctuations in the noise model can be used to capture the influence of an environment on the system (specifically an environment that is modelled classically). We saw that in a given noise realization, the time-variation of the Hamiltonian led to rotations within the ground state subspace when the protecting symmetry was antiunitary, and so the state of the system becomes conditional on the trajectory of the environment. In principle, if the noise profile realised in a given experiment was known, we could reconstruct the quantum information stored in the bound state from measurements on the system at later times. However, in practice, it is impossible to know which noise realisation actually occurs, and so we take a statistical average over the trajectories of the classical environment, resulting in decoherence. For a quantum environment, there is no such averaging over noise trajectories: the evolution of the system is deterministic and not subject to any time dependence. Instead, the system and environment become correlated through the generation of quantum entanglement. In each case, the state of the system at late times is conditional on the outcome of some random processes in the environment, with the randomness being either classical (which noise trajectory?) or quantum (what state is the environment in?) in nature. It is therefore not surprising that our estimates for the decoherence time in each case [Eqs. (2.42), (4.19)] have similar forms (both are proportional to $(V/E_{\mathrm{g}})^4$).

Another connection can be made with our study of the evolution of the entanglement spectrum in Section 2.4. There, we considered the low-energy theory of the entanglement Hamiltonian of the wavefunction as it evolved in time. Dynamically-induced symmetry-breaking gives rise to terms in the entanglement Hamiltonian that break antiunitary symmetries. Therefore, if the phase in question is protected by antiunitary symmetries, then the entanglement edge theory will be gapped out. Analogously, in Section 4.4, we found

that the low-energy edge theory of a quantum spin Hall insulator coupled to an environment generically includes products of TRS-odd operators acting on the system and environment, e.g. Eq. (4.44). It is clear that more generally, such TRS-odd operators will be generated in the low-energy theory of any generic topological edge mode in an open system. We expect that if such operators can induce a gap in the edge mode when included as a static perturbation (as for the entanglement spectrum), then likewise the dynamics of the edge modes in the open system will be strongly affected, and the experimental signatures associated with the topological phase in question will be compromised.

These parallels between our two sets of results suggest that the non-equilibrium classification developed in the context of isolated systems far from equilibrium could be used to identify which topological phases are susceptible to the environment-induced symmetry-breaking effects highlighted in this chapter. In some cases, the analogy is clear. If the non-equilibrium classification for a given symmetry class and spatial dimension is trivial (e.g. quantum spin Hall with TRS only), then all protection is lost once the system is coupled to an environment, and the experimental signatures associated with the phase will be compromised. Additionally, if the classification is unchanged from equilibrium (e.g. topological bound states with unitary symmetries only), then the effective breaking of antiunitary symmetries induced by system-environment interactions does not qualitatively change the dynamics of the system. However, there are more subtle cases where the non-equilibrium classification is only partly reduced from its equilibrium entry, e.g. class BDI topological superconductors in one spatial dimension, which have a classification $\mathbb{Z} \to \mathbb{Z}_2$, where the parity of the number of Majorana fermions on each edge $|\nu|$ is preserved. It is less clear what to expect in these scenarios. In this specific example, it seems plausible that only n out of $n+1$ qubits of information will be subject to decoherence when $|\nu| = 2n+1$ is an odd integer. Numerical simulations could verify this by computing the entanglement generated between the system and environment at late times. Thus, while the connection between open quantum systems and the non-equilibrium classification is established in some cases, more work will need to be done to determine whether the non-equilibrium classification applies to open topological systems in full generality.

It should be noted that alternative schemes for classifying topological matter in open systems have recently been put forward [136, 4]. In contrast to our results, there is no sharp distinction between unitary and antiunitary symmetries in these works. This does not imply that the two are in disagreement – rather, it highlights that there are a number of different ways in which topology influences open quantum systems, according to the physical setting and observables one is interested in. For example, in Ref. [4], the focus is on the topological properties of the system density matrix at late times, as opposed to edge mode

dynamics, which are in fact independent of one another. In Ref. [136], the interest is in the spectral properties of the effective Lindblad generator $\mathscr{L}$, which can still show signatures of topology even if the more traditional quantities associated with topology (bound state coherence and edge mode transport) do not. Furthermore, as discussed in Section 4.2, we defined symmetries at the level of the microscopic Hamiltonian, and in turn asked how these are reflected in the effective equation of motion for the system; in contrast, in these works the Lindblad generators are assumed to have certain symmetry properties, and the consequences are then explored. Our approach is certainly the relevant one when determining whether a given topological system is robust against perturbations that couple system and environment, however evidently there are scenarios where different perspectives are required. It would be interesting to study the relationships between these different classification schemes in future work.

Chapter 5

Summary and Outlook

Our central aim throughout this thesis has been to better understand how topological phenomena manifest themselves in physical settings that are not governed by ground state physics. In studying systems that are either driven out of equilibrium or coupled to their surroundings, we have found that concepts and methods relevant to topology can still be harnessed, but that some of the physical principles that are central to the theory of topological phases must be re-addressed.

Some of the most striking aspects of our results can be traced back to one such principle in particular, concerning the nature of symmetry protection. In systems that are driven out of equilibrium and/or coupled to an environment, antiunitary symmetries – which physically represent a reversal of time – are effectively broken, as is well known in the context of macroscopic irreversibility. We argued that these symmetry-breaking effects have profound consequences for topological phases: While topological phenomena protected by antiunitary symmetries may be robust within the framework of isolated systems at equilibrium, the same is not true of systems that do not fit into this paradigm.

In our treatment of systems undergoing unitary dynamics (Chapter 2), we formalised this intuitive idea in terms of a non-equilibrium topological classification. In this construction, two symmetry-respecting wavefunctions are considered to be equivalent if they can be interconverted via finite-time evolution under a symmetry-respecting Hamiltonian. This differs from the adiabatic deformation procedure, upon which the familiar equilibrium classification is based, in that antiunitary symmetries are not preserved. The two definitions of topology capture the constraints that locality and symmetries impose on quantum systems in a way that naturally pertains to either equilibrium or non-equilibrium scenarios.

Using both general arguments and specific examples, we demonstrated that the content of our topological classification is reflected in a wide range of non-equilibrium settings, as witnessed by certain quantities generally associated with topological phases. Specifically, we

considered the dynamics of the bulk invariants relevant to equilibrium topological phases; the dynamics of the entanglement spectrum; and the susceptibility of topological bound states to noise. All these quantities display qualitatively different behaviour depending on whether the phase in question is trivial or non-trivial in our non-equilibrium classification.

In Chapter 4, we turned our attention to topological phenomena in systems that are at or near equilibrium, but coupled to their surroundings. Again, a dichotomy between unitary and antiunitary symmetries arises in this context, in that the latter are effectively broken by system-environment interactions. This was shown to have consequences for the dynamics of edge modes. We found that systems featuring bound states and one-dimensional helical edge modes are inevitably subject to decoherence and elastic backscattering, respectively, when the equilibrium topological phase to which the system belongs is protected by antiunitary symmetries. The hallmark signatures of topology that have been predicted based on studies of isolated systems (namely, robustness of quantum information and quantized conductance) are therefore compromised when the system is coupled to an environment.

Overall, our results highlight the need to distinguish two types of 'robustness' when discussing topological phases. In the traditional sense, we think of some property of the system as robust if it persists upon introducing arbitrary symmetry-respecting static Hamiltonian-like perturbations. This philosophy is embodied by the equilibrium topological classification. In this thesis, we instead look for quantities that also remain undisturbed when the system is either subjected to time-dependent perturbations or coupled to external degrees of freedom. The relevant formalism that describes this picture is the non-equilibrium classification, which we explicitly computed in Chapter 3 for a broad class of topological phases (Tables 3.1 and 3.3). These tables can be used to quickly determine whether a given topological system will be robust in the latter sense or not (with the possible exception of some subtle cases in open systems, as discussed in Section 4.5).

Not only do the results described here provide new insight into the nature of topological phases in quantum many-body systems, they also have potential practical value. Given that these more general types of perturbation are ubiquitous in experiment (particularly system-environment interactions), we expect that attempts to utilise topological phenomena in designing new technologies will generally be much more successful if the phase in question is non-trivial in our classification. Identifying those topological phases that are fragile to such effects will help future researchers to focus their attention on systems that are more robust, and thus have greater potential utility.

Our findings bring into focus many new open questions. Most immediately, there is certainly more to be understood about the effect of system-environment interactions on

topological boundary modes. In the context of helical edge modes, it remains to be seen how the phenomenological parameters used in our description of the HLL-TLS system depend on microscopic quantities, such that our predictions can be compared to specific experiments. Additionally, so far we have only considered system-environment coupling in the vicinity of a single point. A spatially extended environment (e.g. electron-phonon coupling) could potentially lead to more dramatic deviations from quantized conductance, perhaps even persisting down to zero temperature. Moving beyond helical edge modes, it seems that the RG arguments presented in Section 4.4 give a useful qualitative picture of how the relevant symmetry-breaking effects manifest themselves in general; however a universally applicable *quantitative* description of related scenarios in different spatial dimensions is so far lacking. More generally, it remains to be seen what factors determine the characteristic strength of the symmetry-breaking effects uncovered here.

There are many other systems and phases of matter where our newfound intuition regarding symmetry protection in non-equilibrium and/or open scenarios might prove useful. Most obviously, there are other topological phases not considered here where similar issues could be addressed, such as those featuring spatial symmetries or long-range entanglement (e.g. symmetry-enriched topological phases [38]). However, time-reversal symmetry also plays an important rôle in many non-topological systems. As a simple experimentally relevant example, one could consider how the interactions with the electromagnetic vacuum influence the dynamics of atomic systems featuring Kramers-degenerate internal states. Since the Born-Markov approximation is almost always employed in atomic physics, there could be important indirect transitions of the kind discussed in Section 4.3 which have not yet been properly studied. Our expression for the higher-order Lindblad generator [Eq. (4.17)] might prove useful in this context.

In this thesis, we considered the effects of coherent driving and system-environment interactions separately. However, their combination is generally expected to give rise to a rich variety of driven-dissipative phenomena. It would be interesting to see whether our results could shed light on topological phenomena in scenarios where both are present. A particularly promising arena to study such physics is in periodically driven 'Floquet' topological insulators [123, 186, 225, 63, 174], where dissipation can be exploited to avoid catastrophic heating [54, 102, 197, 64]. While a dynamical version of time-reversal symmetry can be defined for periodic dynamics [123], it may be that the dissipation required to reach a non-trivial steady state invalidates this symmetry, in turn compromising the protection of certain Floquet topological insulators.

References

[1] Aidelsburger, M., Lohse, M., Schweizer, C., Atala, M., Barreiro, J. T., Nascimbène, S., Cooper, N., Bloch, I., & Goldman, N.
Measuring the Chern number of Hofstadter bands with ultracold bosonic atoms. *Nature Physics* **11**(2), 162–166 (2015).

[2] Alba, V. & Calabrese, P.
Entanglement and thermodynamics after a quantum quench in integrable systems. *Proceedings of the National Academy of Sciences* **114**(30), 7947–7951 (2017).

[3] Albert, V. V. & Jiang, L.
Symmetries and conserved quantities in Lindblad master equations. *Physical Review A* **89**, 022118 (2014).

[4] Altland, A., Fleischhauer, M., & Diehl, S.
Symmetry classes of open fermionic quantum matter. Online preprint arXiv:2007.10448 (2020).

[5] Altland, A. & Simons, B. D.
Condensed matter field theory (2nd edition). *Cambridge University Press* (2010).

[6] Altland, A. & Zirnbauer, M. R.
Nonstandard symmetry classes in mesoscopic normal-superconducting hybrid structures. *Physical Review B* **55**, 1142–1161 (1997).

[7] Altshuler, B. L., Aleiner, I. L., & Yudson, V. I.
Localization at the edge of a 2D topological insulator by Kondo impurities with random anisotropies. *Physical Review Letters* **111**, 086401 (2013).

[8] Anderson, P. W., Halperin, B. I., & Varma, C. M.
Anomalous low-temperature thermal properties of glasses and spin glasses. *The Philosophical Magazine* **25**(1), 1–9 (1972).

[9] Anderson, P. W., Yuval, G., & Hamann, D. R.
Exact results in the Kondo problem. II. Scaling theory, qualitatively correct solution, and some new results on one-dimensional classical statistical models. *Physical Review B* **1**, 4464–4473 (1970).

[10] Apel, W. & Rice, T. M.
Combined effect of disorder and interaction on the conductance of a one-dimensional fermion system. *Physical Review B* **26**, 7063–7065 (1982).

[11] Armitage, N. P., Mele, E. J., & Vishwanath, A.
Weyl and Dirac semimetals in three-dimensional solids. *Reviews of Modern Physics* **90**, 015001 (2018).

[12] Atala, M., Aidelsburger, M., Barreiro, J. T., Abanin, D., Kitagawa, T., Demler, E., & Bloch, I.
Direct measurement of the Zak phase in topological Bloch bands. *Nature Physics* **9**, 795–800 (2013).

[13] Babakhanian, A.
Cohomological methods in group theory. *Marcel Dekker, Inc.* (1972).

[14] Bardarson, J. H., Pollmann, F., & Moore, J. E.
Unbounded growth of entanglement in models of many-body localization. *Physical Review Letters* **109**, 017202 (2012).

[15] Bardyn, C.-E., Baranov, M. A., Kraus, C. V., Rico, E., İmamoğlu, A., Zoller, P., & Diehl, S.
Topology by dissipation. *New Journal of Physics* **15**(8), 085001 (2013).

[16] Bardyn, C.-E., Wawer, L., Altland, A., Fleischhauer, M., & Diehl, S.
Probing the topology of density matrices. *Physical Review X* **8**, 011035 (2018).

[17] Baumgartner, B. & Narnhofer, H.
Analysis of quantum semigroups with GKS–Lindblad generators: II. General. *Journal of Physics A* **41**(39), 395303 (2008).

[18] Bernevig, B. A.
Topological insulators and topological superconductors. *Princeton University Press* (2013).

[19] Bernien, H., Schwartz, S., Keesling, A., Levine, H., Omran, A., Pichler, H., Choi, S., Zibrov, A. S., Endres, M., Greiner, M., & Lukin, M.
Probing many-body dynamics on a 51-atom quantum simulator. *Nature* **551**, 579–584 (2017).

[20] Bravyi, S., Hastings, M. B., & Verstraete, F.
Lieb-Robinson bounds and the generation of correlations and topological quantum order. *Physical Review Letters* **97**, 050401 (2006).

[21] Breuer, H. & Petruccione, F.
The theory of open quantum systems. *Oxford University Press* (2002).

[22] Brown, K.
Cohomology of groups. *Springer-Verlag* (1982).

[23] Buča, B. & Prosen, T.
A note on symmetry reductions of the Lindblad equation: transport in constrained open spin chains. *New Journal of Physics* **14**(7), 073007 (2012).

[24] Budich, J. C. & Ardonne, E.
Equivalent topological invariants for one-dimensional Majorana wires in symmetry class D. *Physical Review B* **88**, 075419 (2013).

[25] Budich, J. C. & Ardonne, E.
Topological invariant for generic one-dimensional time-reversal-symmetric superconductors in class DIII. *Physical Review B* **88**, 134523 (2013).

[26] Budich, J. C. & Diehl, S.
Topology of density matrices. *Physical Review B* **91**, 165140 (2015).

[27] Budich, J. C., Dolcini, F., Recher, P., & Trauzettel, B.
Phonon-induced backscattering in helical edge states. *Physical Review Letters* **108**, 086602 (2012).

[28] Budich, J. C., Zoller, P., & Diehl, S.
Dissipative preparation of Chern insulators. *Physical Review A* **91**, 042117 (2015).

[29] Burnell, F. J., Chen, X., Fidkowski, L., & Vishwanath, A.
Exactly soluble model of a three-dimensional symmetry-protected topological phase of bosons with surface topological order. *Physical Review B* **90**, 245122 (2014).

[30] Caio, M. D., Cooper, N. R., & Bhaseen, M. J.
Quantum quenches in Chern insulators. *Physical Review Letters* **115**, 236403 (2015).

[31] Caio, M. D., Cooper, N. R., & Bhaseen, M. J.
Hall response and edge current dynamics in Chern insulators out of equilibrium. *Physical Review B* **94**, 155104 (2016).

[32] Calabrese, P. & Cardy, J.
Evolution of entanglement entropy in one-dimensional systems. *Journal of Statistical Mechanics* P04010 (2005).

[33] Caldeira, A. O. & Leggett, A. J.
Influence of dissipation on quantum tunneling in macroscopic systems. *Physical Review Letters* **46**, 211–214 (1981).

[34] Cardy, J.
Scaling and renormalization in statistical physics. Cambridge Lecture Notes in Physics. *Cambridge University Press* (1996).

[35] Chan, A., De Luca, A., & Chalker, J. T.
Solution of a minimal model for many-body quantum chaos. *Physical Review X* **8**, 041019 (2018).

[36] Chaturvedi, S. & Shibata, F.
Time-convolutionless projection operator formalism for elimination of fast variables. applications to brownian motion. *Zeitschrift für Physik B* **35**(3), 297–308 (1979).

[37] Chen, X., Gu, Z.-C., Liu, Z.-X., & Wen, X.-G.
Symmetry protected topological orders and the group cohomology of their symmetry group. *Physical Review B* **87**, 155114 (2013).

[38] Chen, X., Gu, Z.-C., & Wen, X.-G.
Local unitary transformation, long-range quantum entanglement, wave function renormalization, and topological order. *Physical Review B* **82**, 155138 (2010).

[39] Chen, X., Gu, Z.-C., & Wen, X.-G.
Classification of gapped symmetric phases in one-dimensional spin systems. *Physical Review B* **83**, 035107 (2011).

[40] Chen, X., Gu, Z.-C., & Wen, X.-G.
Complete classification of one-dimensional gapped quantum phases in interacting spin systems. *Physical Review B* **84**, 235128 (2011).

[41] Chen, X., Zhou, T., Huse, D. A., & Fradkin, E.
Out-of-time-order correlations in many-body localized and thermal phases. *Annalen der Physik (Berlin)* **529**(7), 1600332 (2017).

[42] Cheneau, M., Barmettler, P., Poletti, D., Endres, M., Schauß, P., Fukuhara, T., Gross, C., Bloch, I., Kollath, C., & Kuhr, S.
Light-cone-like spreading of correlations in a quantum many-body system. *Nature* **481**, 484–487 (2012).

[43] Chiara, G. D., Montangero, S., Calabrese, P., & Fazio, R.
Entanglement entropy dynamics of heisenberg chains. *Journal of Statistical Mechanics* P03001 (2006).

[44] Chiu, C.-K., Teo, J. C. Y., Schnyder, A. P., & Ryu, S.
Classification of topological quantum matter with symmetries. *Reviews of Modern Physics* **88**, 035005 (2016).

[45] Cooper, N. R., Dalibard, J., & Spielman, I. B.
Topological bands for ultracold atoms. *Reviews of Modern Physics* **91**, 015005 (2019).

[46] Crépin, F., Budich, J. C., Dolcini, F., Recher, P., & Trauzettel, B.
Renormalization group approach for the scattering off a single Rashba impurity in a helical liquid. *Physical Review B* **86**, 121106 (2012).

[47] D'Alessio, L., Kafri, Y., Polkovnikov, A., & Rigol, M.
From quantum chaos and eigenstate thermalization to statistical mechanics and thermodynamics. *Advances in Physics* **65**(3), 239–362 (2016).

[48] D'Alessio, L. & Rigol, M.
Long-time behavior of isolated periodically driven interacting lattice systems. *Physical Review X* **4**, 041048 (2014).

[49] D'Alessio, L. & Rigol, M.
Dynamical preparation of Floquet Chern insulators. *Nature Communications* **6**, 8336 (2015).

[50] Daley, A. J., Kollath, C., Schollwöck, U., & Vidal, G.
Time-dependent density-matrix renormalization-group using adaptive effective Hilbert spaces. *Journal of Statistical Mechanics* P04005 (2004).

[51] Dalibard, J., Castin, Y., & Mølmer, K.
Wave-function approach to dissipative processes in quantum optics. *Physical Review Letters* **68**, 580–583 (1992).

[52] Dalmonte, M., Vermersch, B., & Zoller, P.
Quantum simulation and spectroscopy of entanglement Hamiltonians. *Nature Physics* **14**, 827–831 (2018).

[53] de Léséleuc, S., Lienhard, V., Scholl, P., Barredo, D., Weber, S., Lang, N., Büchler, H. P., Lahaye, T., & Browaeys, A.
Observation of a symmetry-protected topological phase of interacting bosons with Rydberg atoms. *Science* **365**(6455), 775–780 (2019).

[54] Dehghani, H., Oka, T., & Mitra, A.
Dissipative Floquet topological systems. *Physical Review B* **90**, 195429 (2014).

[55] den Nijs, M. & Rommelse, K.
Preroughening transitions in crystal surfaces and valence-bond phases in quantum spin chains. *Physical Review B* **40**, 4709–4734 (1989).

[56] Deutsch, J. M.
Quantum statistical mechanics in a closed system. *Physical Review A* **43**, 2046–2049 (1991).

[57] Diehl, S., Micheli, A., Kantian, A., Kraus, B., Büchler, H. P., & Zoller, P.
Quantum states and phases in driven open quantum systems with cold atoms. *Nature Physics* **4**, 878–883 (2008).

[58] Diehl, S., Rico, E., Baranov, M. A., & Zoller, P.
Topology by dissipation in atomic quantum wires. *Nature Physics* **7**, 971–977 (2011).

[59] Du, L., Knez, I., Sullivan, G., & Du, R.-R.
Robust helical edge transport in gated InAs/GaSb bilayers. *Physical Review Letters* **114**, 096802 (2015).

[60] Dutta, P., Dimon, P., & Horn, P. M.
Energy scales for noise processes in metals. *Physical Review Letters* **43**, 646–649 (1979).

[61] Eisert, J., Cramer, M., & Plenio, M. B.
Colloquium: Area laws for the entanglement entropy. *Reviews of Modern Physics* **82**, 277–306 (2010).

[62] Eisert, J. & Osborne, T. J.
General entanglement scaling laws from time evolution. *Physical Review Letters* **97**, 150404 (2006).

[63] Else, D. V. & Nayak, C.
Classification of topological phases in periodically driven interacting systems. *Physical Review B* **93**, 201103 (2016).

[64] Esin, I., Rudner, M. S., Refael, G., & Lindner, N. H.
Quantized transport and steady states of Floquet topological insulators. *Physical Review B* **97**, 245401 (2018).

[65] Essin, A. M. & Gurarie, V.
Bulk-boundary correspondence of topological insulators from their respective Green's functions. *Physical Review B* **84**, 125132 (2011).

[66] Essin, A. M., Moore, J. E., & Vanderbilt, D.
Magnetoelectric polarizability and axion electrodynamics in crystalline insulators. *Physical Review Letters* **102**, 146805 (2009).

[67] Fan, R., Zhang, P., Shen, H., & Zhai, H.
Out-of-time-order correlation for many-body localization. *Science Bulletin* **62**(10), 707 – 711 (2017).

[68] Fannes, M., Nachtergaele, B., & Werner, R. F.
Finitely correlated states on quantum spin chains. *Communications in Mathematical Physics* **144**, 443–490 (1992).

[69] Fei, Z., Palomaki, T., Wu, S., Zhao, W., Cai, X., Sun, B., Nguyen, P., Finney, J., Xu, X., & Cobden, D. H.
Edge conduction in monolayer WTe_2. *Nature Physics* **13**, 677–682 (2017).

[70] Fidkowski, L.
Entanglement spectrum of topological insulators and superconductors. *Physical Review Letters* **104**, 130502 (2010).

[71] Fidkowski, L. & Kitaev, A.
Topological phases of fermions in one dimension. *Physical Review B* **83**, 075103 (2011).

[72] Foster, M. S., Dzero, M., Gurarie, V., & Yuzbashyan, E. A.
Quantum quench in a $p+ip$ superfluid: Winding numbers and topological states far from equilibrium. *Physical Review B* **88**, 104511 (2013).

[73] Fradkin, E.
Field theories of condensed matter physics (2nd edition). *Cambridge University Press* (2013).

[74] Fu, L.
Topological crystalline insulators. *Physical Review Letters* **106**, 106802 (2011).

[75] Fu, L. & Kane, C. L.
Time reversal polarization and a $\mathbb{Z}_2$ adiabatic spin pump. *Physical Review B* **74**, 195312 (2006).

[76] Fu, L., Kane, C. L., & Mele, E. J.
Topological insulators in three dimensions. *Physical Review Letters* **98**, 106803 (2007).

[77] Geißler, F.
Transport properties of helical Luttinger liquids. Ph.D thesis, Universität Würzburg (2017).

[78] Geissler, F., Crépin, F., & Trauzettel, B.
Random Rashba spin-orbit coupling at the quantum spin Hall edge. *Physical Review B* **89**, 235136 (2014).

[79] Giamarchi, T.
Quantum physics in one dimension. *Clarendon press* (2003).

[80] Goldman, N., Budich, J. C., & Zoller, P.
Topological quantum matter with ultracold gases in optical lattices. *Nature Physics* **12**, 639–645 (2016).

[81] Goldstein, G. & Chamon, C.
Decay rates for topological memories encoded with Majorana fermions. *Physical Review B* **84**, 205109 (2011).

[82] Goldstein, S., Lebowitz, J. L., Tumulka, R., & Zanghì, N.
Long-time behavior of macroscopic quantum systems. *The European Physical Journal H* **35**(2), 173–200 (2010).

[83] Gong, Z., Ashida, Y., Kawabata, K., Takasan, K., Higashikawa, S., & Ueda, M.
Topological phases of non-Hermitian systems. *Physical Review X* **8**, 031079 (2018).

[84] Gong, Z. & Ueda, M.
Topological entanglement-spectrum crossing in quench dynamics. *Physical Review Letters* **121**, 250601 (2018).

[85] Gong, Z.-X., Foss-Feig, M., Brandão, F. G. S. L., & Gorshkov, A. V.
Entanglement area laws for long-range interacting systems. *Physical Review Letters* **119**, 050501 (2017).

[86] Grabecki, G., Wróbel, J., Czapkiewicz, M., Cywiński, L., Gierałtowska, S., Guziewicz, E., Zholudev, M., Gavrilenko, V., Mikhailov, N. N., Dvoretski, S. A., Teppe, F., Knap, W., & Dietl, T.
Nonlocal resistance and its fluctuations in microstructures of band-inverted HgTe/(Hg,Cd)Te quantum wells. *Physical Review B* **88**, 165309 (2013).

[87] Grabert, H. & Weiss, U.
Quantum tunneling rates for asymmetric double-well systems with Ohmic dissipation. *Physical Review Letters* **54**, 1605–1608 (1985).

[88] Greiner, M., Mandel, O., Hänsch, T. W., & Bloch, I.
Collapse and revival of the matter wave field of a Bose-Einstein condensate. *Nature* **419**, 51–54 (2002).

[89] Guardado-Sanchez, E., Brown, P. T., Mitra, D., Devakul, T., Huse, D. A., Schauß, P., & Bakr, W. S.
Probing the quench dynamics of antiferromagnetic correlations in a 2D quantum Ising spin system. *Physical Review X* **8**, 021069 (2018).

[90] Haegeman, J., Pérez-García, D., Cirac, I., & Schuch, N.
Order parameter for symmetry-protected phases in one dimension. *Physical Review Letters* **109**, 050402 (2012).

[91] Haldane, F. D. M.
Model for a quantum Hall effect without Landau levels: Condensed-matter realization of the "parity anomaly". *Physical Review Letters* **61**, 2015–2018 (1988).

[92] Halperin, B. I.
Quantized Hall conductance, current-carrying edge states, and the existence of extended states in a two-dimensional disordered potential. *Physical Review B* **25**, 2185–2190 (1982).

[93] Hastings, M. B.
An area law for one-dimensional quantum systems. *Journal of Statistical Mechanics* P08024 (2007).

[94] Hastings, M. B. & Wen, X.-G.
Quasiadiabatic continuation of quantum states: The stability of topological ground-state degeneracy and emergent gauge invariance. *Physical Review B* **72**, 045141 (2005).

[95] Hatano, N. & Nelson, D. R.
Localization transitions in non-Hermitian quantum mechanics. *Physical Review Letters* **77**, 570–573 (1996).

[96] Ho, W. W. & Abanin, D. A.
Entanglement dynamics in quantum many-body systems. *Physical Review B* **95**, 094302 (2017).

[97] Hsieh, D., Qian, D., Wray, L., Xia, Y., Hor, Y. S., Cava, R. J., & Hasan, M. Z.
A topological Dirac insulator in a quantum spin Hall phase. *Nature* **452**, 970–974 (2008).

[98] Hsieh, T. H., Lin, H., Liu, J., Duan, W., Bansil, A., & Fu, L.
Topological crystalline insulators in the SnTe material class. *Nature Communications* **3**, 982 (2012).

[99] Hu, Y., Cai, Z., Baranov, M. A., & Zoller, P.
Majorana fermions in noisy Kitaev wires. *Physical Review B* **92**, 165118 (2015).

[100] Huang, Y., Zhang, Y.-L., & Chen, X.
Out-of-time-ordered correlators in many-body localized systems. *Annalen der Physik (Berlin)* **529**(7), 1600318 (2017).

[101] Huber, S. D.
Topological mechanics. *Nature Physics* **12**, 621–623 (2016).

[102] Iadecola, T., Neupert, T., & Chamon, C.
Occupation of topological Floquet bands in open systems. *Physical Review B* **91**, 235133 (2015).

[103] Jotzu, G., Messer, M., Desbuquois, R., Lebrat, M., Uehlinger, T., Greif, D., & Esslinger, T.
Experimental realization of the topological Haldane model with ultracold fermions. *Nature* **515**, 237–240 (2014).

[104] Joyner, D.
A primer on computational group homology and cohomology using GAP and SAGE. Extract from 'Aspects of Infinite Groups', Pp. 159–191. *World Scientific* (2008).

[105] Joynt, R. & Prange, R. E.
Conditions for the quantum Hall effect. *Physical Review B* **29**, 3303–3317 (1984).

[106] Jurcevic, P., Lanyon, B. P., Hauke, P., Hempel, C., Zoller, P., Blatt, R., & Roos, C. F.
Quasiparticle engineering and entanglement propagation in a quantum many-body system. *Nature* **511**, 202–205 (2014).

[107] Kampen, N. V.
A cumulant expansion for stochastic linear differential equations. I. *Physica* **74**(2), 215 – 238 (1974).

[108] Kane, C. L. & Fisher, M. P. A.
Transmission through barriers and resonant tunneling in an interacting one-dimensional electron gas. *Physical Review B* **46**, 15233–15262 (1992).

[109] Kane, C. L. & Fisher, M. P. A.
Transport in a one-channel Luttinger liquid. *Physical Review Letters* **68**, 1220–1223 (1992).

[110] Kane, C. L. & Mele, E. J.
$\mathbb{Z}_2$ topological order and the quantum spin Hall effect. *Physical Review Letters* **95**, 146802 (2005).

[111] Kane, C. L. & Mele, E. J.
Quantum spin Hall effect in graphene. *Physical Review Letters* **95**, 226801 (2005).

[112] Karzig, T., Knapp, C., Lutchyn, R. M., Bonderson, P., Hastings, M. B., Nayak, C., Alicea, J., Flensberg, K., Plugge, S., Oreg, Y., Marcus, C. M., & Freedman, M. H.
Scalable designs for quasiparticle-poisoning-protected topological quantum computation with Majorana zero modes. *Physical Review B* **95**, 235305 (2017).

[113] Kawabata, K., Shiozaki, K., Ueda, M., & Sato, M.
Symmetry and topology in non-Hermitian physics. *Physical Review X* **9**, 041015 (2019).

[114] Kennedy, T. & Tasaki, H.
Hidden $\mathbb{Z}_2 \times \mathbb{Z}_2$ symmetry breaking in Haldane-gap antiferromagnets. *Physical Review B* **45**, 304–307 (1992).

[115] Khemani, V., Lazarides, A., Moessner, R., & Sondhi, S. L.
Phase structure of driven quantum systems. *Physical Review Letters* **116**, 250401 (2016).

[116] Khmelnitskii, D.
Quantum Hall effect and additional oscillations of conductivity in weak magnetic fields. *Physics Letters A* **106**(4), 182 – 183 (1984).

[117] Kim, H. & Huse, D. A.
Ballistic spreading of entanglement in a diffusive nonintegrable system. *Physical Review Letters* **111**, 127205 (2013).

[118] King-Smith, R. D. & Vanderbilt, D.
Theory of polarization of crystalline solids. *Physical Review B* **47**, 1651–1654 (1993).

[119] Kitaev, A.
Anyons in an exactly solved model and beyond. *Annals of Physics* **321**(1), 2 – 111 (2006).

[120] Kitaev, A.
Periodic table for topological insulators and superconductors. *AIP Conference Proceedings* **1134**, 22–30 (2009).

[121] Kitaev, A. & Preskill, J.
Topological entanglement entropy. *Physical Review Letters* **96**, 110404 (2006).

[122] Kitaev, A. Y.
Unpaired Majorana fermions in quantum wires. *Physics-Uspekhi* **44**, 131 (2001).

[123] Kitagawa, T., Berg, E., Rudner, M., & Demler, E.
Topological characterization of periodically driven quantum systems. *Physical Review B* **82**, 235114 (2010).

[124] Klitzing, K. v., Dorda, G., & Pepper, M.
New method for high-accuracy determination of the fine-structure constant based on quantized Hall resistance. *Physical Review Letters* **45**, 494–497 (1980).

[125] Kohn, W.
Analytic properties of Bloch waves and Wannier functions. *Physical Review* **115**, 809–821 (1959).

[126] Kondo, J.
Resistance minimum in dilute magnetic alloys. *Progress of Theoretical Physics* **32**(1), 37–49 (1964).

[127] König, M., Baenninger, M., Garcia, A. G. F., Harjee, N., Pruitt, B. L., Ames, C., Leubner, P., Brüne, C., Buhmann, H., Molenkamp, L. W., & Goldhaber-Gordon, D.
Spatially resolved study of backscattering in the quantum spin Hall state. *Physical Review X* **3**, 021003 (2013).

[128] König, M., Wiedmann, S., Brüne, C., Roth, A., Buhmann, H., Molenkamp, L. W., Qi, X.-L., & Zhang, S.-C.
Quantum spin Hall insulator state in HgTe quantum wells. *Science* **318**(5851), 766–770 (2007).

[129] Laughlin, R. B.
Anomalous quantum Hall effect: An incompressible quantum fluid with fractionally charged excitations. *Physical Review Letters* **50**, 1395–1398 (1983).

[130] Lazarides, A., Das, A., & Moessner, R.
Periodic thermodynamics of isolated quantum systems. *Physical Review Letters* **112**, 150401 (2014).

[131] Leggett, A. J., Chakravarty, S., Dorsey, A. T., Fisher, M. P. A., Garg, A., & Zwerger, W.
Dynamics of the dissipative two-state system. *Reviews of Modern Physics* **59**, 1–85 (1987).

[132] Levin, M. & Wen, X.-G.
Detecting topological order in a ground state wave function. *Physical Review Letters* **96**, 110405 (2006).

[133] Li, H. & Haldane, F. D. M.
Entanglement spectrum as a generalization of entanglement entropy: Identification of topological order in non-Abelian fractional quantum Hall effect states. *Physical Review Letters* **101**, 010504 (2008).

[134] Lieb, E. H. & Robinson, D. W.
The finite group velocity of quantum spin systems. *Communications in Mathematical Physics* **28**, 251–257 (1972).

[135] Lieu, S.
Topological symmetry classes for non-Hermitian models and connections to the bosonic Bogoliubov-de Gennes equation. *Physical Review B* **98**, 115135 (2018).

[136] Lieu, S., McGinley, M., & Cooper, N. R.
Tenfold way for quadratic Lindbladians. *Physical Review Letters* **124**, 040401 (2020).

[137] Lindblad, G.
On the generators of quantum dynamical semigroups. *Communications in Mathematical Physics* **48**, 119–130 (1976).

[138] Liu, Z.-G., Xiong, L., Huang, B., Guo, G.-C., & Gong, M.
Topological indexes in symmetry preserving dynamics. arXiv:1802.02931 (2018).

[139] Maciejko, J., Liu, C., Oreg, Y., Qi, X.-L., Wu, C., & Zhang, S.-C.
Kondo effect in the helical edge liquid of the quantum spin Hall state. *Physical Review Letters* **102**, 256803 (2009).

[140] Mahan, G.
Many-particle physics. Physics of Solids and Liquids. *Kluwer Academic/Plenum Publishers* (1981).

[141] Manzano, D. & Hurtado, P. I.
Symmetry and the thermodynamics of currents in open quantum systems. *Physical Review B* **90**, 125138 (2014).

[142] Martin, P. C. & Schwinger, J.
Theory of many-particle systems. I. *Physical Review* **115**, 1342–1373 (1959).

[143] Maslov, D. L. & Stone, M.
Landauer conductance of Luttinger liquids with leads. *Physical Review B* **52**, R5539–R5542 (1995).

[144] Mazza, L., Rizzi, M., Lukin, M. D., & Cirac, J. I.
Robustness of quantum memories based on Majorana zero modes. *Physical Review B* **88**, 205142 (2013).

[145] McGinley, M. & Cooper, N. R.
Topology of one-dimensional quantum systems out of equilibrium. *Physical Review Letters* **121**, 090401 (2018).

[146] McGinley, M. & Cooper, N. R.
Classification of topological insulators and superconductors out of equilibrium. *Physical Review B* **99**, 075148 (2019).

[147] McGinley, M. & Cooper, N. R.
Interacting symmetry-protected topological phases out of equilibrium. *Physical Review Research* **1**, 033204 (2019).

[148] McGinley, M. & Cooper, N. R.
Fragility of time-reversal symmetry protected topological phases. *Nature Physics* (2020).

[149] McGinley, M., Knolle, J., & Nunnenkamp, A.
Robustness of Majorana edge modes and topological order: Exact results for the symmetric interacting Kitaev chain with disorder. *Physical Review B* **96**, 241113 (2017).

[150] McGinley, M., Nunnenkamp, A., & Knolle, J.
Slow growth of out-of-time-order correlators and entanglement entropy in integrable disordered systems. *Physical Review Letters* **122**, 020603 (2019).

[151] Moiseyev, N.
Non-Hermitian quantum mechanics. *Cambridge University Press* (2011).

[152] Moore, G. & Read, N.
Nonabelions in the fractional quantum Hall effect. *Nuclear Physics B* **360**(2), 362 – 396 (1991).

[153] Moore, G. W.
Quantum symmetries and compatible Hamiltonians. Lecture notes at Rutgers. http://www.physics.rutgers.edu/~gmoore/695Fall2013 (2013).

[154] Moore, J. E. & Balents, L.
Topological invariants of time-reversal-invariant band structures. *Physical Review B* **75**, 121306 (2007).

[155] Morimoto, T., Furusaki, A., & Mudry, C.
Breakdown of the topological classification $\mathbb{Z}$ for gapped phases of noninteracting fermions by quartic interactions. *Physical Review B* **92**, 125104 (2015).

[156] Müller, C. & Stace, T. M.
Deriving Lindblad master equations with Keldysh diagrams: Correlated gain and loss in higher order perturbation theory. *Physical Review A* **95**, 013847 (2017).

[157] Nahum, A., Ruhman, J., Vijay, S., & Haah, J.
Quantum entanglement growth under random unitary dynamics. *Physical Review X* **7**, 031016 (2017).

[158] Nandkishore, R. & Huse, D. A.
Many-body localization and thermalization in quantum statistical mechanics. *Annual Review of Condensed Matter Physics* **6**(1), 15–38 (2015).

[159] National Institute of Standards and Technology
CODATA recommended values: von Klitzing constant. https://physics.nist.gov/cgi-bin/cuu/value?rk (2019).

[160] Nayak, C., Simon, S. H., Stern, A., Freedman, M., & Das Sarma, S.
Non-Abelian anyons and topological quantum computation. *Reviews of Modern Physics* **80**, 1083–1159 (2008).

[161] Nicacio, F., Paternostro, M., & Ferraro, A.
Determining stationary-state quantum properties directly from system-environment interactions. *Physical Review A* **94**, 052129 (2016).

[162] Oka, T. & Aoki, H.
Photovoltaic Hall effect in graphene. *Physical Review B* **79**, 081406 (2009).

[163] Oreg, Y. & von Oppen, F.
Majorana zero modes in networks of Cooper-pair boxes: Topologically ordered states and topological quantum computation. *Annual Review of Condensed Matter Physics* **11**(1), 397–420 (2020).

[164] Osborne, T. J.
Efficient approximation of the dynamics of one-dimensional quantum spin systems. *Physical Review Letters* **97**, 157202 (2006).

[165] Ozawa, T., Price, H. M., Amo, A., Goldman, N., Hafezi, M., Lu, L., Rechtsman, M. C., Schuster, D., Simon, J., Zilberberg, O., & Carusotto, I.
Topological photonics. *Reviews of Modern Physics* **91**, 015006 (2019).

[166] Pachos, J. K. & Simon, S. H.
Focus on topological quantum computation. *New Journal of Physics* **16**(6), 065003 (2014).

[167] Perez-Garcia, D., Verstraete, F., Wolf, M. M., & Cirac, J. I.
Matrix product state representations. *Quantum Information and Computation* **7**(5), 401–430 (2007).

[168] Peschel, I.
Calculation of reduced density matrices from correlation functions. *Journal of Physics A* **36**(4), L205 (2003).

[169] Plugge, S., Rasmussen, A., Egger, R., & Flensberg, K.
Majorana box qubits. *New Journal of Physics* **19**(1), 012001 (2017).

[170] Polkovnikov, A., Sengupta, K., Silva, A., & Vengalattore, M.
Colloquium: Nonequilibrium dynamics of closed interacting quantum systems. *Reviews of Modern Physics* **83**, 863–883 (2011).

[171] Pollmann, F. & Turner, A. M.
Detection of symmetry-protected topological phases in one dimension. *Physical Review B* **86**, 125441 (2012).

[172] Pollmann, F., Turner, A. M., Berg, E., & Oshikawa, M.
Entanglement spectrum of a topological phase in one dimension. *Physical Review B* **81**, 064439 (2010).

[173] Popescu, S., Short, A. J., & Winter, A.
Entanglement and the foundations of statistical mechanics. *Nature Physics* **2**, 754–758 (2006).

[174] Potter, A. C., Morimoto, T., & Vishwanath, A.
Classification of interacting topological Floquet phases in one dimension. *Physical Review X* **6**, 041001 (2016).

[175] Preskill, J.
'Quantum information', Chapter 2. Lecture notes at Caltech, physics 219 http://www.theory.caltech.edu/~preskill/ph219/chap2_15.pdf (1998).

[176] Prosen, T. & Žnidarič, M.
Is the efficiency of classical simulations of quantum dynamics related to integrability? *Physical Review E* **75**, 015202 (2007).

[177] Qi, X.-L., Hughes, T. L., & Zhang, S.-C.
Topological field theory of time-reversal invariant insulators. *Physical Review B* **78**, 195424 (2008).

[178] Rainis, D. & Loss, D.
Majorana qubit decoherence by quasiparticle poisoning. *Physical Review B* **85**, 174533 (2012).

[179] Rammer, J. & Smith, H.
Quantum field-theoretical methods in transport theory of metals. *Reviews of Modern Physics* **58**, 323–359 (1986).

[180] Richerme, P., Gong, Z.-X., Lee, A., Senko, C., Smith, J., Foss-Feig, M., Michalakis, S., Gorshkov, A. V., & Monroe, C.
Non-local propagation of correlations in quantum systems with long-range interactions. *Nature* **511**, 198–201 (2014).

[181] Rigol, M., Dunjko, V., & Olshanii, M.
Thermalization and its mechanism for generic isolated quantum systems. *Nature* **452**, 854–858 (2008).

[182] Rigol, M., Dunjko, V., Yurovsky, V., & Olshanii, M.
Relaxation in a completely integrable many-body quantum system: An *ab initio* study of the dynamics of the highly excited states of 1D lattice hard-core bosons. *Physical Review Letters* **98**, 050405 (2007).

[183] Roth, A., Brüne, C., Buhmann, H., Molenkamp, L. W., Maciejko, J., Qi, X.-L., & Zhang, S.-C.
Nonlocal transport in the quantum spin Hall state. *Science* **325**(5938), 294–297 (2009).

[184] Rowell, E. C. & Wang, Z.
Mathematics of topological quantum computing. *Bulletin of the American Mathematical Society* **55**, 183–238 (2018).

[185] Roy, R. & Harper, F.
Periodic table for Floquet topological insulators. *Physical Review B* **96**, 155118 (2017).

[186] Rudner, M. S., Lindner, N. H., Berg, E., & Levin, M.
Anomalous edge states and the bulk-edge correspondence for periodically driven two-dimensional systems. *Physical Review X* **3**, 031005 (2013).

[187] Ryu, S., Schnyder, A. P., Furusaki, A., & Ludwig, A. W. W.
Topological insulators and superconductors: Tenfold way and dimensional hierarchy. *New Journal of Physics* **12**(6), 065010 (2010).

[188] Sacramento, P. D.
Fate of Majorana fermions and Chern numbers after a quantum quench. *Physical Review E* **90**, 032138 (2014).

[189] Safi, I. & Schulz, H. J.
Transport in an inhomogeneous interacting one-dimensional system. *Physical Review B* **52**, R17040–R17043 (1995).

[190] Schindler, F., Cook, A. M., Vergniory, M. G., Wang, Z., Parkin, S. S. P., Bernevig, B. A., & Neupert, T.
Higher-order topological insulators. *Science Advances* **4**(6), EAAT0346 (2018).

[191] Schmidt, T. L., Rachel, S., von Oppen, F., & Glazman, L. I.
Inelastic electron backscattering in a generic helical edge channel. *Physical Review Letters* **108**, 156402 (2012).

[192] Schmitt, F., Kirchmann, P. S., Bovensiepen, U., Moore, R. G., Rettig, L., Krenz, M., Chu, J.-H., Ru, N., Perfetti, L., Lu, D. H., Wolf, M., Fisher, I. R., & Shen, Z.-X.
Transient electronic structure and melting of a charge density wave in TbTe3. *Science* **321**(5896), 1649–1652 (2008).

[193] Schnyder, A. P., Ryu, S., Furusaki, A., & Ludwig, A. W. W.
Classification of topological insulators and superconductors in three spatial dimensions. *Physical Review B* **78**, 195125 (2008).

[194] Schnyder, A. P., Ryu, S., Furusaki, A., & Ludwig, A. W. W.
Classification of topological insulators and superconductors. *AIP Conference Proceedings* **1134**, 10–21 (2009).

[195] Schuch, N., Pérez-García, D., & Cirac, I.
Classifying quantum phases using matrix product states and projected entangled pair states. *Physical Review B* **84**, 165139 (2011).

[196] Schuch, N., Wolf, M. M., Verstraete, F., & Cirac, J. I.
Entropy scaling and simulability by matrix product states. *Physical Review Letters* **100**, 030504 (2008).

[197] Seetharam, K. I., Bardyn, C.-E., Lindner, N. H., Rudner, M. S., & Refael, G.
Controlled population of Floquet-Bloch states via coupling to Bose and Fermi baths. *Physical Review X* **5**, 041050 (2015).

[198] Sharifi, R.
Group and Galois cohomology. Lecture notes at UCLA. http://math.ucla.edu/~sharifi/groupcoh.pdf.

[199] Shibata, F., Takahashi, Y., & Hashitsume, N.
A generalized stochastic Liouville equation. non-markovian versus memoryless master equations. *Journal of Statistical Physics* **17**(4), 171–187 (1977).

[200] Srednicki, M.
Entropy and area. *Physical Review Letters* **71**, 666–669 (1993).

[201] Srednicki, M.
Chaos and quantum thermalization. *Physical Review E* **50**, 888–901 (1994).

[202] Stace, T. M., Doherty, A. C., & Reilly, D. J.
Dynamical steady states in driven quantum systems. *Physical Review Letters* **111**, 180602 (2013).

[203] Su, W. P., Schrieffer, J. R., & Heeger, A. J.
Solitons in polyacetylene. *Physical Review Letters* **42**, 1698–1701 (1979).

[204] Sun, W., Yi, C.-R., Wang, B.-Z., Zhang, W.-W., Sanders, B. C., Xu, X.-T., Wang, Z.-Y., Schmiedmayer, J., Deng, Y., Liu, X.-J., Chen, S., & Pan, J.-W.
Uncover topology by quantum quench dynamics. *Physical Review Letters* **121**, 250403 (2018).

[205] Suzuki, K., Harada, Y., Onomitsu, K., & Muraki, K.
Edge channel transport in the InAs/GaSb topological insulating phase. *Physical Review B* **87**, 235311 (2013).

[206] Tanaka, Y., Furusaki, A., & Matveev, K. A.
Conductance of a helical edge liquid coupled to a magnetic impurity. *Physical Review Letters* **106**, 236402 (2011).

[207] Tanaka, Y., Ren, Z., Sato, T., Nakayama, K., Souma, S., Takahashi, T., Segawa, K., & Ando, Y.
Experimental realization of a topological crystalline insulator in SnTe. *Nature Physics* **8**, 800–803 (2012).

[208] Tarnowski, M., Ünal, F. N., Fläschner, N., Rem, B. S., Eckardt, A., Sengstock, K., & Weitenberg, C.
Measuring topology from dynamics by obtaining the Chern number from a linking number. *Nature communications* **10**, 1728 (2019).

[209] Teo, J. C. Y. & Kane, C. L.
Majorana fermions and non-Abelian statistics in three dimensions. *Physical Review Letters* **104**, 046401 (2010).

[210] Teo, J. C. Y. & Kane, C. L.
Topological defects and gapless modes in insulators and superconductors. *Physical Review B* **82**, 115120 (2010).

[211] Thingna, J., Manzano, D., & Cao, J.
Dynamical signatures of molecular symmetries in nonequilibrium quantum transport. *Scientific Reports* **6**, 28027 (2016).

[212] Thouless, D. J., Kohmoto, M., Nightingale, M. P., & den Nijs, M.
Quantized Hall conductance in a two-dimensional periodic potential. *Physical Review Letters* **49**, 405–408 (1982).

[213] Trotzky, S., Chen, Y.-A., Flesch, A., McCulloch, I. P., Schollwöck, U., Eisert, J., & Bloch, I.
Probing the relaxation towards equilibrium in an isolated strongly correlated one-dimensional bose gas. *Nature Physics* **8**, 325 (2012).

[214] Turner, A. M., Pollmann, F., & Berg, E.
Topological phases of one-dimensional fermions: An entanglement point of view. *Physical Review B* **83**, 075102 (2011).

[215] Ünal, F. N., Mueller, E. J., & Oktel, M. O.
Nonequilibrium fractional Hall response after a topological quench. *Physical Review A* **94**, 053604 (2016).

[216] van Acoleyen, K., Mariën, M., & Verstraete, F.
Entanglement rates and area laws. *Physical Review Letters* **111**, 170501 (2013).

[217] van Caspel, M., Arze, S. E. T., & Castillo, I. P.
Dynamical signatures of topological order in the driven-dissipative Kitaev chain. *SciPost Physics* **6**, 26 (2019).

[218] Verstraete, F. & Cirac, J. I.
Renormalization algorithms for quantum-many body systems in two and higher dimensions. Online preprint arXiv:cond-mat/0407066 (2004).

[219] Verstraete, F., Wolf, M., & Cirac, J. I.
Quantum computation and quantum-state engineering driven by dissipation. *Nature Physics* **5**, 633–636 (2009).

[220] Verstraete, F., Wolf, M. M., Perez-Garcia, D., & Cirac, J. I.
Criticality, the area law, and the computational power of projected entangled pair states. *Physical Review Letters* **96**, 220601 (2006).

[221] Vidal, G.
Efficient classical simulation of slightly entangled quantum computations. *Physical Review Letters* **91**, 147902 (2003).

[222] Vishwanath, A. & Senthil, T.
Physics of three-dimensional bosonic topological insulators: Surface-deconfined criticality and quantized magnetoelectric effect. *Physical Review X* **3**, 011016 (2013).

[223] von Delft, J. & Schoeller, H.
Bosonization for beginners — refermionization for experts. *Annalen der Physik (Berlin)* **7**(4), 225–305 (1998).

[224] von Keyserlingk, C. W., Rakovszky, T., Pollmann, F., & Sondhi, S. L.
Operator hydrodynamics, OTOCs, and entanglement growth in systems without conservation laws. *Physical Review X* **8**, 021013 (2018).

[225] von Keyserlingk, C. W. & Sondhi, S. L.
Phase structure of one-dimensional interacting Floquet systems. I. Abelian symmetry-protected topological phases. *Physical Review B* **93**, 245145 (2016).

[226] von Klitzing, K.
Essay: Quantum Hall effect and the new international system of units. *Physical Review Letters* **122**, 200001 (2019).

[227] von Neumann, J.
Proof of the ergodic theorem and the H-theorem in quantum mechanics. *Zeitschrift für Physik* **57**, 30–70 (1929).

[228] Wang, C. & Senthil, T.
Boson topological insulators: A window into highly entangled quantum phases. *Physical Review B* **87**, 235122 (2013).

[229] Wang, C., Zhang, P., Chen, X., Yu, J., & Zhai, H.
Scheme to measure the topological number of a Chern insulator from quench dynamics. *Physical Review Letters* **118**, 185701 (2017).

[230] Weiss, U.
Quantum dissipative systems (4th edition). *World Scientific* (2012).

[231] Weissman, M. B.
$1/f$ noise and other slow, nonexponential kinetics in condensed matter. *Reviews of Modern Physics* **60**, 537–571 (1988).

[232] Wen, X. G.
Electrodynamical properties of gapless edge excitations in the fractional quantum Hall states. *Physical Review Letters* **64**, 2206–2209 (1990).

[233] Wen, X.-G.
Edge transport properties of the fractional quantum Hall states and weak-impurity scattering of a one-dimensional charge-density wave. *Physical Review B* **44**, 5708–5719 (1991).

[234] Wen, X.-G.
Construction of bosonic symmetry-protected-trivial states and their topological invariants via $G \times \mathrm{SO}(3)$ nonlinear σ models. *Physical Review B* **91**, 205101 (2015).

[235] Wen, X. G. & Niu, Q.
Ground-state degeneracy of the fractional quantum Hall states in the presence of a random potential and on high-genus Riemann surfaces. *Physical Review B* **41**, 9377–9396 (1990).

[236] Weston, T.
The inflation-restriction sequence: An introduction to spectral sequences. Working seminar in mathematics and statistics I & II, Math 666/7. http://www.math.mcgill.ca/goren/seminaroncohomology/infres.pdf (2004).

[237] White, S. R.
Density matrix formulation for quantum renormalization groups. *Physical Review Letters* **69**, 2863–2866 (1992).

[238] Wigner, E.
Group theory and its application to the quantum mechanics of atomic spectra. *Academic Press* (1959).

[239] Wilczek, F. & Zee, A.
Appearance of gauge structure in simple dynamical systems. *Physical Review Letters* **52**, 2111–2114 (1984).

[240] Williamson, D. J., Bultinck, N., Mariën, M., Şahinoğlu, M. B., Haegeman, J., & Verstraete, F.
Matrix product operators for symmetry-protected topological phases: Gauging and edge theories. *Physical Review B* **94**, 205150 (2016).

[241] Wu, C., Bernevig, B. A., & Zhang, S.-C.
Helical liquid and the edge of quantum spin Hall systems. *Physical Review Letters* **96**, 106401 (2006).

[242] Wu, S., Fatemi, V., Gibson, Q. D., Watanabe, K., Taniguchi, T., Cava, R. J., & Jarillo-Herrero, P.
Observation of the quantum spin Hall effect up to 100 kelvin in a monolayer crystal. *Science* **359**(6371), 76–79 (2018).

[243] Xiao, D., Shi, J., Clougherty, D. P., & Niu, Q.
Polarization and adiabatic pumping in inhomogeneous crystals. *Physical Review Letters* **102**, 087602 (2009).

[244] Xu, C. & Moore, J. E.
Stability of the quantum spin Hall effect: Effects of interactions, disorder, and $\mathbb{Z}_2$ topology. *Physical Review B* **73**, 045322 (2006).

[245] Yang, C., Li, L., & Chen, S.
Dynamical topological invariant after a quantum quench. *Physical Review B* **97**, 060304 (2018).

[246] Yang, J. & Liu, Z.-X.
Irreducible projective representations and their physical applications. *Journal of Physics A* **51**(2), 025207 (2017).

[247] Yuval, G. & Anderson, P. W.
Exact results for the Kondo problem: One-body theory and extension to finite temperature. *Physical Review B* **1**, 1522–1528 (1970).

[248] Zak, J.
Berry's phase for energy bands in solids. *Physical Review Letters* **62**, 2747–2750 (1989).

[249] Zhang, L., Zhang, L., Niu, S., & Liu, X.-J.
Dynamical classification of topological quantum phases. *Science Bulletin* **63**, 1385–1391 (2018).

[250] Zhou, H. & Lee, J. Y.
Periodic table for topological bands with non-Hermitian symmetries. *Physical Review B* **99**, 235112 (2019).

[251] Žnidarič, M., Prosen, T., & Prelovšek, P.
Many-body localization in the Heisenberg XXZ magnet in a random field. *Physical Review B* **77**, 064426 (2008).

Appendix A

Computing the image of the restriction functor using the Hochschild-Serre spectral sequence

In this appendix, we describe a method for computing the non-equilibrium classification for strongly interacting bosonic SPTs using certain cohomological methods. In Section 3.2.3, we showed that the non-equilibrium classification is given by the image of the restriction functor from $\mathscr{H}^{d+1}[G, \mathrm{U}_T(1)]$ to $\mathscr{H}^{d+1}[G_T, \mathrm{U}_T(1)]$, where G_T is the subgroup of G containing only unitary elements [Eq. (3.20)]. The restriction functor is a well-studied object in group cohomology, and it features in a theorem known as the Hochschild-Serre (HS) spectral sequence (sometimes referred to as the Lyndon spectral sequence). We provide a brief discussion of spectral sequences, and how they apply to our classification problem; however for a more formal introduction to the methods used, see e.g. Ref. [22].

A spectral sequence is best visualised on a three dimensional grid. Each 2D layer is referred to as a *page* (or sometimes leaf, sheet, or term), labelled by $r \geq 0$. There is some initial page r_0, which is often $r = 1$ or 2. Each page is made up of a square grid, and each point (p,q) of the grid, there is a group, denoted $E_r^{p,q}$. For $p < 0$ or $q < 0$, we have $E_r^{p,q} = \{e\}$, the trivial group. The relationships between different pages are constructed through the 'differentials' $d_r^{p,q} : E_r^{p,q} \to E_r^{p+r,q-r+1}$. Note here that within the page r, the domain and codomain of the differentials are relatively displaced by a vector which depends on r. The differentials satisfy $d_r^{p+r,q-r+1} \circ d_r^{p,q} = 0$, which means that one can form cochain complexes between the groups $E_r^{p+nr,q-nr+1}$, where n runs over the integers.

The groups which constitute the $(r+1)$th page are the cohomology groups of the cochain complexes within the rth page, i.e.

$$E_{r+1}^{p,q} \cong \ker d_r^{p,q} / \operatorname{im} d_r^{p-r,q+r-1} \tag{A.1}$$

The sequence continues for increasing page number $r \to \infty$. In words, spectral sequences are built recursively by constructing cochain complexes between cohomology groups of the previous cochain complexes.

We say that a spectral sequence converges if for r large enough, the groups $E_r^{p,q}$ become independent of r. For example, $E_r^{1,1}$ must converge for $r \geq 3$, since $d_3^{1,1}$ has codomain $E_3^{4,-1} = 0$ and $d_3^{-2,3}$ has domain $E_3^{-2,3} = 0$, hence $E_4^{1,1} = E_3^{1,1}$, and so on. One denotes this convergence as

$$E_r^{p,q} \Rightarrow H^{p+q}. \tag{A.2}$$

Despite the suggestive notation, the groups H^{p+q} are not given by $E_\infty^{p,q}$, but instead have structure related to the converged groups. Specifically, there is a filtration

$$0 = H_{n+1}^n \subseteq H_n^n \subseteq H_{n-1}^n \subseteq \cdots \subseteq H_1^n \subseteq H_0^n = H^n \tag{A.3}$$

such that

$$E_\infty^{p,n-p} \cong H_p^n / H_{p+1}^n \tag{A.4}$$

Thus the diagonals on page $r \to \infty$ with fixed $p+q$ are quotients of successive subgroups of H^{p+q}. Knowledge of the $E_\infty^{p,q}$ thus provides a lot of information about H^{p+q}. Two particularly simple data are the edge maps

$$E_{r_0}^{n,0} \twoheadrightarrow E_\infty^{n,0} \hookrightarrow H^n \tag{A.5a}$$

$$H^n \twoheadrightarrow E_\infty^{0,n} \hookrightarrow E_{r_0}^{0,n}, \tag{A.5b}$$

The surjectivity (indicated by $\twoheadrightarrow$) of the first map of each row follows since $E_\infty^{n,0}$ is a quotient of $E_{r_0}^{n,0}$, and $E_\infty^{0,n} \cong H^n / H_1^n$ is a quotient of H^n. Injectivity (indicated by $\hookrightarrow$) follows since $E_\infty^{n,0} \cong H_n^n$ is a subgroup of H^n, and $E_\infty^{0,n}$ is a subgroup of $E_{r_0}^{0,n}$.

The Hochschild-Serre spectral sequence relates cohomology groups of G to cohomology groups of one of its subgroups. Specifically, if H is a normal subgroup of G, then it is

expressed as

$$E_2^{p,q} = \mathscr{H}^p(G/H, \mathscr{H}^q(H,M)) \Rightarrow \mathscr{H}^{p+q}(G,M) \tag{A.6}$$

where M is an arbitrary G-module. The usage of $\mathscr{H}^q(H,M)$ as a G/H-module means we must understand how elements of G/H act on elements of the cohomology group, via the action of H on M. Examples of this construction can be found in Appendix J.10 of Ref. [37].

The HS spectral sequence is usually applied as a tool for computing cohomology for complicated groups G based on some simpler structure contained in its subgroups. Here, instead, we assume that $\mathscr{H}^{p+q}(G,M)$ is already known by some other method, and make use an important corollary, namely that the composite edge map in Eq. (A.5b) is given by the restriction functor from $H^n = \mathscr{H}^n(G,M)$ to $\mathscr{H}^n(H,M)$ [236]. (Note that $E_{r_0}^{0,n} = \mathscr{H}^0(G/H, \mathscr{H}^n(H,M)) = \mathscr{H}^n(H,M)^{G/H} \leq \mathscr{H}^n(H,M)$, where the superscript $A^{G/H}$ denotes the submodule of A which is invariant under the action of elements of G/H.) Given the respective surjectivity and injectivity of the left and right maps in (A.5b), we have

$$\operatorname{im}\mathrm{Res}_n \cong E_\infty^{0,n}, \tag{A.7}$$

the left hand side of which gives the non-equilibrium classification in dimension $d = n-1$, by the arguments of Section 3.2.3. Our task is now reduced to finding how the HS spectral sequence (A.6) converges along the $(0,n)$ axis, using $H = G_T$ as the subgroup, and $M = \mathrm{U}_T(1)$ as the G-module. We can also simplify matters further by using the isomorphism $\mathscr{H}^n(G, \mathrm{U}_T(1)) \cong \mathscr{H}^{n+1}(G, \mathbb{Z}_T)$, where $\mathbb{Z}_T$ is a G-module with underlying group $\mathbb{Z}$, transforming as $T : a \mapsto -a$ for antiunitary elements T.

We now describe how to obtain $E_\infty^{0,n}$ for the group $G = \mathbb{Z}_n \times \mathbb{Z}_m \times \mathbb{Z}_2^T$, module $M = \mathbb{Z}_T$, and $n = 2, \ldots, 5$ corresponding to spatial dimension $d = 0, \ldots, 3$. The other groups in Table 3.3 can be obtained in similar ways.

The second page of the sequence $E_2^{p,q} = \mathscr{H}^p(\mathbb{Z}_2^T, \mathscr{H}^q(\mathbb{Z}_n \times \mathbb{Z}_m, \mathbb{Z}_T))$ can be calculated using cohomology identities for finite cyclic groups [104], giving

p / q	0	1	2	3	4	5
5	$B_{n,m}\times B_{n,m}$	$B_{n,m}\times B_{n,m}$	$B_{n,m}\times B_{n,m}$	$B_{n,m}\times B_{n,m}$	$B_{n,m}\times B_{n,m}$	$B_{n,m}\times B_{n,m}$
4	$A_{n,m}\times B_{n,m}$	$A_{n,m}\times B_{n,m}$	$A_{n,m}\times B_{n,m}$	$A_{n,m}\times B_{n,m}$	$A_{n,m}\times B_{n,m}$	$A_{n,m}\times B_{n,m}$
3	$B_{n,m}$	$B_{n,m}$	$B_{n,m}$	$B_{n,m}$	$B_{n,m}$	$B_{n,m}$
2	$A_{n,m}$	$A_{n,m}$	$A_{n,m}$	$A_{n,m}$	$A_{n,m}$	$A_{n,m}$
1	0	0	0	0	0	0
0	0	$\mathbb{Z}_2$	0	$\mathbb{Z}_2$	0	$\mathbb{Z}_2$

(A.8)

where we have used the shorthand

$$\begin{aligned} A_{n,m} &\coloneqq \mathbb{Z}_{(2,n)}\times\mathbb{Z}_{(2,m)} \\ B_{n,m} &\coloneqq \mathbb{Z}_{(2,n,m)} \end{aligned} \tag{A.9}$$

and $(a,b,c,\ldots)$ denotes the greatest common divisor of the integers in the brackets. The converged page $E_\infty^{p,q}$ is obtained by applying the differentials $d_r^{p,q}$ sequentially, however there is generally no explicit expression for these $d_r^{p,q}$. Instead, we can note from Eqs. (A.3), (A.4), that the diagonals of $E_\infty^{p,q}$ with $p+q=n$ provide a filtration of $\mathscr{H}^n(\mathbb{Z}_n\times\mathbb{Z}_m\times\mathbb{Z}_2^T,\mathbb{Z}_T)$, which itself was calculated by independent means using the torsion product in Appendix J.7 of Ref. [37]. For example, when $n=5$ (corresponding to 3 spatial dimensions), we have $\mathscr{H}^5(\mathbb{Z}_n\times\mathbb{Z}_m\times\mathbb{Z}_2,\mathbb{Z}_T)=\mathbb{Z}_2\times B_{n,m}^{\times 4}\times A_{n,m}^{\times 2}$.

Now, with increasing r, the group $E_{r+1}^{p,q}=\ker d_r^{p,q}/\operatorname{im} d_r^{p-r,q+r-1}$ can either remain the same as $E_r^{p,q}$ (if $d_r^{p,q}$ and $d_r^{p-r,q+r-1}$ are both the zero map), or become a smaller group. However, we see that already at the $r=2$ page, the product of the orders of the groups is $\prod_p|E_2^{p,5-p}|=|\mathbb{Z}_2||B_{n,m}|^4|A_{n,m}|^2$, which matches the order of the previously obtained cohomology group $=|\mathscr{H}^5(\mathbb{Z}_n\times\mathbb{Z}_m\times\mathbb{Z}_2,\mathbb{Z}_T)|$. We also know from the filtration Eqs. (A.3), (A.4) that $|\mathscr{H}^5(\mathbb{Z}_n\times\mathbb{Z}_m\times\mathbb{Z}_2,\mathbb{Z}_T)|=\prod_p|E_\infty^{p,5-p}|$. Given that $|E_\infty^{p,q}|\le|E_2^{p,q}|$, with equality implying $E_\infty^{p,q}=E_2^{p,q}$, we conclude that along this diagonal, the sequence already converges at the 2nd page. The same turns out to be true for all the diagonals $p+q=2,\ldots,5$. Therefore, in this case, the non-equilibrium classification equals $E_2^{0,d+2}$, given by the first non-trivial column of (A.8).

The remaining symmetry classes can be obtained using the same method. However, some follow more easily: if the only homomorphism from $\mathscr{H}^{1+d}[G,\mathrm{U}_T(1)]$ to $\mathscr{H}^{1+d}[G_T,\mathrm{U}_T(1)]$ is the trivial map, then its image must be trivial. For example in the case of $G=\mathrm{U}(1)\rtimes\mathbb{Z}_2^T$ in $d=2$ dimensions, there is no non-trivial homomorphism from $\mathbb{Z}_2$ to $\mathbb{Z}$.

Appendix B

Derivation of the higher order master equation

In this appendix, we derive the higher order corrections to the master equation for a system with a topological bound state in contact with an environment [Eq. (4.17)]. This derivation is based on the assumption that the system is well-described by a quantum Markov process. Before beginning the derivation, we provide a semi-quantitative justification for why such an assumption is expected to hold in regimes where the criterion $\tau_{\mathrm{m}} \ll \tau_S$ [Eq. (4.15)] is satisfied. (Recall that τ_{m} is the 'memory time' for the environment spectral functions, and τ_S is the typical timescale over which the state of the system changes appreciably.)

The true dynamics of the open system is governed by the composite Hamiltonian (4.2). Consider the corresponding von Neumann equation of motion

$$\frac{\mathrm{d}\hat{\rho}_I(t)}{\mathrm{d}t} = -\mathrm{i}[\hat{H}_I(t), \hat{\rho}_I(t)] \tag{B.1}$$

where $\hat{\rho}_I(t)$ and $\hat{H}_I(t)$ are the interaction picture representations of $\hat{\rho}(t)$ and $\hat{H}_{SE}$, respectively, the latter of which can be decomposed as $\hat{H}_{SE} = \sum_\alpha \hat{A}_\alpha \otimes \hat{B}_\alpha$, with $\hat{A}_\alpha$ acting on the system and $\hat{B}_\alpha$ acting on the bath. This has a formal solution in a superoperator formalism. Define the superoperator for the commutator $\mathscr{L}_H(t)[\hat{\rho}] = -\mathrm{i}[\hat{H}_I(t), \hat{\rho}]$, and in turn the time-evolution superoperator

$$\mathscr{U}(t_2, t_1) \coloneqq \mathscr{T} \exp\left(\int_{t_1}^{t_2} \mathrm{d}t' \, \mathscr{L}_H(t') \right). \tag{B.2}$$

The system density matrix in the interaction picture $\hat{\rho}_{S,I}(t) = e^{\mathrm{i}\hat{H}_S t}\hat{\rho}_S(t)e^{-\mathrm{i}\hat{H}_S t}$ can then be written

$$\begin{aligned}\hat{\rho}_{S,I}(t) &= \mathrm{Tr}_E\left(\mathscr{U}(t,0)[\hat{\rho}_I(0)]\right)\\ &= \mathrm{Tr}_E\left(\sum_{n=0}^{\infty}(-\mathrm{i})^n\sum_{\alpha_1\ldots\alpha_n}\int_0^t \mathrm{d}t_1\int_0^{t_1}\mathrm{d}t_2\cdots\int_0^{t_{n-1}}\mathrm{d}t_n\right.\\ &\left.\times\,[\hat{A}_{\alpha_1}(t_1)\otimes\hat{B}_{\alpha_1}(t_1),[\cdots[\hat{A}_{\alpha_n}(t_n)\otimes\hat{B}_{\alpha_n}(t_n),\hat{\rho}_S(0)\otimes\hat{\rho}_E]\cdots]]\right)\end{aligned} \tag{B.3}$$

For simplicity, we will assume that the environment is Gaussian, and that all one-point expectation values vanish $\mathrm{Tr}_E[\hat{\rho}_E\hat{B}_\alpha]=0$. The partial trace can then in principle be evaluated by summing over all pairs of insertions according to Wick's theorem[1]. A given term in which times t_i and t_j are paired will involve the two-time correlation function $\tilde{\Gamma}_{\alpha_i\alpha_j}(t_i-t_j)$. These functions have a typical range in time τ_m, and so contributions for which $|t_i-t_j|\gtrsim\tau_\mathrm{m}$ will be small. Now, let us consider how $\hat{\rho}_{S,I}(t)$ changes between times t and $t+\Delta t$. We split the time integrations into regions $[0,t]$ and $[t,t+\Delta t]$, giving

$$\begin{aligned}\hat{\rho}_{S,I}(t+\Delta t) = \mathrm{Tr}_E\left(\sum_{n=0}^{\infty}\sum_{m=0}^{\infty}(-\mathrm{i})^{n+m}\sum_{\substack{\alpha_1\ldots\alpha_n\\ \beta_1\ldots\beta_m}}\int_0^t\mathrm{d}t_1\int_0^{t_1}\mathrm{d}t_2\cdots\int_0^{t_{n-1}}\mathrm{d}t_n\int_t^{t+\Delta t}\mathrm{d}t'_1\cdots\int_t^{t'_{m-1}}\mathrm{d}t'_m\right.\\ \left.\times\,[\hat{A}_{\beta_1}(t'_1)\otimes\hat{B}_{\beta_1}(t'_1),\cdots[\hat{A}_{\alpha_1}(t_1)\otimes\hat{B}_{\alpha_1}(t_1),[\cdots[\hat{A}_{\alpha_n}(t_n)\otimes\hat{B}_{\alpha_n}(t_n),\hat{\rho}_S(0)\otimes\hat{\rho}_E]\cdots]]\cdots]\right)\end{aligned} \tag{B.4}$$

The insertions at times $t'_j\in[t,t+\Delta t]$ can be Wick-paired among themselves or with insertions at earlier times $t_i\in[0,t]$. If $\Delta t\gg\tau_\mathrm{m}$, then the latter terms will be small, since the correlators are short-ranged in time relative to Δt. If we neglect these terms, we can identify the part of (B.4) involving operators at times $t_i\le t$ with the expression (B.3), giving

$$\begin{aligned}\hat{\rho}_{S,I}(t+\Delta t) = \mathrm{Tr}_E\left(\sum_{m=0}^{\infty}(-\mathrm{i})^m\int_t^{t+\Delta t}\mathrm{d}t'_1\cdots\int_t^{t'_{m-1}}\mathrm{d}t'_m\right.\\ \left.\times\,[\hat{A}_{\beta_1}(t'_1)\otimes\hat{B}_{\beta_1}(t'_1),[\cdots[\hat{A}_{\beta_n}(t'_m)\otimes\hat{B}_{\beta_n}(t'_m),\hat{\rho}_{S,I}(t)\otimes\hat{\rho}_E]\cdots]]\right)\\ +\,(\text{terms higher order in }\tau_\mathrm{m}/\Delta t)\end{aligned} \tag{B.5}$$

[1] For non-Gaussian environments, similar arguments can be formulated where one includes contributions from all cumulants [107].

We now undo the interaction picture rotation, and use the fact that contractions between the $\hat{B}_{\beta_i}(t_i')$ operators only depend on the differences between time coordinates

$$\hat{\rho}_S(t+\Delta t) = e^{-\mathrm{i}\Delta t\hat{H}_S}\,\mathrm{Tr}_E\left(\sum_{m=0}^{\infty}(-\mathrm{i})^m\int_0^{\Delta t}\mathrm{d}t_1'\cdots\int_0^{t_{m-1}'}\mathrm{d}t_m'\right.$$
$$\left.\times\,[\hat{A}_{\beta_1}(t_1')\otimes\hat{B}_{\beta_1}(t_1'),[\cdots[\hat{A}_{\beta_n}(t_m')\otimes\hat{B}_{\beta_n}(t_m'),\hat{\rho}_S(t)\otimes\hat{\rho}_E]\cdots]]\right)e^{\mathrm{i}\Delta t\hat{H}_S} \tag{B.6}$$

While the above still looks forbidding, we have arrived at an expression for the system density matrix at a time $t+\Delta t$ where the only dependence on t comes through $\hat{\rho}_S(t)$. We can therefore write

$$\hat{\rho}_S(t+\Delta t) = \mathscr{U}_{\Delta t}[\hat{\rho}_S(t)] \tag{B.7}$$

for some superoperator $\mathscr{U}_{\Delta t}$. Again we emphasise that this expression relies on $\tau_\mathrm{m}\ll\Delta t$, such that we can safely neglect the additional terms in Eq. (B.5), which capture the dependence of the system's dynamics on the state of the system at times before t. Now, if Δt is sufficiently small, then we may expand $\mathscr{U}_{\Delta t}=\mathscr{I}+\Delta t\mathscr{L}+\mathscr{O}([\Delta t]^2)$ for some $\mathscr{L}$, where $\mathscr{I}$ is the identity superoperator. If this is the case, then (B.7) can be cast as a differential equation

$$\frac{\mathrm{d}\hat{\rho}_S(t)}{\mathrm{d}t} = \mathscr{L}[\hat{\rho}_S(t)] \tag{B.8}$$

Therefore, provided that there exists a timescale $\Delta t\gg\tau_\mathrm{m}$ for which $\Delta t\mathscr{L}[\hat{\rho}_S(t)]\ll 1$, the system density matrix is governed by an effective Markovian master equation generated by the superoperator $\mathscr{L}$, which on mathematical grounds must take the Lindblad form (4.3). Note that in taking the differential limit of (B.7), we discard information about the temporal variation of $\hat{\rho}_S(t)$ over timescales shorter than τ_m. Thus, while the dynamics of the system is strictly non-Markovian, it is effectively Markovian over sufficiently coarse-grained timescales. We can characterize the magnitude of $\mathscr{L}[\hat{\rho}_S]$ by the timescale τ_S, describing the typical times over which the state of the system changes appreciably. The criterion for such a Markovian description of the system is then given by Eq. (4.15), as stated in the main text. Note that all these arguments regarding Markovianity can be formulated more rigorously in terms of a systematic expansion in τ_m/τ_S for both classical and quantum problems; see Refs. [107, 199, 36] for more details.

With this understood, we are now in a position to derive an explicit expression for the generator $\mathscr{L}$, which unlike the Born-Markov expression (4.12) will include terms up to fourth

order in V. Specifically, we are interested in scenarios where the system has degenerate ground states separated in energy from excited states by a finite gap E_{g}, and the environment is in thermal equilibrium at a temperature $T \ll E_g$.

While the expression (B.6) could in principle be used to infer $\mathscr{L}$, it is actually easier to compute $\hat{\rho}_S(t)$ using conventional time-dependent perturbation theory and compare to the formal solution of Eq. (B.8) $\hat{\rho}_S(t) = e^{\mathscr{L}t}[\hat{\rho}_S(0)]$. Specifically, for $t \ll \tau_S$, we expect that the perturbative expansion will converge well, and the linear-in-time component of $\hat{\rho}_S(t)$ will be $t\,\mathscr{L}[\hat{\rho}_S(0)]$, up to oscillations on timescales of order τ_{m}. (This is analogous to the derivation of transition rates in Fermi's golden rule.) To help perform the necessary coarse-graining, it is helpful to consider the Laplace transform

$$\tilde{\rho}_S(s) := \int_0^\infty \mathrm{d}t\, e^{-st}\hat{\rho}_S(t). \tag{B.9}$$

For $s \ll \tau_{\mathrm{m}}^{-1}$, any fast oscillations will be averaged out; thus the effective Lindblad generator $\mathscr{L}$ describing Markovian dynamics on coarse-grained timescales can be inferred from the small-s behaviour of $\tilde{\rho}_S(s)$. The Taylor expansion of $e^{\mathscr{L}t}$ generates a Laurent series in s

$$\tilde{\rho}_S(s) = \frac{1}{s}\hat{\rho}_S(0) + \frac{1}{s^2}\mathscr{L}\hat{\rho}_S(0) + \frac{1}{s^3}\mathscr{L}^2\hat{\rho}_S(0) + \cdots. \tag{B.10}$$

We will compute $\tilde{\rho}_S(s)$ in perturbation theory, and extract the coefficient of s^{-2} therein[2], allowing us to infer $\mathscr{L}$. (This strategy partly resembles one used to derive higher order master equations for atomic systems [202, 156].)

The system density matrix at later times is given by the formal expression

$$\hat{\rho}_{S,I}(t) = \mathrm{Tr}_E\left[\hat{U}(t,0)\,(\hat{\rho}_S(0)\otimes\hat{\rho}_E)\,\hat{U}(t,0)^\dagger\right], \tag{B.11}$$

where $\hat{U}(t_2,t_1) = \mathscr{T}\exp(-\mathrm{i}\int_{t_1}^{t_2}\mathrm{d}t'\hat{H}_I(t'))$ is the time-evolution operator for the composite system in the interaction picture. If we work to second order in V, we expect to arrive at the Born-Markov expression (4.12). Here, we will include all terms to fourth order in V, and then take the Laplace transform as described above. Let us write $\hat{\rho}_{S,I}^{(i,j)}(t)$ for the component

[2]The Laurent series (B.10) evidently breaks down as $s \to 0$. This is because the Taylor expansion of $e^{\mathscr{L}t}$ converges poorly for times $t \gg \tau_S$. Indeed if we did not Taylor expand before taking the Laplace transform (or if we somehow re-summed the Laurent series), then we would have found that the only singularities of $\tilde{\rho}_S(s)$ were simple poles located at $s = -\lambda_i$, where λ_i are the eigenvalues of $\mathscr{L}$. The expansion should therefore only be trusted in the region $\tau_S^{-1} \ll s \ll \tau_{\mathrm{m}}^{-1}$, such that oscillatory terms are suppressed and the Laurent series is reliable. Fortunately, if we work to finite order in time-dependent perturbation theory, then the region $s \ll \tau_S^{-1}$ will not be resolved, and so the expansion (B.10) emerges naturally without us having to explicitly impose any restrictions on s.

that comes from expanding $\hat{U}(t,0)$ to ith order and $\hat{U}(t,0)^\dagger$ to jth order. One such term is $\hat{\rho}_{S,I}^{(2,2)}(t)$, which can be written using the decomposition of the coupling operators (4.13)

$$\begin{aligned}\hat{\rho}_S^{(2,2)}(t) = &\sum_{\alpha_1\ldots\alpha_4}\sum_{\omega_1\ldots\omega_4}\int_0^t \mathrm{d}t_1\int_0^{t_1}\mathrm{d}t_2\int_0^t\mathrm{d}t_3\int_0^{t_3}\mathrm{d}t_4\\ &\times \mathrm{Tr}_E[\hat{B}^\dagger_{\alpha_4}(t_4)\hat{B}^\dagger_{\alpha_3}(t_3)\hat{B}_{\alpha_1}(t_1)\hat{B}_{\alpha_2}(t_2)\hat{\rho}_E]\exp\left(-\mathrm{i}\omega_1 t_1-\mathrm{i}\omega_2 t_2+\mathrm{i}\omega_3 t_3+\mathrm{i}\omega_4 t_4\right)\\ &\times \hat{A}_{\alpha_1}(\omega_1)\hat{A}_{\alpha_2}(\omega_2)\hat{\rho}_S(0)\hat{A}^\dagger_{\alpha_4}(\omega_4)\hat{A}^\dagger_{\alpha_3}(\omega_3).\end{aligned} \tag{B.12}$$

For simplicity, here we will consider a Gaussian environment. (We expect that non-Gaussian corrections will not change the qualitative aspects of our results.) The four-point correlator for the environment can then be evaluated using Wick's theorem. There are three contributions corresponding to the different ways to pair the insertions. Let us consider the term where times (t_1,t_4) and (t_2,t_3) are paired, which after a Fourier transform of the two-time correlators gives

$$\begin{aligned}\hat{\rho}_S^{(2,2)}(t) \ni &\sum_{\alpha_1\ldots\alpha_4}\sum_{\omega_1\ldots\omega_4}\int_0^t \mathrm{d}t_1\int_0^{t_1}\mathrm{d}t_2\int_0^t\mathrm{d}t_3\int_0^{t_3}\mathrm{d}t_4\int_{-\infty}^{\infty}\frac{\mathrm{d}\varepsilon_A}{2\pi}\int_{-\infty}^{\infty}\frac{\mathrm{d}\varepsilon_B}{2\pi}\Gamma_{\alpha_4\alpha_1}(\varepsilon_A)\Gamma_{\alpha_3\alpha_2}(\varepsilon_B)\\ &\times\exp\left[-\mathrm{i}(\omega_1-\varepsilon_A)t_1-\mathrm{i}(\omega_2-\varepsilon_B)t_2+\mathrm{i}(\omega_3-\varepsilon_B)t_3+\mathrm{i}(\omega_4-\varepsilon_A)t_4\right]\\ &\times\hat{A}_{\alpha_1}(\omega_1)\hat{A}_{\alpha_2}(\omega_2)\hat{\rho}_S(0)\hat{A}^\dagger_{\alpha_4}(\omega_4)\hat{A}^\dagger_{\alpha_3}(\omega_3).\end{aligned} \tag{B.13}$$

Since all the time-dependence is now in the exponential factor, the Laplace transform can be performed easily. The relevant integral is

$$\begin{aligned}&\int_0^\infty\mathrm{d}t\int_0^t\mathrm{d}t_1\int_0^{t_1}\mathrm{d}t_2\int_0^t\mathrm{d}t_3\int_0^{t_3}\mathrm{d}t_4\, e^{-\mathrm{i}\Delta_1 t_1-\mathrm{i}\Delta_2 t_2+\mathrm{i}\Delta_3 t_3+\mathrm{i}\Delta_4 t_4-s(t-t_0)}\\ &=\sum_{c_1,\ldots c_4=0}^{1}\frac{(-1)^{c_1+c_2+c_3+c_4}}{\Delta_2(\Delta_1+c_2\Delta_2)\Delta_4(\Delta_3+c_4\Delta_4)}\frac{-\mathrm{i}}{-\mathrm{i}s+c_1(\Delta_1+c_2\Delta_2)-c_3(\Delta_3+c_4\Delta_4)}\end{aligned} \tag{B.14}$$

with the substitutions $\Delta_1=\omega_1-\varepsilon_A$, $\Delta_2=\omega_2-\varepsilon_B$, $\Delta_3=\omega_3-\varepsilon_B$, and $\Delta_4=\omega_4-\varepsilon_A$. Although the expression (B.14) contains many terms with different poles, it is possible to extract its analytical properties near $s=0$ in the regimes of interest to us. Much like our treatment of the lowest order master equation (4.12), we have $\omega_2,\omega_4\le -E_\mathrm{g}$, since the system is gapped and $\hat{A}_\alpha$ have no off-diagonal matrix elements within the ground state subspace. Similarly, we can split the contributions into terms for which $\omega_1+\omega_2=0$ versus those with $\omega_1+\omega_2\le -E_\mathrm{g}$ (similarly for $\omega_3+\omega_4$). We anticipate that the latter can be neglected, since they represent thermally activated processes where the final state is excited. We are left with a sum over ω_2 and ω_4 only, and we have $\Delta_1=\Delta_4-\omega_2-\omega_4$; $\Delta_3=\Delta_2-\omega_2-\omega_4$. Thus for a given $\omega_{2,4}$ in

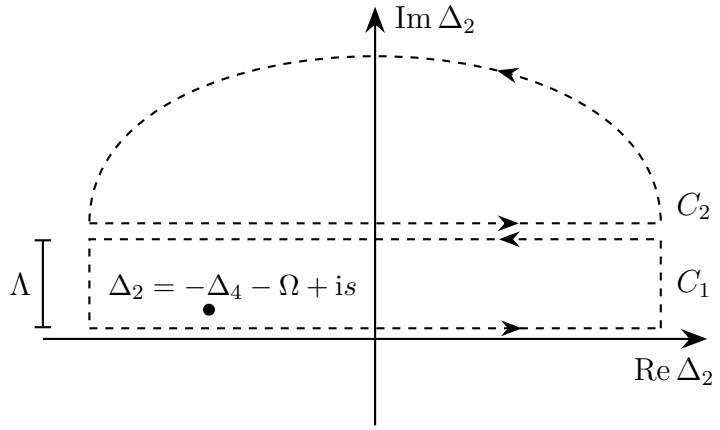

Fig. B.1 Contours C_1 and C_2 along which the integrals over Δ_2 and Δ_4 in Eq. (B.15) are taken. The spectral functions are assumed to be non-singular within a distance Λ from the real axis (see main text). For $c_1 = c_2 = 1$, $c_3 = 0$, a simple pole is enclosed within C_1.

the sum, the integrals over ε_A, ε_B can be written as integrals over Δ_4, Δ_2, respectively, giving

$$\begin{aligned}\tilde{\rho}_S^{(2,2)}(s) \ni -\mathrm{i} \sum_{\alpha_1 \ldots \alpha_4} \sum_{\omega_2,\omega_4 \leq -E_\mathrm{g}} \sum_{c_1,\ldots c_4=0}^{1} \int \frac{\mathrm{d}\Delta_2}{2\pi} \int \frac{\mathrm{d}\Delta_4}{2\pi} \Gamma_{\alpha_4\alpha_1}(\omega_4 - \Delta_4)\Gamma_{\alpha_3\alpha_2}(\omega_2 - \Delta_2) \\ \times \frac{(-1)^{c_1+c_2+c_3+c_4}}{-\mathrm{i}s + \Delta_2(c_1c_2 - c_3) + \Delta_4(c_1 - c_3c_4) + \Omega(c_3 - c_1)} \\ \times \frac{\hat{A}_{\alpha_1}(-\omega_2)\hat{A}_{\alpha_2}(\omega_2)\hat{\rho}_S(0)\hat{A}^\dagger_{\alpha_4}(\omega_4)\hat{A}^\dagger_{\alpha_3}(-\omega_4)}{\Delta_2\Delta_4(\Delta_4 + c_2\Delta_2 - \Omega)(\Delta_2 + c_4\Delta_4 - \Omega)},\end{aligned} \tag{B.15}$$

where $\Omega = \omega_2 + \omega_4$. We must now deal with the integrals over $\Delta_{2,4}$. While the integrand appears to be singular at $\Delta_2 = 0$, $\Delta_4 = 0$, $\Delta_4 + c_2\Delta_2 - \Omega = 0$, and $\Delta_2 + c_4\Delta_4 - \Omega = 0$, it is in fact analytic at these points, provided one includes all terms in the sum over $\{c_i\}$. We can therefore shift the denominators of the third line of the above such that they vanish infinitesimally below the real axis, and close the Δ_2, Δ_4 contours in the upper half plane; the expression can then be safely analysed term by term.

We can distinguish contributions to the integrals from the nonanalyticities of the spectral functions versus those due to the simple pole in the second line of (B.15). Since the environment correlation functions are short-ranged in time, the spectral functions will be smooth on the real axis, and so we assume that the former contributions occur at $|\mathrm{Im}\,\Delta_2| > \Lambda$ for some $\Lambda \gg \tau_S^{-1}$. Each integral can therefore be split into contours C_1 and C_2, where C_1 bounds the region $0 < \mathrm{Im}\,\Delta_2 < \Lambda$ and C_2 encloses the rest of the upper-half plane (see Fig. B.1). Integrating over Δ_2 first, we see that $\int_{C_1} \mathrm{d}\Delta_2(\cdots)$ only encloses the pole if $c_1 = c_2 = 1$, $c_3 = 0$ (taking s to be a positive real variable). If we then integrate Δ_4 around

C_1, we must have $c_4 = 0$, such that a pole at $\Delta_4 = is$ is enclosed. This contribution will be suppressed by a factor $\Gamma_{\alpha_4\alpha_1}(\omega_4 - is) \sim e^{-E_g/T}$, and can therefore neglected. If, instead, both integrals are taken over C_2, then no s^{-2} term is generated. Therefore, we must take one integral over C_1 and the other over C_2. One finds that the only terms that contribute to the coefficient of s^{-2} are $(c_1, c_2, c_3, c_4) = (1, 1, 0, 1)$, giving

$$\begin{aligned}(\text{B.15}) \; &= -s^{-2} \sum_{\substack{\alpha_1 \ldots \alpha_4 \\ \omega_2, \omega_4 \leq -E_g}} \int \frac{d\varepsilon}{2\pi} \frac{\Gamma_{\alpha_4\alpha_1}(\varepsilon)\Gamma_{\alpha_3\alpha_2}(-\varepsilon)}{(\varepsilon + \omega_2)(\varepsilon - \omega_4)} \hat{A}_{\alpha_1}(-\omega_2)\hat{A}_{\alpha_2}(\omega_2)\hat{\rho}_S(0)\hat{A}^\dagger_{\alpha_4}(\omega_4)\hat{A}^\dagger_{\alpha_3}(-\omega_4) \\ &+ \; (\text{terms less singular than } s^{-2}) \qquad \text{(B.16)}\end{aligned}$$

These arguments can be repeated for the other Wick pairings and for all $\hat{\rho}_S^{(i,j)}(t)$ with $i + j = 4$. To combine them into a concise form, we need to make use of certain properties of the spectral functions. Since the operators $\hat{B}_\alpha$ are Hermitian, we have

$$\Gamma_{\alpha\beta}(\varepsilon)^* = \Gamma_{\beta\alpha}(\varepsilon) \qquad \text{(B.17)}$$

i.e. the spectral function is a Hermitian matrix. Additionally, as we are concerned with cases where $\hat{B}_\alpha$ and $\hat{H}_E$ (and hence $\hat{\rho}_E$) are invariant under some antiunitary symmetry $\hat{T}_E \hat{B}^*_\alpha \hat{T}^\dagger_E = \hat{B}_\alpha$, we have

$$\begin{aligned}\tilde{\Gamma}_{\alpha\beta}(t) &= \mathrm{Tr}_E \left(\hat{\rho}_E \hat{B}_\alpha(t)\hat{B}_\beta(0)\right) \\ &= \mathrm{Tr}_E \left(\hat{T}_E \hat{\rho}^*_E \hat{T}^\dagger_E \; \hat{T}_E \hat{B}_\alpha(-t)^* \hat{T}^\dagger_E \; \hat{T}_E \hat{B}_\beta(0)^* \hat{T}^\dagger_E\right) \\ &= \mathrm{Tr}_E \left(\hat{\rho}_E \hat{B}_\alpha(-t)\hat{B}_\beta(0)\right)^* \\ &= \tilde{\Gamma}_{\alpha\beta}(-t)^* \\ &\Rightarrow \Gamma_{\alpha\beta}(\varepsilon) \in \mathbb{R} \qquad \text{(B.18)}\end{aligned}$$

i.e. the spectral function is a real symmetric matrix. Altogether, we arrive at the expression for the master equation (4.17) quoted in the main text.

Appendix C

Derivation of the resistance of the helical Luttinger liquid coupled to a two-level system

In this appendix, we derive expressions for the electrical conductance of a helical Luttinger liquid coupled to a two-level system via electrostatic interactions, which in the main text was argued to be governed by the effective low-energy Hamiltonian (4.47).

Before beginning a calculation, we must carefully consider exactly what quantity we aim to compute. In the absence of the coupling $y = 0$, the helical modes described by (4.46) are perfect conductors. More precisely, a four-terminal resistance measurement on a single edge would give zero resistance (infinite conductance), while a two-terminal measurement would give a finite conductance $G_0 = \kappa e^2/2\pi\hbar$ per edge channel, associated with transmission from the leads to the sample. The universal constant κ is equal to K for interacting one-dimensional leads [10], or 1 if the leads are well-described by Fermi liquids [143, 189]. For example, in a typical solid-state experiment in a Hall bar geometry, the are two helical channels (one at each edge) and the leads are Fermi liquids, so the combined conductance is $G_0^{\text{bar}} = 2e^2/2\pi\hbar$ [128, 183]. Our interest is in the deviations from perfect conduction due to interactions with the TLS. Unlike the conductances, the various resistances in a single-channel geometry combine additively. Therefore, we will aim to determine the residual resistance $\delta R = R - R_0$ for the channel to which the TLS is coupled, where R (R_0) is the resistance with (without) the TLS. For computational convenience, we will calculate the correction to the two-terminal conductance $\delta G = G - G_0$ for a single spatially homogeneous helical channel (i.e. one where the leads have the same interaction strength as the bulk of the system, so $\kappa = K$). For small

δG, this allows us to determine the resistance via

$$\delta R = \frac{-\delta G}{G_0^2}. \tag{C.1}$$

While the values of G_0 and δG quoted here are specific to the two-terminal conductance protocol with interacting leads, the residual resistance δR is entirely associated with the HLL-TLS interactions, and is independent of the measurement geometry and properties of the leads.

Our calculation is an extension of Kane and Fisher's derivation for the conductance of a Luttinger liquid coupled to a static impurity [109]. We first integrate out the bosonic fields for all $x \neq 0$, leaving only $\hat{\phi}(x=0)$. One obtains the Matsubara action

$$S_{\text{eff}}\left[\phi, \vec{S}\,\right] = S_{\text{WZ}}\left[\vec{S}\,\right] + \frac{1}{\pi K}\sum_{\mathrm{i}\omega_n} |\omega_n||\phi(\mathrm{i}\omega_n)|^2 + \int_0^\beta \mathrm{d}\tau\, \varepsilon S^z(\tau) + (y/\sigma) S^y(\tau)\cos[2\phi(\tau)] \tag{C.2}$$

where $\omega_n = 2\pi n/\beta$ are the bosonic Matsubara frequencies, and $\varepsilon = \sqrt{E^2+\Delta^2}$. The frequency space representation of the field ϕ is given by [140]

$$\phi(\mathrm{i}\omega_n) = \int_0^\beta \mathrm{d}\tau\, e^{\mathrm{i}\omega_n \tau}\phi(\tau) \tag{C.3}$$

The field $\phi(\tau)$ can be coupled to a classical gauge field $a(\tau)$ via the standard coupling $S_a[\phi] = \int \mathrm{d}\tau\, j(\tau)a(\tau)$, where $j(\tau) = -\mathrm{i}e\partial_\tau\phi(\tau)/\pi$ is the current operator [79]. The continuation of the gauge field to real time is related to the voltage applied across the point $x=0$ by $V(t) = \partial_t a(t)$ [109]. The term $S_a[\phi]$ can then be removed by a shift of variables $\phi(\tau) \to \phi(\tau) - eKa(\tau)/2$, giving[1]

$$\begin{aligned} S_{\text{eff}}\left[\phi, \vec{S}\,\right] = S_{\text{WZ}}\left[\vec{S}\,\right] &+ \frac{1}{\pi K}\sum_{\mathrm{i}\omega_n} |\omega_n||\phi(\mathrm{i}\omega_n)|^2 + \frac{Ke^2}{4\pi}\sum_{\mathrm{i}\omega_n} |\omega_n||a(\mathrm{i}\omega_n)|^2 \\ &+ \int_0^\beta \mathrm{d}\tau\, \varepsilon S^z(\tau) + (y/\sigma) S^y(\tau)\cos[2\phi(\tau) - eKa(\tau)] \end{aligned} \tag{C.4}$$

[1] One must use the fact that $a(\tau)$ is imaginary, which follows from the realness of $V(t) = \partial_t a(t)$.

As explained in the main text, we will treat y perturbatively here. The partition function for the action (C.4) can be expanded in powers of y, and at leading order we have

$$\mathscr{Z}[a] = \mathscr{Z}_0[a]\left(1 + \frac{y^2}{4\sigma^2}\int_0^\beta \mathrm{d}\tau_1 \int_0^\beta \mathrm{d}\tau_2\, F^{\mathrm{m}}(\tau_1-\tau_2)C^{\mathrm{m}}(\tau_1-\tau_2)\cos[eKa(\tau_1)-eKa(\tau_2)]\right) \tag{C.5}$$

where we have defined the imaginary time correlators

$$F^{\mathrm{m}}(\tau_1-\tau_2) := \left\langle \mathscr{T}_\tau e^{2\mathrm{i}\phi(\tau_1)}e^{-2\mathrm{i}\phi(\tau_2)}\right\rangle_0, \qquad C^{\mathrm{m}}(\tau_1-\tau_2) := \langle \mathscr{T}_\tau S^y(\tau_1)S^y(\tau_2)\rangle_0 . \tag{C.6}$$

Here, $\mathscr{Z}_0[a]$ and $\langle\cdot\rangle_0$ are the partition function and expectation values with respect to the action (C.4) at zero coupling $y=0$. The current in imaginary time is given by the derivative of the generating functional $I(\tau) = \delta \log \mathscr{Z}[a]/\delta a(\tau)$, giving

$$I(\tau) = I_0(\tau) - \frac{eKy^2}{2\sigma^2}\int_0^\beta \mathrm{d}\tau' F^{\mathrm{m}}(\tau-\tau')C^{\mathrm{m}}(\tau-\tau')\sin[eKa(\tau)-eKa(\tau')] \tag{C.7}$$

where $I_0(\tau) = \delta\mathscr{Z}_0/\delta a(\tau)$ is the contribution for the unperturbed HLL, which is responsible for the conductance of the clean system $G_0 = Ke^2/2\pi$. We now perform an analytic continuation to the Keldysh contour in real time $t = -\mathrm{i}\tau$, which runs from $t' = -\infty$ to $t' = t$ and then back to $t' = -\infty - \mathrm{i}\beta$ [179]. This gives a correction $\delta I(t) = I(t) - I_0(t)$ of

$$\delta I(t) = \frac{-\mathrm{i}eKy^2}{2\sigma^2}\int_{-\infty}^{t}\mathrm{d}t'\left[F^{>}(t-t')C^{>}(t-t') - F^{<}(t-t')C^{<}(t-t')\right]\sin(eK[a(t)-a(t')]) \tag{C.8}$$

where $F^{>(<)}(t)$ is the greater (lesser) Green's function, which for $t>0$ can be obtained by analytically continuing the imaginary time Green's function $F^{\mathrm{m}}(\tau)$ to $\tau \to \pm\mathrm{i}t$, with the $+$ sign for $F^{>}(t)$ [similar for $C^{>,<}(t)$]. By standard techniques, one finds [79]

$$F^{>(<)}(t) = e^{\mp\mathrm{i}\pi K\,\mathrm{sgn}(t)}\left(\frac{\pi\sigma/\beta}{\sinh(\pi|t|/\beta)}\right)^{2K} \tag{C.9}$$

$$C^{>(<)}(t) = \frac{1}{4}\left[\cos(\varepsilon t) \mp \mathrm{i}\tanh(\beta\varepsilon/2)\sin(\varepsilon t)\right] \tag{C.10}$$

To obtain the linear conductance, we expand to first order in the voltage $V(t) = V_0 e^{-\mathrm{i}\omega_0 t}$ which gives

$$\delta I_{\mathrm{lin}}(t) = V_0 e^{-\mathrm{i}\omega_0 t} \frac{-\mathrm{i}e^2K^2y^2}{4\omega_0\sigma^2} \int_0^\infty \mathrm{d}t' \left(1 - e^{\mathrm{i}\omega_0 t'}\right) \left(\frac{\pi\sigma/\beta}{\sinh(\pi t'/\beta)}\right)^{2K} \times \left[\sin(\pi K)\cos(\varepsilon t') + \cos(\pi K)\tanh(\beta\varepsilon/2)\sin(\varepsilon t')\right] \tag{C.11}$$

The above can be evaluated using the standard integral $\int_0^\infty \mathrm{d}x\, e^{\mathrm{i}qx} \sinh^{-2K}(x) = 2^{2K-1} P_K(-q)$, where we define $P_K(q) \coloneqq B(K + \mathrm{i}q/2, 1-2K)$, with $B(a,b) = \Gamma(a)\Gamma(b)/\Gamma(a+b)$ the Euler beta function. Using the identity $\sin(\pi K) \pm \mathrm{i}\cos(\pi K)\tanh(\beta\varepsilon/2) \equiv \mathrm{sech}(\beta\varepsilon/2)\sin(\pi K \pm \mathrm{i}\beta\varepsilon/2)$ and employing the relation (C.1), we find the residual AC resistance within the linear response regime

$$\begin{aligned}\delta R(\omega) = R_K \times \frac{\mathrm{i}\pi y^2}{4\omega\sigma} \left(\frac{2\pi\sigma}{\beta}\right)^{2K-1} \mathrm{sech}(\beta\varepsilon/2) \\ \times \Big[\big(P_K[\varepsilon\beta/\pi] - P_K[(\varepsilon-\omega)\beta/\pi]\big)\sin(\pi K + \mathrm{i}\beta\varepsilon/2) \\ + \big(P_K[-\varepsilon\beta/\pi] - P_K[(-\varepsilon-\omega)\beta/\pi]\big)\sin(\pi K - \mathrm{i}\beta\varepsilon/2)\Big].\end{aligned} \tag{C.12}$$

where R_K is the von Klitzing constant $R_K = 2\pi\hbar/e^2$. Using the identity

$$B(K \pm \mathrm{i}q/2, 1-2K) = \frac{|\Gamma(K + \mathrm{i}q/2, 1-2K)|^2}{\sin(2\pi K)\Gamma(2K)} \sin(\pi K \mp \mathrm{i}\pi q/2), \tag{C.13}$$

Eq. (C.12) can be evaluated in the DC limit $\omega \to 0$, giving Eq. (4.49). Additionally, using the limiting behaviour

$$P_K(q) \underset{|q|\to\infty}{=} -\mathrm{i}\,\mathrm{sgn}(q)\Gamma(1-2K)e^{\mathrm{i}\pi K\,\mathrm{sgn}(q)} \left(\frac{|q|}{2}\right)^{2K-1} \qquad q \in \mathbb{R}, \tag{C.14}$$

we can compute the AC resistance at zero temperature. The real part is given in (4.50), and the imaginary part is

$$\begin{aligned}\mathrm{Im}\,\delta R_{T=0}(\omega) = -R_K \times \frac{\pi^2 y^2}{4\sigma\omega}\Gamma(1-2K) \\ \times \begin{cases} (\sigma[\varepsilon+\omega])^{2K-1} + (\sigma[\varepsilon-\omega])^{2K-1} - 2(\sigma\varepsilon)^{2K-1} & |\omega| < \varepsilon, \\ (\sigma[|\omega|+\varepsilon])^{2K-1} - \cos(2\pi K)(\sigma[|\omega|-\varepsilon])^{2K-1} - 2(\sigma\varepsilon)^{2K-1} & |\omega| \geq \varepsilon. \end{cases}\end{aligned} \tag{C.15}$$

Note that at leading order in y, the imaginary part $\mathrm{Im}\,\delta R_{T=0}(\omega)$ only contributes to an overall phase shift of the linear conductance. The real part describes the rate of backscattering.

We can also obtain an expression for the nonequilibrium current at finite DC bias by substituting $a(t)-a(t')=V\times(t-t')$ in Eq. (C.8). By analogy to Eq. (C.1), the resistance due to the TLS can be identified as $\delta R(V)=V[I_0(V)+\delta I(V)]^{-1}-G_0^{-1}\approx-\delta I(V)/(VG_0^2)$, having used $I_0(V)=G_0V$ (which still holds at finite bias). This gives

$$\begin{aligned}\delta R(V)=R_K\times\frac{\pi y^2}{4eKV\sigma}(2\pi\sigma T)^{2K-1}\,\mathrm{sech}(\varepsilon/2T)\\ \times\,\mathrm{Im}\left\{\sin(\pi K+\mathrm{i}\varepsilon/2T)\left[P_K\left(\frac{\varepsilon-eKV}{\pi T}\right)-P_K\left(\frac{\varepsilon+eKV}{\pi T}\right)\right]\right\}\end{aligned}\tag{C.16}$$

which in the zero temperature limit gives Eq. (4.51).

We note that in the limit $\varepsilon\ll\max(T,\omega,eV)$, our expressions for the resistance exactly coincide with those of Kane and Fisher for a Luttinger liquid coupled to a static impurity, i.e. a perturbation of the form $(y/\sigma)\cos[2\hat{\phi}]$, without the pseudospin operator. This is because the correlator $C^{>,<}(t)$ [Eq. (C.10)] becomes time-independent in this regime, and so the system behaves as if a TRS-breaking static magnetic impurity were present.

As a point of interest, the effective low-energy Hamiltonian (4.47) is closely related to the spin boson model, which describes a two-level system coupled to a bath of harmonic oscillators (see Ref. [131] for an introduction). In fact, the two theories are dual to each other at low energies. To see this, we rescale the fields $\hat{\phi}\to\sqrt{K}\hat{\phi}$, $\hat{\theta}\to\sqrt{1/K}\,\hat{\theta}$ and then perform a unitary transformation using the operator $\hat{U}=e^{-2\mathrm{i}\sqrt{K}\hat{\phi}\hat{S}^z}$. The transformed Hamiltonian $\hat{H}'=\hat{U}^\dagger\hat{H}_{\mathrm{eff}}\hat{U}$ takes the form

$$\hat{H}'=\frac{u}{2\pi}\int\mathrm{d}x\,\left[(\nabla\hat{\phi})^2+(\nabla\hat{\theta})^2\right]+\varepsilon\hat{S}^z-2u\sqrt{K}\hat{S}^z\nabla\hat{\theta}+(y/\sigma)\left[\hat{S}^y+\frac{\hat{S}^+e^{-4\mathrm{i}\sqrt{K}\hat{\phi}}-\mathrm{H.c.}}{2\mathrm{i}}\right].\tag{C.17}$$

The terms involving $e^{\pm4\mathrm{i}\sqrt{K}\hat{\phi}}$ have a scaling dimension of $4K$, and are therefore RG-irrelevant for sufficiently weak interactions $K>1/4$. These terms can accordingly be neglected at low energies. The rescaled bosonic fields can then be expressed in terms of harmonic oscillator operators [79], and one finds that the remaining terms in $\hat{H}'$ are exactly the spin boson Hamiltonian for an Ohmic bath. Using the notation of Ref. [131], the dual spin boson system has a dimensionless friction coefficient of $\alpha_{\mathrm{SB}}=K$, a bias of $\varepsilon_{\mathrm{SB}}=\varepsilon$, and a tunnelling matrix element $\Delta_{\mathrm{SB}}=(y/\sigma)$ [not to be confused with the physical tunnelling matrix element Δ in Eq. (4.29)].

The spin boson model is known to exhibit a crossover[2] from coherent oscillations of the spin for $\alpha_{\mathrm{SB}} < 1/2$ to overdamped behaviour for $\alpha_{\mathrm{SB}} > 1/2$ (see Ref. [230], Section 22.6). In the coherent regime, methods that are based on perturbation theory in Δ_{SB} may be unreliable at low temperatures [87]. The same point $K = 1/2$ in our model marks the onset of resonances in the perturbative expressions for the AC and finite-bias resistance [Eqs. (4.50), (4.51)]. For strong interactions $K < 1/2$, it is possible that the methods used here – which have so far only been justified based on semi-quantitative RG arguments – may run in to similar problems. Nevertheless, for $K > 1/2$ (corresponding to the overdamped spin-boson model), methods based on perturbation theory in y are known to be safe [131]. More generally, we expect that better insight into the low-energy properties of the HLL-TLS Hamiltonian (4.47) can be obtained by harnessing the extensive literature on the spin boson model.

[2] This crossover is distinct from the localization transition at $\alpha_{\mathrm{SB}} = 1$.